

# VYSOKÉ UČENÍ TECHNICKÉ V BRNĚ

## FAKULTA CHEMICKÁ

Alkalicky aktivovaná vysokopeční struska:  
vliv organických a anorganických přísad

Habilitační práce v oboru

Chemie, technologie a vlastnosti materiálů

Ing. Lukáš Kalina, Ph.D.

Brno 2020

Ing. Lukáš Kalina. Ph.D.

Email: kalina@fch.vut.cz

Tel: 541 149 366

Brno

Vysoké učení technické v Brně

Fakulta chemická

Ústav chemie materiálů

Centrum materiálového výzkumu

Purkyňova 464/118

612 00 Brno

[www.fch.vut.cz](http://www.fch.vut.cz)

[www.materials-research.cz](http://www.materials-research.cz)



Poloprovozní výroba betonových dílců z alkalicky aktivované strusky, Běstovice 2019

### **Poděkování:**

*Děkuji především skvělému týmu mých kolegů, bez kterých by tato práce a výsledky společného výzkumu vznikaly jen velmi obtížně. Zvláštní poděkování patří zejména doc. Ing. Františku Šoukalovi, Ph.D., který mi poskytl vždy cenné rady ať už s řešením otázek týkající se základního, tak i aplikovaného výzkumu. Dále bych rád poděkoval Ing. Vlastimilovi Bílkovi, Ph.D. (ml.) za sdílené nadšení ve výzkumu alkalicky aktivovaných materiálů a dlouholetou spolupráci, která přerostla až v přátelský vztah našich rodin i mimo akademickou sféru. Poděkování patří i Fakultě chemické a Centru materiálového výzkumu za možnost profesního růstu a poskytnutí přístrojového vybavení. Speciální dík věnuji mé rodině, jmenovitě mým „holkám“ Helence a Anetce, které mi byly a stále jsou velkou oporou.*

## Abstrakt

Ekologické a ekonomické důvody mají za následek, že v posledních letech stoupá zájem o netradiční cementy a anorganické kompozity. Alkalicky aktivované materiály, zejména pak ty na bázi alkalicky aktivované strusky (AAS), disponují velkým potenciálem pro uplatnění ve stavebnictví. Mnohé přednosti, které tato pojiva nabízí, jsou však ve stínu některých nevýhod bránící širšímu využití v mnoha praktických aplikacích. Těmto negativním aspektům lze předcházet použitím vhodně zvolených přísad a příměsí. Práce proto shrnuje dosavadní poznatky našeho a celosvětového výzkumu týkající se působení různých typů chemických přísad v AAS. Jsou diskutovány skupiny přísad, které mohou významně zlepšit vlastnosti AAS a současně je popsán i vliv přísad přispívající ke zmírnění negativních jevů spojených s produkcí těchto netradičních materiálů. Dosažené výsledky naznačují, že již mnohé problémy byly pomocí přísad vyřešeny, nicméně je třeba se této oblasti i nadále věnovat a posouvat alkalicky aktivované materiály do oblastí vyšší atraktivnosti a zájmu z pohledu stavebního průmyslu.

**Klíčová slova:** *alkalicky aktivovaná struska, přísada, hydratace, stavebnictví, ekologie*

## Abstract

Ecological and economic interests in recent years have resulted in an increased demand for non-traditional types of cement and inorganic composites. Alkali-activated materials, especially those based on alkaline activation of blast furnace slag (AAS), have been shown to have high potential in the construction industry. However, many of the advantages that these binders offer are overshadowed by some of the drawbacks that hinder their wider use in many practical applications. This work summarizes our current understanding and the worldwide research concerning the effects of different types of chemical admixtures in AAS. Discussed are the admixtures which significantly improve properties of AAS, as well as their contribution to the mitigation of negative effects associated with the production of these non-traditional materials. The obtained results suggest that many of the problems have already been addressed with the use of chemical admixtures, however further research into this subject would be paramount in order to make alkali-activated materials more enticing for practical use within the construction industry.

**Key words:** *alkali-activated slag, admixture, hydration, building industry, ecology*

## Obsah

Předmluva .....	1
1. Úvod do řešené problematiky .....	2
2. Alkalická aktivace: základní principy .....	3
2.2 Alkalická aktivace vysokopecní strusky .....	5
2.2.1 Faktory ovlivňující proces alkalické aktivace vysokopecní strusky .....	5
2.2.2 Hydratační produkty .....	9
2.2.3 Aplikační potenciál.....	10
3. Chemické přísady: proč, co a jak? .....	12
3.1 Organické přísady .....	14
3.1.1 Plastifikační přísady.....	15
3.1.2 Přísady redukující smrštění .....	21
3.1.3 Pro vzdušňovací přísady .....	29
3.1.4 Ostatní organické přísady.....	31
3.2 Anorganické přísady .....	32
3.2.1 Anorganické přísady ovlivňující dobu tuhnutí AAS .....	32
3.2.2 Minerální přísady/příměsi .....	34
Mikrosilika a speciálně upravený křemen .....	34
Popílek.....	36
Metakaolin.....	38
Portlandský cement.....	39
Hašené vápno .....	42
4. Závěrečné shrnutí.....	45
5. Zkratky a symboly.....	47
6. Literatura .....	48
7. Přílohy .....	59

## Předmluva

Čas neúprosně utíká a už je to více než jedenáct let, kdy začala má cesta k hlubšímu poznání problematiky alkalicky aktivovaných materiálů. Fascinace výroby betonu bez použití tradičního cementu mě tehdy natolik nadchla, že jsem ani na vteřinu nezaváhal a přijal nabídku se této problematice naplno věnovat. Počáteční nadšení z propagovaných úžasných vlastností zmíněných materiálů však brzy vystřídalo rychlé vystřízlivění. Postupem času jsem čím dál tím víc docházel k názoru, že alkalicky aktivované materiály představují jakési zamotané klubko různých neduhů a úskalí, které významně ovlivňuje jejich použití v průmyslové praxi. Řada výzkumníků proto na tyto materiály postupně zanevřela, nebo je již na počátku své vědecké kariéry hodila přes palubu. Cílem vědy však je a vždy bude tato pomyslná klubka rozmotávat, což mě stále nabíjí potřebou pochopit procesy probíhající uvnitř těchto materiálů, které lze následně vhodným způsobem ovlivnit za účelem získání jejich požadovaných vlastností. Inspirací mi byl samotný beton. Tento heterogenní materiál je v novodobé historii o mnoho let starší nežli alkalicky aktivované materiály, a proto se stal předmětem dlouhodobého testování, ale i mnohého vylepšení, za kterým stojí zejména použití rozličných přísad a příměsí. Chemické přísady mohou neuvěřitelným způsobem měnit charakteristiky betonu, což znamenalo v polovině dvacátého století doslova revoluční zvrát v technologii betonu. V této souvislosti proto vyvstává řada otázek: Dokáží vhodně zvolené přísady rovněž zlepšovat, či eliminovat negativní vlastnosti alkalicky aktivovaných materiálů? Jaké přísady tedy použít a jaké bude jejich chování v silně zásaditém prostředí? Hledáním odpovědí na tyto otázky se již řadu let zabývá mnoho světových výzkumných center. Mým cílem a cílem celé naší malé vědecké skupiny je rovněž přispět námi dosaženými výsledky celosvětovému výzkumu na poli alkalické aktivace a přivést tak tyto materiály na pomyslné výsluní stavebního průmyslu.

Alkalicky aktivované materiály na bázi vysokopecní strusky mají z historického hlediska zřejmě největší potenciál pro využití v praxi. Z tohoto důvodu práce shrnuje dosavadní poznatky týkající se využití organických a anorganických přísad a příměsí v těchto materiálech. Většina kapitol je navíc obohacena diskuzí nad výsledky našeho výzkumu, které byly publikovány v prestižních impaktovaných časopisech daného oboru nebo byly představeny na mezinárodních vědeckých konferencích. Nejvýznamnější odborné publikace jsou rovněž součástí této práce. Věřím, že naše poznatky přispěly k pochopení účinku mnoha chemických přísad a pomohly tak nalézt řešení některých úskalí spojených s produkcí těchto netradičních materiálů.

## 1. Úvod do řešené problematiky

Alkalicky aktivované materiály jsou netradiční stavební pojiva, jejichž výzkum a následná praktická aplikace zažívá v současné době nebývalého rozvoje. Proces alkalické aktivace není žádnou novinkou, nicméně nezadržitelný výzkum a vývoj těchto materiálů můžeme dnes definovat jakousi pomyslnou vývojovou spirálou, kdy v současné době vytváříme z již objevených materiálů materiály nové, ve smyslu komplexního řízení jejich vlastností. Alkalicky aktivované materiály (AAM) si tak nacházejí čím dál tím rozsáhlejší uplatnění v průmyslové praxi.

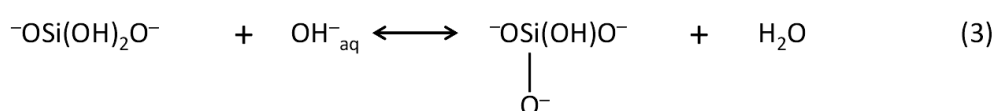
Navzdory citátu amerického průmyslníka Henryho Forda: „Historie je blbost...Jediná historie, která za něco stojí, je ta, kterou vytváříme teď“ je zcela namístě připomenou některé důležité významné milníky související s vývojem AAM, které dokládají, že rozvoj těchto materiálů neprobíhal tak rychle, jak by si zaslouhoval. V technických kruzích představovaly AAM donedávna spíše raritu na poli stavebních materiálů, což se v současné době velmi rychle mění. Výzkum alkalicky aktivovaných materiálů začal v novodobé historii již před více než sto lety prací Kühla [1], který aktivoval vysokopecní strusku silnými zásadami. Od této doby, vývoj alkalicky aktivovaných materiálů zcela jistě významně pokročil. V této souvislosti nelze opomenout práci Purdona [2] probíhající v letech 1930–1950. Aktivací vysokopecní strusky zjistil, že alkalické hydroxidy mají ve směsi podobné chování jako katalyzátory. Po rozpuštění strusky a následné tvorbě hydrátů dochází i k částečnému obnovení původního alkalického aktivátoru, což bylo potvrzeno o mnoho let později na základě výzkumu s použitím moderních analytických metod. Dále pak nutno zmínit rozsáhlý výzkumný program Glukhovského [3], který probíhal v padesátých letech minulého století s cílem o velkoobjemou produkci těchto materiálů. V průběhu tohoto výzkumu se dospělo k závěru, že vznikající pojivové fáze AAM jsou velmi podobné jak fázím utvářející se v průběhu hydratace portlandského cementu (OPC), tak i přírodním horninám. Na základě těchto skutečností byla vysvětlena i vysokou trvanlivost těchto materiálů v okolním prostředí. Významnou popularizaci alkalicky aktivovaných materiálů přinesla práce Davidovitse [4] v sedmdesátých letech minulého století, který patentoval pojiva založená na alkalické aktivaci metakaolinu, pojmenoval je „geopolymery“ a dal těmto materiálům atraktivní historický podtext o možnostech jejich používání ve starém Egyptě při stavbě pyramid. K celosvětovému výzkumu alkalicky aktivovaných materiálů přispěla i odborná veřejnost v Československu a potažmo v České republice, zejména díky soustavné práci Brandštetra, Rovnaníkové, Škváry nebo Bílka (st.). V současné době se zabývá alkalickou aktivací mnoho výzkumných pracovišť po celém světě. Lze říci, že jejich společným cílem je rozsáhlejší využití těchto materiálů v praxi.

V dnešní době je bezesporu nejrozšířenějším stavebním pojivem portlandský cement. Můžeme se tedy ptát, proč se zabývat i jinými anorganickými pojivy jakými mohou být alkalicky aktivované materiály? Důležitost poznání nových materiálů souvisí především s objevením jejich potenciálních možností, které jsou v mnoha případech zcela zásadní v porovnání s konvenční cestou. Klíčovým důvodem, proč po více než 100 letech sporadického využití alkalicky aktivovaných materiálů o ně opět roste zájem, souvisí zejména s potenciálním snížením emisí CO<sub>2</sub>, které mají velmi pravděpodobně vliv na globální oteplování celé planety. Rovněž je zapotřebí zmínit, že většina alkalicky aktivovaných materiálů vychází z průmyslových odpadních a sekundárních surovin, což významně

přispívá k ochraně přírodních zdrojů. Potenciální výroba alkalicky aktivovaných materiálů je spojena i s nižší energetickou náročností v porovnání s produkcí portlandského cementu. Zmíněné souvislosti vedou k závěru, že i když portlandský cement bude ještě minimálně několik desetiletí naší nejrozšířenější maltovinou, pokroky aplikovaného výzkumu v oblasti alkalické aktivace vedlejších průmyslových produktů nenechávají na pochybách, že se AAM stanou jedním z ekologicky i ekonomicky významných materiálů 21. století.

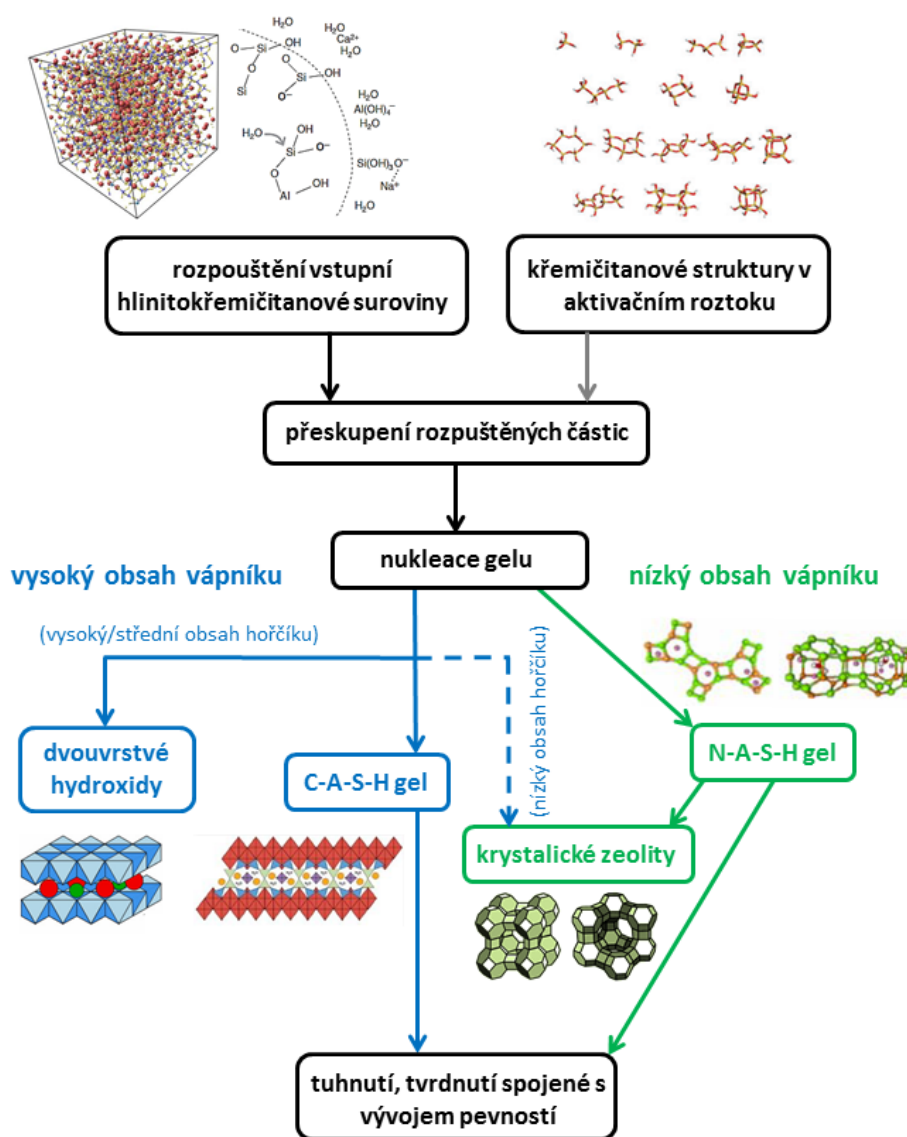
## 2. Alkalická aktivace: základní principy

Základním předpokladem alkalické aktivace je vždy schopnost docílit rozpuštění základní hlinitokřemičitanové suroviny v alkalickém prostředí. Rozpuštěné hlinitanové a křemičitanové fragmenty následně vzájemně polykondenzují a vytváří tak vždy specifický typ pojivové fáze. Proces rozpouštění je založen na rozkladu iontových nebo kovalentních vazeb. Vyšší stupeň vazeb s iontovým charakterem vede ke snadnější hydrataci materiálu ve vodě. Tento jev je typický například pro fáze portlandského cementu, kde křemičitanové a hlinitanové tetraedry přítomné v disktrétním stavu jsou obklopeny vápenatými ionty. V okamžiku kontaktu s vodou dochází k protonizaci Ca–O vazeb, což vede k autokatalytické destrukci příslušné fáze [5]. Odlišná situace nastává v případě, kdy má být rozpuštěna fáze obsahující vazby s nižším stupněm iontového charakteru. V této situaci iontová síla vody není dostačující pro rozklad kovalentních vazeb. Nicméně pokud roztok obsahuje ionty s charakterem donoru elektronů, jako jsou například ionty alkalických kovů, pH roztoku je zvýšeno, což umožní účinný rozklad příslušných vazeb, tedy rozpuštění vstupní suroviny. Hydrolytickou destrukci hlinitokřemičitanu lze popsat dle následujících reakcí [6]:



V počáteční fázi dochází k rozkladu kovalentních vazeb v alkalickém roztoku, ve kterém hrají hlavní roli  $\text{OH}^-$  ionty, ale i ionty alkalického kovu. Vyšší koncentrace alkalického roztoku podporuje průběh výše zmíněných reakcí zleva doprava. Rovnice 1–3 představují hydratační reakce, ve kterých anionty  $\text{OH}^-$  reagují s povrchem Al-Si prekurzoru za vzniku komplexních aniontů  $\text{Al(OH)}_4^-$ ,  $^-\text{OSi(OH)}_3$  a příslušných dvojmocných či trojmocných forem. Reakce 4–5 mají fyzikálně elektrostatický charakter, kde kation alkalického kovu vyvažuje záporný náboj

rozpuštěných částic. Poté následují kation-aniontové kondenzační interakce (reakce 6) založené na principu Coulombických sil, které vedou k tvorbě výsledné struktury. Dle výzkumu Glassera a Harveyho [7] nebyly prokázány kation-aniontové kondenzační interakce přímo mezi  $\text{Al}(\text{OH})_4^-$  tetraedry, což významně zpomaluje rozpouštění hliníku do roztoku. Z tohoto důvodu je přítomnost hlinitanových tetraedrů v pojivové fázi vždy nižší nežli křemičitanových. Reakce 4–6 naznačují, že kation alkalického kovu má nejen významný vliv na rozpouštění hlinitokřemičitanové fáze, ale i na utváření výsledné struktury pojivových fází. Mezi nejpoužívanější alkalické aktivátory patří sodné a draselné sloučeniny. I přesto, že  $\text{Na}^+$  a  $\text{K}^+$  mají stejný náboj, jejich účinek v roztoku je odlišný, především díky jejich rozdílné velikosti iontu. Bylo prokázáno, že kation-aniontové kondenzační interakce probíhají pomaleji s rostoucí velikostí kationtu. Z tohoto důvodu lze usoudit, že  $\text{Na}^+$  s menším iontovým poloměrem bude více aktivní v porovnání s  $\text{K}^+$ , což bylo ověřeno i vyšší rozpustností vstupních surovin [8].



Obr. 1: Proces alkalické aktivace hlinitokřemičitanových prekurzorů

Dle chemického složení vstupních surovin, lze rozdělit alkalicky aktivované materiály na dva základní typy; AAM s vysokým, nebo nízkým obsahem vápničku. Charakter vznikajících fází v procesu alkalické aktivace je schematicky zobrazen na Obr. 1. Je patrné, že alkalická aktivace surovin s vyšším obsahem vápničku (portlandský cement, vysokopecní struska) vede k vytvoření hlavní pojivové fáze C-A-S-H gelu, ve které může docházet k částečné náhradě chemicky vázaných  $\text{Ca}^{2+}$  za  $\text{Na}^+$  ionty. Bližší charakterizace této fáze, stejně tak i dalších hydratačních produktů vysokopecní strusky je shrnuta v kapitole 2.2.2. Alkalická aktivace nízko-vápenatých prekurzorů (jíly, elektrárenské popílky s nízkým obsahem vápničku, metakaolin) dává vzniknout zejména trojrozměrnému anorganickému N(K)-A-S-H gelu, někdy nazývanému též „geopolymer“, který může rovněž sloužit jako vhodný prekurzor pro vznik zeolitických struktur.

## 2.2 Alkalická aktivace vysokopecní strusky

Princip hydratace portlandského cementu je poměrně dobře zmapován. Přesto však dochází i nadále k zpřesnění popisu jednotlivých dějů během hydratace slínkových fází a to zejména díky vývoji a modernizaci nových analytických metod [9]. Systém alkalicky aktivované vysokopecní strusky (AAS) se zdá být ještě mnohem komplikovanější. Záleží totiž na více faktorech, které mohou zásadním způsobem ovlivnit proces alkalické aktivace. Následující kapitoly proto shrnují dosavadní poznatky týkající se průběhu hydratace a tvorby hydratačních produktů související s charakterem mikrostruktury AAS.

### 2.2.1 Faktory ovlivňující proces alkalické aktivace vysokopecní strusky

#### Vliv chemických a fyzikálních vlastností vysokopecní strusky

Pokud se zaměříme na samotné složení strusky, můžeme s jistotou říct, že důležitou vlastností strusky z pohledu alkalické aktivace je obsah amorfní fáze. Dobře zchlazená struska neobsahuje žádné krystality. Chemické složení této strusky je definováno systémem  $\text{CaO-SiO}_2\text{-MgO-Al}_2\text{O}_3$  a je popsáno jako směs amorfních fází o složení podobné gehlenitu ( $2\text{CaO}\cdot\text{Al}_2\text{O}_3\cdot\text{SiO}_2$ ) a akermanitu ( $2\text{CaO}\cdot\text{MgO}\cdot 2\text{SiO}_2$ ). Obsah amorfní fáze lze odhadnout pomocí tzv. stupně depolymerace ( $DP$ ), který definuje poměr „volného“ vápničku a křemíku. Pokud předpokládáme, že veškerý hořčík je přítomný v krystalické fázi akermanitu a hliník v gehlenitu můžeme  $DP$  vypočítat následovně:

$$DP = \frac{n(\text{CaO}) - 2n(\text{MgO}) - n(\text{Al}_2\text{O}_3) - n(\text{SO}_3)}{n(\text{SiO}_2) - 2n(\text{MgO}) - 0,5n(\text{Al}_2\text{O}_3)} \quad (1)$$

Tento poměr je obvykle pro granulovanou vysokopecní strusku v rozmezí 1,3–1,5. Vyšší hodnota signalizuje více depolymerovaný, tedy víc reaktivní systém [10].

Je rovněž velmi dobře známo, že reaktivita vysokopecní strusky stoupá s klesající velikostí zrn strusky. V silně alkalickém prostředí je rozpouštění částic nad 20  $\mu\text{m}$  podstatně nižší v porovnání s částicemi s velikostí pod 2  $\mu\text{m}$ , která jsou kompletně zreagovány již do 24 hodin od aktivace [11,12]. Někteří autoři rovněž dávají do souvislosti měrný povrch dle Blainea s dlouhodobými pevnostmi AAS. Talling a Brandštetr [13] došli k závěru, že optimální měrný povrch pro alkalickou aktivaci vysokopecní strusky je kolem 4 000  $\text{cm}^2/\text{g}$ .

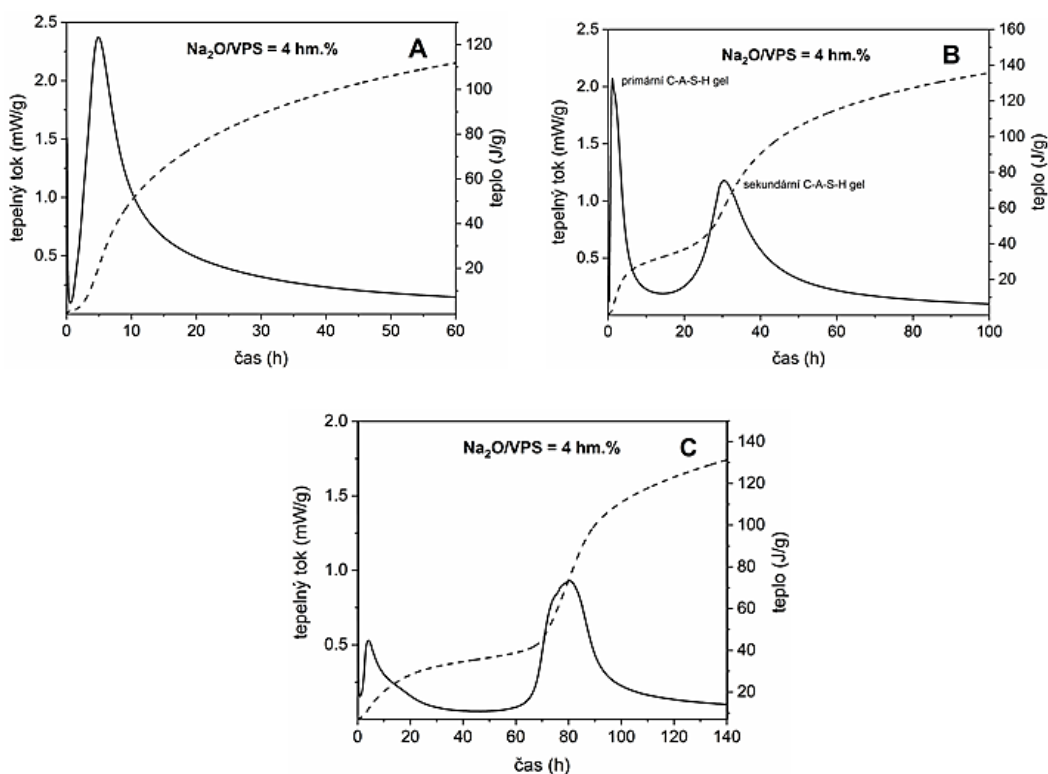
Některé práce se zabývaly i zkoušením vyšších měrných povrchů, což vždy pozitivně ovlivnilo pevnosti AAS [14,15].

### Vliv koncentrace a vybraného druhu alkalického aktivátoru

Druh použitého aktivátoru předurčuje, jakým reakčním mechanismem bude alkalická aktivace probíhat. Dle tvaru křivek z isothermální kalorimetrie popsali Shi a Day [16] průběh alkalické aktivace s použitím nejběžnějších alkalických aktivátorů, jakými jsou hydroxid, křemičitan a uhličitan alkalického kovu. Nicméně první pokusy se týkaly pouhého smíchání vysokopecní strusky s **vodou** bez přítomnosti alkalického aktivátoru. V tomto případě dochází k narušení vazeb Si–O, Al–O, Ca–O a Mg–O na povrchu zrn strusky v důsledku polarizačního efektu  $\text{OH}^-$  iontů [17]. Jelikož mají vazby Ca–O a Mg–O mnohem nižší energii, než vazby Si–O a Al–O, koncentrace  $\text{Ca}^{2+}$  a  $\text{Mg}^{2+}$  iontů v roztoku je mnohem vyšší, než koncentrace křemičitanových a hlinitanových aniontů a na povrchu zrn strusky začíná vznikat vrstva bohatá na křemík a hliník [18]. Tato vrstva má schopnost adsorbovat  $\text{H}^+$ , což způsobuje zvýšení koncentrace  $\text{OH}^-$  iontů v roztoku. Nicméně bez přítomnosti alkalického aktivátoru není koncentrace  $\text{OH}^-$  iontů dostačující k narušení většího množství vazeb Si–O a Al–O, nezbytné pro vyšší tvorbu hydratačních produktů. Kalorimetrická křivka v tomto případě vykazuje pouze jedno, velmi slabé maximum, které odpovídá smáčení strusky, částečnému rozpuštění povrchu zrn a adsorpci iontů na povrch částic strusky.

V přítomnosti **hydroxidu alkalického kovu** je počáteční pík mnohem výraznější, než v předchozím případě. Vysoké pH roztoku má za následek rozrušení velkého množství vazeb Si–O a Al–O. Na povrchu zrn strusky začne ihned vznikat vrstva hydratačních produktů [19]. Jelikož  $\text{Ca}(\text{OH})_2$  má vyšší rozpustnost nežli C-S-H respektive C-A-S-H gel, budou přednostně právě tyto pojivové fáze velmi rychle precipitovat z roztoku. V případě, že struska obsahuje velké množství hořčíku, je velmi pravděpodobná i tvorba hydrotalcitu ( $\text{Mg}_6\text{Al}_2\text{CO}_3(\text{OH})_{16}\cdot 4\text{H}_2\text{O}$ ). Kalorimetrická křivka v tomto případě vykazuje dvě maxima. První maximum (v prvních minutách od aktivace), velmi dobře měřitelné s použitím tzv. AdMix ampulí [20], odpovídá smáčení a rozpouštění zrn strusky. Daleko výraznější vývoj tepla je následně pozorován po několika desítkách minut až hodin od zamíchání, což odpovídá tvorbě již zmíněných pojivových fází (Obr. 2A).

Alkalická aktivace strusky pomocí **vodního skla** vykazuje odlišný hydratační mechanismus (Obr. 2B). Začátek hydratačního procesu zahrnuje stejné děje jak v předchozím případě. Nicméně díky vysoké koncentraci  $(\text{SiO}_4)^{4-}$  iontů, přítomných v roztoku po přidání vodního skla a rozpouštěním strusky, dochází velmi brzo k vytvoření tzv. „primárního“ C-A-S-H gelu. V některých případech lze pozorovat i zdvojení příslušného hydratačního maxima, což lze vysvětlit následovně. Roztok vodního skla má zpravidla nižší pH v porovnání s hydroxidem, tedy koncentrace  $\text{Ca}^{2+}$  iontů z rozpuštěné strusky nebude v roztoku tak vysoká. V prvním kroku je tedy vytvořeno určité množství pojivové fáze. Jakmile však dojde k vyčerpání  $\text{Ca}^{2+}$  iontů, křemičitanové ionty se mohou polymerizovat a dochází tak k uvolnění dalšího hydratačního tepla. Poté nastává „indukční perioda“, která může trvat i několik hodin. V tomto čase dochází k opětovnému a postupnému rozpouštění částic strusky. V okamžiku, kdy je pórový roztok přesycen rozpuštěnými ionty, dochází ke vzniku tzv. „sekundárního“ C-A-S-H gelu [16].



**Obr. 2: Kalorimetrické křivky hydratačního procesu AAS s použitím různého druhu alkalického aktivátoru: roztok hydroxidu sodného (A); roztok sodného vodního skla (B); roztok uhličitanu sodného (C); převzato z DP Langová (školitel: Kalina L.) [21]**

Hydratační průběh alkalické aktivace s využitím **uhličitanu alkalického kovu** (Obr. 2C) má velmi podobný průběh jako v případě aktivace vodním sklem. Nutno však zmínit, že nižší pH roztoku uhličitanu povede k nižšímu vývoji hydratačního tepla v porovnání s aktivací vodním sklem. Charakter vznikajících produktů je rovněž odlišný. Díky vysoké koncentraci uhličitanových aniontů dochází v předindukční periodě především k jejich reakci s rozpuštěnými  $\text{Ca}^{2+}$  ionty a následné tvorby podvojného uhličitanu, gaylussitu ( $\text{Na}_2\text{Ca}(\text{CO}_3)_2 \cdot 5\text{H}_2\text{O}$ ), za předpokladu aktivace sodným uhličitanem. Roztok je tak ochuzen o vápenaté ionty, což podmiňuje vývoj zeolitických struktur z rozpuštěných křemičitanových a hlinitanových jednotek. Během indukční periody pokračuje rozpouštění strusky, fáze gaylussitu se mění na  $\text{CaCO}_3$  za současného uvolnění  $\text{Na}^+$  iontů podporující opět tvorbu zeolitů. Poslední hydratační maximum je stejně jako v případě aktivace vodním sklem přiřazeno vývoji C-A-S-H gelu, jehož precipitace je výrazně podpořena snížením koncentrace uhličitanových aniontů v roztoku [22].

Obecně lze říci, že hydratační teplo v průběhu alkalické aktivace vysokopecní strusky roste s přidáním alkalického aktivátoru. Výrazný vliv byl pozorován v případě aktivace vodním sklem. Vyšší koncentrace alkalického kovu vede ke zkrácení indukční periody a zároveň k významnému nárůstu hydratačního tepla zejména během prvních 24 hodin související s vyšší tvorbou pojivové fáze, což vede k pozitivnímu ovlivnění mechanických vlastností připravovaných materiálů [19]. Aktivace vodním sklem je ovlivněna i silikátovým modulem použitého vodního skla, kdy nižší moduly spíše zpomalují hydratační procesy [23].

Další faktor, který byl již zmíněn a má velký vliv na vlastnosti AAS, je druh používaného aktivátoru z hlediska příslušného alkalického kovu. Kationty  $\text{Na}^+$  a  $\text{K}^+$  mají rozdílný iontový poloměr, proto lze očekávat i odlišné chování v průběhu alkalické aktivace. Kation s menší velikostí ( $\text{Na}^+$ ) podporuje tvorbu malých silikátových oligomerů, jako například silikátové monomery, dimery a trimery. Proto můžeme očekávat, že sodné aktivátory budou v reakcích více aktivní než draselné, což vede k lepšímu rozpuštění základního hlinitokřemičitanu. Tuto teorii potvrdili ve své studii Xu a van Deventer [8], kteří zkoumali chování přírodních aluminosilikátů aktivovaných buď  $\text{NaOH}$ , nebo  $\text{KOH}$ . Výsledky ukázaly, že všechny alkalicky aktivované materiály vykazovaly větší pevnosti při použití  $\text{KOH}$  aktivátoru, navzdory tomu, že se základní suroviny rozpouštěly lépe při užití  $\text{NaOH}$ . Tuto skutečnost vysvětlil Phair a van Deventer [24] následovně; jelikož  $\text{K}^+$  kationy mají menší solvatační obal než  $\text{Na}^+$ , dochází k reakcím, které vytvářejí těsnější a hustší zesílení vedoucí k celkově větší pevnosti alkalicky aktivované matrice.

Použitý druh alkalického aktivátoru má rovněž vliv na tvorbu výkvětů. Na základě MAS NMR spektroskopie bylo prokázáno, že se alkalické ionty v alkalicky aktivovaných strukturách vyskytují ve formě  $\text{Na},\text{K}(\text{H}_2\text{O})_n^+$  [25]. Začlenění  $\text{Na},\text{K}(\text{H}_2\text{O})_n^+$  ve struktuře materiálu je slabší nežli za situace, kdyby se alkalické kovy vyskytovaly ve formě samostatných  $\text{Na}^+$  a  $\text{K}^+$  iontů, což usnadňuje jejich migraci na povrch vzorku a tím tvorbu výkvětů. Výkvětům lze předcházet záměnou sodného za draselný alkalický aktivátor. Draselné ionty jsou totiž hůře vyluhovatelné ze struktury [26], navíc reakce se vzdušným  $\text{CO}_2$  dává vznik  $\text{K}_2\text{CO}_3$ , který nevytváří viditelné hydráty. Rozpustnost  $\text{K}_2\text{CO}_3$ , který se tvoří na povrchu alkalicky aktivovaného materiálu je vyšší než u  $\text{Na}_2\text{CO}_3 \cdot n\text{H}_2\text{O}$ , proto v kontaktu s vodním prostředím se rozpouští prakticky bez tvorby viditelných výkvětů [27].

### Vliv vodního součinitele

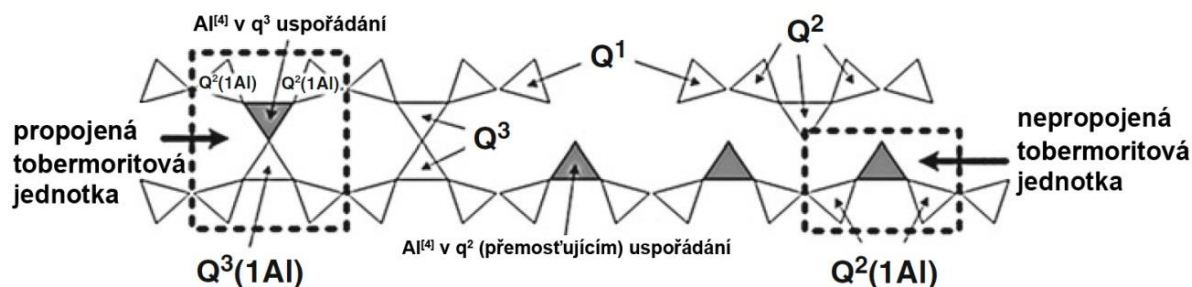
Je velmi dobře známo, že vodní součinitel má podstatný vliv na vlastnosti cementových pojiv. Stejně tak je tomu i v případě alkalicky aktivovaných materiálů. Nicméně vstup další proměnné, v podobě různého druhu použitého alkalického aktivátoru se stává opět velmi klíčovým faktorem. Nižší hodnota vodního součinitele způsobuje vyšší nárůst hydratačního tepla spojeného s vývojem pojivových fází. Toto pravidlo platí rovněž i pro systém aktivovaný vodním sklem, zároveň však dochází vlivem nižšího vodního součinitele k podstatnému urychlení hydratace a to až o několik hodin [28]. Výrazné změny hydratačního procesu souvisí především s distribucí křemičitanových aniontů, která je ovlivněna několika faktory (křemičitý modul, teplota, pH ...) [19].

### Vliv teploty

Nárůst teploty, při které je vzorek vytvrzován vykazuje velmi podobný vliv na hydrataci AAS, jako je tomu v případě nárůstu koncentrace aktivátoru. Vyšší teplota, při které probíhá alkalická aktivace, vede k uvolnění vyššího hydratačního tepla související s tvorbou pojivových fází [29].

## 2.2.2 Hydratační produkty

Dosavadní studie se shodují na tom, že hlavním hydratačním produktem alkalicky aktivované strusky je hliníkem částečně substituovaný C-S-H gel [30-32]. Určité množství chemicky vázaných  $\text{Ca}^{2+}$  může být také nahrazeno ionty alkalického kovu. Přítomnost hlinitanového tetraedru a kationtu alkalického kovu (např.  $\text{Na}^+$ ) v gelu vede k jeho označování zkratkou C-A-S-H nebo C-(N)-A-S-H fáze, aby byl zřetelně odlišen od hydratačních produktů portlandského cementu. Obecně platí, že se snižujícím se poměrem Ca/Si v pojivové fázi roste schopnost gelu vázat ostatní alkalické ionty, což bylo potvrzeno i výzkumem **Kaliny a kol.** [33]. Geometrie křemičitanových řetězců limituje množství hlinitanových jednotek, které je C-S-H gel schopný pojmout. Maximální poměr Al/Si byl stanoven na 0,20 [34]. Struktura C-A-S-H gelu je podobná struktuře neuspořádaného tobermoritu. Vysoká míra neuspořádanosti na delší vzdálenosti způsobuje, že se při identifikaci tradičními krystalografickými technikami gel jeví jako převážně amorfní [35]. Tvorba gelu alkalicky aktivované vysokopeční strusky vychází z modelu navrženého Myersem [36], ve kterém se hlinitanové tetraedry včleňují do struktury a nahrazují tak křemičitanové „přemostující“ tetraedry, což vede k prodloužení lineárních řetězců a k možnému nahodilému meziřetězcovému zesílení skrze Si–O–Al vazby (Obr. 3). Množství  $\text{Q}^3$  jednotek a tedy stupeň propojení je relativně nízký při aktivaci roztokem hydroxidů, zatímco při použití vodního skla výrazně vzrůstá [32].



Obr. 3: Schematické znázornění propojených a nepropojených tobermoritových struktur, které reprezentují obecnou strukturu C-(N)-A-S-H gelu, převzato z [36]

Alkalickou aktivací strusky vznikají kromě C-(N)-A-S-H gelu také sekundární produkty. Jejich tvorba a charakter je silně ovlivněn řadou faktorů, které již byly diskutovány v předchozí kapitole. Nicméně v obecné rovině lze na minoritní hydratační produkty AAS uplatnit několik následujících všeobecných zákonitostí:

- Stupeň substituce hlinitanového tetraedru do struktury C-S-H gelu je, jak již bylo zmíněno, omezený. Z termodynamického hlediska je navíc přítomnost vazby Al–O–Al v gelu zcela vyloučena [36,37]. Z toho vyplývá, že sekundární produkty alkalické aktivace budou bohaté na hliník.
- Substituce hořčíku do pojivové fáze je rovněž omezena. Z tohoto důvodu se velmi často v systémech AAS nachází fáze hydrotalcitu. Při alkalické aktivaci vysokopeční strusky s nízkým množstvím hořčíku je velmi pravděpodobná tvorba zeolitických struktur namísto tvorby hydrotalcitu [38].

- AFm fáze, jako například strätlingit ( $\text{Ca}_2\text{Al}_2\text{SiO}_7 \cdot 8\text{H}_2\text{O}$ ), vykazují v prvních fázích alkalické aktivace silnou neuspořádanost. Krystalizují až v dlouhodobých stádiích hydratace [39].
- N-A-S-H gel je rovněž minoritním sekundárním produktem AAS. Jeho obsah stoupá s využitím příměsí, s nízkým obsahem vápníku, jako jsou vysokoteplotní popílky [40] nebo metakaolin [41].
- Přítomnost aluminátových hydrátů ( $\text{C}_4\text{AH}_{13}$ ,  $\text{C}_2\text{AH}_8$ ) ovlivňuje především složení vstupní suroviny. V alkalické aktivaci strusek bohatých na hořčík může Mg nahradit v hydrátech Ca za vzniku  $\text{M}_4\text{AH}_{13}$  [28].
- Stejně tak typ aktivátoru rozhoduje o vzniku minoritních hydratačních produktů. Strusky aktivované sírany vykazují přítomnost AFt fáze (ettringit) [42], zatímco aktivace uhličitany dávají vznik karbonátovým hydrátům AFm [19].

### 2.2.3 Aplikační potenciál

AAM založené na aktivaci vysokopecní strusky byly využívány ve stavebním průmyslu již od roku 1950 v bývalém Sovětském svazu, Číně, ale i v jiných státech světa. Zejména na území dnešní Ukrajiny bylo v minulosti přikročeno k produkci alkalicky aktivovaných prefabrikátů zahrnující drenážní trubky, silážní panely nebo betonové prvky zpevňující železniční násypy. Od produkce těchto jednoduchých výrobků bylo v roce 1988 následně přistoupeno k výrobě předpjatých železničních pražců a výstavbě 24-podlažní budovy v Lipetsku (Obr. 4A), která byla dokončena v roce 1994. Všechny zmíněné výrobky a stavby byly důkladně testovány v různých časových obdobích. Bylo zjištěno, že betony na bázi AAM překračují možnosti běžně používaných betonů na bázi portlandského cementu. Aplikace AAM se v minulém století rozvíjela i v ostatních státech. V roce 1974 bylo v polském Krakově postaveno skladiště z prefabrikovaných železobetonových panelů. Dále byly vyráběny například betonové pražce (Španělsko a Japonsko, 1980), střešní krytina (Finsko, 1988) nebo mostní prvky a chodníky (Austrálie, 2006) [28]. V Austrálii byl v roce 2014 proveden jeden z nejrozsáhlejších projektů výroby alkalicky aktivovaného betonu z vysokopecní strusky, kde letištní runway West Wellcamp Brisbane byla vystavěna s použitím betonových panelů o objemu přibližně 40 000 m<sup>3</sup> (Obr. 4C) [43].

Od roku 2003 byly v České republice rovněž zahájeny poloprovozní zkoušky s cílem produkovat beton na bázi alkalicky aktivovaného elektrárenského popílku. Tento beton, který byl pojmenován POPbeton<sup>®</sup> [44], vznikl ve spolupráci mezi Ústavem skla a keramiky VŠCHT a Katedrou technologie staveb ČVUT v Praze. V roce 2016 byl patentován naším výzkumným týmem na FCH VUT Brno způsob výroby alkalicky aktivovaných materiálů s použitím odpadních produktů z výroby vodního skla [45]. Především díky nahrazení finančně nákladných alkalických aktivátorů odpadními surovinami byl tento patent následně komercializován a prostřednictvím spolupráce s ŽPSV a.s. byly v poloprovozních podmínkách vyrobeny betonové prvky dělicích stěn sloužící jako silniční záchytné systémy (Obr. 4B) [46,47]. AAM skýtají možnost využití i pro speciální aplikace jakými jsou například lehčené materiály, materiály pro vysokoteplotní aplikace, vláknobetony, stejně tak i pro stabilizaci/solidifikaci nebezpečných a radioaktivních materiálů. Produkce zmíněných AAM vždy spojuje kombinace vhodného pojiva, kameniva a přísad, které výrazně ovlivňují požadované vlastnosti produkovaných materiálů.



**Obr. 4: Příklady aplikace alkalicky aktivované vysokopecní strusky. 24-podlažní budova v Lipetsku (A); betonová svodidla v ŽPSV a.s. (B); letištní runway West Wellcamp Brisbane (C)**

## Shrnutí

Krátký úvod k těmto netradičním materiálům poskytuje čtenáři přehled o základních principech alkalické aktivace a možnostech jejich využití v produkci stavebních materiálů. V současné době tato pojiva přitahují velkou pozornost jak z hlediska technického, tak i environmentálního významu. Stále však zůstává řada nedořešených souvislostí týkající se zejména reakčních principů a trvanlivosti, které je třeba pochopit natolik, aby zmíněné materiály dostaly svým propagovaným vlastnostem. Tento vytyčený cíl lze dosáhnout především multioborovým výzkumem zahrnující znalosti z fyziky, chemie, materiálních věd a stavebního inženýrství. Každý obor přináší jiný pohled na danou problematiku, což vede k velmi účinnému řešení klíčových otázek. Alkalicky aktivované materiály byly a jsou předmětem zájmu mnoha výzkumných institucí, nicméně stále zbývá odhalit mnoho nových poznatků, které pomohou těmto materiálům na trnité cestě od výzkumu k praktické aplikaci.

### 3. Chemické přísady: proč, co a jak?

#### Proč?

V posledních desetiletích bylo dosaženo obrovského úspěchu s použitím chemických přísad pro výrobu betonových produktů. Správné použití přísad totiž nabízí příznivé účinky na beton, ať už se jedná o vyšší trvanlivost, zlepšenou zpracovatelnost, ale i kontrolu nad tuhnutím celého systému. Vlastnosti finálního produktu lze tak s využitím přísad modifikovat pro konkrétní účel použití, což vede v konečném důsledku ke snížení celkových finančních nákladů. V dnešní době tak bezesporu chemické přísady hrají hlavní roli v moderních betonových materiálech a technologiích. Chemické přísady obecně zlepšují jak výše uvedené vlastnosti betonu tak napomáhají vývoji novým betonovým technologiím, jako jsou například čerpané a samonivelační betony, betonáže pod vodou, či možnosti využití stříkaných betonů.

#### Co?

Myšlenka přidávání chemických látek o malé koncentraci s potenciálem významně ovlivnit vlastnosti stavebních materiálů není žádnou novinkou. Již staří Římané a Egypťané několik stovek let před Kristem popsali účinek organických materiálů, jako například volská krev, vejce nebo ovocné šťávy, na vlastnosti produkovaných malt a betonů tehdejšího typu [48,49]. Moderní přísady jsou spíše na bázi syntetických molekul a polymerů vyráběných speciálně pro betonářský průmysl. Rozdělení přísad do jednotlivých skupin však v celosvětovém měřítku přináší více zmatku než objasnění, což je spojeno především s faktem, že dlouhou dobu byly používány přísady na bázi odpadních průmyslových produktů s více než jedním konkrétním účinkem na čerstvý či ztuhlý beton. K velmi logickému členění přísad však bylo přistoupeno v případě ČR. Přísady jsou vždy zařazeny do příslušných skupin souvisejících s jejich konkrétním modifikačním účinkem na betonovou záměs:

- vodoredukující/plastifikační
- silně vodoredukující/superplastifikační
- stabilizační
- provzdušňovací
- urychlující tuhnutí a tvrdnutí
- zpomalující tuhnutí
- těsnící
- ostatní (injektažní, inhibitory koroze, biocidní, plynotvorné, pěnotvorné, adhezivní)

#### Jak?

Přísady jsou definovány jako zcela jiný materiál než cement, voda nebo kamenivo. Používají se jako složka betonu, která se přidává do betonové záměsi bezprostředně před nebo během míchání. Jejich dávkování je velmi malé a pohybuje se nejčastěji v rozmezí od 0,005 do 2 hm. % na celkovou hmotnost složek tvořících cementové pojivo. Celkové množství přísady však nesmí překročit 5 hm. % [50]. V mnoha případech je přísada přidávána do betonu i v tekuté formě. Pokud však její množství převyšuje 3 l/m<sup>3</sup> betonu, musí být brána v úvahu i voda přítomná v přísadě a následně započtena do vodního součinitele [51]. V situaci, kdy je použita více než jedna přísada, je rovněž velmi důležité ověřit jejich vzájemnou koexistenci v systému. V některých případech se totiž různé typy přísad mohou vzájemně negativně ovlivňovat. Naproti tomu existuje i celá řada příkladů, kdy jednotlivé přísady vykazují vzájemně synergické účinky.

## Chemické přísady v AAS

Předtím, nežli budou v následujících kapitolách diskutovány přísady v AAS, je nezbytné nejdříve krátce definovat samotný pojem "přísada" z pohledu alkalické aktivace. Měli bychom vzít totiž na vědomí, že mnoho sloučenin, které patří mezi nezbytné složky při tvorbě alkalicky aktivovaných materiálů, jsou běžně definovány jako přísady, či příměsi v systémech na bázi portlandského cementu. V kontextu alkalické aktivace tedy není samotný alkalický aktivátor, či snad aktivovaný hliníkokřemičitan považován za přísadu, protože vytváří pojivo jako takové. Obecně lze říci, že účinek organických a anorganických přísad (používaných pro běžné cementy) na chování a vlastnosti alkalicky aktivovaných materiálů dosud nebyl v dosavadním výzkumu příliš popsán. Krom toho je třeba zmínit i publikování naprosto protichůdných výsledků popisující účinky konkrétní přísady, což souvisí zejména s použitím různých typů alkalicky aktivovaných materiálů. Je více než pravděpodobné, že chování použité přísady bude ovlivněno několika faktory: tj. typem hliníkokřemičitanu, který je aktivován (struska, popílek, metakaolin ...), ale i koncentrací, přídatkem a druhem alkalického aktivátoru. Co však dosavadní studie jednoznačně prokázaly, je většinou naprosto odlišné chování přísad v alkalicky aktivovaném materiálu v porovnání s jejich účinkem v systému na bázi portlandského cementu. Řada prací se zabývala i vysvětlením těchto odlišností, nicméně i tak je v této oblasti potřeba dalšího výzkumu [52]. Následující kapitoly proto shrnují dosavadní poznatky výzkumu týkající se působení různých typů chemických přísad v AAS. Jsou diskutovány skupiny přísad, které mohou významně zlepšit vlastnosti AAS a současně je popsán i vliv přísad přispívající ke zmírnění negativních jevů spojených s produkcí těchto netradičních materiálů.

Z pohledu využití různých druhů chemických přísad v AAS však stále existuje řada obecných souvislostí a otázek, které by měly být v budoucích výzkumech řešeny:

- Většina přísad je navržena pro cementové systémy, ve kterých hodnota pH pórového roztoku je nižší nežli v AAS. Některé přísady se tak ve vysokém alkalickém prostředí rozkládají, například reakčním mechanismem alkalické hydrolýzy, a ztrácí tak svůj původní účinek. Obecné principy týkající se vlivu silně zásaditého prostředí na chemickou strukturu přísady by měly být v budoucnu diskutovány s cílem napovědět potenciálnímu uživateli, zda je vhodné přísadu použít, či nikoli.
- V cementových systémech se velmi často využívá synergických efektů některých různých druhů chemických přísad. Navzdory tomuto se v současnosti jen velmi málo výzkumných prací zabývá kombinací jednotlivých přísad v AAS.
- Pokud je přísada přidávána v tekuté formě do záměsi AAS, má být voda v přísadě započtena do vodního součinitele? Je totiž velmi dobře známo, že i velmi malá změna ve vodním součiniteli může výrazně ovlivnit vlastnosti alkalicky aktivované záměsi.
- Systémy na bázi AAS jsou bezesporu díky různým možným typům alkalických aktivátorů mnohem komplexnější v porovnání s materiály na bázi portlandského cementu. Sjednocení a popis účinku jednotlivých přísad v závislosti na použitém aktivátoru představuje do budoucna další důležitý krok k pochopení reakčního mechanismu přísad v AAS.

## 3.1 Organické přísady

### Úvod do problematiky organických povrchově aktivních látek

Povrchově aktivní látky, známé jako surfaktanty, představují v cementových systémech skupinu chemických přísad s širokým a dnes již zcela nenahraditelným použitím. Obecně je lze nazvat jako interaktivní přísady spojené vždy s mezifázovým rozhraním kapalina-vzduch, nebo pevná látka-kapalina, kde dochází k jejich orientaci a adsorpci. Je tak všeobecně známo, že typickými povrchově aktivními přísadami v technologii silikátových pojiv jsou provzdušňovací přísady, plastifikátory, ale i přísady redukující smrštění. Pro pochopení mechanismu jejich působení je proto nezbytné představit jejich samotnou koncepci. Základním znakem těchto přísad je jejich amfifilní charakter sestávající se z hydrofobní části (většinou dlouhý alkylový řetězec) a hydrofilní hlavy. V případě, že je taková molekula obsažena ve vodném prostředí, hydrofobní část má vždy snahu minimalizovat kontakt s rozpouštědlem [53]. Na základě povahy hydrofilní hlavy můžeme povrchově aktivní látky rozdělit do následujících skupin:

- aniontové
- kationtové
- amfoterní
- neionogenní

Důležitým parametrem, který určuje charakter povrchově aktivních látek je tzv. hydrofilně-lipofilní rovnováha (HLB). Hodnota HLB charakterizuje poměr vlivu hydrofilní a lipofilní části molekuly surfaktantu na její vlastnosti. Vysoké hodnoty HLB mají hydrofilní surfaktanty s velkou rozpustností ve vodě, naopak nízké hodnoty HLB jsou typické pro sloučeniny ve vodě málo rozpustné. Hodnoty HLB mohou být počítány dle různých empirických vzorců, nejčastěji je však používán vztah (2) založený na příspěvcích jednotlivých skupin v molekule, kde parametr  $k$  představuje individuální hydrofilní a lipofilní skupiny, člen  $i$  množství skupin  $k$  a  $GN$  číselnou hodnotu skupiny určenou dle Daviese [54].

$$HLB = \frac{\sum_{k=0}^n (i_k GN_k)}{2} \quad (2)$$

Chování povrchově aktivních látek v různých prostředích lze odhadnout i z charakteru hydrofobní části [49].

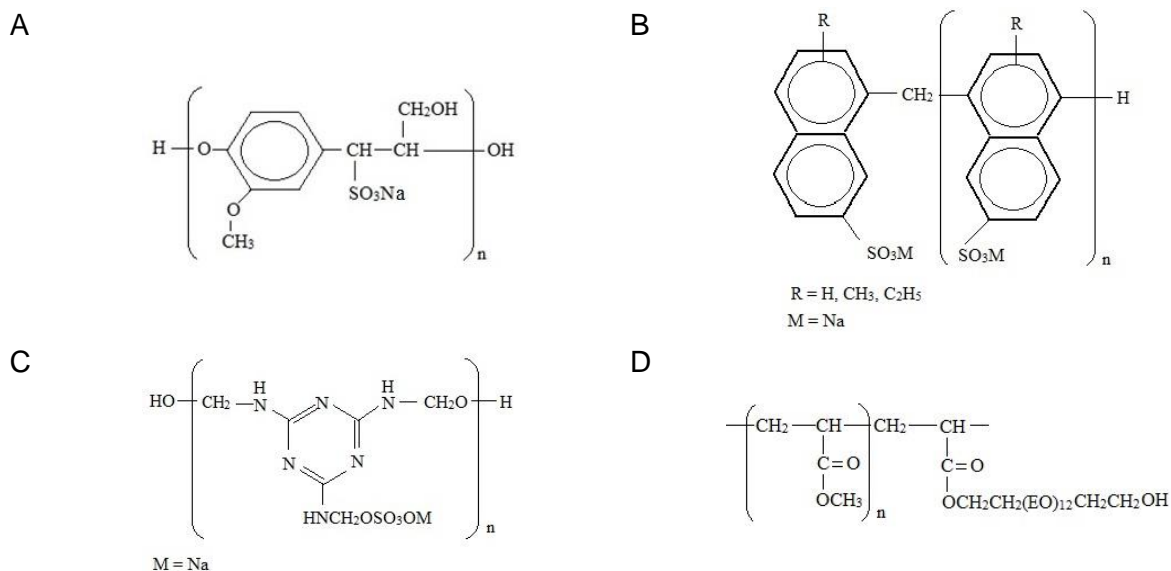
- dlouhý hydrofobní řetězec
  - snížená rozpustnost ve vodě, zvýšená v organických rozpouštědlech
  - těsnější uspořádání molekul na mezifázovém rozhraní
  - vyšší možnost precipitace částic s opačným nábojem v případě iontových surfaktantů
- rozvětvený řetězec a přítomnost nenasycených vazeb
  - vyšší rozpustnost ve vodě v porovnání s přísadou s lineárním řetězcem nebo řetězcem obsahující nasycené vazby
  - nižší tendence k vzájemnému sdružování
- přítomnost aromatických jader
  - vyšší adsorpce surfaktantu na pozitivně nabitý povrch
  - volnější uspořádání molekul na mezifázovém rozhraní

### 3.1.1 Plastifikační přísady

Plastifikační přísady jsou polymerní látky, které patří bezesporu k nejdůležitějším chemickým přísadám. Přidávají se do betonu pro zlepšení jeho zpracovatelnosti, stejně tak pro snížení množství záměsové vody. Takto lze dosáhnout lepších vlastností ztvrdlého betonu, konkrétně pevnosti a trvanlivosti. Snížení obsahu záměsové vody je dáno evropskou normou EN 934-2 [50] a musí být nejméně 5 % při nárůstu 28-denní pevnosti v tlaku betonu o 10 %. Tyto přísady lze použít i takovým způsobem, že kromě vody je možné snížit i obsah cementu v betonu při zachování původního vodního součinitele, zpracovatelnosti a pevnosti v porovnání s betonem bez přísady. Kromě úspory cementu je dalším přínosem i snížení hydratačního tepla. Povrchově aktivní látky, které snižují obsah záměsové vody minimálně o 10 % oproti kontrolnímu betonu se stejnou zpracovatelností se dnes nazývají superplastifikátory. Norma EN 934-2 [50] rovněž ukládá pevnost v tlaku superplastifikovaného betonu vyšší nejméně o 40 % po dvou dnech a o 15 % po 28 dnech oproti kontrolnímu betonu [55].

Na trhu se vyskytovalo v uplynulých letech značné množství plastifikačních přísad. Ve většině případů jsou připraveny v podobě vodných roztoků, jejichž hustoty se pohybují v rozmezí 1,10 až 1,15 g/cm<sup>3</sup> a koncentrace účinných složek 35 až 40 %. Dnes rozdělujeme plastifikační přísady podle jejich struktury na 4 základní typy (Obr. 5) [56]:

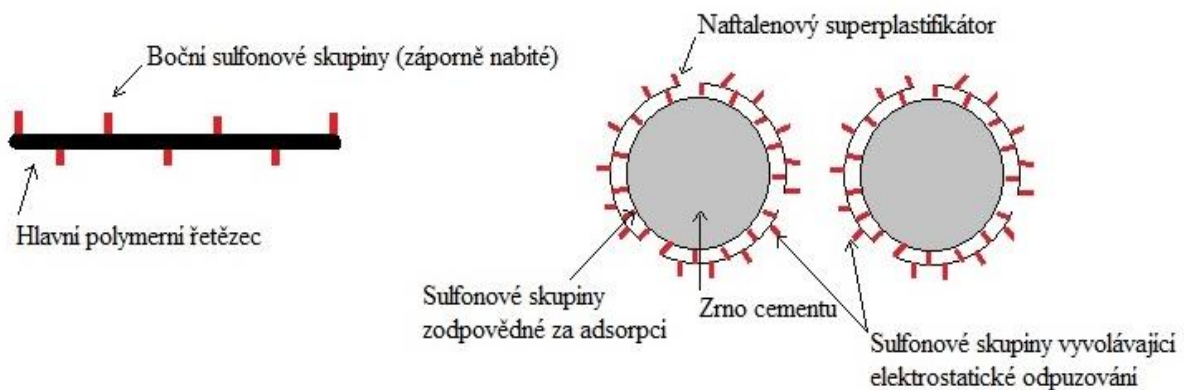
- sulfonované soli polykondenzátů naftalenu a formaldehydu, obvykle označované jako sulfonáty polynaftalenů, nebo jednoduše naftalenové superplastifikátory
- sulfonované soli polykondenzátů melaminu a formaldehydu, obvykle označované jako sulfonáty polymelaminu, tedy melaminové superplastifikátory
- lignosulfonáty s velmi nízkým obsahem sacharidů a povrchově aktivních činidel
- polyakryláty (polykarboxyláty)



Obr. 5: Chemické struktury plastifikačních přísad na bázi lignosulfonátu (A); polynaftalenů (B); polymelaminu (C) a polykarboxylátu (D)

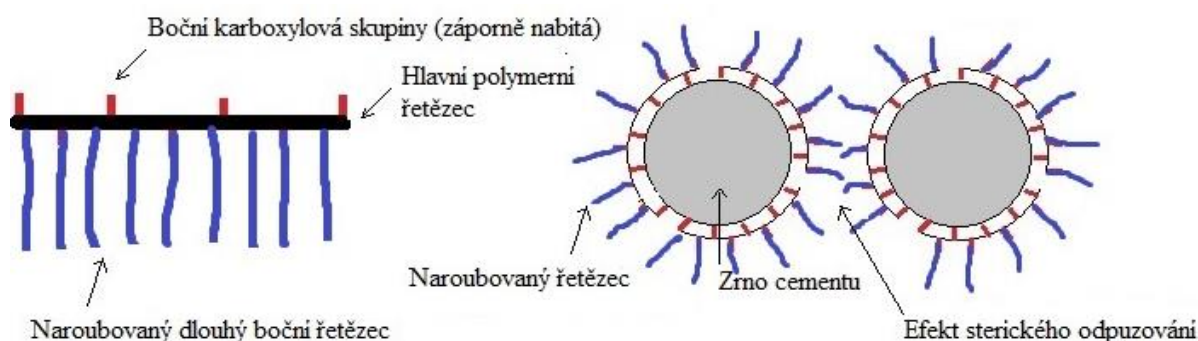
## Mechanismus působení plastifikačních přísad

Během hydratace cementu dochází díky přítomnosti velkého množství nenasycených povrchových nábojů na částicích cementu k jejich flokulaci. V takové flokulované struktuře se zachycuje určité množství vody, která následně není k dispozici na ztekucení směsi. Pro dosažení požadované zpracovatelnosti je nutné použít více vody, než je třeba k úplné hydrataci všech cementových zrn. Tento nadbytek vody, která nikdy nezreaguje s cementem, přispívá porézности cementové pasty a způsobuje zhoršení mechanických vlastností a trvanlivosti betonu. Účinek plastifikačních přísad tkví ve schopnosti dispergovat částice cementu díky neutralizaci jejich povrchových nábojů, čímž významně omezují přirozený sklon k flokulaci. Tímto způsobem lze docílit značného snížení množství záměsové vody [56]. V minulých letech byl dispergační účinek přisuzován pouze vytvářením záporného elektrostatického náboje na částicích cementu. Na tomto principu spolehlivě fungují plastifikátory disponující záporně nabitými skupinami navázanými na hlavní polymerní řetězci (např. lignosulfonáty). V alkalickém prostředí dochází u sulfonovaných plastifikačních přísad obsahujících  $-SO_3^-$  skupinu k její disociaci. Přitažlivé síly mezi částicemi jsou neutralizovány díky adsorpci aniontových polymerů na cementová zrna právě pomocí zmíněných  $-SO_3^-$  skupin. Na druhém konci polymerního řetězce jsou vytvořeny záporně nabitě skupiny  $SO_3^-$ , čímž dochází k elektrostatickému odpuzování částic cementu (Obr. 6).



**Obr. 6: Znázornění superplastifikátoru na bázi naftalenu a jeho účinek elektrostatického odpuzování cementových částic, převzato z [55]**

Naproti tomu účinek superplastifikátorů na bázi polykarboxylátů je odlišný. Disperzní mechanismus těchto superplastifikátorů je připisován spíše sterickému odpuzování díky přítomnosti neutrálně nabitých dlouhých bočních řetězců, nežli přítomností nabitých aniontových skupin  $COO^-$ , které způsobují adsorpci polymeru na povrch cementových částic (Obr. 7). Řetězce naroubované na molekulách polymeru, který je navázán na povrch cementových částic, má schopnost tyto částice od sebe odtlačovat, což brání jejich spojení do velkých a nepravidelných aglomerátů [55].

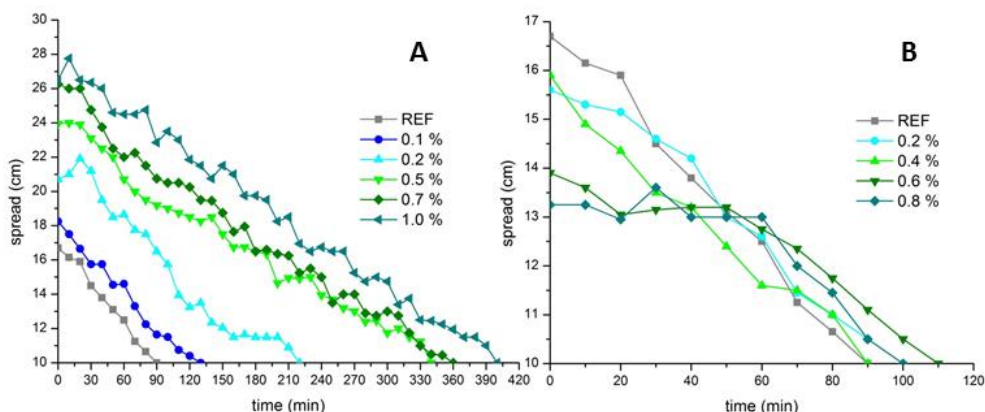


**Obr. 7: Znázornění superplastifikátoru na bázi polykarboxylátu a jeho účinek sterického odpuzování cementových částic, převzato z [55]**

### Plastifikační přísady v AAS

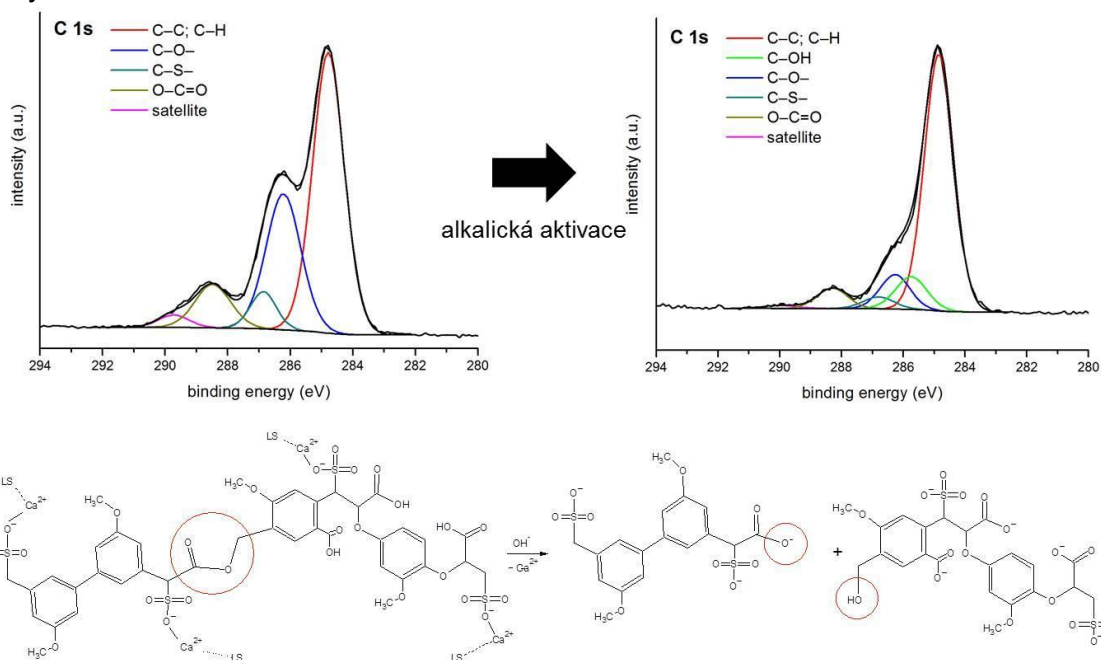
První pokusy zakomponování plastifikačních přísad do alkalicky aktivovaných systémů se datují do osmdesátých let minulého století, kdy ve Finsku a Norsku byly poprvé použity přísady na bázi lignosulfonátů redukující množství záměsové vody [57,58]. Tyto studie však nevedly k objasnění chování zmíněných přísad v alkalicky aktivovaných materiálech. Douglas a Brandštetr [59] v devadesátých letech rovněž použili plastifikační přísady na bázi ligno- a naftalensulfonátu v alkalicky aktivované vysokopecní strusce. Přísady byly však shledány jako neúčinné. Velmi podobné chování těchto povrchově aktivních látek popsali ve své studii i Wang a kol. [15], kteří testovali plastifikátory na bázi lignosulfonátu. Došli k závěru, že při použití těchto přísad dochází ke snížení pevnosti bez viditelných změn zpracovatelnosti. Bakharev a kol. [60] naopak dospěli k opačnému závěru než jejich předchůdci. Jejich systém založený na bázi vysokopecní strusky aktivovaný roztokem NaOH a vodním sklem vykazoval při přidavku lignosulfonátu podobné chování jako v pojivo na bázi portlandského cementu. Bylo pozorováno významné zlepšení zpracovatelnosti při současném snížení smrštění. Přídavek přísady nicméně zpomaloval tuhnutí a vývoj mechanických pevností.

Obdobné výsledky byly dosaženy i ve studii **Kaliny a kol.** [61]. Malty připravené aktivací vysokopecní strusky roztokem NaOH s velmi malým přídavkem lignosulfonátu vykazovaly výrazný nárůst zpracovatelnosti (Obr. 8A). Mechanické vlastnosti byly ovlivněny pouze v počátečních stádiích hydratace. Již po sedmi dnech dosahovaly všechny vzorky s přídavkem lignosulfonátu (0,1–1,0 hm. % přepočteno na množství VPS) obdobné pevnosti jako referenční směs. Stejně tak tomu bylo i po 28 dnech zrání. V této studii byl navíc popsán i mechanismus působení přísad na bázi lignosulfonátu v AAS. Pomocí metody XPS byl prokázán silný vliv alkalického prostředí na chemickou strukturu molekul lignosulfonátů (Obr. 9). Díky alkalické hydrolyze dochází k rozkladu polymerních řetězců na menší fragmenty, což bylo potvrzeno výrazným úbytkem jednoduchých vazeb mezi uhlíkem a kyslíkem ( $-C-O-$ ) a zároveň detekcí nově vytvořených hydroxylových skupin. Záporně nabitá sulfonátová skupina však ve struktuře molekuly zůstává nezměněna, a proto je elektrostatický účinek přísady stále zachován.



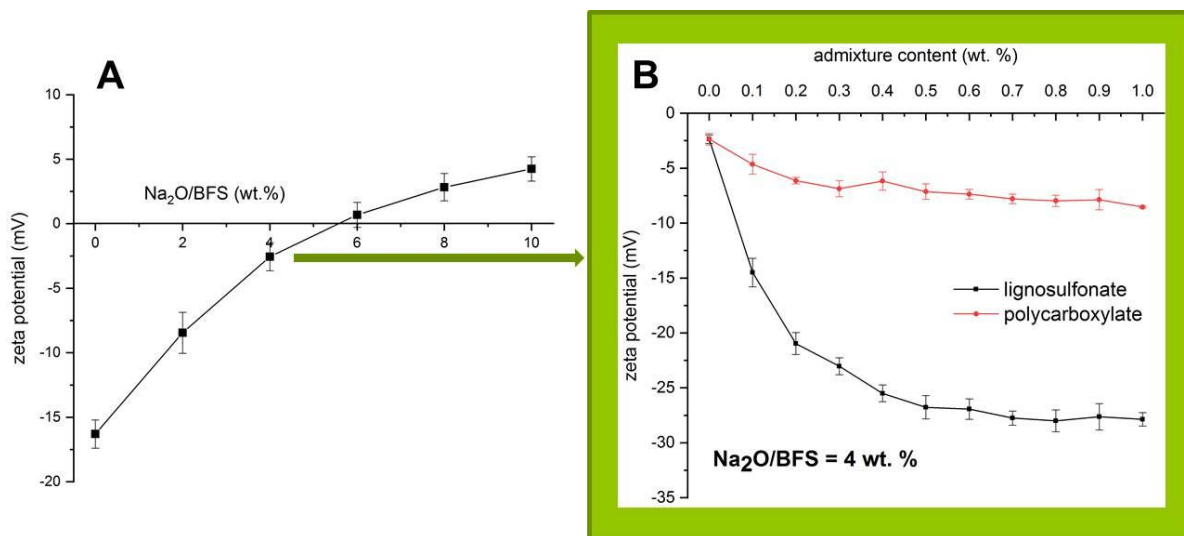
**Obr. 8: Zpracovatelnost rozlíváním na střešacím stolek AAS aktivované roztokem NaOH s použitím přídatku plastifikátoru na bázi lignosulfonátu (A); polykarboxylátu (B); převzato z Kalina a kol. [61]**

Potvrzení interakce mezi částicemi VPS a přísady přinesly výsledky měření zeta potenciálu suspenze částic strusky v alkalickém roztoku NaOH. V průběhu alkalické aktivace VPS dochází díky vysoké hodnotě pH k rozpuštění částic strusky za současného uvolnění  $\text{Ca}^{2+}$  iontů do roztoku. Díky tomu by měla být povrchová vrstva strusky tvořená silanolovými skupinami deprotonována, tedy záporně nabitá [62]. Vzhledem k přítomnosti kationtů alkalických kovů, pocházejících z roztoku hydroxidu, však rozpuštěné  $\text{M}^+$  ionty interagují s povrchem strusky, což vede k jeho kladnému nabití, které je závislé na koncentraci použitého aktivátoru (Obr. 10A). Účinek lignosulfonátového plastifikátoru je velmi dobře patrný z Obr. 10B, kdy jeho přidavek způsobuje výrazné snížení hodnot zeta potenciálu. Interakce mezi kladně nabitými částicemi strusky a přísadou obsahující záporně nabitě sulfonátové skupiny je tak nezpochybnitelná, stejně tak i zachování elektrostatického efektu přísady.



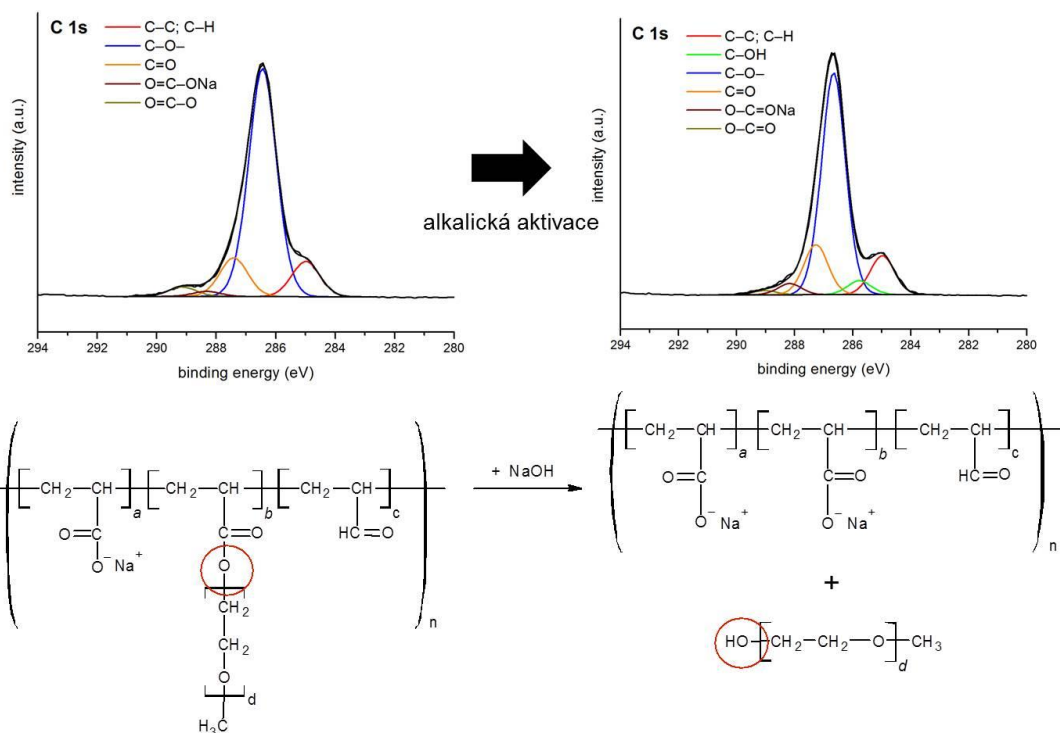
**Obr. 9: Mechanismus rozkladu molekuly lignosulfonátu v silně alkalickém prostředí vytvořeném na základě výsledků z XPS analýzy; převzato z Kalina a kol. [61]**

V poslední době se výzkum zaměřil i na superplastifikátory na bázi polykarboxylátů. Tato nová generace přísad dosahuje velmi dobrých výsledků v systémech na bázi portlandského cementu, nicméně jejich použití v alkalicky aktivovaných pojivech byla donedávna velkou neznámou. Puertas a kol. [63] studovali efekt polykarboxylátového superplastifikátoru jak na systémech alkalicky aktivované strusky, tak i popílku. Příklad přísady však nepřinesl kýžené zlepšení zpracovatelnosti ani mechanických vlastností testovaných směsí. K velmi podobným závěrům došel i Criado a kol. [64]. Puertas a Palacios [65] se následně zabývaly chemickou stabilitou polykarboxylátů ve vysoce zásaditém prostředí. Výsledky výzkumu naznačují, že přísady na bázi polykarboxylátů byly v alkalickém prostředí při pH vyšším než 13 chemicky nestabilní.



**Obr. 10: Měření zeta potenciálu suspenze vysokopecní strusky s různou koncentrací NaOH aktivátoru (A) a po přidavku plastifikační přísady (B); převzato z Kalina a kol. [61]**

Studie **Kaliny a kol.** [61] potvrzuje výsledky tohoto výzkumu a přináší jasné zdůvodnění velmi nízké efektivity těchto přísad. Příklad přísady do AAS nejenže nezlepšil zpracovatelnost záměsi, ale navíc ve větším přídávku docházelo dokonce k jejímu poklesu (Obr. 8B). Naprosto žádné zlepšení zpracovatelnosti je opět spojeno s alkalickou hydrolyzou polymerního řetězce (Obr. 11). Dlouhý boční řetězec, který by měl v těchto systémech plnit funkci sterické zábrany mezi jednotlivými částicemi strusky, je v důsledku hydrolyzy esterové skupiny odštěpen od hlavního řetězce, čímž celá molekula kompletně ztratí svůj účinek. Molekuly polykarboxylátu se díky COO<sup>-</sup> skupině sice navazují na zrna strusky (Obr. 10B), nicméně k silnému ovlivnění náboje částic, které by případně plnilo funkci elektrostatického odpuzování, nedochází.



**Obr. 11: Mechanismus rozkladu molekuly polykarboxylátu v silně alkalickém prostředí vytvořené na základě výsledků z XPS analýzy); převzato z Kalina a kol. [61]**

Detailní studium účinnosti superplastifikátorů na bázi polykarboxylátů v AAS aktivované křemičitanem sodným přinesl výzkum Kashani a kol. [66] Díky nižšímu pH v porovnání s předchozími systémy aktivovanými roztokem NaOH zřejmě nedochází k hydrolyze esterové skupiny, a proto lze studovat jak vliv délky hlavních a bočních polymerních řetězců molekuly, stejně tak i náboje (kladný × záporný), který byl vymezen na základě naroubování konkrétních funkčních skupin na boční polymerní řetězec. Bylo zjištěno, že molekuly s dlouhým hlavním a krátkými postranními řetězci způsobují znatelné zvýšení napětí meze toku, což vede k poklesu zpracovatelnosti v porovnání s alkalicky aktivovanou vysokopeční struskou bez dané přísady. Vše je zapříčiněno tím, že dochází k vysokému stupni můstkové vazby, jelikož nabitý řetězec může být současně adsorbován na více částicích vysokopeční strusky. V souladu s tímto mechanismem je ve výsledku přítomno více přitažlivých mezičásticových sil, které zvyšují seskupení částic a způsobují zvýšení meze toku. Zmíněného efektu lze zamezit zavedením sterické zábrany pomocí delších postranních řetězců a zkrácením hlavního řetězce. Mírně pozitivního efektu polykarboxylátového superplastifikátoru lze rovněž docílit přítomností kladně nabitých funkčních skupin na bočním řetězci z důvodu vyšší adsorpce přísady na zrna strusky, která mají v prostředí aktivace křemičitanem alkalického kovu spíše záporný náboj.

Ostatní druhy plastifikačních přísad byly studovány zejména díky rozsáhlému výzkumu Palacios a kol. [65,67-69], kteří zjistili například velmi dobrou chemickou stabilitu plastifikátoru na bázi polynaftalenu v silně alkalickém prostředí. Nízká dávka této přísady (cca 0,1 hm. %) vedla k účinnému snižování napětí na mezi toku připravené záměsi. Dále byla studována i povrchová aktivita plastifikátorů na bázi melaminu a vinylového kopolymeru. V této souvislosti bylo zjištěno, že adsorpce výše jmenovaných přísad je v AAS 3 až 10× nižší v porovnání v systému na bázi OPC. Jejich účinnost v prostředí s vysokými hodnotami

pH značně klesá. Během aktivace roztoky vodních skel, kde lze očekávat méně alkalické prostředí v porovnání s hydroxidy, byl zaznamenán pozitivní efekt přísad ve smyslu zvýšení tekutosti připravených záměsí, nicméně současně bylo stanoveno prodloužení času počátku a konce tuhnutí až o několik hodin.

Vzhledem k výsledkům uvedeným v literatuře je tedy zřejmé, že případný vývoj nové generace plastifikačních přísad, použitelných pro alkalicky aktivované materiály, musí být zejména zaměřen na zlepšení chemické stability polymerních struktur ve vysoce alkalickém prostředí. Při vývoji je nutné rovněž docílit potlačení retardačního účinku na průběh hydratace, což je v současné době při použití běžně dostupných komerčních plastifikačních přísad obvyklým jevem.

### 3.1.2 Přísady redukující smrštění

#### Úvod do problematiky smrštění cementových systémů

Smrštění je definováno jako snižování objemu materiálu za konstantní teploty bez vnějšího zatěžování. Je to velmi důležitá materiálová vlastnost, která výrazně ovlivňuje chování materiálu z dlouhodobého hlediska [70]. Silikátové materiály mohou podléhat následujícím typům smrštění:

- plastické smrštění
- autogenní smrštění
- smrštění vysycháním
- dekalciфикаční smrštění

Všechny zmíněné typy smrštění mohou vést až ke vzniku trhlin, ke kterému dochází, pokud napětí v tahu  $\sigma$ , vyvolané smrštěním způsobující deformaci při dotvarování  $\epsilon$ , dosáhne vyšší hodnoty, než je pevnost v tahu daného materiálu  $f$  dle vztahu (3).

$$\sigma = E\epsilon > f \quad (3)$$

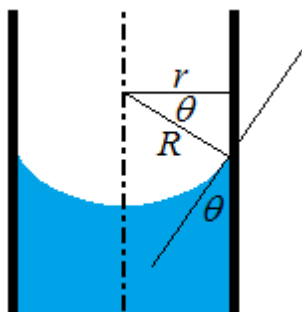
Tvorba trhlin samozřejmě negativně ovlivňuje jak mechanické vlastnosti materiálu, tak i jeho trvanlivost. Nejvyšší životnosti betonových konstrukcí lze tedy přispět potlačením smrštění. Dle Wittmanna a kol. [71] je obecně smrštění výsledkem několika nezávislých faktorů jako jsou změny ve vlhkosti materiálu, chemické reakce a fyzikální interakce povrchů hydratačních produktů a pórového roztoku. V případě AAS je smrštění obvykle několikanásobně vyšší než u systémů založených na bázi portlandského cementu, což se většinou připisuje vyššímu obsahu mesopórů [72], rozdílné povaze C-S-H gelu, nižšímu množství vytvořených krystalických hydratačních produktů [73] a v případě aktivace vodním sklem i vzniku křemičitého gelu, který má vyšší sklon ke smrštění [23,74]. Není divu, že snížení smrštění AAS je jedním z hlavních cílů současného výzkumu. Pochopení příčin a mechanismu smrštění je tak bezpochyby klíčem k jeho účinné redukci v AAS. Díky značné podobnosti mikrostruktury běžného hydratovaného cementu a AAS lze principy smrštění charakterizovat dle obecně známých teorií platných pro cementové systémy.

V třicátých letech Bangham [75] publikoval první průkopnické studie týkající se souvislostí mezi vysycháním a smrštěním porézní hmoty a během následujících desetiletí byly popsány různé přístupy popisující smrštění vysycháním vzniklých cementových systémů. Teorie

kapilárního a rozpojovacího tlaku jsou známy a hojně používány k vysvětlení příčiny smrštění. První je založena na předpokladu vzniku menisků, jež se vytváří během vysychání cementové matrice jako důsledek sil povrchového napětí. Rozdíl mezi tlakem v kapalně fázi  $p_l$  a v plynné fázi  $p_v$  je nazýván tzv. kapilárním tlakem  $\Delta p_c$  a je dle rovnice (4), která se nazývá Laplaceovou-Youngovou, roven součinu zakřivení rozhraní kapalina-pára  $\kappa$  a povrchového napětí  $\gamma$ . Zakřivení mezifázového rozhraní  $\kappa$  lze charakterizovat pomocí jeho poloměru křivosti  $R$  a následně zjednodušit rovnici (4) na výsledný tvar (5). Pokud chceme vyjádřit kapilární tlak v závislosti na poloměru velikosti pórů  $r$ , je možné poloměr křivosti vypočítat dle smáčecího úhlu  $\theta$  (Obr. 12).

$$\Delta p_c = p_l - p_v = \kappa \gamma \quad (4)$$

$$\Delta p_c = \frac{2\gamma}{R} = -\frac{2\gamma}{r} \cos \theta \quad (5)$$



**Obr. 12: Závislost poloměru křivosti fázového rozhraní  $R$  a poloměrem póru  $r$ , převzato z [70]**

Vzhledem k jistým pochybnostem o použitelnosti této teorie na cementový systém s velmi jemnými póry (několik nanometrů) a za podmínek hydratace s okolní relativní vlhkostí pod 50 %, byla v roce 2006 představena teorie, založená na konceptu rozdělovacích tlaků, podle níž jsou disjunkční síly hlavním mechanismem smrštění vysycháním. Pojem rozpojovací tlak  $p_d$  představuje komplexní interakce mezi vodou a dvěma pevnými povrchy, které mohou být ve zjednodušené verzi psané jako superpozice přínosu přitažlivých nebo molekulárních sil (převážně van der Waalsových sil)  $p_m$ , odpudivých sil elektrické dvojvrstvy  $p_e$  a strukturních složek  $p_s$  dle rovnice (3).

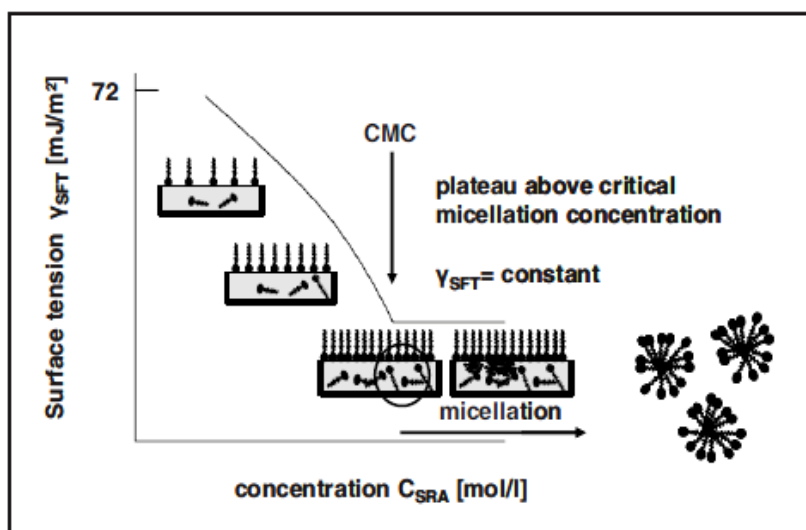
$$p_d = p_m + p_e + p_s \quad (6)$$

Pokud jsou dva pevné povrchy ve vakuu nebo suchém vzduchu blízko sebe, dominují přitažlivé síly a pevné povrchy jsou v těsném kontaktu. Se vzrůstající relativní vlhkostí vytváří adsorbovaná a kapilární voda film způsobující jejich rozdělení [76].

### Přísady redukující smrštění v cementových systémech

S ohledem na kapilární model, popsáný v předchozí kapitole, je jednou z možností jak účinně snižovat smrštění použití přísad redukujících smrštění na bázi organických povrchově aktivních látek, které snižují povrchového napětí pórového roztoku [77].

Přísady redukující smrštění (SRA) byly použity ke snížení smrštění cementových systémů před více než třiceti lety. Obecně patří do skupiny organických sloučenin nazývaných povrchově aktivní látky, které jsou chemickými látkami s amfifilním charakterem, tj. jsou složeny z hydrofilní hlavy a hydrofobního řetězce. Z tohoto důvodu se mohou adsorbovat na rozhraní a měnit jejich vlastnosti. Jejich adsorpce na rozhraní kapaliny a páry je zásadní pro snížení smrštění porézního systému, a to především díky snižování povrchového napětí kapaliny přítomné v pórech, které však může být omezeno jejich mísitelností v pórovém roztoku nebo jejich interakcí s jinými složkami v systému. Obecně lze říci, že povrchové napětí postupně klesá s rostoucí dávkou SRA, avšak za určitým bodem, nazývaným kritická koncentrace micel (CMC), se jejich vliv na povrchové napětí snižuje (Obr. 1 Obr. 13). Díky vytvoření micel následně nedochází k jejich adsorpci na rozhraní mezi kapalnou a plynnou fází [78]. SRA molekuly mohou také adsorbovat na rozhraní pevná látka-kapalina, což v cementových systémech obvykle znamená fyzickou adsorpci polární části SRA na polární povrch částice. Tato vlastnost je rovněž nežádoucí, protože snižuje účinnost SRA, neboť tyto molekuly již nejsou schopné se podílet na snížení povrchového napětí pórového roztoku. Rovněž dochází i k negativnímu ovlivnění hydratačních procesů, které jsou v přímé souvislosti s konečnými vlastnostmi malty nebo betonu. Pro zabránění této adsorpce se v cementových systémech používají převážně neionogenní SRA [49].



Obr. 13: Závislost povrchového napětí na koncentraci SRA, převzato z [79]

Dle molekulové struktury lze neionogenní SRA rozdělit do následujících skupin:

- monoalkoholy (lineární, rozvětvené, cyklické)
- glykoly (alkandioly nebo oxyalkylenglykoly)
- alkylether polyoxyalkylenglykoly
- polymerní surfaktanty
- jiné SRA (aminoalkoholy, amidy atd.)

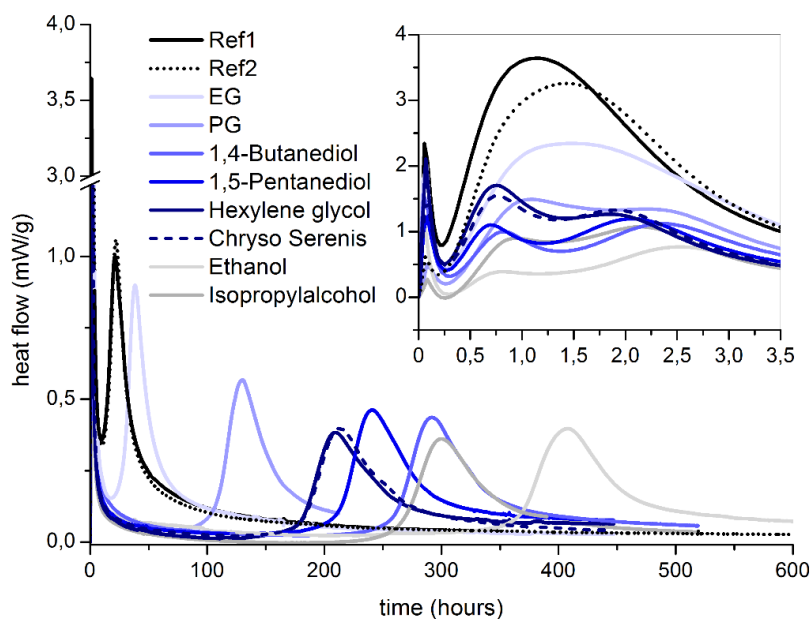
### Přísady redukující smrštění v AAS

Dosud bylo publikováno pouze několik studií, které zkoumaly účinek organických přísad redukující smrštění v AAS. Jak už bývá železným pravidlem na poli alkalicky aktivovaných

materiálů, přísady, které spolehlivě fungují v běžných cementových systémech, naprosto selhávají v případě AAS. Ukázalo se, že účinnost komerčních produktů efektivně snižovat smrštění AAS je nedostačující a spíše funguje principem výrazného zpomalení hydratace. Z tohoto důvodu byl celosvětový výzkum zaměřen na studium různých skupin organických látek, které by účinně redukovaly smrštění a zároveň nezhoršovaly ostatní vlastnosti alkalicky aktivovaného materiálu. Následující kapitola shrnuje dosavadní výzkum v této oblasti a přináší tak naději pochopení problematiky smrštění AAS vedoucí k volbě vhodného druhu a dávkování SRA.

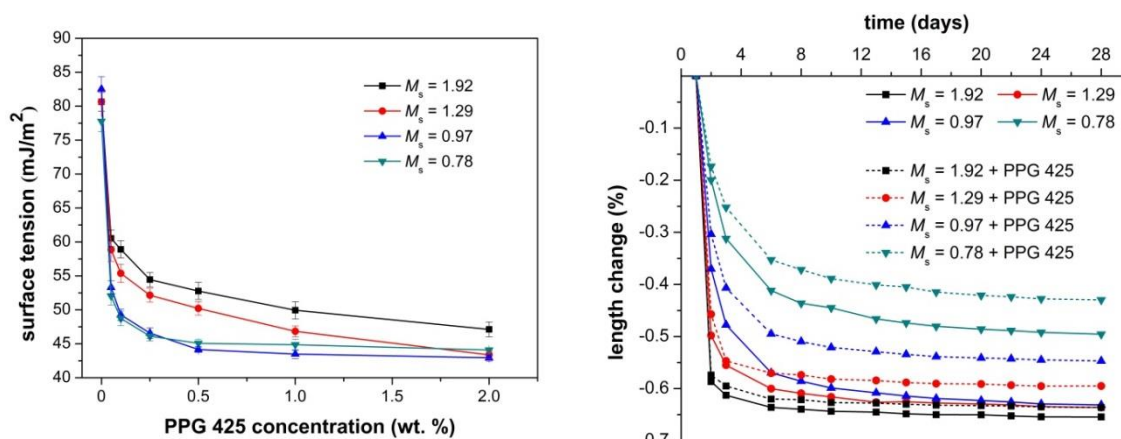
Řada komerčních SRA navržených pro systémy s běžným portlandským cementem jsou na bázi neionogenních povrchově aktivních látek, zejména alkoholů a glykolů. Palacios a Puertas [80] studovaly vliv SRA na bázi polypropylenglykolu na smrštění a další vlastnosti AAS aktivované pomocí vodního skla. Při relativní vlhkosti 50 % se smrštění malty AAS snížilo přibližně o 7 a 35 % při 1%, respektive 2% dávky SRA. Naproti tomu snížení smrštění při 99% relativní vlhkosti bylo podstatně větší: přibližně 50 % a 75 % při zachování stejných dávek SRA. Z těchto výsledků lze říci, že SRA postupně ztrácejí schopnost snižovat smrštění při nižších hodnotách relativní vlhkosti. V této práci byl rovněž studován vliv vodního součinitele na rozsah smrštění AAS. Bylo zjištěno, že přídavek SRA snížil spotřebu vody pro stejnou konzistenci, jakož to i povrchového napětí v pórovém roztoku. Zároveň docházelo k odlišné distribuci velikosti pórů směrem k větším pórům ve srovnání s referenčním vzorkem, což zapříčinilo nižší kapilární napětí. Také Bilim a kol. [81,82] používali SRA na bázi polypropylenglykolu pro zmírnění smrštění AAS. Při vytvrzování za vysoké hodnoty relativní vlhkosti se opět smrštění vysycháním výrazně snížilo (až o 40 % po 180 dnech) a to jak při aktivaci metakřemičitanem sodným, tak i roztokem vodního skla. Výzkum potvrdil, že během prvních dnů vysychání bylo snižování smrštění mnohem větší, např. po 3 dnech asi 80 %.

Studie **Bílka a Kaliny** [83-85] potvrdily až 70% snížení smrštění vysycháním s použitím 2 hm. % komerční přísady na bázi hexylenglykolu oproti referenční maltě. Zjistilo se však, že komerční přísady obecně vykazují značný retardační účinek na hydratační proces AAS, tedy i tvorbu pojivové fáze (Obr. 14). Při testovaných komerčních přísad v AAS je tak výsledkem materiál, který se jen velmi málo smršťuje, ale důležité vlastnosti jako počáteční a dlouhodobé pevnosti jsou silně potlačeny. Toto zjištění vedlo ke zkoumání jiných skupin povrchově aktivních látek s lepším potenciálem pro užití v AAS.



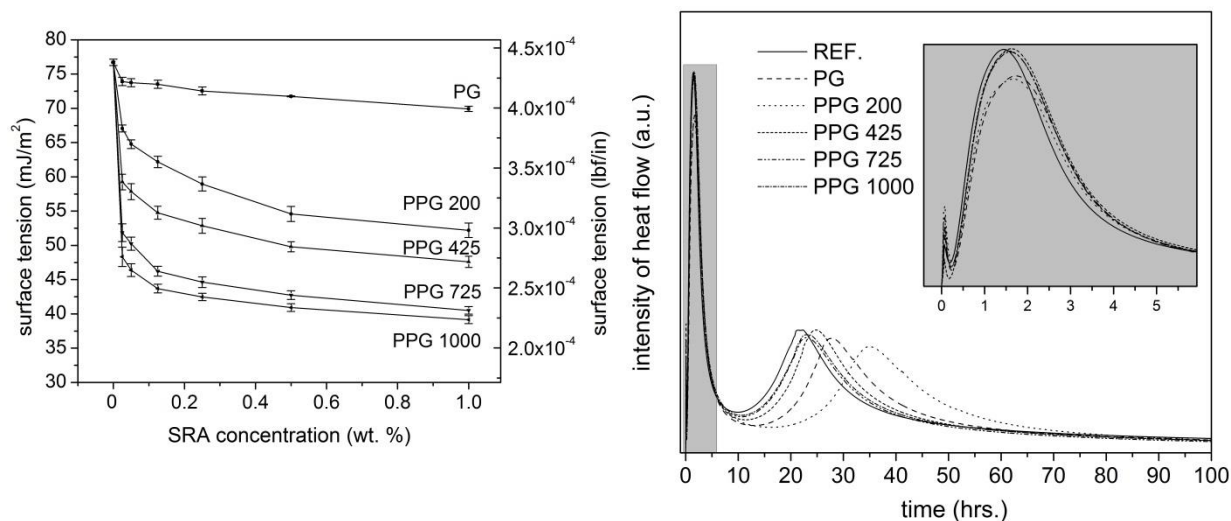
Obr. 14: Účinek různých alkoholů a glykolů na hydrataci AAS; převzato z Bílek, Kalina a kol. [84]

Polyoxyalkylen glykoly se ukázaly jako velmi slibná skupina organických látek, která byla podrobena dalšímu výzkumu. Kalina a Bílek [86] prokázali, že charakter alkalického prostředí významně ovlivňuje schopnost polyoxyalkylen glykolových přísad redukovat smrštění v AAS (Obr. 15). Ve stručnosti lze shrnout, že s klesajícím molárním poměrem oxidu křemičitého a oxidu alkalického kovu ( $\text{Na}_2\text{O}$ ,  $\text{K}_2\text{O}$ ) v použitém aktivačním roztoku dochází ke zvyšování účinnosti protismršťovacích přísad (použit polypropylen glykol;  $M_n=425$ ). Zároveň byla pozorována i jejich lepší mísitelnost s aktivačním roztokem. Mísitelnost přísady s aktivačním, resp. pórovým roztokem se zvyšuje také během hydratace AAS, neboť zejména v prvních hodinách hydratace dochází k rychlému spotřebování křemičitanových iontů, které mají na mísitelnost negativní vliv.



Obr. 15: Závislost povrchového napětí (vlevo) a smrštění vysycháním (vpravo) s použitím PPG 425 v AAS aktivované roztokem vodního skla s různým silikátovým modulem; převzato z Kalina a kol. (Příloha V) [86]

**Kalina, Bílek a kol.** [87] rovněž zkoumali vliv délky řetězce vybraných polyoxyalkylenglykolů na schopnost účinně redukovat smrštění. Jako slibnou skupinou se obecně ukázaly být polypropylenglykoly se spíše vyšší molekulovou hmotností (cca 700–1 000), které výrazně neovlivňují hydratační procesy AAS a zároveň jsou efektivnější ve snižování povrchového napětí pórového roztoku (Obr. 16). Svou roli hrají také změny v distribuci velikosti pórů a celková porozita. U některých nižších polyalkylenglykolů sice bylo zaznamenáno velmi výrazné snížení smrštění, nicméně hlavní příčinou bylo zpomalení hydratace AAS, což se velmi nepříznivě projevilo na zvýšení porozity těchto materiálů a ve svém důsledku znamenalo zhoršení mechanických a dalších vlastností. Dále bylo prokázáno, že míra zpomalení hydratace AAS v přítomnosti přísad úzce souvisí s dávkou alkalického aktivátoru, kdy lze jejím navýšením řadu negativních vlivů na hydrataci potlačit [88]. Molekulová hmotnost polyoxyalkylenglykolů má vliv i na možné vyluhování přísady ze systému, kde byla použita. Ve studii **Bílka, Kaliny a kol.** [89] bylo posouzeno, do jaké míry zůstávají použité organické přísady v AAS v „aktivní“ formě, tedy v pórovém roztoku, schopné migrovat k rozhraní kapalina-plyn a tím snižovat povrchové napětí roztoku, a v jaké míře dochází k jejich imobilizaci, například jejich zakomponováním do postupně se vyvíjejících hydratačních produktů, popř. adsorpcí. Konkrétně byly studovány polyethyenglykoly až do molekulové hmotnosti 35 000 a bylo zjištěno, že množství vyluhované povrchově aktivní látky výrazně klesá s rostoucí molekulovou hmotností.



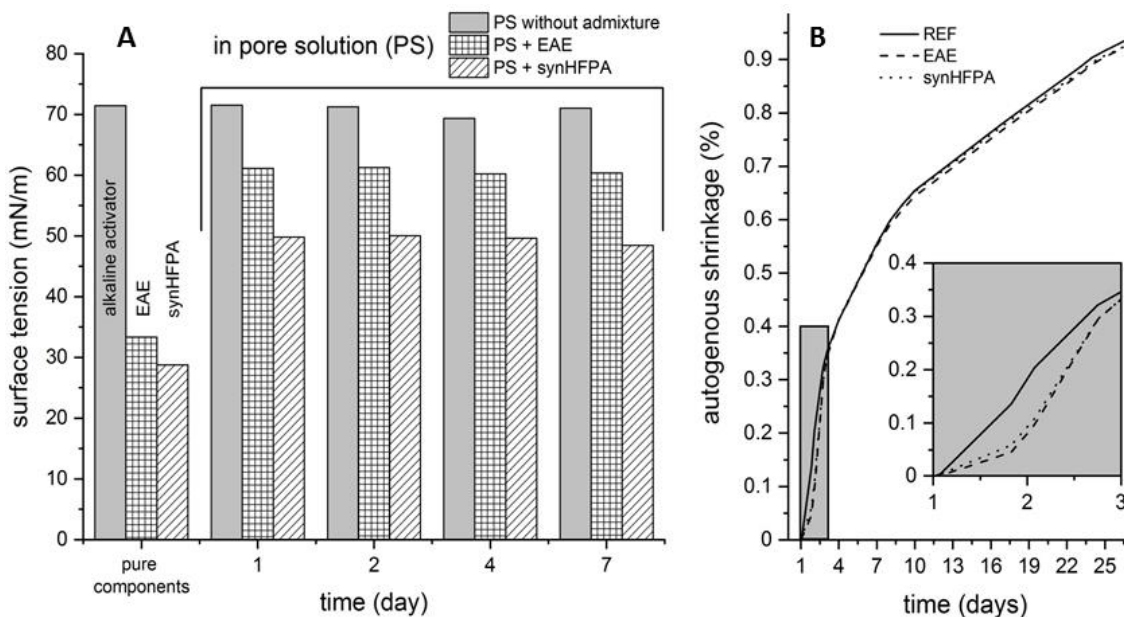
**Obr. 16: Závislost povrchového napětí (vlevo) a hydratačního procesu (vpravo) s použitím PPG o různé molekulové hmotnosti v AAS aktivované roztokem sodného vodního skla; převzato z Kalina a kol. (Příloha VII) [87]**

Další slibnou skupinou SRA s potenciálem pro použití v AAS jsou organické sloučeniny na bázi aminoalkoholů. Tyto povrchově aktivní látky snižují, obdobně jako již testované polyoxyalkylenglykoly, povrchové napětí pórového roztoku AAS. Navíc však přináší některé významné pozitivní vlastnosti. Obecně lze říci, že se stoupajícím polymerním stupněm polyoxyalkylenglykolů sice klesá povrchové napětí pórového roztoku, ale zároveň i klesá mísitelnost těchto polymerních látek v alkalickém roztoku, což negativně ovlivňuje rovnoměrnou distribuci povrchově aktivní látky. Naproti tomu aminoalkoholy vykazují dobrou mísitelnost ve vodném prostředí, zejména díky aminové skupině, která zvyšuje hodnotu HLB, tedy i hydrofilní charakter přísady. Dostatečná mísitelnost s alkalickým roztokem tak přináší

podstatné zvýšení jejich účinnosti. Výzkum prokázal významný účinek různých typů alkylových skupin navázaných na aminovou funkční skupinu. Práce **Kaliny a kol.** [90,91] potvrdila, že více rozvětvený alkylový řetězec snižuje povrchové napětí pórového roztoku i smrštění vysycháním AAS. Účinný přídatek aminoalkoholů na výsledné smrštění však stále negativně ovlivňuje hydratační procesy, což má opět dopad i na mechanické vlastnosti AAS.

V několika studiích byly zkoušeny i účinky různých organických přísad, které nepatří do skupiny neionogenních povrchově aktivních látek. Bakharev a kol. [60] například dospěli k závěru, že směs AAS, po přidání provzdušňovací přísady v kombinaci s blíže nespecifikovanou SRA, vykazovala výrazně lepší zpracovatelnost a rovněž i redukcí smrštění. Tyto dvě přísady snížily dlouhodobé smrštění o cca 70 %. Snížení smrštění, ačkoli podstatně nižší, bylo dosaženo i u plastifikačních přísad na bázi lignosulfonátu. Nutno však zmínit, že jiný typ plastifikátoru na bázi modifikovaných naftalenformaldehydových polymerech zvýšil smrštění vysycháním o téměř 40 %. Z tohoto důvodu nelze potvrdit obecně příznivý efekt plastifikačních přísad na redukcí smrštění AAS.

Cesta k účinné redukcí smrštění AAS pomocí organických přísad se zdá být více komplikovaná, než se na první pohled může zdát. V mnoho případech je snížení smrštění doslova vykoupeno výrazným zpomalením procesu hydratace mající za následek podstatné zhoršení mechanických vlastností. Přesto však bylo prokázáno, že použití některých povrchově aktivních látek je příslibem k efektivní redukcí smrštění AAS. Skupiny látek na bázi polyoxyalkylenglykolů a aminoalkoholů se zdají být použitelné v určité koncentraci s nižším vlivem negativních vedlejších účinků. Nicméně rozsáhlé smrštění AAS, zejména pak v případě aktivace roztokem vodního skla, nelze zcela potlačit ani s použitím zmíněných přísad. Na základě teorie kapilárního tlaku se jako možné řešení nabízí syntéza nových typů SRA, které budou mít vyšší potenciál ke snižování povrchového napětí pórového roztoku. Řešený projekt GAČR GA17-03670S „Vývoj přísad redukcí smrštění navržených pro alkalicky aktivované systémy“ (odpovědný řešitel **Kalina L.**) [92] měl ambice na možný posun v této oblasti. Díky modifikaci popsanych přísad pomocí vybraných funkčních skupin, lze docílit výrazného snížení povrchového napětí, což poskytuje možnost nižšího, avšak účinnějšího dávkování přísady. Nukleofilní acylací aminoalkoholů estery karboxylové kyseliny byly syntetizovány nové typy SRA pomocí naroubování různých hydrofobních řetězců na aminovou funkční skupinu. V práci **Kaliny a kol.** [93] byla zkoumána zejména syntetizovaná přísada na bázi sekundárních fluorovaných aminů z hlediska její účinnosti efektivně snižovat jak autogenní smrštění, tak smrštění vysycháním. V případě autogenního smrštění bylo prokázáno, že výsledné smrštění vykazuje obdobný vývoj jako u vzorků bez přísady, přestože povrchové napětí pórového roztoku zůstávalo velmi nízké i po několika dnech od počátku alkalické aktivace (Obr. 17).



**Obr. 17: Vliv přísad na bázi aminoalkoholů na povrchové napětí pórového roztoku (A); autogenního smrštění (B) AAS, převzato z Kalina a kol. (Příloha I) [93]**

Rozdíl mezi testovanými vzorky byl pozorován pouze v průběhu počátečních stádií hydratace, kdy u AAS záměsí s přísadou byla oddálena tvorba hlavní hydratační fáze C-A-S-H gelu o několik hodin. Rovněž bylo zjištěno, že přidavek použitých přísad velmi málo ovlivňuje celkovou porozitu systému. V této souvislosti nelze opomenout zcela rozdílné chování SRA v OPC materiálech, kde byl jasně prokázán jejich pozitivní účinek při snižování smrštění v autogenních podmínkách [94,95]. Mnohé studie navíc jednoznačně potvrzují, že přidavek surfaktantů má za následek udržení vysoké vnitřní relativní vlhkosti [94,96]. Z tohoto důvodu by měl být hlavní mechanismus, který řídí smrštění, primárně připisován kapilárním tlakům na rozdíl od rozpojovacího tlaku působícím zejména při nižší vlhkosti systému. Nicméně dle výsledků výzkumu lze dospět k závěrům, že výrazný pokles povrchového napětí nemusí vést nutně ke snížení smrštění, tedy teorii kapilárního tlaku v AAS nelze vždy striktně aplikovat. Významně odlišné chování AAS s přidavkem SRA bylo pozorováno při testování vývoje smrštění vysycháním. Vzorky s přísadou dosáhly podstatně nižšího výsledného smrštění v porovnání s referencí. Zároveň však byla naměřena vysoká ztráta hmotnosti v průběhu prvních dní hydratace. Vše souvisí opět s negativním dopadem SRA na průběh hydratačního procesu AAS. Nižší stupeň hydratace v počátečních fázích alkalické aktivace vede k nižšímu vyvázání vody do hydratačních produktů, což má za následek její vyšší odpar do okolního prostředí. Voda v systému chybí, tudíž lze očekávat významně nižší tvorbu pojivové fáze a následně i vyšší porozitu výsledného materiálu. V tomto ohledu je tedy otázkou, zda pozorované snížení smrštění vysycháním je zapříčiněno přítomností přísady z hlediska její schopnosti účinně snižovat povrchové napětí v kapilárách. Nabízí se spíše vysvětlení, které stojí na přímé souvislosti mezi retardačním účinkem přísady z pohledu hydratace a vývojem smrštění vysycháním. Vzhledem k podobné chemické povaze komerčně používaných SRA lze očekávat analogické chování. Využití neionogenních povrchově aktivních látek v AAS při účinné redukci smrštění tak bohužel nepřináší požadované výsledky, a proto zůstává i nadále snaha o nalezení vhodných přísad, které by tento problém komplexně vyřešily.

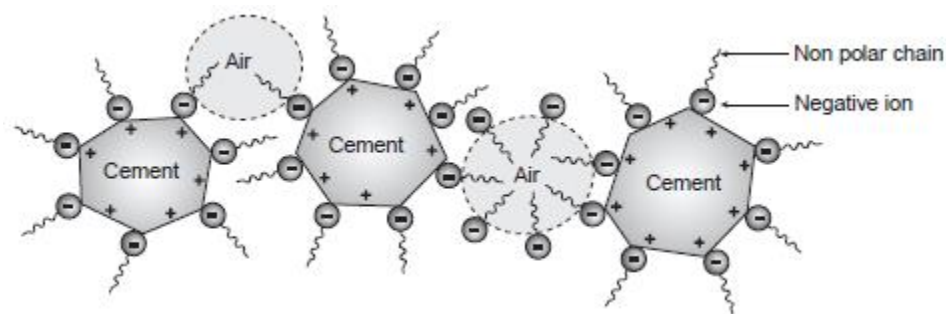
### 3.1.3 Provzdušňovací přísady

Zřejmě nejdůležitější použití provzdušňovacích přísad (AEA) souvisí se zvyšováním odolnosti anorganických pojiv proti zmrazování a rozmrazování. Jejich funkce spočívá ve vytvoření velkého množství uzavřených vzduchových pórů obsažených v čerstvé záměsi. Provzdušněním vytvořené vzduchové póry jsou expansním prostorem pro zvětšující se objem krystalů ledu. Velikost pórů se obvykle pohybuje od 0,05 do 0,3 mm a zpravidla nejsou nikdy vyplněny hydratačními produkty, protože k vytvoření pojivové fáze je třeba voda, která zde není obsažena. Míru provzdušnění určuje několik faktorů, jakými jsou obsah cementu, vodní součinitel, rychlost a doba míchání nebo typ a množství použité přísady. Zajímavým vedlejším účinkem provzdušnění je i zlepšení zpracovatelnosti, což v konečném důsledku znamená menší spotřebu vody a cementu. Provzdušňovací přísady rovněž umožňují produkci lehčených betonů bez nutnosti užití lehčeného kameniva [28,97].

#### Mechanismus účinku provzdušňovacích přísad

Působení provzdušňovacích přísad v cementových systémech zachycuje Obr. 18. Je velmi dobře vidět, že na mezifázovém rozhraní kapalina-vzduch se povrchově aktivní molekula přísady vždy orientuje polární skupinou k vodnému roztoku, což způsobuje snižování povrchového napětí, podporuje tvorbu bublin a zároveň působí proti jejich slučování. Na rozhraní pevná látka-voda je hydrofilní skupina přísady vázána na částici cementu, zbylá část molekuly směřuje do vodného roztoku. Dochází tedy k tomu, že vzduch vytlačí vodný roztok z okolí cementu a sám zůstává připojen v těsné blízkosti částic jako soubor bublin. Zmíněný způsob provzdušnění je velmi účinný, nicméně je třeba vzít v úvahu, že přísada adsorbovaná na povrch cementu, či jiné částice, vyvolá její hydrofobní povahu. Jakékoli možné předávkování provzdušňovací přísady tedy může vést ke značnému zpomalení hydratačních procesů související se ztrátou mechanických vlastností [97,98]. V této souvislosti uvádí Aitcin [56], že v rozsahu od 4 do 6 % provzdušnění, se zvýšením obsahu vzduchu o 1 % sníží pevnost v tlaku o 4 až 6 %. Z tohoto důvodu je nutné, aby AEA byla účinná jen v tak malém množství, které nebude mít negativní dopad na vlastnosti pojiva.

V současné době máme k dispozici jen omezený počet organických sloučenin, které jsou vhodné k použití jako provzdušňovací přísada. Nejstarší a jedna z neúčinnějších je vinsolová pryskyřice extrahovaná z borovicového dřeva. Účinnou složkou je abietát sodný, sodná sůl kyseliny abietové, což je aromatická sloučenina získaná z rozkladu přírodních dřevních pryskyřic. Složení nových generací AEA je založeno spíše na směsi syntetických chemikálií, zejména pak na aniontových povrchových látkách, které jsou tvořeny hydrofilní hlavou na bázi karboxylátů, sulfonátů, síranů nebo fosfátů. Dále jsou známé i kationtové a amfoterní povrchově aktivní sloučeniny. Jejich výhodou je vyšší adsorpce na převážně záporně nabitá zrna cementu [49,98]. V AAS systémech může být situace odlišná. Povrchový náboj strusky je totiž silně ovlivněn použitým typem aktivátoru, jak bylo potvrzeno ve studii Kashaniho a kol. [62]. V případě aktivace roztokem křemičitanu sodného je povrchový náboj strusky záporný, stejně jako u hydratovaných zrn cementu, z důvodu adsorpce rozpuštěných záporně nabitých křemičitanových fragmentů na povrchu strusky. Opačná situace nastává při aktivaci hydroxidy alkalických kovů, kde díky adsorpci  $\text{Na}^+$  ( $\text{K}^+$ ) na silanolové skupiny, které se vyskytují na povrchu strusky, dochází k vytvoření kladného náboje (viz Obr. 10).

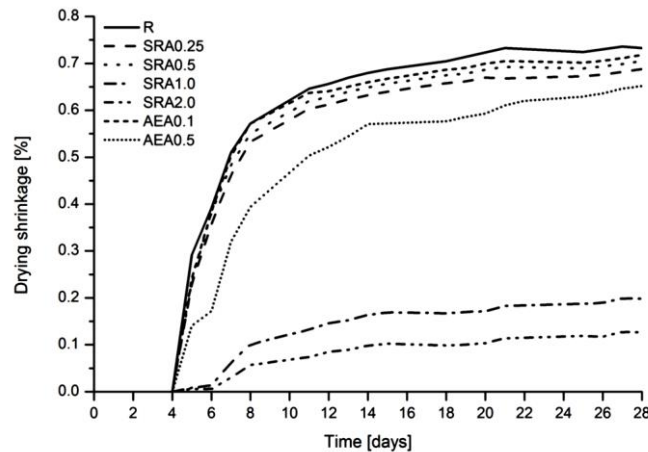


Obr. 18: Mechanismus účinku aniontové provzdušňovací přísady v cementové pastě, převzato z [97]

### Provzdušňovací přísady v AAS

Různé typy provzdušňujících přísad byly testovány i v AAS. Douglas a kol. [99] zjistili, že AEA na bázi sulfonátu dokáže zvýšit provzdušnění alkalicky aktivovaného betonu až na 6 %. V této souvislosti bylo potvrzeno, že výše zmíněná přísada měla naprosto stejný účinek jak v AAS, tak OPC systémech. Nejen provzdušnění, ale i ostatní vlastnosti AAS lze ovlivnit přidáním AEA. Bakharev a kol. [60] zkoumali vliv alkyl aryl sulfonátu na zpracovatelnost, mechanické vlastnosti a smrštění AAS betonu aktivované NaOH a  $\text{Na}_2\text{CO}_3$ . Zjistili, že alkalicky aktivovaný beton dosáhl s přísadou lepší zpracovatelnosti, mechanické vlastnosti nebyly ovlivněny a navíc došlo k významnému snížení autogenního smrštění a smrštění vysycháním.

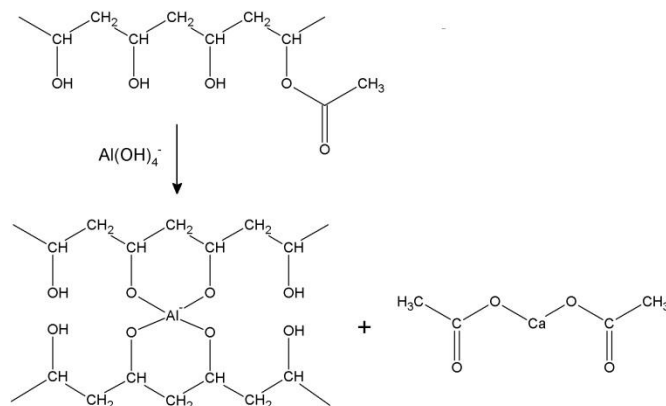
Jak již bylo zmíněno v předchozí kapitole, distribuce velikosti pórů má zásadní vliv na smrštění AAS. Provzdušnění tedy nemusí být nutně užitečné jen z hlediska zvýšení odolnosti proti zmrazování a rozmrazování, ale může hrát podstatnou roli i v redukci rozsáhlého smrštění AAS materiálů. **Bílek, Kalina a kol.** [83] studovali účinek komerčně vyráběných SRA na bázi 2-methyl-2,4-pentandiolu a AEA, kde hlavní složky tvořily zejména kyselina sulfonová a kokosový olej. Bylo zjištěno, že již malý přírůstek SRA (0,25–2,0 hm. %), nebo EAE (0,1; 0,5 hm. %) negativně ovlivňuje mechanické vlastnosti. Naopak smrštění vysycháním bylo s použitím obou přísad sníženo (Obr. 19). Z výsledků lze navíc vysledovat, že účinnost AEA byla v porovnání s SRA vyšší. Této skupině povrchově aktivních látek je proto zapotřebí do budoucna věnovat vyšší pozornost. Hledání vzájemného vztahu mezi charakterem hydrofilní nebo hydrofobní částí molekuly a jejich mechanismem účinku v alkalicky aktivovaném systému, může být klíčem k řešení nejpálčivějšího problému AAS, kterým je rozsáhlé smrštění.



Obr. 19: Vývoj smrštění vysycháním ovlivněný pomocí různých přísad redukující smrštění (SRA) a provzdušňovacích přísad (AEA); převzato z Bílek, Kalina a kol. [83]

### 3.1.4 Ostatní organické přísady

Mezi ostatní organické přísady, které byly testovány v systému AAS, patří různé typy kopolymerů [100,101]. Velmi malé množství (1 hm. %) těchto organických sloučenin (např. poly(ethylen-vinylacetát), polyvinylacetát) zvyšoval významně pevnosti v tlaku a tahu za ohybu a zároveň přispěl i k udržení vnitřní vlhkosti materiálu. Reakční mechanismus mezi polymerní látkou (polyvinylacetát) a anorganickou maticí, spočívající v zesílení řetězců polymeru pomocí hlinitanových tetraedrů (Obr. 20), byl vysvětlen ve studii Kaliny a kol. [102]. Dá se předpokládat, že velmi podobné interakce budou probíhat i v systémech na bázi AAM. Organické látky byly použity i jako alternativní regulátory tuhnutí AAS [103,104]. V tomto smyslu byly testovány organické kyseliny, jako je kyselina vinná a jablečná. Doba tuhnutí s použitím těchto sloučenin byla významně oddálena, nicméně jejich přídavek silně ovlivnil počáteční a dlouhodobé pevnosti materiálu. Za účelem zvýšení trvanlivosti AAS materiálů byl zkoušen i přídavek stearátu vápenatého [105]. S použitím této přísady byla významně snížena nasákavost AAS a to především díky vytvoření vodě odpudivému filmu pokrývající povrch materiálu. Hydrofobní část molekuly však zároveň ovlivnila samotný průběh alkalické aktivace, což se opět projevilo z pohledu snížení mechanických vlastností AAS.



Obr. 20: Zesílení řetězců polymeru (polyvinylacetát) hlinitanovými tetraedry; převzato z Kalina a kol. (Příloha XIII) [102]

## 3.2 Anorganické přísady

Kromě popsaných organických povrchově aktivních sloučenin existuje i řada anorganických přísad. Do této skupiny přísad patří zejména chemické látky, které nacházejí využití zejména v oblasti ovlivnění rychlosti tuhnutí a tvrdnutí cementových směsí. Mechanismus jejich účinku vychází ze skutečnosti, že první reakce v systému voda-cement probíhají ve vodném roztoku. Je proto zřejmé, že přidání určité ve vodě rozpustné chemikálie do zmíněného systému povede k ovlivnění míry ionizace cementových částic a k tvorbě hydratačních produktů. V důsledku toho lze velmi účinně ovlivnit charakteristiky tuhnutí a tvrdnutí. V případě AAS materiálů je situace velmi podobná. Hydratační produkty se tvoří rovněž z roztoku, stejně jak je tomu i v případě cementových systémů. Z tohoto důvodu můžeme využít obecně platná pravidla, formulovaná již v roce 1973 Joiselem [106], založených na principu změny typu a koncentrace ionizovaných složek v roztoku:

- přísady, které urychlují rozpouštění složek tvořící pojivovou fázi, se řadí do skupiny urychlovačů tuhnutí, naopak přísady, které brání rozpouštění fází a snižují tak koncentrací kationtů a aniontů v roztoku se nazývají zpomalovače tuhnutí a tvrdnutí
- přítomnost jednomocných kationtů (např.  $\text{Na}^+$ ,  $\text{K}^+$ ) o nízkých koncentracích snižuje obsah rozpuštěných  $\text{Ca}^{2+}$  iontů v roztoku, naopak vyšší koncentrace alkalických iontů zvyšuje rozpustnost silikátových a hlinitanových fází za současného potlačení předchozího efektu
- přítomnost určitých jednomocných aniontů (např.  $\text{Cl}^-$ ,  $\text{NO}_3^-$ ) nebo  $\text{SO}_4^{2-}$ , snižuje rozpustnost silikátových a hlinitanových fází, nicméně zvyšuje obsah rozpuštěného  $\text{Ca}^{2+}$ . Stejně tak jako v předchozím případě, nižší koncentrace aniontů podporuje prvně zmíněný účinek, jejich vyšší množství v roztoku však vede k upřednostnění druhého účinku

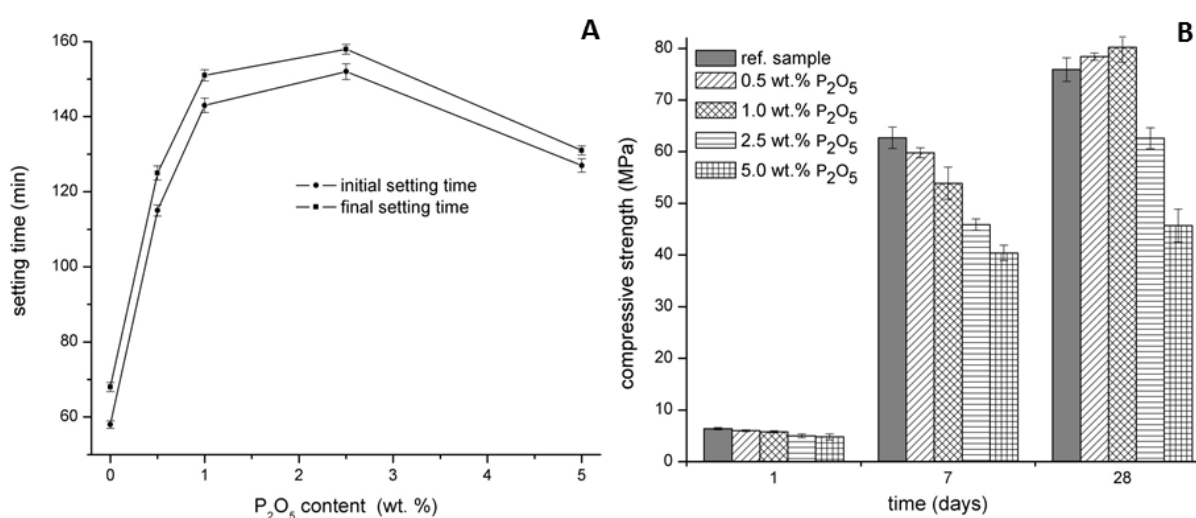
### 3.2.1 Anorganické přísady ovlivňující dobu tuhnutí AAS

Jedním z limitujících faktorů, které podstatně ovlivňuje širší využití AAS materiálů je jejich rychlá doba tuhnutí související s rychlou ztrátou zpracovatelnosti. Z tohoto důvodu není divu, že výzkum přísad ovlivňující dobu tuhnutí AAS je zaměřen téměř výhradně na zpomalovače tuhnutí, zatímco urychlující látky jsou popsány spíše z pohledu nežádoucího vlivu. Obecně existuje celá řada sloučenin, které mohou být použity jako retardéry tuhnutí. Velkou skupinu tvoří zejména organické sloučeniny, které se běžně používají jako přísady snižující obsah vody. Účinek tohoto typu přísad byl detailně popsán v předchozí kapitole 3.1.1. V rámci problematiky AAS je výzkum retardérů tuhnutí zaměřen zejména na využití anorganických solí. V běžných cementech působí vybrané anorganické soli doslova super-retardačním účinkem, což zřejmě vedlo i k jejich použití v AAS. Nevýhodou však zůstává relativně vysoká cena oproti organickým alternativám [55].

Se skupinou látek na bázi kyseliny fosforečné a jejích solí bylo provedeno a popsáno nejvíce experimentů, protože vykazovala nejvýraznější vliv na zpomalení tuhnutí alkalicky aktivovaných pojiv. Chang [107] ve své studii popisuje účinek  $\text{H}_3\text{PO}_4$  v AAS, kdy byla zjištěna silná závislost ovlivňující tuhnutí na přídatku této kyseliny o různé molární koncentraci. Při koncentraci 0,78 M byl zjištěn nepatrný vliv na dobu tuhnutí, o něco větší vliv byl zaznamenán při koncentraci v rozmezí 0,80–0,84 M a extrémně silný retardační účinek byl

pozorován při koncentraci 0,87 M. Přídavek kyseliny, však souvisel s vysokým smrštěním a snížením pevností v tlaku. Gong a Yang [108] pozorovali silný retardační vliv fosforečnanu sodného. Mechanismus účinku této soli byl vysvětlen precipitací fosforečnanu vápenatého, který v počáteční hydrataci vázal vápenaté ionty v roztoku, což způsobilo zpomalení tvorby pojivových fází.

Zpřesněním chemického působení fosforečnanu sodného v AAS byla věnována studie **Kaliny a Bílka** [109]. V této práci byly ověřeny retardační účinky  $\text{Na}_3\text{PO}_4$ , které souvisely s výrazným prodloužením počátku a konce tuhnutí a vlivem i na mechanické vlastnosti AAS (Obr. 21).

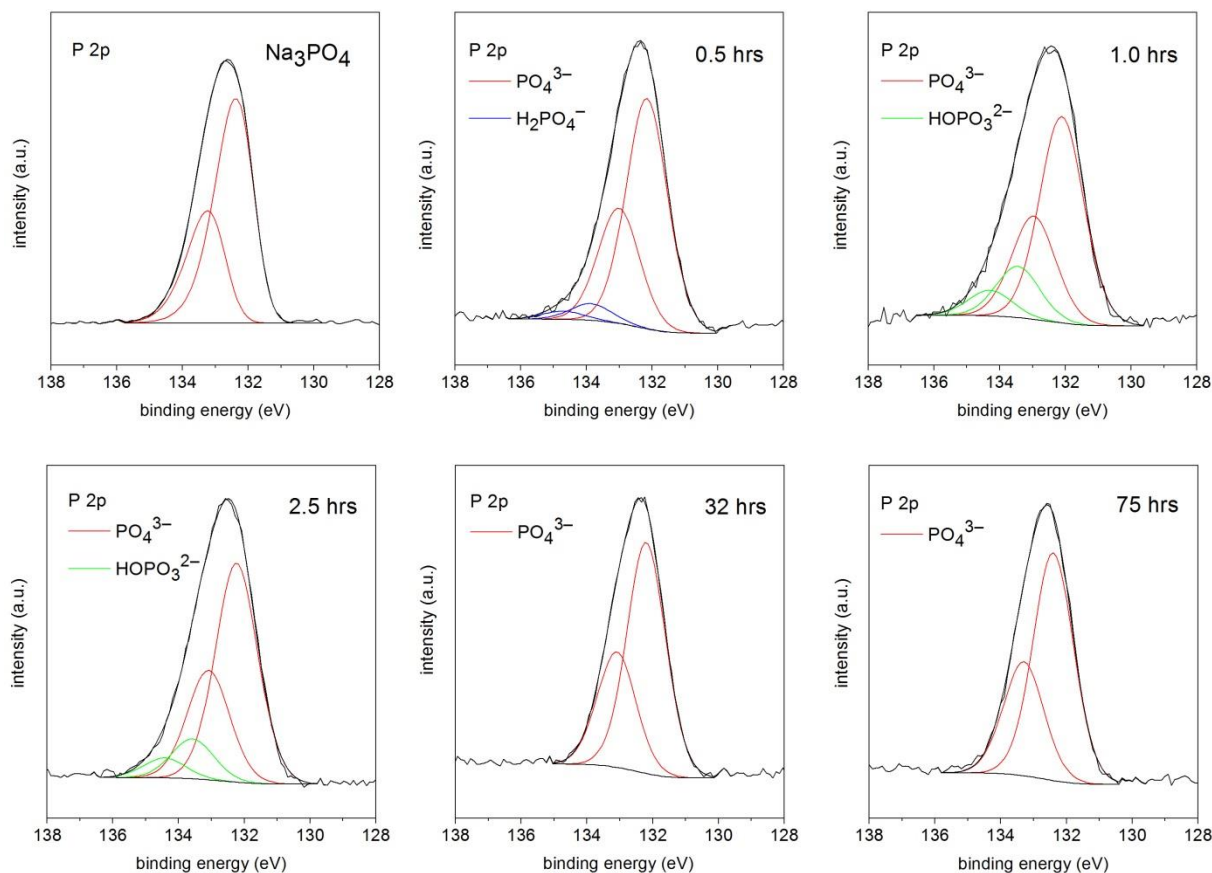


**Obr. 21: Vliv přídavku  $\text{Na}_3\text{PO}_4$  (přepočteno na  $\text{P}_2\text{O}_5$ ) na počátek a konec tuhnutí (A), mechanické vlastnosti (B) AAS; převzato z Kalina a kol. (Příloha XI) [109]**

Zároveň však bylo popsáno i působení fosforečnanu sodného během prvních hodin hydratačního procesu. Kombinací Ramanovy a rentgenové fotoelektronové spektroskopie (Obr. 22) bylo prokázáno, že vápenaté ionty jsou v počáteční fázi hydratace vázány ve struktuře dihydrogen a hydrogenfosforečnanů a brání tak nukleaci a růstu vznikajícího C-S-H gelu. Stabilita vápenatých hydrogenfosforečnanů v alkalickém prostředí AAS je však nízká, což vede k jejich opětovnému rozpuštění a následné tvorbě méně rozpustných fází jako je C-S-H gel a vápenatý hydroxyapatit.

Zpomalovače tuhnutí na bázi fosforečných solí se ukazují jako velmi vhodné přísady jak v systémech AAS, tak i v jiných alkalicky aktivovaných pojivech [110]. Tyto sloučeniny dokáží nejen účinně zpomalit proces tuhnutí, ale mají i pozitivní efekt na dlouhodobé pevnosti zkoumaných materiálů [109,110]. V alkalicky aktivovaných systémech byl ověřen i účinek boritanů, jejichž retardační účinky v pojivech z portlandského cementu je velmi dobře znám [111]. Nicholson a kol. [112] však zjistili, že výraznějšího zpomalení hydratace je dosaženo až při vysoké dávce soli (konkrétně 7 hm. %). Při takové koncentraci boritanů je však pevnost těchto pojiv výrazně negativně ovlivněna. Zajímavým zpomalovačem z pohledu AAS je i chlorid sodný. Ve studii Tallinga a Brandštetra [13] fungoval nízký přídavek NaCl (4 hm. %) jako urychlovač tuhnutí, naopak jeho vyšší množství (8 hm. %) vykazovalo nejen zpomalení hydratace, ale dokonce došlo k zastavení reakcí i vývoje mechanických pevností.

V jiném systému AAS byly pozorovány významné retardační účinky této soli při koncentracích přesahujících 20 hm. %, kdy konečná pevnost pojiva nebyla téměř ovlivněna [113]. Z dlouhodobého hlediska jsou však dávky tak velkého množství chloridu zejména v rámci vyztužených betonů dosti problematické.



**Obr. 22: XPS spektra různých stádií hydratace AAS s přidavkem fosforečnanu sodného; převzato z Kalina a kol. (Příloha XI) [109]**

### 3.2.2 Minerální přísady/příměsi

V následujících kapitolách jsou sumarizovány dosavadní výsledky výzkumu týkající se anorganických látek, které většinou známe v systémech na bázi OPC jako tzv. příměsi. Dále uvedené látky však i ve velmi malém množství dokáží významně ovlivnit vlastnosti připravených AAS. Zároveň je diskutován vliv těchto anorganických látek ve vyšším obsahu než 5 hm. %, což neodpovídá dle normy EN 934-2 [50] definici označující „chemická přísada do betonu“. Nicméně vzhledem k absenci norem, které by definovaly pojem chemické přísady v alkalicky aktivovaných systémech je zcela namístě shrnout účinek těchto látek v AAS i ve vyšších koncentracích.

#### Mikrosilika a speciálně upravený křemen

Mikrosilika nebo speciálně upravený křemen (SUK) jsou minerální příměsi široce využívané pro zvýšení mechanických vlastností AAS. Rashad a kol. [114] studovali přidavek SUK (od 5 do 30 hm. %) jako náhradu strusky v AAS aktivovaného pomocí sodného vodního skla. Výsledky prokázaly jednoznačně pozitivní vliv na vývoj pevností v tlaku po 28 dnech. Bylo

zjištěno, že vyšší přídavek SUK vede k nárůstu pevností. Pozitivní vliv na dlouhodobé pevnosti v tlaku (7 a 28 dní) byly pozorovány u AAS malt, ve kterých byl použit přídavek mikrosiliky (8 hm. %) a vápna (2 hm. %) spolu s  $\text{Na}_2\text{SO}_4$  (1 hm. %). Douglas a Brandštetr [59,115] vysvětlili, že přídavek mikrosiliky přímo souvisí se změnou distribuce velikosti pórů. Částice mikrosiliky s vysokým měrným povrchem působí jako filer a zaplňují tak intersticiální prostory uvnitř vytvrzené matrice, což vede ke zvýšení objemové hmotnosti a pevnosti materiálu. Kromě toho lze očekávat i příspěvek pucolánové reakce, což má opět pozitivní vliv na pevnosti materiálu. Zajímavé výsledky přinesla studie Rashada a Khalila [116], kde byla jako náhrada strusky využita mikrosilika (od 5 do 15 hm. %). Využití této příměsi opět přineslo zvýšení pevností v tlaku v porovnání s referenčním vzorkem. Nejlepší výsledky však vykazovaly AAS pasty s nejnižším testovaným přídavkem mikrosiliky (5 hm. %). Velmi podobné chování ukázal i systém AAS aktivovaný roztokem hydroxidu sodného [117]. Přídavek mikrosiliky (od 5 do 20 hm. %) vykazoval zvýšení pevností v tlaku, kdy nevyšších hodnot bylo dosaženo opět s nízkými náhradami strusky, konkrétně od 5 do 10 hm. %. Pokles pevností s vyšší přídavkem mikrosiliky zřejmě úzce souvisí se snížením zpracovatelnosti záměsi, jejímž výsledkem je nárůst nehomogenity výsledného systému. Vztah mezi přídavkem mikrosiliky a zpracovatelností prokázali Collins a Sanjayan [118]. Bylo zjištěno, že 10% náhrada strusky mikrosilikou vede k významné ztrátě zpracovatelnosti oproti referenčnímu AAS vzorku. Nutno však dodat, že některé studie [119] naopak zaznamenaly zlepšení zpracovatelnosti s přídavkem mikrosiliky. V této souvislosti bylo potvrzeno, že za zlepšením, či zhoršením zpracovatelnosti stojí zejména užití specifické kombinace mikrosilika/aktivátor nežli přídavek mikrosiliky jako takové.

Z uvedených studií lze konstatovat, že vhodný přídavek mikrosiliky a SUK má pozitivní vliv na zvýšení pevností AAS materiálů v podmínkách blízké laboratorním teplotám. Odlišná situace nastává vystavením AAS s přídavkem mikrosiliky nebo SUK vysokým teplotám. Rashad a Khalil [116] pozorovali velmi dobrou objemovou stálost referenčních vzorků AAS při nárůstu teploty až do 1 000 °C, zatímco alkalicky aktivované pasty s rostoucím přídavkem mikrosiliky jevíly značnou objemovou nestabilitu související s výrazným poklesem pevností materiálu. AAS systémy s přídavkem mikrosiliky rovněž neobstály v průběhu vystavení teplotním šokům. V procesu žíhání na teplotu 800 °C a následného rychlého zchlazení na laboratorní teplotu vykazovaly referenční vzorky AAS až 1,75krát vyšší odolnost, než vzorky s mikrosilikou. Autoři vysvětlují horší teplotní odolnost vzorků s mikrosilikou na základě pozorované vyšší tvorby akermanitu v referenčním vzorku, která „přechází“ do pojivové fáze.<sup>1</sup> Výrazné objemové změny však spíše souvisí s charakterem vytvořené pojivové fáze a její devitifikací s rostoucí teplotou, což bylo potvrzeno výzkumem Bernal a kol. [120].

Pozitivní účinek přídavku mikrosiliky v souvislosti se snížením smrštění vysycháním AAS byl studován Aydinem [121]. Vzorky aktivované sodným vodním sklem vykazovaly výraznou redukci smrštění s rostoucím přídavkem mikrosiliky (až do 20 hm. %). Rozdílné výsledky však představuje výzkum Matalkah a kol. [122], kteří studovali vliv různých přísad a příměsí na smrštění vysycháním AAS aktivované rovněž sodným vodním sklem. Bylo zjištěno, že přídavek mikrosiliky (5 hm. %) vykázal o 11 % vyšší smrštění po 60 dnech ve srovnání s

---

<sup>1</sup> Zmíněné vysvětlení založené na XRD analýze se jeví jako více než nepřesvědčivé, neboť zkoumané vzorky nebyly měřeny pomocí Rietveldovy metody, tedy nelze výsledná spektra kvantifikovat.

kontrolním vzorkem. Je patrné, že názory na užití mikrosiliky jako účinné přísady k redukcí smrštění AAS se liší. Vzhledem k velmi nízkému počtu publikovaných výsledků je zapotřebí dalšího výzkumu v této oblasti.

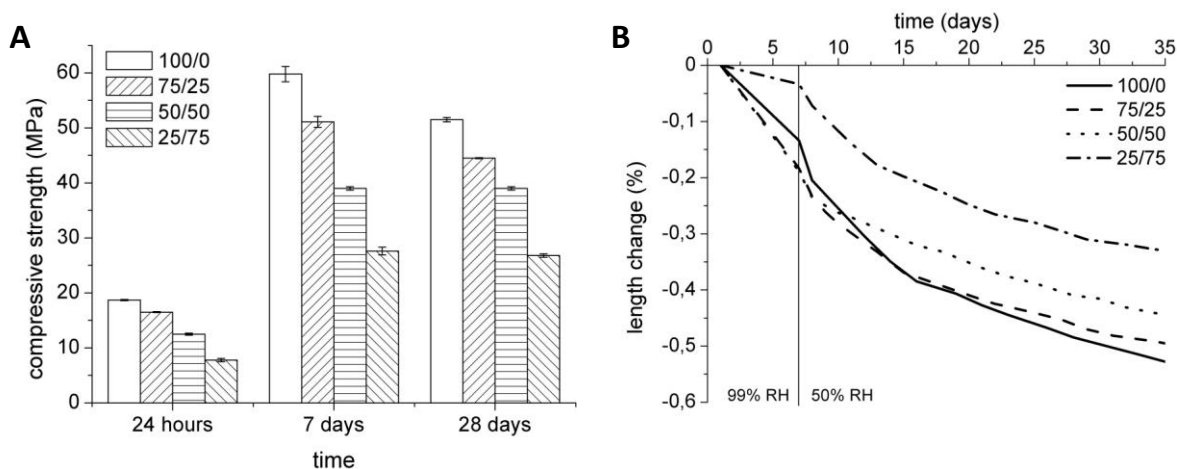
## Popílek

Účinek popílků byl v AAS systémech studován zejména z pohledu vlivu na zpracovatelnost, dobu tuhnutí a pevnost materiálu. Nutno zmínit, že níže diskutované výsledky jednotlivých výzkumů jsou založeny zejména na přidavku vysokoteplotních popílků s typickým složením a charakterem daným procesem jejich vzniku. Collins a Sanjayan [118] studovali částečné nahrazení VPS popílkem a zjistili jeho pozitivní efekt na zpracovatelnost celého systému. K velmi podobným výsledkům dospěly nezávisle na sobě i ostatní studie [13,15]. Přídavek popílku má vliv i na dobu tuhnutí AAS. Bylo zjištěno [123], že náhrada VPS popílkem ve vysokém množství (90% náhrada) oddaluje dobu tuhnutí až o několik hodin. Důležitým faktorem je i typ použitého aktivátoru. Sugama a kol. [124] prokázali, že doba tuhnutí AAS s náhradou VPS (do 50 %) vzrůstá při aktivaci sodným vodním sklem s vysokým silikátovým modulem (3,22; 2,50). Naproti tomu užitím roztoku vodního skla s nižším modulem (2,00) došlo k podstatnému urychlení doby tuhnutí.

Z hlediska vlivu přidavku popílku na pevnosti AAS lze obecně říci, že dochází spíše k jejímu zhoršení [15,74,121,123,125,126]. Nicméně i zde hraje zásadní roli volba alkalického aktivátoru, která tuto situaci může významně změnit. Shi a Day [127] testovali pevnost v tlaku a tahu za ohybu vzorků s 50% náhradou VPS popílkem. Alkalickou aktivací pomocí roztoků hydroxidu sodného a vodního skla bylo zjištěno, že vzorky s přidavkem popílku vykazovaly vždy nižší pevnosti v porovnání s referencí. Nepříznivou situaci při aktivaci vodním sklem z pohledu pevností lze změnit přidavkem vápna. Douglas a Brandštetr [59] potvrdili, že 5 a 10% náhrada strusky popílkem, ve směsi aktivované roztokem obsahující sodné vodní sklo a 2 % vápna, má sice negativní dopad na krátkodobé jednodenní pevnosti materiálu, ale z dlouhodobého hlediska (7 a 28 dní) bylo dosaženo vyšších pevností. Příznivý vliv přidavku malého množství vápna na vývoj pevností byl sledován i ve výzkumu Guerrieri a Sanjayana [128], kde vzorky s 35% náhradou strusky popílkem vykazovaly nejvyšších hodnot pevností v tlaku.

Pevnost AAS je rovněž úzce spojena s podmínkami vytvrzování. Výsledky výzkumného projektu TAČR-GAMA TG01010054-4 (odpovědný řešitel **Kalina L.**) [129] naznačují přímou souvislost mezi vývojem pevností v tlaku a smrštěním vysycháním. Bylo potvrzeno, že vysoká míra smrštění AAS uložených za podmínek relativní vlhkosti přibližně 50 % zapříčinila z dlouhodobého hlediska pokles pevností, které byly důsledkem tvorby trhlin iniciované vysokým smrštěním materiálu. **Kalina a kol.** [130] prokázali, že náhrada strusky vysokoteplotním popílkem vedla ke snížení nežádoucího smrštění a postupnému nárůstu pevností (Obr. 23). Přestože vzorky s popílkovou náhradou nedosáhly po 28 dnech pevností vzorků připravených aktivací samotné VPS, výsledné betonové prefabrikáty nevykazovaly viditelné trhliny, což v konečném důsledku vedlo ke zvýšení trvanlivosti vyrobených betonových dílců. Redukce smrštění přidavkem popílků může být vysvětlena následovně. Jedním z možných důvodů je celkový charakter pojivových fází. Aktivací strusky a popílku vznikají dva typy gelů, konkrétně C-A-S-H a N-A-S-H gel [131]. Rozdílný poměr vytvořených gelů, které mají odlišnou hustotu [132], ovlivňuje celkovou distribuci velikosti pórů [72], což je jedním z klíčových parametrů z hlediska vývoje smrštění. Důležitou roli hraje rovněž tzv.

„zředovací efekt“. V případě použití popílků lze očekávat nižší vývoj pojivové fáze, matrice je tedy více porézní a mechanismy kapilárních, nebo rozpojovacích tlaků diskutovaných v kapitole 3.1.2 přestávají být tak dominantní.



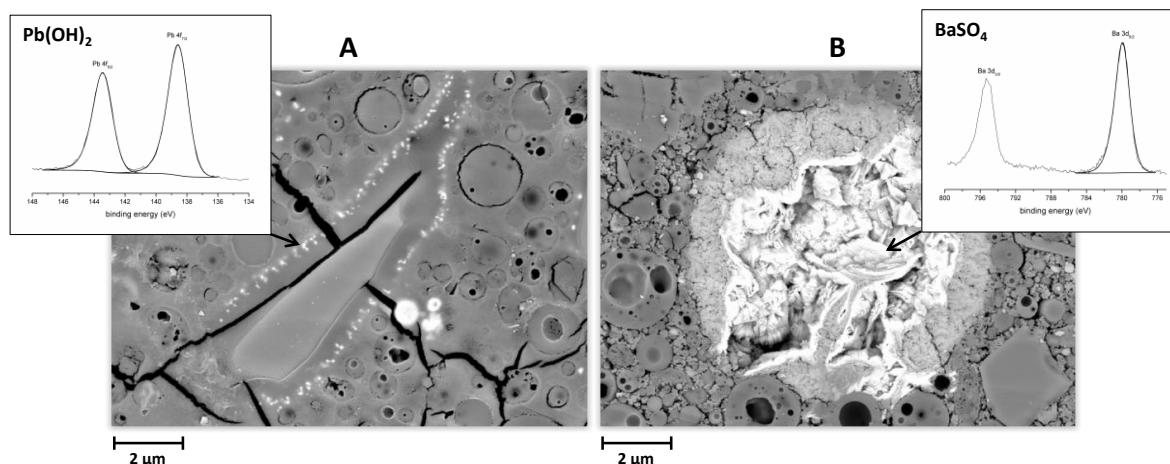
**Obr. 23: Vývoj pevností v tlaku (A) a smrštění vysycháním (B) betonových vzorků s postupnou náhradou strusky vysokoteplotním popílkem, převzato z Kalina a kol. [130]**

Přídavek popílku v AAS rovněž zvyšuje odolnost materiálu v agresivním prostředí. Sugama a kol. [124] vystavili vzorky s různým poměrem struska/popílek působení roztoku kyseliny sírové o pH = 1,1. Ukázalo se, že záměsí se stejným množstvím strusky a popílku měly v průběhu testovacího období nejnižší úbytek hmotnosti, což svědčí o jejich vyšší stabilitě v kyselém prostředí oproti materiálům aktivovaným pouze s VPS, které naopak vykazovaly nejvyšší úbytek hmotnosti. Alkalicky aktivované materiály s přídavkem popílků byly testovány i v prostředí síranů. Ismail a kol. [133] potvrdili, že v roztoku  $\text{Na}_2\text{SO}_4$  nebyl zaznamenán žádný negativní vliv. Naopak při expozici roztoku  $\text{MgSO}_4$  došlo k vysoké expanzi, která měla za následek úplnou ztrátu mechanických vlastností. V podmínkách síranu hořečnatého dochází k dekalifikaci pojivového systému za současné precipitace dihydrátu síranu vápenatého odpovědného za nežádoucí objemové změny.

Rozsáhlým studiem trvanlivosti strusko-popílkových alkalicky aktivovaných pojiv (50 hm. % popílku) se zabývali Šafář a Kalina [134], kteří hodnotil její aspekty z pohledu síranové odolnosti, odolnosti vůči kyselinám, karbonatoci, mrazuvzdornosti a odolnosti povrchové vrstvy vůči vodě a chemickým rozmrazovacím látkám. Bylo zjištěno, že 5% roztok  $\text{Na}_2\text{SO}_4$  nezpůsobil po 84 dnech působení žádné výrazné změny pevnosti v tahu za ohybu a pevnosti v tlaku. Rozměry všech vzorků taktéž zůstaly nezměněny. Alkalicky aktivovaný materiál vykazoval stejnou odolnost vůči působení  $\text{Na}_2\text{SO}_4$  jako materiál na bázi portlandského cementu. Po 56 dnech ponoření betonových těles v roztoku kyseliny octové o pH 4,0–4,5 vykazoval AAM mnohem nižší relativní ztrátu hmotnosti v čase v porovnání se vzorky na bázi OPC. Orientační zkoušky pevnosti v tlaku ukázaly, že zatímco pevnost AAM se nezměnila, pevnost cementového betonu klesla přibližně o polovinu. V prostředí 1%obj.  $\text{CO}_2$  nevykazoval cementový beton po 56 dnech téměř žádné projevy karbonatace, zatímco hloubka karbonatace AAM byla dle fenolftaleinové metody v průměru 8–11 mm. Odolnost AAM vůči karbonatoci je tedy značně nižší, než odolnost cementového betonu. Mrazuvzdornost materiálů byla zkoumána cyklickým zmrazováním a rozmrazováním vodou

nasycených betonových vzorků. Po 100 cyklech nedošlo v žádném z materiálů k výraznému poklesu pevností. Alkalicky aktivovaný materiál byl v testu shledán minimálně stejně mrazuvzdorným, jako cementový beton. Odolnost povrchu betonových krychlí vůči působení vody a chemických rozmrazovacích látek byla zkoumána ponořením jedné ze stěn krychle do 3% roztoku NaCl a následně vystavena cyklickému zmrazování/rozmrazování. Povrch AAM byl rozpadlý již po 25 cyklech, zatímco cementový beton vydržel 50 cyklů. Povrchová vrstva AAM tedy byla v tomto testu méně odolná, než povrch cementového betonu.

Směsná alkalicky aktivovaná pojiva strusky a popílku byla rovněž testována z pohledu jejich schopnosti imobilizovat těžké kovy. **Kalina, Koplík a kol.** [135,136] prokázali, že pojiva s přísadkou popílku mají velký potenciál účinně imobilizovat těžké kovy (Pb, Zn, Cu, Ni, Cr, Ba) ve své struktuře. Imobilizační mechanismus může probíhat na základě jejich fixace v matici chemickou vazbou nebo fyzikálním procesem zapouzdření. Bylo zjištěno, že olovo se může zabudovávat do struktury chemickou vazbou za vytvoření  $Pb_3SiO_4$  [137]. Metodou XPS byla rovněž prokázána schopnost tvorby nerozpustných sloučenin hydroxidů ( $Pb(OH)_2$ ,  $Cu(OH)_2$ ), v případě Ba a Hg pak síranů ( $BaSO_4$ ) nebo sulfidů ( $HgS$ ,  $Hg_2S$ ) [138,139] (Obr. 24).



**Obr. 24: Imobilizace olova tvorbou nerozpustného hydroxidu olovnatého – drobné bílé útvary (A) a barya ve formě síranu barnatého (B); převzato z Koplík, Kalina a kol. (Příloha IX) [138]**

### Metakaolin

Alkalická aktivace metakaolinu je velmi dobře známá z pohledu tvorby tzv. geopolymerních struktur. Důležitá je však i jeho role z hlediska použití jako přísady/příměsi v AAS. Částečná náhrada strusky metakaolinem například významně ovlivňuje dobu tuhnutí celého systému, kdy dochází ke zpomalení počátku tuhnutí [38,140]. Na proces hydratace má metakaolin vliv i ve vztahu k polykondenzačním reakcím, které jsou podpořeny díky vyššímu začleňování hlinitanového tetraedru do struktury gelu [141]. Bylo zjištěno, že náhrada strusky metakaolinem má za určitých podmínek pozitivní efekt na vývoj pevností [41,142,143]. Tento jev zřejmě souvisí s vyšší koncentrací rozpuštěných hlinitanových tetraedrů, které se následně mohou začleňovat do struktury pojivové fáze. Rovnaník [144] prokázal, že teplota vytvrzení hraje velmi důležitou roli v procesu utváření pojivové fáze aktivovaného metakaolinu. Důležitým faktorem je i charakter vzniklého gelu. Fernandez-Jimenez a

Palomo [145] potvrdili, že tvorba hlinitokřemičitanového gelu bohatého na hliník významně zvyšuje pevnost materiálu. Přídavek metakaolinu do AAS však nemusí vždy nutně vést ke zvýšení mechanických vlastností. Vysoký měrný povrch a vrstevnatá struktura částic metakaolinu může mít za následek potřeby vyššího vodního součinitele [146]. Nadbytek vody následně souvisí s nižším vývojem pevností, naopak nedostatek s rychlou ztrátou zpracovatelnosti, která rovněž ovlivňuje výsledné mechanické vlastnosti [38,147]. Přídavek metakaolinu ovlivňuje také trvanlivost připravovaného materiálu. Bernal a kol. [143] studovali absorpci vody, kapilární nasákavost a s tím související průnik chloridových iontů do struktury betonu. Výsledky naznačují, že přídavek metakaolinu významně snižuje zmíněné testované parametry, což obecně souvisí s vyšší odolností materiálu vůči pronikání nežádoucích látek do jeho struktury.

Motivací pro samotný výzkum a vývoj pojiv na bázi alkalicky aktivovaného metakaolinu se staly série požárů ve Francii mezi roky 1970–72. Zvýšení ohnivzdornosti hořlavých materiálů bylo docíleno použitím ochranné vrstvy na bázi aktivovaného metakaolinu, později patentovaného pod názvem „geopolymer“ [148]. Z tohoto důvodu byl sledován i vliv přídavku metakaolinu v AAS související se zvýšením žáro- a ohnivzdornosti. Z hlediska odolnosti materiálu vůči vysokým teplotám (~1 000 °C) a následnému zchlazení na laboratorní teplotu bylo zjištěno, že směsná pojiva na bázi strusky a metakaolinu vykazovala vysokou ztrátu pevností v porovnání se vzorky aktivované pouze metakaolinem. Důvodem je koexistence geopolymerní fáze společně s C-A-S-H gelem. Přítomnost vápníku v C-A-S-H gelu způsobuje snížení podílu skelné fáze, která je nosičem pevností po zchlazení celého systému [41]. Při vystavení AAS plamenu o teplotě 1 100 °C byla prokázána vyšší ohnivzdornost se stoupajícím množstvím metakaolinu v záměsi [140].

### Portlandský cement

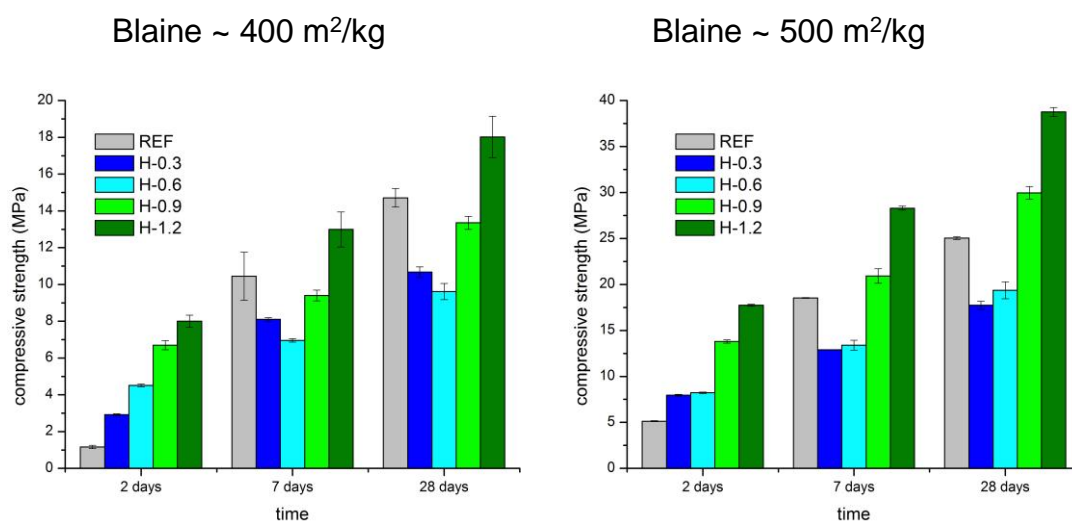
Přídavek portlandského cementu do AAS může způsobovat změny v samotném procesu tuhnutí [149,150]. Nicméně jeho přídavek do AAS souvisí především s pozitivním efektem na vývoj pevností, což bylo zaznamenáno v mnoha studiích [149,151-153]. Důvodem je vyšší koncentrace rozpuštěných hlinitanových a křemičitanových fragmentů v roztoku, které principem polykondenzačních reakcí dávají vzniknout většímu množství pojivové fáze odpovědné za nárůst pevností materiálu. Některé studie [74,149,154] však zaznamenaly pokles pevností s přídavkem OPC. Tento negativní jev úzce souvisí s volbou a především koncentrací použitého alkalického aktivátoru. Martinez-Ramirez a Palomo [155] proto zkoumali, jak ovlivní vysoká koncentrace  $\text{OH}^-$  iontů hydratační mechanismus portlandského cementu. Bylo zjištěno, že ačkoli je hydratace cementu v prvních minutách od smíchání s alkalickým aktivátorem rychlejší, celkové teplo, uvolněné po 24 hodinách, je výrazně vyšší při hydrataci s vodou. Vysvětlení je následující: V prvních minutách hydratace dochází k velmi rychlému rozpouštění  $\text{C}_3\text{S}$  fáze a následně precipitaci nerozpustných vápenatých sloučenin, což vede k poklesu koncentrace  $\text{Ca}^{2+}$  v roztoku a tedy k opětovnému zvýšení rozpouštění trikalciem silikátu. Na druhou stranu, hydratační proces je následně velmi rychle zpomalen a to zejména díky vysoké koncentraci  $\text{OH}^-$ , které posouvají rovnováhu hydratačních reakcí  $\text{C}_3\text{S}$  a  $\text{C}_2\text{S}$  na opačnou stranu, což zabraňuje normálnímu průběhu hydratace. Alkálie mají rovněž vliv i na hydrataci aluminátových fází. Díky silně zásaditému prostředí přechází sádrovec v cementu do roztoku tvořeného hydroxidem vápenatým a síranem alkalických kovů. Hydratace  $\text{C}_3\text{A}$  tak není regulována běžně vznikajícím ettringitem,

což podporuje tvorbu kalcium-alumino-hydrátů. V systémech s vysokou koncentrací alkalického aktivátoru bylo navíc překvapivě zjištěno vyšší množství tvorby portlanditu než u cementu hydratovaného vodou. Extrémně vysoká hladina alkality může dokonce způsobovat rozklad vznikajícího C-S-H gelu vedoucí v silně zásaditých podmínkách k tvorbě  $\text{Ca}(\text{OH})_2$ , ale i  $\text{SiO}_2$ , jehož přítomnost byla detekována metodou rentgenové difrakce.

### Hybridní systémy

Zajímavou kombinací, která spojuje charakteristiky tradičního portlandského cementu a alkalicky aktivovaných materiálů, představují tzv. hybridní systémy. Produkce hybridních pojiv může být docílena pomocí dvou různých přístupů. Prvním z nich je aktivace směsi hlinítkřemičitanů (OPC+VPS) vhodným aktivátorem, což představuje konvenční způsob přípravy AAM. Druhou možností je produkce speciálního typu cementu, kde aktivátor je již v pevné formě smíchán společně s ostatními složkami. Taková pojiva poskytují některé zajímavé výhody. Především mohou být aktivovány pouze vodou, což přináší značné usnadnění jejich produkce v porovnání s běžně používaným postupem přípravy AAM, kde práce se silně alkalickými roztoky mohou způsobovat jistá omezení ve výrobním procesu. Další výhoda spočívá v jejich případném zařazení do Evropské normy EN 197-1 [156], ve které mohou být klasifikovány jako CEM III vysokopecní cementy. Obsah alkálií, běžně vyjádřeno jako  $\text{Na}_2\text{O}_{\text{EKV}}$ , se v požadavcích na chemické vlastnosti cementů v této normě nepředepisuje, což poskytuje těmto hybridním systémům bezproblémové začlenění mezi ostatní typy produkovaných cementů.

Výzkumem hybridních cementů s možným aplikačním potenciálem se zabýval ve své studii **Kalina a kol.** [33] Podle požadavků normy EN 197-1 [156] na fyzikální a chemické vlastnosti cementů byl navržen nový typ cementu příslušící do skupiny CEM III/C, jehož hlavní složkou je vysokopecní struska, portlandský slínek (5 hm. %) a alkalický aktivátor získaný z průmyslového odpadu. Navržené typy hybridních cementů splňovaly všechny požadavky vyplývající z výše uvedené normy. Nicméně některé parametry vstupních surovin musí být pečlivě kontrolovány. Výsledky výzkumu prokázaly silnou souvislost mezi testovanými mechanickými vlastnostmi a měrným povrchem vysokopecní strusky (Obr. 25).



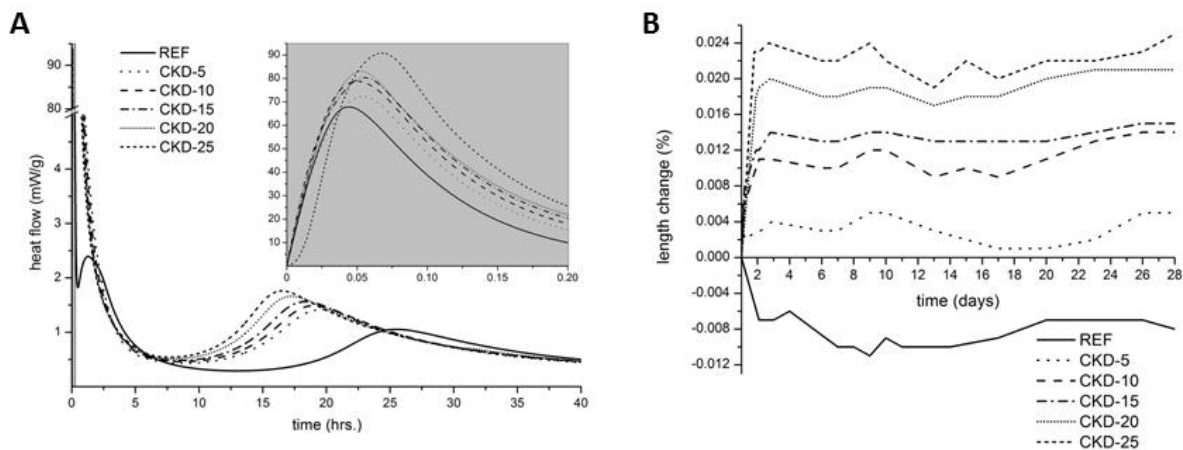
Obr. 25: Vývoj pevností v tlaku hybridních cementů s různou jemností částic strusky a dávkou aktivátoru vyjádřenou hmotnostním poměrem  $\text{Na}_2\text{O}/\text{VPS}$ ; převzato z Kalina a kol. [33]

Pro potřeby produkce hybridních systémů je v tomto případě nezbytným požadavkem vysoká jemnozrnnost strusky s hodnotami měrného povrchu přesahující 500 m<sup>2</sup>/kg, stejně tak i dostatečného množství alkalického aktivátoru. Splněním těchto požadavků, lze docílit produkce netradičního typu cementu s vysokým ekologickým i ekonomickým přínosem. Nutné je však zmínit, že v této oblasti je třeba dalšího výzkumu, který bude cílit především na posouzení trvanlivosti materiálů připravených s použitím těchto hybridních cementů.

### Vedlejší produkty z výroby portlandského cementu

Zajímavou přísadou/příměsí z pohledu řešení některých nežádoucích vlastností AAS je použití sekundárních surovin z výroby portlandského cementu, konkrétně cementářských by-passových odprašků. Chemické složení odprašků velmi závisí na charakteru vstupních surovin, ale i na používaném palivu v průběhu výpalu portlandského slínku. Obecně lze říct, že odprašky obsahují sloučeniny s nízkou teplotou tání, jako jsou například sírany a chloridy alkalických kovů, dále pak surovinovou moučku, stejně tak i slínkové fáze (belit, vápno). Z důvodu vysokého obsahu alkálií nemohou být navraceny zpět do výrobního procesu, proto jsou velmi často odváženy na skládky. Pouze malá část je přimíchávána společně s cementem, tak aby neovlivnila jeho výsledné chování v průběhu hydratačního procesu. Chemické složení odprašků může být nicméně velmi výhodné z hlediska aktivačního procesu VPS.

**Kalina a kol.** [157-160] popsali účinek odprašků v AAS v několika odborných pojednáních. Bylo zjištěno, že obsah alkálií významně zvyšuje pH aktivačního roztoku, podporuje tak rozpouštění částic strusky, což přispívá k vyšší a zároveň rychlejší tvorbě pojivové fáze. Tyto předpoklady byly potvrzeny na základě stanovení pomocí isotermické kalorimetrie (Obr. 26A). Příliš vysoký obsah odprašků však může vést i k velmi rychlé ztrátě zpracovatelnosti a následné nehomogenitě vzorků související s poklesem mechanických vlastností. Tento negativní aspekt zřejmě souvisí s rychlou spotřebou záměsové vody na hydrataci volného CaO. Volný CaO se v odprašcích vyskytuje i ve formě tzv. mrtvě páleného vápna, které vzniká při teplotách nad 1 000 °C. Jeho pomalá reakce s vodou dává vznik vápennému hydrátu Ca(OH)<sub>2</sub>, který vykazuje expanzivní účinky projevující se až v průběhu tvrdnutí záměsi. Rozsáhlé smrštění AAS materiálů tak může být tímto způsobem značně kompenzováno (Obr. 26B). I přes některé výhody, které odprašky poskytují, však musíme konstatovat, že jejich použití v AAS se jeví jako neperspektivní. Mezi hlavní důvody patří zejména vysoký obsah chloridů, což zcela vylučuje jejich použití společně s ocelovou výztuží. Problematickým faktorem je i jejich nestálé složení. Během řešení evropského projektu H2020-GeoDust [161] byly sledovány změny v chemickém a fázovém složení odprašků odebraných v průběhu různých časových období. Odprašky vykazovaly poměrně značné výkyvy ve složení, zejména pak v obsahu volného CaO. Z uvedených důvodů je jejich použití pro průmyslovou produkci AAS materiálů nevhodné.



**Obr. 26: Vývoj tepelného toku (A) a délkových změn při RH = 100 % (B) alkalicky aktivované strusky s různým přidavkem by-passových cementářských odprašků (CKD), převzato z Kalina a kol. (Příloha IV) [157]**

### Hašené vápno

Využití samotného hašeného vápna jakožto alkalického aktivátoru VPS dalo vzniknout již na počátku minulého století prvním typům AAS [1]. Jeho přidavek zvyšuje především počáteční pevnosti materiálu, což bylo potvrzeno v několika výzkumných pracích [13,15,127,162]. Vysoká koncentrace vápenatých kationtů vede k tvorbě jak C-S-H, respektive C-A-S-H gelu, tak kalcium-aluminátovým fázím, jako například  $C_4AH_{13}$ . Charakter AAS pojiv s přidavkem hašeného vápna může být ovlivněn i jeho kombinací s jinými aktivátory. Shi a kol. [28] prokázali, že užitím  $Na_2SO_4$  dochází k vyššímu rozpouštění strusky, což přispívá k vyššímu vytvoření C-S-H gelu. Zároveň dochází i k tvorbě AFt fází. Obě vytvořené fáze jsou odpovědné za zvýšení počátečních pevností. Byly zkoumány i účinky hašeného vápna v kombinaci s jinými aktivátory. Collins a Sanjayan [162] pozorovali zvýšení zpracovatelnosti a oddálení doby tuhnutí záměsi při aktivaci společně se sodným vodním sklem. K podobným závěrům došel i Yang a kol. [163], kteří využívali jak roztok sodného vodního skla, tak uhličitanu sodného. Vliv hašeného vápna však přináší i negativní aspekty, především se jedná o nárůst vývoje smrštění vysycháním [162].

## Shrnutí vlivu minerálních přísad/příměsí v AAS

přísada/příměs	přídavek (hm. %)	pozitivní efekt	negativní efekt
mikrosilika a SUK	5–30	zvýšení pevnosti [114,116,117]	
	5–30		zhoršení mechanických vlastností při vysokých teplotách [114,120]
vysokoteplotní popílek	10	zlepšení zpracovatelnosti [13,15,118]	
	< 50 ( $M_s=3,22; 2,50$ )	oddálení tuhnutí [124]	
	< 50 ( $M_s= 2.00$ )		zrychlení doby tuhnutí [124]
	> 90		výrazné prodloužení doby tuhnutí [123]
	50		snížení pevností [127]
	5 (+ 2 % hašeného vápna)	zvýšení pevností (7 a 28 dní) [59]	snížení pevností (1 den) [59]
	10 (+ 2 % hašeného vápna)	zvýšení pevností (28 dní) [59]	snížení pevností (1 a 7 dní) [59]
	75; 50; 25	snížení smrštění [130]	pokles pevností [130]
	50	dobrá odolnost v kyselém prostředí $H_2SO_4$ [124] a $CH_3COOH$ [134]	
	50	žádné změny v prostředí $Na_2SO_4$ [133,134]	
	50		ztráta mechanických vlastností v prostředí $MgSO_4$ [133]
	50		vysoká míra karbonatace [134]
	50	vysoká mrazuvzdornost [134]	
50		nízká odolnost vůči CHRL [134]	
50	výborná schopnost imobilizace těžkých kovů [135,136]		
metakaolin	< 20	prodloužení doby tuhnutí [38,140]	
	25; 50	zrychlení polykondenzačních reakcí [141]	
	> 0	nárůst pevností [41,142,143]	
	> 0		riziko ztráty zpracovatelnosti a pevností [38,147]
	10; 20	snížení absorpce vody, kapilární nasákavosti a průniku chloridových iontů [143]	
	20		žádný pozitivní vliv na žárovzdornost materiálu [41]
	> 0	zvýšení ohnivzdornosti [140]	

přísada/příměs	přídavek (hm. %)	pozitivní efekt	negativní efekt
portlandský cement	30–80	zvýšení pevností (aktivátor 1% Na <sub>2</sub> SiO <sub>3</sub> ) [151]	
	50; 70	zvýšení dlouhodobých pevností (aktivátor Na <sub>2</sub> SO <sub>4</sub> ) [149,153]	snížení počátečních pevností (aktivátor Na <sub>2</sub> SO <sub>4</sub> ) [149]
	40	zvýšení počátečních pevností (aktivátor 2M NaOH) [152]	
	20; 40; 60; 80		snížení pevností (aktivátor 4; 6; 8 % Na <sub>2</sub> SiO <sub>3</sub> ) [154]
	30		snížení pevností (aktivátor 4 % Na <sub>2</sub> SiO <sub>3</sub> ) [74]
	30	žádný vliv na dobu tuhnutí (aktivátor Na <sub>2</sub> SO <sub>4</sub> ) [149]	
	0–30		výrazné zrychlení doby tuhnutí (aktivátor Na <sub>2</sub> SiO <sub>3</sub> ) [150]
cementářské by-passové odprašky	5–25	zrychlení a zvýšení tvorby pojivové fáze (RH=100%) [157]	
	5–20	zvýšení pevností (RH=100%) [157]	
	> 20		výrazná ztráta zpracovatelnosti, snížení pevností (RH=100%) [157]
	5–50	zvýšení počátečních pevností (autogenní podmínky) [160]	snížení dlouhodobých pevností (autogenní podmínky) [160]
	10–50		snížení počátečních a dlouhodobých pevností (RH = 99 %) [158]
	5–25	snížení smrštění (RH=100%) [157]	
	5–25	snížení autogenního smrštění [160]	
	50		vysoký expanzní účinek [159,160]
hašené vápno	< 5	zvýšení počátečních pevností [13,15,121,155]	
	1; 7,5	zvýšení zpracovatelnosti [162,163]	nárůst smrštění vysycháním [162]
	7,5	oddálení doby tuhnutí [163]	

## 4. Závěrečné shrnutí

Alkalicky aktivované materiály jsou velmi slibně se rozvíjející skupinou stavebních poživ. Jejich vyšší aplikační potenciál, který je v současnosti omezen z důvodu některých negativních vlastností, lze podpořit užitím různých přísad, ať už na organické, nebo anorganické bázi. V práci byly představeny účinky nejvíce používaných přísad, které zásadním způsobem ovlivňují charakter alkalicky aktivované strusky. Použití přísad v AAS vychází z potřeby řešení nejdůležitějších technologických omezení, jakými jsou zejména vysoké smrštění, nízká zpracovatelnost a rychlý počátek tuhnutí.

Byly diskutovány přísady, které redukuje rozsáhlé smrštění těchto materiálů. Z hlediska organických přísad vykazují sloučeniny na bázi oxyalkylenglykolů a aminoalkoholů schopnost redukce smrštění. Nicméně jejich přídavek musí být vždy pečlivě zváženo s ohledem na jejich negativní dopad na průběh hydratačních procesů. V této souvislosti bylo potvrzeno, že cesta snižování povrchového napětí pórového roztoku působením zmíněných přísad, na jejímž principu je postavena teorie kapilárního tlaku, nemusí vždy vést k účinné redukci smrštění. Zde je zapotřebí dalšího výzkumu, který by odhalil možnosti některých, dosud netestovaných látek účinně snižovat smrštění AAS bez nežádoucích vedlejších vlivů. Z tohoto důvodu je nutné se zaměřit na možnosti ovlivnění jiných kritérií, které by hrály významnou roli ve snižování smrštění. Velikost distribuce pórů je právě jedním z klíčových parametrů ovlivňující rozsah smrštění. Testování účinku provzdušňovacích přísad tak může představovat jistý posun v této oblasti výzkumu. Jako alternativa se nabízí i využití anorganických přísad a příměsí. Snižování smrštění bylo dosaženo přídavkem jak vysokoteplotního popílku, tak pomocí cementářských by-passových odprašků. Z dlouhodobého hlediska jsou však tyto přísady neperspektivní a to zejména díky prokazatelnému negativnímu dopadu na mechanické vlastnosti AAS, stejně tak i z pohledu jejich nestálého chemického složení.

K většímu úspěchu vedlo úsilí o zvýšení zpracovatelnosti připravovaných čerstvých záměsí AAS. V této oblasti došlo k pochopení mechanismu účinku běžně používaných plastifikačních přísad v systému AAS, což má za následek možnost výběru přísady s vhodným chemickým složením. Sloučeniny na bázi lignosulfonátů ukázaly, že i ve velmi malém množství dokáží výrazně zvýšit zpracovatelnost čerstvě namíchané AAS. Nicméně zásadní proměnnou řídicí efektivnost těchto přísad představuje samotná volba alkalického aktivátoru. Typ aktivátoru ovlivňuje náboj na zrnech strusky a tím i to, zda tyto povrchově aktivních látek budou v systému fungovat dle našich požadavků. Velkým překvapením se stalo úplné selhání použitelnosti nové generace superplastifikátorů na bázi polykarboxylátů v AAS systémech. Vysoké pH způsobuje rozklad těchto polymerních látek a jejich funkční mechanismus postavený na bázi sterického bránění je tak zcela eliminován. Z tohoto důvodu musí být do budoucna kladen vyšší důraz na zjištění stability organických přísad v silně alkalickém prostředí.

K dalším významným pokrokům došlo i z hlediska řešení předčasného tuhnutí AAS. Anorganické přísady na bázi fosforečnanů vykazují velmi silné retardační účinky a mohou být s výhodou využity v AAS. K oddálení počátku tuhnutí lze docílit i již zmiňovanými lignosulfonátovými plastifikátory. Oba typy přísad však mohou negativně ovlivnit počáteční

pevnosti materiálu, nicméně z dlouhodobého hlediska byl prokázán spíše pozitivní vliv na vývoj mechanických vlastností AAS.

Výzkum AAS byl zaměřen i na zhodnocení vlivu nejvíce používaných minerálních přísad a příměsí, které mohou rovněž přinést některé pozitivní účinky. Mnohé výzkumné práce řešily zvýšení mechanických vlastností AAS dosažených přidávkem mikrosiliky, SUKu, portlandského cementu nebo vápna. Vyšší trvanlivosti AAS z pohledu jejich odolnosti v silně chemicky agresivních prostředích lze docílit například přidávkem vysokoteplotního popílku nebo metakaolinu. Vytvořené pojivové fáze s použitím těchto přísad/příměsí mají rovněž výbornou schopnost imobilizovat toxické kovy ve své struktuře. Minerální přísady/příměsí tak mohou poskytnout mnohé benefity AAS materiálů ve smyslu jejich následného použití v praxi. V této souvislosti se otvírá možnost využití i některých netradičních nebo málo používaných minerálních přísad a příměsí, které jsou dostupné v dané lokalitě potenciální výroby AAS.

Bylo prokázáno, že využití organických a anorganických přísad a příměsí má mnohdy zcela zásadní vliv na chování alkalicky aktivované vysokopecní strusky. Současný výzkum musí nadále směřovat cestou vývoje charakteristických typů přísad, které by byly navrženy tak, aby jejich účinek nebyl negativně ovlivněn silně zásadité prostředí alkalické aktivace. Tímto způsobem lze následně připravit unikátní skupiny modifikovaných alkalicky aktivovaných materiálů, které by odkryly zcela nové možnosti jejich využití v průmyslové sféře.

## 5. Zkratky a symboly

AAM	alkalicky aktivovaný materiál
AAS	alkalicky aktivovaná struska
AEA	provzdušňovací přísada
AFm fáze	$[\text{Ca}_2(\text{Al,Fe})(\text{OH})_6] \cdot \text{X} \cdot n\text{H}_2\text{O}$ ; X=dvojmocný anion
AFt fáze	$[\text{Ca}_3(\text{Al,Fe})(\text{OH})_6 \cdot 12\text{H}_2\text{O}]_2 \cdot \text{X}_3 \cdot n\text{H}_2\text{O}$ ; X=dvojmocný anion
C <sub>3</sub> A	trikalcium aluminát
C-A-S-H gel	kalcium-aluminát-silikát-hydrát
CMC	kritická micelární koncentrace
C-(N)-A-S-H gel	kalcium-aluminát-silikát-hydrát s alkalickým kovem ve své struktuře
C-S-H gel	kalcium-silikát-hydrát
C <sub>2</sub> S	dikalcium silikát
C <sub>3</sub> S	trikalcium silikát
DP	stupeň depolymerace
HLB	hydrofilně-lipofilní rovnováha
MAS-NMR	nukleární magnetická rezonance (magic angle spinning)
N(K)-A-S-H gel	aluminát-silikát-hydrát s alkalickým kovem ve své struktuře
OPC	běžný portlandský cement
SRA	přísada redukující smrštění
SUK	speciálně upravený křemen
VPS	vysokopecní struska
XPS	rentgenová fotoelektronová spektroskopie
XRD	rentgenová difrakční analýza

## 6. Literatura

1. Kuhl, H. Slag cement and process of making the same. 1908.
2. Purdon, A.O. The action of alkalis on blast-furnace slag. *Journal of the Society of Chemical Industry* **1940**, *59*, 191-202.
3. Glukhovskiy, V.D. *Soil silicates*. Gostroiizdat Publish: Kyjev, 1959.
4. Davidovits, J. *Geopolymer chemistry and applications*. Institut Ge'opolyme`re: Saint-Quentin, 2008.
5. Krivenko, P. Why alkaline activation-60 years of the theory and practice of alkali-activated materials. *Journal of Ceramic Science and Technology* **2017**, *8*, 323-334.
6. McCormick, A.V.; Bell, A.T.; Radke, C.J. Influence of alkali-metal cations on silicon exchange and si-29 spin relaxation in alkaline silicate solutions. *Journal of Physical Chemistry* **1989**, *93*, 1737-1741.
7. Glasser, L.S.D.; Harvey, G. The unexpected behavior of potassium aluminosilicate solutions. *Journal of the Chemical Society-Chemical Communications* **1984**, 664-665.
8. Xu, H.; Van Deventer, J.S.J. The geopolymerisation of alumino-silicate minerals. *International Journal of Mineral Processing* **2000**, *59*, 247-266.
9. Scrivener, K.L.; Juilland, P.; Monteiro, P.J.M. Advances in understanding hydration of portland cement. *Cement and Concrete Research* **2015**, *78*, 38-56.
10. Duxson, P.; Provis, J.L. Designing precursors for geopolymer cements. *Journal of the American Ceramic Society* **2008**, *91*, 3864-3869.
11. Wan, H.W.; Shui, Z.H.; Lin, Z.S. Analysis of geometric characteristics of ggbs particles and their influences on cement properties. *Cement and Concrete Research* **2004**, *34*, 133-137.
12. Wang, P.Z.; Trettin, R.; Rudert, V. Effect of fineness and particle size distribution of granulated blast-furnace slag on the hydraulic reactivity in cement systems. *Advances in Cement Research* **2005**, *17*, 161-166.
13. Talling, B.; Brandstetr, J. Present state and future of alkali-activated slag concretes. *Fly Ash, Silica Fume, Slag, and Natural Pozzolans in Concrete, Vol 1-2* **1989**, *114*, 1519-1545.
14. Brough, A.R.; Atkinson, A. Sodium silicate-based, alkali-activated slag mortars part i. Strength, hydration and microstructure. *Cement and Concrete Research* **2002**, *32*, 865-879.
15. Wang, S.D.; Scrivener, K.L.; Pratt, P.L. Factors affecting the strength of alkali-activated slag. *Cement and Concrete Research* **1994**, *24*, 1033-1043.
16. Shi, C.J.; Day, R.L. A calorimetric study of early hydration of alkali-slag cements. *Cement and Concrete Research* **1995**, *25*, 1333-1346.
17. Teoreanu, I. The interaction mechanism of blast-furnace slag with water; the role of activating agents. *Cemento* **1991**, *8*, 91-97.

18. Rajaokarivonyandriambololona, Z.; Thomassin, J.H.; Baillif, P.; Touray, J.C. Experimental hydration of 2 synthetic glassy blast-furnace slags in water and alkaline-solutions (naoh and koh0.1n) at 40-degrees-c - structure, composition and origin of the hydrated layer. *Journal of Materials Science* **1990**, *25*, 2399-2410.
19. Shi, C.J.; Day, R.L. Some factors affecting early hydration of alkali-slag cements. *Cement and Concrete Research* **1996**, *26*, 439-447.
20. Novotný, R., Másilko, J., Šoukal, F. Admix ampule izotermického kalorimetru tamair. 2015.
21. Langová, M. Účinek plastifikátorů na chování a vlastnosti alkalicky aktivovaných materiálů. *diplovová práce* **2016**, *Vysoké učení technické v Brně*, školitel: Ing. Lukáš Kalina, Ph.D.
22. Bernal, S.A.; Provis, J.L.; Myers, R.J.; San Nicolas, R.; van Deventer, J.S.J. Role of carbonates in the chemical evolution of sodium carbonate-activated slag binders. *Materials and Structures* **2015**, *48*, 517-529.
23. Krizan, D.; Zivanovic, B. Effects of dosage and modulus of water glass on early hydration of alkali-slag cements. *Cement and Concrete Research* **2002**, *32*, 1181-1188.
24. Phair, J.W.; Van Deventer, J.S.J. Effect of silicate activator ph on the leaching and material characteristics of waste-based inorganic polymers. *Minerals Engineering* **2001**, *14*, 289-304.
25. Barbosa, V.F.F.; MacKenzie, K.J.D.; Thaumaturgo, C. Synthesis and characterisation of materials based on inorganic polymers of alumina and silica: Sodium polysialate polymers. *International Journal of Inorganic Materials* **2000**, *2*, 309-317.
26. Szklorzová, H., Bílek, V. Influence of alkali ions in the activator on the performance of alkali-activated mortars. In *3rd International Symposium on Non-Traditional Cement and Concrete*, ZPSV a.s.: Brno, 2008; pp 777-784.
27. Skvara, F.; Kopecky, L.; Kyskova, L.; Smilauer, V.; Alberovska, L.; Vinsova, L. Aluminosilicate polymers - influence of elevated temperatures, efflorescence. *Ceramics-Silikaty* **2009**, *53*, 276-282.
28. Shi, C.; Krivenko, P.V.; Roy, D.M. *Alkali-activated cements and concretes*. Taylor & Francis: London ; New York, 2006; p ix, 376 p.
29. FernandezJimenez, A.; Puertas, F. Influence of the activator concentration on the kinetics of the alkaline activation process of a blastfurnace slag. *Materiales De Construccion* **1997**, *47*, 31-42.
30. Richardson, I.G.; Brough, A.R.; Groves, G.W.; Dobson, C.M. The characterization of hardened alkali-activated blast-furnace slag pastes and the nature of the calcium silicate hydrate (c-s-h) phase. *Cement and Concrete Research* **1994**, *24*, 813-829.
31. Richardson, I.G.; Groves, G.W. The structure of the calcium silicate hydrate phases present in hardened pastes of white portland cement blast-furnace slag blends. *Journal of Materials Science* **1997**, *32*, 4793-4802.

32. Fernandez-Jimenez, A.; Puertas, F.; Sobrados, I.; Sanz, J. Structure of calcium silicate hydrates formed in alkaline-activated slag: Influence of the type of alkaline activator. *Journal of the American Ceramic Society* **2003**, *86*, 1389-1394.
33. Kalina, L.; Bílek, V.; Bradová, L.; Novotný, R.; Opravil, T.; Šoukal, F. In *Hybrid alkali-activated cements*, SynerCrete18 International Conference on Interdisciplinary Approaches for Cement-based Materials and Structural Concrete, Funchal, 2018; RILEM Publications: Funchal.
34. Provis, J.L. Alkali-activated materials. *Cement and Concrete Research* **2018**, *114*, 40-48.
35. Provis, J.L. Geopolymers and other alkali activated materials: Why, how, and what? *Materials and Structures* **2014**, *47*, 11-25.
36. Myers, R.J.; Bernal, S.A.; San Nicolas, R.; Provis, J.L. Generalized structural description of calcium-sodium aluminosilicate hydrate gels: The cross-linked substituted tobermorite model. *Langmuir* **2013**, *29*, 5294-5306.
37. Richardson, I.G. Tobermorite/jennite- and tobermorite/calcium hydroxide-based models for the structure of c-s-h: Applicability to hardened pastes of tricalcium silicate, beta-dicalcium silicate, portland cement, and blends of portland cement with blast-fumace slag, metakaolin, or silica fume. *Cement and Concrete Research* **2004**, *34*, 1733-1777.
38. Bernal, S.A.; Provis, J.L.; Rose, V.; de Gutierrez, R.M. Evolution of binder structure in sodium silicate-activated slag-metakaolin blends. *Cement & Concrete Composites* **2011**, *33*, 46-54.
39. Bernal, S.A.; Provis, J.L.; Walkley, B.; Nicolas, R.S.; Gehman, J.D.; Brice, D.G.; Kilcullen, A.R.; Duxson, P.; van Deventer, J.S.J. Gel nanostructure in alkali-activated binders based on slag and fly ash, and effects of accelerated carbonation. *Cement and Concrete Research* **2013**, *53*, 127-144.
40. Ismail, I.; Bernal, S.A.; Provis, J.L.; Nicolas, R.S.; Hamdan, S.; van Deventer, J.S.J. Modification of phase evolution in alkali-activated blast furnace slag by the incorporation of fly ash. *Cement & Concrete Composites* **2014**, *45*, 125-135.
41. Bernal, S.A.; Rodriguez, E.D.; de Gutierrez, R.M.; Gordillo, M.; Provis, J.L. Mechanical and thermal characterisation of geopolymers based on silicate-activated metakaolin/slag blends. *Journal of Materials Science* **2011**, *46*, 5477-5486.
42. Regourd, M.; Thomassin, J.H.; Baillif, P.; Touray, J.C. Blast-furnace slag hydration - surface-analysis. *Cement and Concrete Research* **1983**, *13*, 549-556.
43. Glasby, T.D., J.; Genrich, R.; Aldred, J. Efc geopolymer concrete aircraft pavements at brisbane west wellcamp airport. In *Concrete 2015 Conference*, Melbourne Australia, 2015.
44. Svoboda, P.; Doležal, J.; Škvára, F.; Kopecký, L.; Lucuk, M. Beton bez cementu s názvem popbeton. *Silika* **2006**, *16*, 150-152.
45. Kalina, L.B., V.; Koplík, J.; Másilko, J.; Opravil, T.; Šoukal, F. Způsob výroby bezslínkových hydraulických geopolymerních materiálů s využitím odpadních technologických kalů z výroby vodního skla. 2016.

46. Kalina, L.B., V.; Koplík, J.; Novotný, R.; Mončeková, M.; Opravil, T. Výroba prvků dělicích stěn z alkalicky aktivovaného betonu. 2016.
47. Kalina, L.B., V.; Koplík, J.; Novotný, R.; Mončeková, M.; Opravil, T. Výroba prvků dělicích stěn z bezslínkového betonu. 2016.
48. Rovnaníková, P. *Omítky*. Společnost pro technologie ochrany památek: Praha, 2002; Vol. 1.
49. Aïtcin, P.C., Flatt, R.J. *Science and technology of concrete admixtures*. Woodhead Publishing ed.; 2015.
50. Přísady do betonu, malty a injektážní malty - část 2: Přísady do betonu - definice, požadavky, shoda, označení a značení štítkem. 2012; Vol. ČSN EN 934-2.
51. *Příručka technologa - beton*. Heidelberg cement group: 2010; Vol. 1.
52. Provis, J.L. *Alkali activated materials*. Springer: 2016; p 402.
53. Rosen, M.J. *Surfactants and interfacial phenomena*. 3rd ed.; Wiley-Interscience: Hoboken, N.J., 2004; p xiii, 444 p.
54. Davies, J.T., Rideal, E.K. *Interfacial phenomena*. 1961; Vol. 2.
55. Collepardi, M. *The new concrete*. Grafiche Tintoretto: 2006.
56. Aïtcin, P.-C. *High-performance concrete*. E. & F.N. Spon: London ; New York, 1998; p xxxii, 591 p.
57. Kukko, H., Mannonen, R. Chemical and mechanical properties of alkali-activated blast furnace slag (f-concrete). *Nord Concrete Research* **1982**, *1*.
58. Byfors, K.; Klingstedt, G.; Lehtonen, V.; Pyy, H.; Romben, L. Durability of concrete made with alkali activated slag. *Fly Ash, Silica Fume, Slag, and Natural Pozzolans in Concrete, Vol 1-2* **1989**, *114*, 1429-1466.
59. Douglas, E.; Brandstetr, J. A preliminary-study on the alkali activation of ground granulated blast-furnace slag. *Cement and Concrete Research* **1990**, *20*, 746-756.
60. Bakharev, T.; Sanjayan, J.G.; Cheng, Y.B. Effect of admixtures on properties of alkali-activated slag concrete. *Cement and Concrete Research* **2000**, *30*, 1367-1374.
61. Kalina, L.; Bílek, V.; Novotný, R.; Šoukal, F. Effect of plasticizing admixtures on the behavior and properties of alkali activated materials. In *5th International Congress on the Chemistry of Cement. 5th International Congress on the Chemistry of Cement (ICCC 2019)*, Research Institute of Binding Materials Prague: Prague, 2019.
62. Kashani, A.; Provis, J.L.; Qiao, G.G.; van Deventer, J.S.J. The interrelationship between surface chemistry and rheology in alkali activated slag paste. *Construction and Building Materials* **2014**, *65*, 583-591.

63. Puertas, F.; Palomo, A.; Fernandez-Jimenez, A.; Izquierdo, J.D.; Granizo, M.L. Effect of superplasticisers on the behaviour and properties of alkaline cements. *Advances in Cement Research* **2003**, *15*, 23-28.
64. Criado, M.; Palomo, A.; Fernandez-Jimenez, A.; Banfill, P.F.G. Alkali activated fly ash: Effect of admixtures on paste rheology. *Rheologica Acta* **2009**, *48*, 447-455.
65. Palacios, M.; Puertas, F. Effect of superplasticizer and shrinkage-reducing admixtures on alkali-activated slag pastes and mortars. *Cement and Concrete Research* **2005**, *35*, 1358-1367.
66. Kashani, A.; Provis, J.L.; Xu, J.T.; Kilcullen, A.R.; Qiao, G.G.; van Deventer, J.S.J. Effect of molecular architecture of polycarboxylate ethers on plasticizing performance in alkali-activated slag paste. *Journal of Materials Science* **2014**, *49*, 2761-2772.
67. Palacios, M.; Houst, Y.F.; Bowen, P.; Puertas, F. Adsorption of superplasticizer admixtures on alkali-activated slag pastes. *Cement and Concrete Research* **2009**, *39*, 670-677.
68. Palacios, M.; Banfill, P.F.G.; Puertas, F. Rheology and setting of alkali-activated slag pastes and mortars: Effect of organ admixture. *Aci Materials Journal* **2008**, *105*, 140-148.
69. Palacios, M.; Puertas, F. Stability of superplasticizer and shrinkage-reducing admixtures in high basic media. *Materiales De Construccion* **2004**, *54*, 65-86.
70. Bílek, V. Alkalicky aktivované systémy. Ph.D., Brno University of Technology, Brno, 2017.
71. Wittmann, F.H.; Beltzung, F.; Zhao, T.J. Shrinkage mechanisms, crack formation, and service life of reinforced concrete structures. *Advances in Concrete Structural Durability, Proceedings of Icdcs2008, Vols 1 and 2* **2008**, 52-63.
72. Collins, F.; Sanjayan, J.G. Effect of pore size distribution on drying shrinkage of alkali-activated slag concrete. *Cement and Concrete Research* **2000**, *30*, 1401-1406.
73. Yang, L.Y.; Jia, Z.J.; Zhang, Y.M.; Dai, J.G. Effects of nano-tio<sub>2</sub> on strength, shrinkage and microstructure of alkali activated slag pastes. *Cement & Concrete Composites* **2015**, *57*, 1-7.
74. Bakharev, T.; Sanjayan, J.G.; Cheng, Y.B. Alkali activation of australian slag cements. *Cement and Concrete Research* **1999**, *29*, 113-120.
75. Bangham, D.H. The gibbs adsorption equation and adsorption on solids. *Transactions of the Faraday society* **1937**, *33*.
76. Wittmann, F.H. Useful fundamentals of shrinkage and creep of concrete. *Concreep 10: Mechanics and Physics of Creep, Shrinkage, and Durability of Concrete and Concrete Structures* **2015**, 84-93.
77. Lura, P.; Pease, B.; Mazzotta, G.B.; Rajabipour, F.; Weiss, J. Influence of shrinkage-reducing admixtures on development of plastic shrinkage cracks. *Aci Materials Journal* **2007**, *104*, 187-194.
78. Rajabipour, F.; Sant, G.; Weiss, J. Interactions between shrinkage reducing admixtures (sra) and cement paste's pore solution. *Cement and Concrete Research* **2008**, *38*, 606-615.

79. Eberhardt, A.B. On the mechanisms of shrinkage reducing admixtures in self consolidating mortars and concretes. Bauhaus University, Weimar, 2011.
80. Palacios, M.; Puertas, F. Effect of shrinkage-reducing admixtures on the properties of alkali-activated slag mortars and pastes. *Cement and Concrete Research* **2007**, *37*, 691-702.
81. Bilim, C.; Karahan, O.; Atis, C.D.; Ilkentapar, S. Influence of admixtures on the properties of alkali-activated slag mortars subjected to different curing conditions. *Materials & Design* **2013**, *44*, 540-547.
82. Bilim, C.; Karahan, O.; Atis, C.D.; Ilkentapar, S. Effects of chemical admixtures and curing conditions on some properties of alkali-activated cementless slag mixtures. *Ksce Journal of Civil Engineering* **2015**, *19*, 733-741.
83. Bílek, V., Kalina, L., Koplík, J., Novotný, R., Hajdúchová, M., Opravil, T. Influence of chemical admixtures on properties of alkali-activated slag-based mortars. *Advanced Materials Research* **2015**, *1124*.
84. Bílek, V., Kalina, L., Novotný, R., Pořízka, J., Opravil, T., Šoukal, F. Effect of alcohol structure on hydration of alkali-activated slag. In *10th International conference on cementitious materials and alternative binders for sustainable concrete*, Montreal, 2017.
85. Bilek, V.; Kalina, L.; Novotny, R.; Tkacz, J.; Parizek, L. Some issues of shrinkage-reducing admixtures application in alkali-activated slag systems. *Materials* **2016**, *9*.
86. Kalina, L.; Novotny, R.; Bilek, V. Influence of alkali ions on the efficiency of shrinkage reduction by polypropylene glycol in alkali activated systems. *Advances in Cement Research* **2018**, *30*, 240-244.
87. Kalina, L.; Bilek, V.; Bartonickova, E.; Krouska, J. Polypropylene glycols as effective shrinkage-reducing admixtures in alkali-activated materials. *Aci Materials Journal* **2018**, *115*, 251-256.
88. Bilek, V.; Kalina, L.; Novotny, R. Polyethylene glycol molecular weight as an important parameter affecting drying shrinkage and hydration of alkali-activated slag mortars and pastes. *Construction and Building Materials* **2018**, *166*, 564-571.
89. Bilek, V.; Kalina, L.; Bartonickova, E.; Porizka, J. Evaluation of the surfactant leaching from alkali-activated slag-based composites using surface-tension measurements. *Materiali in Tehnologije* **2019**, *53*, 33-38.
90. Kalina, L. Effect of chemical structure on the efficiency of shrinkage reducing admixtures in alkali activated systems. In *Alkali Activated Materials and Geopolymers: Versatile Materials Offering High Performance and Low Emissions*, ECI: Tomar, 2018.
91. Kalina, L.; Bílek Jr., V.; Bartoníčková, E. Effect of amino alcohol admixtures on alkali-activated materials. *Materials and Technology* **2020**, *54*.
92. Vývoj přísad redukující smrštění navržených pro alkalicky aktivované systémy. Grantová agentura České republiky GA17-03670S: 2017; Vol. (hl. řešitel: Ing. Lukáš Kalina, Ph.D.).

93. Kalina, L.; Bílek, V.; Bartoníčková, E.; Kalina, M.; Hajzler, J.; Novotny, R. Doubts over capillary pressure theory in context with drying and autogenous shrinkage of alkali activated materials. *Construction and Building Materials* **2020**.
94. Weiss, J.; Lura, P.; Rajabipour, F.; Sant, G. Performance of shrinkage-reducing admixtures at different humidities and at early ages. *Aci Mater J* **2008**, *105*, 638-638.
95. Bentz, D.P.; Geiker, M.R.; Hansen, K.K. Shrinkage-reducing admixtures and early-age desiccation in cement pastes and mortars. *Cement and Concrete Research* **2001**, *31*, 1075-1085.
96. He, Z.H.; Qian, C.X. Internal relative humidity and creep of concrete with modified admixtures. *Progress in Natural Science-Materials International* **2011**, *21*, 426-432.
97. Mehta, P.K.; Monteiro, P.J.M. *Concrete : Microstructure, properties, and materials*. 3rd ed.; McGraw-Hill: New York, 2006; p xxi, 659 p.
98. Lea, F.M.; Hewlett, P.C. *Lea's chemistry of cement and concrete*. 4th ed.; Copublished in North, Central, and South America by J. Wiley: London, 1998; p 1053.
99. Douglas, E.; Bilodeau, A.; Malhotra, V.M. Properties and durability of alkali-activated slag concrete. *Aci Materials Journal* **1992**, *89*, 509-516.
100. Zhang, Y.J.; Wang, Y.C.; Xu, D.L.; Li, S. Mechanical performance and hydration mechanism of geopolymer composite reinforced by resin. *Materials Science and Engineering a-Structural Materials Properties Microstructure and Processing* **2010**, *527*, 6574-6580.
101. Zhang, Y.J.; Li, S.; Wang, Y.C.; Xu, D.L. Microstructural and strength evolutions of geopolymer composite reinforced by resin exposed to elevated temperature. *Journal of Non-Crystalline Solids* **2012**, *358*, 620-624.
102. Kalina, L.; Masilko, J.; Koplík, J.; Soukal, F. Xps characterization of polymer-monocalcium aluminate interface. *Cement and Concrete Research* **2014**, *66*, 110-114.
103. Zhang, Z., Zhou, D., Pan, Z. Selection of setting retarding substances for alkali activated slag cement. *Concrete* **2008**.
104. Zhu, X., Shi, C. Research on new type setting retarder for alkali activated slag cement. *China Building Materials* **2008**.
105. Li, Q.; Yang, K.; Yang, C.H. An alternative admixture to reduce sorptivity of alkali-activated slag cement by optimising pore structure and introducing hydrophobic film. *Cement & Concrete Composites* **2019**, *95*, 183-192.
106. Joisel, A. *Admixtures in cement*. Soisy, 1973.
107. Chang, J.J. A study on the setting characteristics of sodium silicate-activated slag pastes. *Cement and Concrete Research* **2003**, *33*, 1005-1011.
108. Gong, C.M.; Yang, N.R. Effect of phosphate on the hydration of alkali-activated red mud-slag cementitious material. *Cement and Concrete Research* **2000**, *30*, 1013-1016.

109. Kalina, L.; Bilek, V.; Novotny, R.; Moncekova, M.; Masilko, J.; Koplík, J. Effect of  $\text{Na}_3\text{PO}_4$  on the hydration process of alkali-activated blast furnace slag. *Materials* **2016**, *9*.
110. Lee, W.K.W.; van Deventer, J.S.J. Effects of anions on the formation of aluminosilicate gel in geopolymers. *Industrial & Engineering Chemistry Research* **2002**, *41*, 4550-4558.
111. Bensted, J.; Callaghan, I.C.; Lepre, A. Comparative-study of the efficiency of various borate compounds as set-retarders of class g oilwell cement. *Cement and Concrete Research* **1991**, *21*, 663-668.
112. Nicholson, C.L., Murray, B.J., Fletcher, R.A., Brew, D.R.M., MacKenzie, K.J.D., Schmucker, M. Novel geopolymer materials containing borate structural units. In *World Congress Geopolymer*, Saint-Quentin, 2005.
113. Sakulich, A.R.; Anderson, E.; Schauer, C.; Barsoum, M.W. Mechanical and microstructural characterization of an alkali-activated slag/limestone fine aggregate concrete. *Construction and Building Materials* **2009**, *23*, 2951-2957.
114. Rashad, A.M.; Zeedan, S.R.; Hassan, H.A. A preliminary study of autoclaved alkali-activated slag blended with quartz powder. *Construction and Building Materials* **2012**, *33*, 70-77.
115. Douglas, E.; Bilodeau, A.; Brandstetr, J.; Malhotra, V.M. Alkali activated ground granulated blast-furnace slag concrete - preliminary investigation. *Cement and Concrete Research* **1991**, *21*, 101-108.
116. Rashad, A.M.; Khalil, M.H. A preliminary study of alkali-activated slag blended with silica fume under the effect of thermal loads and thermal shock cycles. *Construction and Building Materials* **2013**, *40*, 522-532.
117. Escalante-Garcia, J.I.; Palacios-Villanueva, V.M.; Gorokhovskiy, A.V.; Mendoza-Suarez, G.; Fuentes, A.F. Characteristics of a  $\text{NaOH}$ -activated blast furnace slag blended with a fine particle silica waste. *Journal of the American Ceramic Society* **2002**, *85*, 1788-1792.
118. Collins, F.; Sanjayan, J.G. Effects of ultra-fine materials on workability and strength of concrete containing alkali-activated slag as the binder. *Cement and Concrete Research* **1999**, *29*, 459-462.
119. Gifford, P.M.; Gillott, J.E. Behaviour of mortar and concrete made with activated blast furnace slag cement. *Canadian Journal of Civil Engineering* **1997**, *24*, 237-249.
120. Bernal, S.A.; Rodriguez, E.D.; de Gutierrez, R.M.; Provis, J.L. Performance at high temperature of alkali-activated slag pastes produced with silica fume and rice husk ash based activators. *Materiales De Construccion* **2015**, *65*.
121. Aydin, S. A ternary optimisation of mineral additives of alkali activated cement mortars. *Construction and Building Materials* **2013**, *43*, 131-138.
122. Matalkah, F.; Salem, T.; Shaafaey, M.; Soroushian, P. Drying shrinkage of alkali activated binders cured at room temperature. *Construction and Building Materials* **2019**, *201*, 563-570.

123. Kumar, S.; Kumar, R.; Mehrotra, S.P. Influence of granulated blast furnace slag on the reaction, structure and properties of fly ash based geopolymer. *Journal of Materials Science* **2010**, *45*, 607-615.
124. Sugama, T.; Brothers, L.E.; Van de Putte, T.R. Acid-resistant cements for geothermal wells: Sodium silicate activated slag/fly ash blends. *Advances in Cement Research* **2005**, *17*, 65-75.
125. Wang, S.D. Review of recent research on alkali-activated concrete in china. *Magazine of Concrete Research* **1991**, *43*, 29-35.
126. Shen, W.G.; Wang, Y.H.; Zhang, T.; Zhou, M.K.; Li, J.S.; Cui, X.Y. Magnesia modification of alkali-activated slag fly ash cement. *Journal of Wuhan University of Technology-Materials Science Edition* **2011**, *26*, 121-125.
127. Shi, C.; Day, R.L. Early strength development and hydration of alkali-activated blast furnace slag/fly ash blends. *Advances in Cement Research* **1999**, *11*, 189-196.
128. Guerrieri, M.; Sanjayan, J.G. Behavior of combined fly ash/slag-based geopolymers when exposed to high temperatures. *Fire and Materials* **2010**, *34*, 163-175.
129. Bezcementové betony. Technologická agentura České republiky: 2015; Vol. (hl. řešitel: Ing. Lukáš Kalina, Ph.D.).
130. Kalina, L.; Bílek, V.; Šoukal, F.; Opravil, T. In *Recycling of waste technological sludge in alkali activated concretes*, Performance-based approaches for concrete structures, 2016.
131. Marjanovic, N.; Komljenovic, M.; Bascarevic, Z.; Nikolic, V.; Petrovic, R. Physical-mechanical and microstructural properties of alkali-activated fly ash-blast furnace slag blends. *Ceramics International* **2015**, *41*, 1421-1435.
132. Provis, J.L.; Myers, R.J.; White, C.E.; Rose, V.; van Deventer, J.S.J. X-ray microtomography shows pore structure and tortuosity in alkali-activated binders. *Cement and Concrete Research* **2012**, *42*, 855-864.
133. Ismail, I.; Bernal, S.A.; Provis, J.L.; Hamdan, S.; van Deventer, J.S.J. Microstructural changes in alkali activated fly ash/slag geopolymers with sulfate exposure. *Materials and Structures* **2013**, *46*, 361-373.
134. Šafář, M. Trvanlivost alkalicky aktivovaných systémů. *diplomová práce* **2015**, *Vysoké učení technické v Brně*, školitel: Ing. Lukáš Kalina, Ph.D.
135. Kalina, L.; Koplík, J.; Soukal, F.; Masilko, J.; Jaskowiecova, L. Potential uses of geopolymers to immobilize toxic metals from by-products materials. *Environmental Engineering and Management Journal* **2012**, *11*, 579-584.
136. Koplík, J.; Porizka, J.; Kalina, L.; Masilko, J.; Brezina, M. Influence of pb dosage on immobilization characteristics of different types of alkali-activated mixtures and mortars. *Advances in Materials Science and Engineering* **2018**.
137. Palomo, A.; Palacios, M. Alkali-activated cementitious materials: Alternative matrices for the immobilisation of hazardous wastes - part ii. Stabilisation of chromium and lead. *Cement and Concrete Research* **2003**, *33*, 289-295.

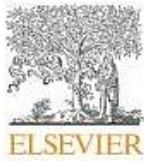
138. Koplík, J.; Kalina, L.; Masilko, J.; Soukal, F. The characterization of fixation of ba, pb, and cu in alkali-activated fly ash/blast furnace slag matrix. *Materials* **2016**, *9*.
139. Donatello, S.; Fernandez-Jimenez, A.; Palomo, A. An assessment of mercury immobilisation in alkali activated fly ash (aafa) cements. *Journal of Hazardous Materials* **2012**, *213*, 207-215.
140. Cheng, T.W.; Chiu, J.P. Fire-resistant geopolymer produced by granulated blast furnace slag. *Minerals Engineering* **2003**, *16*, 205-210.
141. Buchwald, A.; Tatarin, R.; Stephan, D. Reaction progress of alkaline-activated metakaolin-ground granulated blast furnace slag blends. *Journal of Materials Science* **2009**, *44*, 5609-5617.
142. Bernal, S.A.; Rodriguez, E.D.; de Gutierrez, R.M.; Provis, J.L.; Delvasto, S. Activation of metakaolin/slag blends using alkaline solutions based on chemically modified silica fume and rice husk ash. *Waste and Biomass Valorization* **2012**, *3*, 99-108.
143. Bernal, S.A.; de Gutierrez, R.M.; Provis, J.L. Engineering and durability properties of concretes based on alkali-activated granulated blast furnace slag/metakaolin blends. *Construction and Building Materials* **2012**, *33*, 99-108.
144. Rovnanik, P. Effect of curing temperature on the development of hard structure of metakaolin-based geopolymer. *Construction and Building Materials* **2010**, *24*, 1176-1183.
145. Fernandez-Jimenez, A.; Palomo, A.; Sobrados, I.; Sanz, J. The role played by the reactive alumina content in the alkaline activation of fly ashes. *Microporous and Mesoporous Materials* **2006**, *91*, 111-119.
146. Li, C.; Sun, H.H.; Li, L.T. A review: The comparison between alkali-activated slag (si plus ca) and metakaolin (si plus al) cements. *Cement and Concrete Research* **2010**, *40*, 1341-1349.
147. Buchwald, A.; Hilbig, H.; Kaps, C. Alkali-activated metakaolin-slag blends - performance and structure in dependence of their composition. *Journal of Materials Science* **2007**, *42*, 3024-3032.
148. Davidovits, J. *Geopolymer*. Institut Géopolymère: 2008.
149. Wu, X.Q.; Jiang, W.M.; Roy, D.M. Early activation and properties of slag cement. *Cement and Concrete Research* **1990**, *20*, 961-974.
150. Wang, F.S.; Sun, R.L.; Cui, Y.J. Study on modification of the high-strength slag cement material. *Cement and Concrete Research* **2005**, *35*, 1344-1348.
151. Roy, S.; Chanda, S.; Bandopadhyay, S.K.; Ghosh, S.N. Investigation of portland slag cement activated by waterglass. *Cement and Concrete Research* **1998**, *28*, 1049-1056.
152. Roy, D.M.; Jiang, W.M.; Silsbee, M.R. Chloride diffusion in ordinary, blended, and alkali-activated cement pastes and its relation to other properties. *Cement and Concrete Research* **2000**, *30*, 1879-1884.

153. Singh, N.; Rai, S.; Singh, N.B. Effect of sodium sulphate on the hydration of granulated blast furnace slag blended portland cement. *Indian Journal of Engineering and Materials Sciences* **2001**, *8*, 110-113.
154. Bilim, C.; Atis, C.D. Alkali activation of mortars containing different replacement levels of ground granulated blast furnace slag. *Construction and Building Materials* **2012**, *28*, 708-712.
155. Martinez-Ramirez, S.; Palomo, A. Opc hydration with highly alkaline solutions. *Advances in Cement Research* **2001**, *13*, 123-129.
156. Cement - část 1: Složení, specifikace a kritéria shody cementů pro obecné použití. 2013; Vol. ČSN EN 197-1.
157. Kalina, L.; Bilek, V.; Kiripolsky, T.; Novotny, R.; Masilko, J. Cement kiln by-pass dust: An effective alkaline activator for pozzolanic materials. *Materials* **2018**, *11*.
158. Bilek, V.; Parizek, L.; Kalina, L. Effect of the by-pass cement-kiln dust and fluidized-bed-combustion fly ash on the properties of fine-grained alkali-activated slag-based composites. *Materiali in Tehnologije* **2015**, *49*, 549-552.
159. Kalina, L. Syntéza aluminátosilikátových systémů na bázi geopolymérů orientovaná na využití sekundárních surovin. *disertační práce* **2011**, *Vysoké učení technické v Brně*, školitel: doc. Ing. František Šoukal, Ph.D.
160. Štěpánková, E.; Kalina, L.; Bilek, V.; Bartoníčková, E. Utilization of by-pass cement kiln dust in alkali-activated materials. In *Non-Traditional Cement and Concrete*, Key Engineering Materials: Brno.
161. Geodust. H2020 - Marie Sklodowska-Curie - Research and Innovation Staff Exchange: 2017; Vol. (hl. řešitel: doc. Ing. Tomáš Opravil, Ph.D.).
162. Collins, F.G.; Sanjayan, J.G. Workability and mechanical properties of alkali activated slag concrete. *Cement and Concrete Research* **1999**, *29*, 455-458.
163. Yang, K.H.; Cho, A.R.; Song, J.K. Effect of water-binder ratio on the mechanical properties of calcium hydroxide-based alkali-activated slag concrete. *Construction and Building Materials* **2012**, *29*, 504-511.

## 7. Přílohy

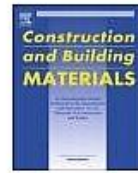
Seznam impaktovaných článků, které shrnují poznatky našeho výzkumu a vytváří obsahovou stránku práce, doplněný kvartilem časopisů dle AIS:

Příloha I	Kalina, L.; Bílek, V.; Bartoníčková, E.; Kalina, M.; Hajzler, J.; Novotny, R. Doubts over capillary pressure theory in context with drying and autogenous shrinkage of alkali activated materials. <i>Construction and Building Materials</i> <b>2020</b> .	Q1
Příloha II	Kalina, L.; Bílek, V.; Bartoníčková, E. Effect of amino alcohol admixtures on alkali-activated materials. <i>Materials and Technology</i> <b>2020</b> , 54, 19-23.	Q4
Příloha III	Bílek, V.; Kalina, L.; Bartonickova, E.; Porizka, J. Evaluation of the surfactant leaching from alkali-activated slag-based composites using surface-tension measurements. <i>Materiali in Tehnologije</i> <b>2019</b> , 53, 33-38.	Q4
Příloha IV	Kalina, L.; Bílek, V.; Kiripolsky, T.; Novotny, R.; Masilko, J. Cement kiln by-pass dust: An effective alkaline activator for pozzolanic materials. <i>Materials</i> <b>2018</b> , 11.	Q2
Příloha V	Kalina, L.; Novotny, R.; Bílek, V. Influence of alkali ions on the efficiency of shrinkage reduction by polypropylene glycol in alkali activated systems. <i>Advances in Cement Research</i> <b>2018</b> , 30, 240-244.	Q3
Příloha VI	Bílek, V.; Kalina, L.; Novotny, R. Polyethylene glycol molecular weight as an important parameter affecting drying shrinkage and hydration of alkali-activated slag mortars and pastes. <i>Construction and Building Materials</i> <b>2018</b> , 166, 564-571.	Q1
Příloha VII	Kalina, L.; Bílek, V.; Bartonickova, E.; Krouska, J. Polypropylene glycols as effective shrinkage-reducing admixtures in alkali-activated materials. <i>ACI Materials Journal</i> <b>2018</b> , 115, 251-256.	Q2
Příloha VIII	Koplik, J.; Porizka, J.; Kalina, L.; Masilko, J.; Brezina, M. Influence of Pb dosage on immobilization characteristics of different types of alkali-activated mixtures and mortars. <i>Advances in Materials Science and Engineering</i> <b>2018</b> .	Q3
Příloha IX	Koplik, J.; Kalina, L.; Masilko, J.; Soukal, F. The characterization of fixation of Ba, Pb, and Cu in alkali-activated fly ash/blast furnace slag matrix. <i>Materials</i> <b>2016</b> , 9.	Q2
Příloha X	Bílek, V.; Kalina, L.; Novotny, R.; Tkacz, J.; Parizek, L. Some issues of shrinkage-reducing admixtures application in alkali-activated slag systems. <i>Materials</i> <b>2016</b> , 9.	Q2
Příloha XI	Kalina, L.; Bílek, V.; Novotny, R.; Moncekova, M.; Masilko, J.; Koplik, J. Effect of Na <sub>3</sub> PO <sub>4</sub> on the hydration process of alkali-activated blast furnace slag. <i>Materials</i> <b>2016</b> , 9.	Q2
Příloha XII	Bílek, V.; Parizek, L.; Kalina, L. Effect of the by-pass cement-kiln dust and fluidized-bed-combustion fly ash on the properties of fine-grained alkali-activated slag-based composites. <i>Materiali in Tehnologije</i> <b>2015</b> , 49, 549-552.	Q4
Příloha XIII	Kalina, L.; Masilko, J.; Koplik, J.; Šoukal, F. XPS characterization of polymer-monocalcium aluminate interface. <i>Cement and Concrete Research</i> <b>2014</b> , 66, 110-114.	Q1
Příloha XIV	Kalina, L.; Koplik, J.; Soukal, F.; Masilko, J.; Jaskowiecova, L. Potential uses of geopolymers to immobilize toxic metals from by-products materials. <i>Environmental Engineering and Management Journal</i> <b>2012</b> , 11, 579-584.	Q4



Contents lists available at ScienceDirect

Construction and Building Materials

journal homepage: [www.elsevier.com/locate/conbuildmat](http://www.elsevier.com/locate/conbuildmat)

## Doubts over capillary pressure theory in context with drying and autogenous shrinkage of alkali-activated materials



Lukáš Kalina\*, Vlastimil Bílek Jr., Eva Bartoníčková, Michal Kalina, Jan Hajzler, Radoslav Novotný

Brno University of Technology, Faculty of Chemistry, Materials Research Centre, Purkyňova 464/118, Brno CZ-612 00, Czech Republic

### HIGHLIGHTS

- Amino alcohol surfactants reduced the surface tension of AAS pore solutions.
- Surfactants had a minor effect on autogenous shrinkage.
- Drying shrinkage was reduced mainly thanks to hydration retardation caused by surfactants.
- Decrease in surface tension does not necessarily lead to decrease in shrinkage.
- Adsorption of surfactants on slag particles were observed.

### ARTICLE INFO

#### Article history:

Received 10 September 2019

Received in revised form 27 February 2020

Accepted 28 February 2020

#### Keywords:

Alkali-activated slag  
Shrinkage  
Admixture  
Hydration  
Capillary pressure  
Surface tension

### ABSTRACT

One of the most important technological problems associated with alkali-activated materials is high shrinkage. In this study, shrinkage reducing admixtures (SRAs) based on amino alcohols were used in alkali-activated slag (AAS) as strong surfactants that should, in terms of capillary pressure theory, decrease shrinkage via the decrease in surface tension. Although the surface tension of the pore solution was reduced by SRAs, autogenous shrinkage was not affected in the long run, while drying shrinkage was noticeably reduced and simultaneous weight changes were dramatically increased. The expected retardation effect of SRAs on hydration was confirmed using isothermal calorimetry, strength development, mercury intrusion porosimetry and scanning electron microscopy. The obtained results suggest that the observed effect of SRAs on drying shrinkage was caused by coarser pore structure rather than by a decrease in surface tension of the pore solution. Since the decrease in surface tension does not necessarily lead to decrease in shrinkage, the application of capillary pressure theory in AAS can sometimes be an issue.

© 2020 Elsevier Ltd. All rights reserved.

### 1. Introduction

Alkali-activated materials (AAM) are non-traditional cementitious materials, the research and subsequent practical applications of which are currently undergoing an unprecedented development. The increased interest in these materials is primarily related to the revelation of their potential options, which are in many cases crucial in comparison with the conventional way represented by the usage of ordinary Portland cement (OPC). The main reason why AAM are gaining increased recognition and interest is connected with the reduction of CO<sub>2</sub> emissions which are lower compared to the emissions coming from Portland cement-based materials [1]. It should also be noted that most AAM are based on industrial

waste and secondary raw materials which significantly contribute to the saving of natural resources.

Generally AAM show very good chemical [2] and high-temperature [3] resistance. High early strength is also an advantageous property typical for alkaline activated blast furnace slag-based systems (AAS) cured under ambient conditions [4]. Nevertheless, these materials also have some disadvantages considerably limiting their practical applications, especially their high autogenous and drying shrinkage [5].

The capillary pressure theory and disjoining pressure theory are known and abundantly used to explain the origin of shrinkage phenomena [6]. The former theory was based on the formation of menisci which arise during the drying of cementitious matrix as a consequence of surface tension forces. The difference between the pressures in liquid and vapour phase  $\Delta p$  comprises a meniscus curvature. For a spherical liquid/vapour interfaces the Laplace equation can be used:

\* Corresponding author.

E-mail address: [kalina@fch.vut.cz](mailto:kalina@fch.vut.cz) (L. Kalina).

$$\Delta p = \frac{2\gamma}{r} \quad (1)$$

where  $r$  is the radius of the largest solution-filled cylindrical pore and  $\gamma$  is the surface tension at the liquid/vapour interface.

However, there are some doubts about the applicability of this theory to the cementitious systems with very fine pores (below 10 nm) regarding the pore shape, the existence of menisci and also the relative humidity lower than 50% [7,8]. According to these authors, disjoining forces play the main role in the shrinkage mechanism, particularly in mature hydrated cement paste. The term "disjoining pressure" represents the complex interactions between water and two solid surfaces, which may be written in simplified version as a superposition of the contribution of dispersive attractive or molecular forces (predominantly van der Waals forces), repulsive electric double layer components and structural components. When the solid surfaces are close to each other in a vacuum or in dry air, the attractive contributions dominate, and the solid surfaces are in close contact. As the relative humidity increases, water that is adsorbed and condensed within the capillaries forms a film separating the solid surfaces. This theory is applicable throughout the whole range of relative humidity [6].

Additionally, recent investigations [9,10] also showed that extensive shrinkage of AAS is created by the contribution of visco-elastic/visco-plastic behaviour during drying related to the rearrangement of C-(A)-S-H under capillary stresses. This could be more pronounced by the presence of alkalis and results in chemical and physical changes in AAS.

With respect to the capillary model described above, one of the ways to effectively reduce the shrinkage phenomenon is by using the organic surfactants-based shrinkage reducing admixtures (SRAs). The basic premise of the SRAs function is the reduction of surface tension of the capillary fluid, i.e. pore solution, which also decreases the capillary forces described by the Laplace equation (Eq. (1)). This results in the mitigation of drying [11] as well as autogenous [12] shrinkage. According to certain studies [13,14], the correlations between the shrinkage reduction and the reduction of surface tension of pore solution exhibit direct dependence. Thus, the assumption of good efficiency of SRAs according to the previous studies should particularly lie on the ability to decrease the surface tension of pore solution in alkali-activated systems as well.

Contrary to the above mentioned well-established findings regarding the Portland cement-based systems and also to some studies in AAS [15,16] we have observed some problems when using SRAs in waterglass-activated slag [17]. During the drying of porous immature AAS with delayed hydration, very low drying shrinkage was observed, while after prolonged curing, SRAs lost its efficiency. Similar observations of other SRAs and other related organic substances of various types led us to a more in-depth analysis including the context of the surface tension of the pore solution, i.e. in relation to original working mechanism of SRAs. Therefore, this paper provides information about the efficiency of non-ionic amino alcohol surfactants upon the ability to reduce both drying and autogenous shrinkage in alkali-activated blast furnace slag. The presented results discussed are regarding surface tension of the pore solution, hydration process and physical-mechanical properties of AAS, and suggest that the decrease in surface tension by SRAs does not necessarily lead to expected shrinkage reduction.

## 2. Experimental part

### 2.1. Materials

Commercial blast furnace slag (BFS) (ArcellorMittal Ostrava, a. s.) with the Blaine fineness of 400 m<sup>2</sup>/kg was the main aluminosil-

icate material for alkaline activation. The phase composition was determined using X-Ray powder diffraction (XRD) analyser EMPYREAN (PANalytical, Netherland) in a central focusing arrangement using CuK $\alpha$  radiation with step 0.013 °2 $\theta$ . The method of internal standard (calcium fluorite) for the amorphous part determination was applied. The XRD analysis showed the content of an amorphous phase of about 90%. The evaluation of the crystallographic structure and quantitative analysis was done by a Highscore programme using the Rietveld method. The crystal phases identified in BFS were melilite, calcite and merwinite. The chemical composition of BFS determined by X-ray fluorescence (XRF) is given in Table 1 and was performed with the spectrometer VANTA VRC (BAS, CZE). Quantification of elements was calculated via the internal mode in Geochem and represented as oxides. Sodium waterglass (Vodní sklo, a.s.) with the silicate modulus of 1.96 was used as an alkaline activator. Silicate modulus was determined by conductometry analysis.

2-(Ethylamino)ethanol (non-fluorinated secondary amine, further EAE) obtained from Sigma-Aldrich (per analysis grade) and self-synthesized N-ethyl,N-hydroxyethyl-heptafluoropropylamid (fluorinated secondary amide further synHFPA) were used as the SRA additives with assumed potential to reduce the surface tension of a pore solution. SynHFPA was prepared according to the patent CN106831504 by nucleophile acylation of 2-(Ethanolamino) ethanol with perfluoroester of carboxylic acid, i.e Methyl heptafluorobutyrate (99%, Sigma-Aldrich). The concentration of added surfactants was set to 0.5 wt% (by weight of BFS).

### 2.2. Testing methods

#### 2.2.1. Physical-mechanical properties

Testing samples for the measurements of compressive strength as well as drying and autogenous shrinkage evolution were prepared as follows. BFS was activated by using sodium waterglass in an automatic mortar mixer set to exact mixing cycle in compliance with EN 196-1. The mass ratio Na<sub>2</sub>O/BFS was set to 0.04 and water to BFS ratio was adjusted to 0.35 including the water presented in the alkaline activator. Prepared alkali-activated pastes were cast into steel moulds with the dimensions of 25 × 25 × 285 mm, which were moistly cured for the next 24 h. Both, mixing and curing were performed at laboratory temperature of 25 °C. Two different curing conditions after demoulding the samples were chosen for the strength and shrinkage measurements. One set of species was placed in the curing chamber with a defined relative humidity (65%, humidity chamber HC 105 Memmert), whereas the other one was wrapped into plastic foil to ensure autogenous conditions. Compressive strength measurements were carried out by a compressive and bending tester Destest 3310 (Betonsystem, CZE) at 1, 7 and 28 days. Observed data were statistically processed (standard average and deviation from 6 samples). The length changes were measured in short time intervals using the ASTM C490 apparatus until the age of 28 days. Observed data were also statistically processed as standard average from three separately measurements.

To observe the autogenous volume changes during the first 24 h, Archimedes principle measurements were carried out. The mixtures of AAS were placed into the elastic membranes of commercially available non-lubricated, non-reservoir condoms. The condoms were then tied by a thin fishing line and hung to an analytical balance (Mettler Toledo ME 204, USA). The sample weight of air ( $w_{air}$ ) was obtained. Subsequently, the condom was submerged into a beaker filled with paraffin oil and the weight of the sample ( $w_{is}$ ) in the initial setting time was determined. The initial setting time was identified simultaneously using the Vicat needle. Thereafter the weights ( $w_i$ ) were monitored during the setting and hardening of the binder every minute. The change of sample volume  $\Delta V$

**Table 1**  
Chemical compositions of blast furnace slag.

Raw material	Chemical composition/wt.%									
	SiO <sub>2</sub>	Al <sub>2</sub> O <sub>3</sub>	CaO	MgO	SO <sub>3</sub>	Na <sub>2</sub> O	K <sub>2</sub> O	TiO <sub>2</sub>	MnO	Fe <sub>2</sub> O <sub>3</sub>
Blast furnace slag	34.7	9.1	41.1	10.5	1.4	0.4	0.9	1.0	0.6	0.3

at a constant laboratory temperature  $T$  (25 °C) was calculated as follows:

$$-\Delta V(T) = \frac{W_{is} - W_t}{W_{air} - W_{is}} (\%) \quad (2)$$

### 2.2.2. Isothermal calorimetry

The evolution of hydration heat was measured using the TAM Air isothermal microcalorimeter (TA instruments, USA). The measurements of heat evolution were performed at constant temperature of 25 °C. BFS and alkaline activator were mixed together by injecting the solution into a 15 mL Admix<sup>®</sup> vial and stirring it for 3 min, immediately after the thermal equilibrium of placed BFS was reached. Water/BFS (0.35) as well as the Na<sub>2</sub>O/BFS (0.04) ratios were the same as in the preparation process of testing samples. The heat evolution was immediately recorded as the heat flow. These measurements were performed against a reference sample which has a similar heating capacity (i.e. water).

### 2.2.3. Porosimetry

The total porosity and the pore size distribution were determined by mercury intrusion porosimeter Poremaster (Quantachrome Instruments, USA). The working pressure range was from 0.14 to 231 MPa which covered the pore diameter range from 6.5 to 1000 nm. These measurements were carried out using Hg with the surface tension of 0.480 N/m and the contact angle of 140°. The contact angle value was selected according to Collins and Sanjayan study [18] focused on the measurement of pore size distribution of AAS-based systems. Nevertheless, the contact angle is dependent on several factors [19] which can affect the value of calculated pore diameter. The scan mode was chosen to average from 11 points. Obtained intrusion data were processed by the Poremaster program and normalized by sample weight and volume. Observed experimental data were presented as standard averaged values from three measurements. The chosen experimental parameters should provide information about the trend of porosity evolution due to the different mechanism of hydration in the presence of different SRA and not determine the exact pore distribution which could be given by the innovative MIP methods [19].

### 2.2.4. Surface tension

The dynamic surface tensions of pore solutions as well as pure amino alcohol admixtures were measured by the tensiometer BPA-800P (KSV Instruments, Finland) with the maximum bubble pressure method. Measurements were carried out at a constant temperature of 25 °C. Pore solutions were obtained from hardened samples stored in autogenous conditions in different time periods (1 and 7 days) using the steel die-and-piston system subjected to a pressure of 300 kN.

### 2.2.5. Zeta potential

The effect of surfactant addition on the values of zeta potential of slag suspension was investigated by the method of electrophoretic light scattering using Zetasizer Nano ZS (Malvern Panalytical Ltd., UK). Our main goal in this part of measurement was mainly to confirm the relative effect of used SRAs on surface chemistry of BFS grains in comparison with the sample without admix-

ture. For this purpose, 10 mL of slag suspension (1 g BFS/ 100 mL H<sub>2</sub>O) with alkaline activator (4 wt% Na<sub>2</sub>O/BFS) was titrated with the surfactants solutions using the MPT-2 titration unit (Malvern Panalytical Ltd., UK) in the concentration range 0-5 wt% by mass of BFS. The surfactant addition was performed stepwise with defined concentration steps (0.25 wt%). After each step, the pH, the conductivity, the average scattered light intensity and the zeta potential of the suspension were measured. The above described titrations were performed for all investigated surfactants under a controlled temperature (25.0 ± 0.2 °C) in three independently prepared replicates. Electrophoretic light scattering (ELS) was done for each of these replicates after individual surfactant additions in three repeated scans (results are presented in the form of mean values ± SD, n = 9 (three repeated measurements of three sample replicates)). The obtained data from ELS titration were processed using the Zetasizer software (version 7.11; Malvern Panalytical Ltd., UK). It should be noted that the values of zeta potential determined by electrophoretic light scattering for colloidal particles are also influenced by the concentration and by the size of analysed particles. The measurement of zeta potential in concentrated suspensions such as AAS suspensions with SRAs admixtures is generally a great technological challenge, due to the high sample turbidity. As a consequence the measurable concentrations using this method must be in comparison with real used concentrations in formulations significantly lower. On the other hand, the dilution can be beneficial for the measurement because of suppressing the changes in particle size thanks to slowed down hydration, i.e. dissolution of slag particles and growth of hydration products.

## 3. Results and discussion

### 3.1. Surface activity of amino alcohols

Surface activity is an essential property of surface-active agents (surfactants) and can be evaluated by means of the surface tension measurements. Fig. 1 shows the values of surface tension of pure amino alcohol admixtures, as well as pore solutions. The solution of alkaline activator exhibited relatively high surface tension (71.4 mN/m at 25 °C), very similar to distilled water (72.0 mN/m at 25 °C) and the surface tension of EAE and synHFPA showed more than halved values, 33.2 and 28.7 mN/m respectively. The addition of surfactants into the activated BFS sample resulted in a decrease of surface tension in pore solution, especially when the synthesized fluorocarbon surfactant was used. In the case of EAE addition, a 15% reduction was achieved. The synthesized fluorocarbon (synHFPA) admixture decreased surface tension by about 30%. From Fig. 1 it is evident that the surface tension of pore solution did not change during the hydration process, although the bulk concentration of SRA should be increased due to the chemical bonding of water into the hydration products. Similar values and trends of surface tension of AAS pore solution without SRAs, where the surface tension increased only very slightly from 24 h to seven days have previously been published [20].

### 3.2. Autogenous shrinkage

It is well known that capillary stress occurs due to internal drying during autogenous conditions. The consumption of water for

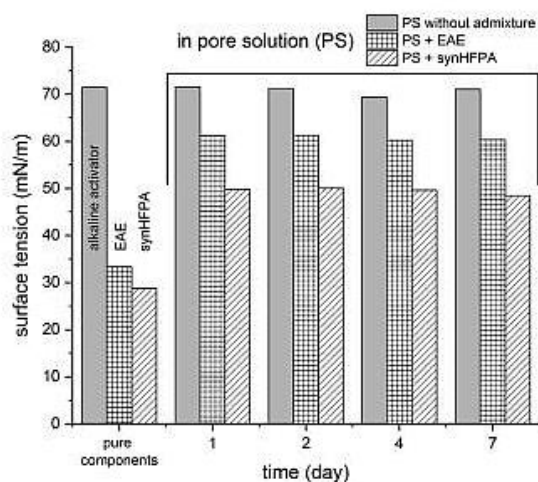


Fig. 1. Surface tension of pure amino alcohol admixtures and pore solutions.

the hydration products formation, i.e. self-desiccation, results in a decrease in relative humidity in the whole system and therefore curved menisci are created. Weiss et al. [21] and Bentz et al. [22] confirmed that the presence of SRAs in autogenous conditions leads to lower development of shrinkage. The utilization of some types of commercial SRAs can even lead to an initial expansion which decreases a part of the autogenous shrinkage later on. Sant et al. [23] explained that this behaviour should be connected with the amplification in portlandite oversaturation and its precipitation causes an early-age expansion. Several studies also confirm that the addition of the SRAs causes high internal relative humidity retention [21,24,25]. For this reason, the main mechanism controlling the shrinkage is attributed primarily to the capillary stress while disjoining pressure or another mechanism may dominate the shrinkage response at lower relative humidity [26]. Nevertheless, it should be noted that previous studies were mainly focused on cementitious systems based on Portland cement. The situation in the case of AAS seems to be different which is shown in Fig. 2.

From a long-term point of view, the autogenous shrinkage evolution exhibits very similar progress whether the systems contain SRAs or not. The distinction among the samples was observed only during the early timeframes of the hydration process. The samples containing SRAs showed a lower shrinkage rate up to 72 h from the start of alkaline activation, which can be related to the changes of hydration in the presence of SRAs. Therefore, microcalorimetry measurements were implemented. Fig. 3 shows two peaks appearing in the first minutes and hours of hydration process and one peak occurring after tens of hours. Typologically the same shape of the calorimetric curve for waterglass-activated BFS was reported by Shi and Day [27]. According to them, the initial peak is attributed to the wetting and dissolution of slag grains and adsorption of ions onto them while the additional initial peak is connected with the formation of a primary binder phase resulting mainly from the reaction of  $(\text{SiO}_4)^{4-}$  ions from sodium waterglass and  $\text{Ca}^{2+}$  ions dissolved from the surface of BFS. The third hydration peak is the main one where the bulk hydration of the slag takes place [28] resulting in the fast evolution of the gel-like interstitial matrix among the slag grains [29]. C-(A)-S-H gel is a typical binder phase which occurs during alkaline activation of BFS [30]. It is evident that the presence of SRAs somewhat decreased the content of the binder phase formed during the initial hydration phase and noticeably retarded the peak corresponding to bulk hydration. It can be

seen that once the C-(A)-S-H gel started to form, the autogenous shrinkage increased sharply. After 3 days, all samples behaved the same way, despite the different shapes of testing samples and the beginning of autogenous shrinkage measurement, i.e. 1 day from the start of mixing (Fig. 2A) or the time of initial settings (Fig. 2B). The calorimetry measurements were also in accordance with the compressive strength development (Fig. 4). After 1 day, the samples containing an SRA showed significantly lower values of compressive strengths in comparison with the reference samples. The retardation effect of SRAs was undoubtedly manifested. After 7 and 28 days, the compressive strength values of all samples were very similar.

An important factor that controls the capillary pressure is also the pore size distribution. The magnitude of shrinkage predominantly depends on the loss of water from mesopores (2–50 nm) [31]. In the case of AAS, the proportion of pores in the mentioned region is higher compared to hydrated OPC which is the main reason for its higher shrinkage [18]. The effect of SRAs addition on the change of porosity is one of the crucial factors which influence the shrinkage phenomena. Shah et al. [32] revealed a minor influence of SRAs on the pore size distribution of hydrated OPC. However, Kalina and Bilek [17,33] showed that some surfactants increase the porosity of AAS very strongly. Therefore, the differences in pore size distribution and total porosity of hardened samples were examined. Fig. 5A shows that MIP response under the autogenous treatment is very similar up to the pore diameter of 50 nm for all samples after just 7 days. Simultaneously, it is evident that all samples have a high concentration of pores within the mesopore size range, responsible for magnification of capillary tensile forces set up at the menisci. Therefore, the effect of surface tension should play the key role for the reduction of capillary pressure. However, the autogenous shrinkage rate remains unchanged with or without the SRA addition, even though the surface tension of the pore solution seems to be effectively reduced.

### 3.3. Drying shrinkage

According to the Wittmann and Splittgerber studies [34,35], a relative humidity above 55% of the surrounding air ensures that the capillary pressure outweighs the disjoining pressure because the van der Waals attractive forces among the pore walls are minimized. Therefore, the verification of the capillary force shrinkage model was further based on the measurements of length change during the curing process with controlled relative humidity (65%). The results in Fig. 6A show that the usage of SRAs decreased the drying shrinkage by about 35% compared to the reference samples. Consequently, one fundamental question arises: Does the decrease of surface tension by the addition of SRAs affect the drying shrinkage reduction? The combination of several measurements suggests that a different explanation should be offered.

During the drying shrinkage measurement, the weight changes of tested specimens were also obtained (Fig. 6B). A significant weight loss was observed in the case of samples with SRAs, especially when EAE was used. This can be related to the reduced surface tension of the pore solution, but also to the porosity and pore size distribution. The latter is supported by the comparison of the weight loss and drying shrinkage development. It can be seen that for the reference paste both drying and shrinkage rate is the highest at the beginning of drying while for both pastes with SRAs, extensive initial drying is not accompanied by rapid shrinking. The highest shrinkage rate is somewhat delayed and can be seen after around two days. This suggests that after 24 h, SRA-containing specimens had much larger pores whose emptying does not lead to severe shrinkage. Coarser porosity is related to the retardation of hydration by SRAs, particularly to the delay of the third peak on the calorimetric curve (Fig. 4), which was also

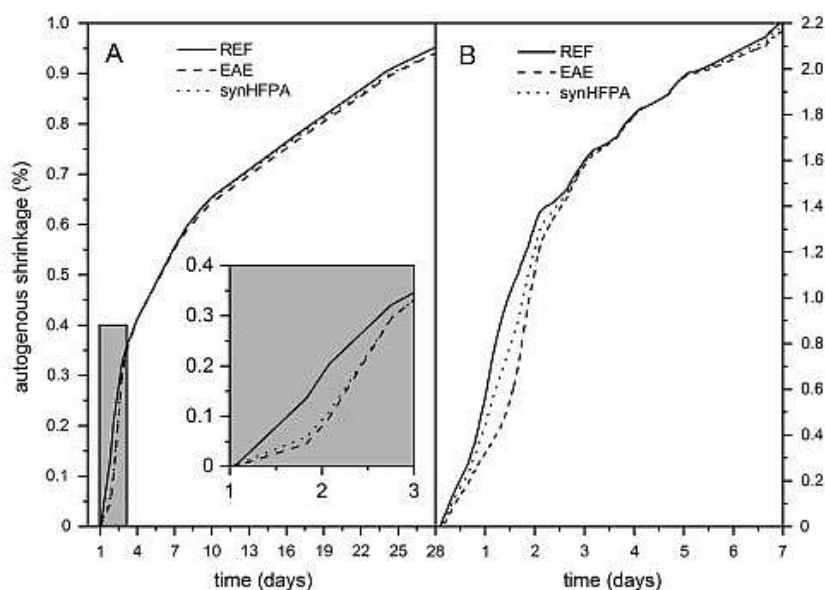


Fig. 2. Autogenous shrinkage of alkali-activated blast furnace slag samples measured on the test beams (A) and in the elastic membrane (B).

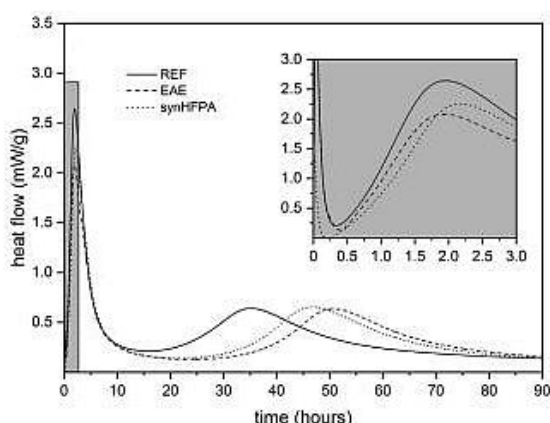


Fig. 3. Effect of surfactants on hydration process of alkali-activated blast furnace slag.

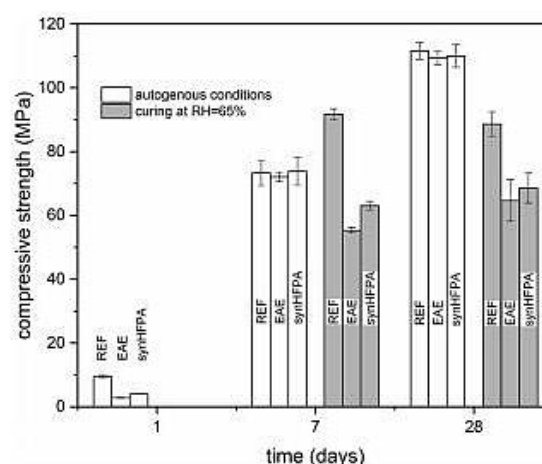


Fig. 4. Effect of surfactants on compressive strength development of alkali-activated blast furnace slag.

reported in the Bilek et al. study [17]. Simultaneously, due to a lower degree of hydration at the start of drying (24 h), a lower amount of water is bound in the hydration products and thus more water can freely evaporate out which increases total weight loss during drying. Consequently, less water is available for the creation of hydration products which is the main difference between autogenous conditions and controlled curing at RH = 65%. The lower amount of formed binder phase has a direct impact on total porosity and mechanical properties as well. Fig. 5B shows that the porosity is greatly influenced. After 7 days; the total porosity of the samples with SRA addition was more than five times higher than that of the reference ones. This porosity and the slowing down of the hydration process also reduced strength development. Fig. 4 shows that the compressive strength of samples with SRA cured at 65% of relative humidity was always noticeably lower compared to the reference samples. It is obvious that a lower degree of hydra-

tion also results in a lower extent of drying shrinkage. For this reason, it is difficult to conclude whether the decline in drying shrinkage is related to the reduction of surface tension of the pore solution or the creation of a coarser microstructure (Fig. 7) with a lower proportion of mesopores.

It should be noted that the usage of SRAs in improving the drying shrinkage performance of OPC systems shows a somewhat different effect. Namely, it has been observed that the cement binders containing SRAs exhibit the reduction in the rate of cement hydration and strength development. Nevertheless, the reduction takes place mainly in the early-age compressive and tensile strength [32,36] but a noticeable strength improvement was later confirmed with simultaneous reduction of drying shrinkage [36,37]. It is obvious that the behaviour of AAS with the addition of SRAs is quite different. The reason may be related to the AAS pore

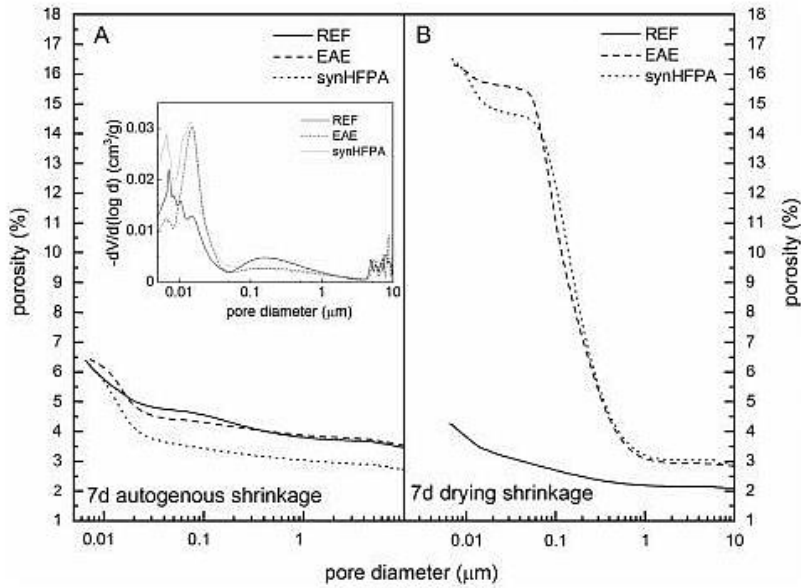


Fig. 5. Porosity of alkali-activated blast furnace slag in autogenous conditions (A) and cured at RH = 65% (B).

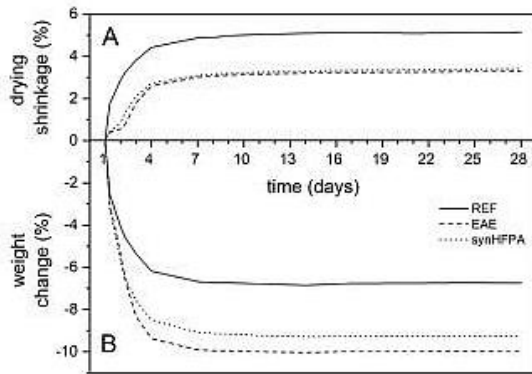


Fig. 6. Drying shrinkage (A) and weight changes (B) of alkali-activated blast furnace slag samples.

structure being generally more refined when compared to Portland cement. This implies that the lack of SRA molecules at the liquid-vapour interface can occur at a higher relative humidity compared to Portland cement and thus SRA loses its efficiency during the earlier drying stages. This can be partially slowed down by an increased dose of the SRA beyond its critical micelle concentration (CMC). Although it does not lead to a further decrease of the bulk pore solution surface tension, micelles can serve as a buffer for later stages of drying and interfacial area increase [6]. In this context, the issues of immobilization of SRA molecules by interactions with AAS through adsorption on slag particles and hydration products, as well as their consumption by hydration product may occur. Our recent study [38] showed that depending on the structure of SRAs, only a relatively small fraction of SRA remains in the pore solution in the mobile form, capable of migrating to the interfacial area to reduce surface tension. If the portion of the immobilized SRA is so high that its concentration in the pore solution is below CMC, the above described buffering effect is lost resulting in an earlier decrease of SRA efficiency.

Initially high but subsequently decreasing SRA efficiency can be seen in previous research by Bilim et al. [16], while work by

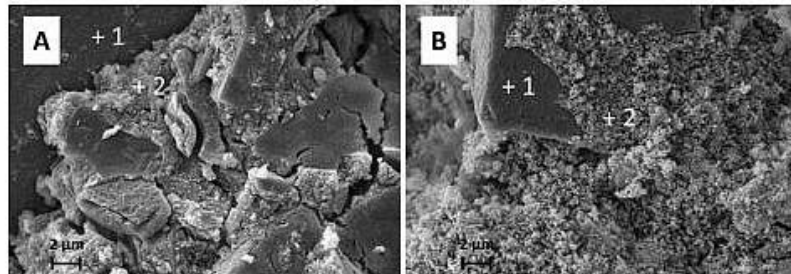


Fig. 7. SEM images of alkali-activated blast furnace slag with (B) and without (A) SRA addition after 7 days of hydration; RH = 65%; 1 – blast furnace slag particle, 2 – binder phase.

Palacios and Puertas [15] reported much higher SRA efficiency at the relative humidity of 99% compared to 50%. These results correlate well with the increase interfacial area during drying discussed above. However, findings presented in this study are rather opposite due to unaffected autogenous shrinkage and reduced drying shrinkage. It is true that during initial stages of autogenous shrinkage both SRAs seem to be efficient, but the decrease in shrinkage correlates better with the retardation of hydration than with the decrease in surface tension. The same stands for the initial stages of drying shrinkage and for weight loss during drying. These results, therefore suggest that at least in some cases of AAS, the effects of hydration degree and related pore structure or surface area on shrinkage prevail over the (bulk) pore solution surface tension.

#### 3.4. Action of amino alcohols in alkali-activated systems

The efficiency of SRAs can be affected if they adsorb at the solid/liquid interfaces. The adsorption of non-ionic surfactants was observed in various studies focused on different silicate solid materials such as precipitated silica [39], ground quartz [40], soils [41] or clays [42]. The consequence of adsorption closely related to the development of undesired properties of mortar or concrete and changed working mechanism of SRA at the liquid/air interface. Therefore, the examination of how the molecular nature of used surfactants affects the adsorption at the solid/liquid interfaces is critical for their utilization in alkali-activated systems.

This paper provided an investigation of SRAs adsorption based on the zeta potential measurement which gives information about the electrokinetic potential in the interfacial double layer of BFS grains. Several factors such as different pH, the nature of used alkaline activator or the addition of some admixture can fundamentally change the charge on BFS grain surface. If the BFS particles are in contact with water, the Si-O, Al-O and Ca-O bonds on their surface are broken under the polarization effect of OH<sup>-</sup> [43]. The strength of Ca-O bonds is weaker than that of Si-O or Al-O bonds resulting in a higher concentration of Ca<sup>2+</sup> ions in the solution [44] and very quick Si-Al-rich layer creation on the surface of BFS particles [45]. The Si-Al-rich layer can adsorb H<sub>3</sub>O<sup>+</sup> ions causing the increase of OH<sup>-</sup> concentration and consequently increasing the pH of the solution. An alkaline pH means that some silanol groups on wetted particle surface deprotonate and a negative charge is induced [46]. When alkaline activator (sodium waterglass) was added into the BFS suspension, a higher negative value of zeta potential was observed (Fig. 8). Kashani et al. [47] explained negative zeta potential through the presence of additional silicate species from the alkaline activator which can be adsorbed or can precipitate on the BFS particle surface. However, the situation will quickly change if an SRA is added to the alkaline suspension. Fig. 8 shows that a higher content of amino alcohol surfactants decreased the zeta potential values, as well as the surface charge. The effect of particle size variation on actual determined values of zeta potentials after individual SRA addition was neglected due to the minimal observed changes in average scattered light intensity during the performed experiments. It should follow that used surfactants were adsorbed on the BFS surface. The adsorption mechanism of surfactants may be explained by the hydrogen bonding between the polar hydrophilic head of SRAs (C-OH) and the silanol groups on the slag surface [48]. Due to the amphiphilic nature of the most used SRAs for which the non-ionic character is typical, the tendency to adsorb onto hydrophilic surfaces is always expected. The adsorption is more accelerated if a fluorinated surfactant with a longer hydrophobic tail is used. Similar results were achieved in the Partyka et al. [39] study. Moreover, the authors observed that the CMC of surfactant with longer hydrophobic chain was drastically decreased which is related to the maximum degree of adsorp-

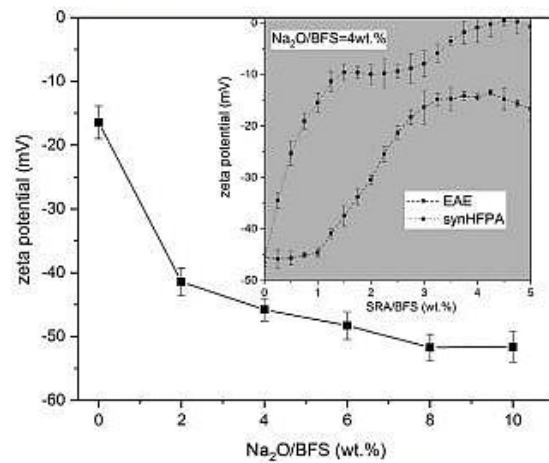


Fig. 8. Zeta potential of slag suspensions with different sodium waterglass dosage and after the addition of amino alcohol admixtures.

tion. The dissolution of BFS is then negatively affected and the hydration process slows down as was shown in the formation of a primary C-(A)-S-H gel in the previous results (see Fig. 3). The delay in the creation of the secondary C-(A)-S-H gel probably also depends on the length of the hydrophobic tail and molecular structure of SRAs in general as was showed by Bilek et al. [49]. However, further and deeper investigation between the character of organic admixtures and the hydration mechanism of AAM is necessary.

#### 4. Conclusion

Based on obtained results, the essential conclusions may be summarized as follows:

- The addition of surfactants with a higher potential to reduce the surface tension of pore solution does not have any influence on the autogenous shrinkage or on the hydration process of AAS from a long-term point of view. The decrease in capillary pressure does not lead to the shrinkage reduction. Therefore, the basic principle of the working mechanism of SRAs in alkali-activated systems ceases to be applicable.
- The effect of SRAs on the drying shrinkage reduction is also speculative. Observed shrinkage reduction with the SRAs content is caused by the smaller amount of binder phase formation, rather than by the effective action of used admixtures.
- A great influence on the hydration process of AAS in the presence of SRAs was shown. The molecular character of used non-ionic surfactants causes a noticeable adsorption on slag particles during the alkaline activation resulting in the retardation of the hydration process. Due to similar nature of the most commercially used SRAs, the analogous behaviour can be expected. Therefore, the development of specific admixtures designed exclusively for AAM will be necessary for the future.

#### CRedit authorship contribution statement

**Lukáš Kalina:** Conceptualization, Investigation, Writing - original draft, Writing - review & editing, Methodology. **Vlastimil Bilek:** Validation, Methodology, Writing - review & editing. **Eva Bartoníčková:** Visualization. **Michal Kalina:** Formal analysis. **Jan Hajzler:** Formal analysis. **Radoslav Novotný:** Formal analysis.

### Acknowledgements

This work was financially supported by the project: GA17-03670S, "Development of shrinkage reducing agents designed for alkali activated systems," with financial support from the Czech science foundation.

### References

- [1] J.L. Provis, Geopolymers and other alkali activated materials: why, how, and what?, *Mater. Struct.* 47 (2014) 11–25, <https://doi.org/10.1617/s11527-013-0211-5>.
- [2] A. Palomo, M.T. Blanco-Varela, M.L. Granizo, F. Puertas, T. Vazquez, M.W. Grutzeck, Chemical stability of cementitious materials based on metakaolin, *Cement Concrete Res.* 29 (1999) 997–1004, [https://doi.org/10.1016/S0008-8846\(99\)00074-5](https://doi.org/10.1016/S0008-8846(99)00074-5).
- [3] J. Davidovits, Geopolymers – inorganic polymeric new materials, *J. Therm. Anal.* 37 (1991) 1633–1656, <https://doi.org/10.1007/B01912193>.
- [4] W.K.W. Lee, J.S.J. van Deventer, The effect of ionic contaminants on the early-age properties of alkali-activated fly ash-based cements, *Cem. Concr. Res.* 32 (2002) 577–584, [https://doi.org/10.1016/S0008-8846\(01\)00724-4](https://doi.org/10.1016/S0008-8846(01)00724-4).
- [5] A.A.M. Neto, M.A. Cincotto, W. Repette, Drying and autogenous shrinkage of pastes and mortars with activated slag cement, *Cem. Concr. Res.* 38 (2008) 565–574, <https://doi.org/10.1016/j.cemconres.2007.11.002>.
- [6] P.C. Aitcin, R.J. Flair, *Science and Technology of Concrete Admixtures*, Woodhead Publishing, Cambridge, 2015.
- [7] F. Beltzung, F.H. Wittmann, Role of disjoining pressure in cement based materials, *Cem. Concr. Res.* 35 (2005) 2364–2370, <https://doi.org/10.1016/j.cemconres.2005.04.004>.
- [8] G.W. Scherer, Drying, shrinkage, and cracking of cementitious materials, *Transport Porous Med.* 110 (2015) 311–331, <https://doi.org/10.1007/s11242-015-0518-5>.
- [9] H.L. Ye, A. Radlinska, Shrinkage mechanisms of alkali-activated slag, *Cem. Concr. Res.* 88 (2016) 126–135, <https://doi.org/10.1016/j.cemconres.2016.07.001>.
- [10] H.L. Ye, C. Cartwright, F. Rajabipour, A. Radlinska, Understanding the drying shrinkage performance of alkali-activated slag mortars, *Cem. Concr. Comp.* 76 (2017) 13–24, <https://doi.org/10.1016/j.cemconcomp.2016.11.010>.
- [11] P.K. Mehta, P.J.M. Monteiro, *Concrete: Microstructure, Properties, and Materials*, third ed., McGraw-Hill, New York, 2006.
- [12] G. Sant, The influence of temperature on autogenous volume changes in cementitious materials containing shrinkage reducing admixtures, *Cem. Concr. Comp.* 34 (2012) 855–865, <https://doi.org/10.1016/j.cemconcomp.2012.04.003>.
- [13] P. Lura, B. Pease, G.B. Mazzotta, F. Rajabipour, J. Weiss, Influence of shrinkage-reducing admixtures on development of plastic shrinkage cracks, *ACI Mater. J.* 104 (2007) 187–194, <https://doi.org/10.14359/18582>.
- [14] D.P. Bentz, Influence of shrinkage-reducing admixtures on early-age properties of cement pastes, *J. Adv. Concr. Technol.* 4 (2006) 423–429, <https://doi.org/10.3151/jact.4.423>.
- [15] M. Palacios, F. Puertas, Effect of shrinkage-reducing admixtures on the properties of alkali-activated slag mortars and pastes, *Cem. Concr. Res.* 37 (2007) 691–702, <https://doi.org/10.1016/j.cemconres.2006.11.021>.
- [16] C. Bilim, O. Karahan, C.D. Atis, S. Ilkentapar, Influence of admixtures on the properties of alkali-activated slag mortars subjected to different curing conditions, *Mater. Des.* 44 (2013) 540–547, <https://doi.org/10.1016/j.matdes.2012.08.049>.
- [17] V. Bilek, L. Kalina, R. Novotny, J. Tkacz, L. Parizek, Some issues of shrinkage-reducing admixtures application in alkali-activated slag systems, *Materials* 9 (2016), <https://doi.org/10.3390/Ma9060462>.
- [18] F. Collins, J.G. Sanjayan, Effect of pore size distribution on drying shrinkage of alkali-activated slag concrete, *Cem. Concr. Res.* 30 (2000) 1401–1406, [https://doi.org/10.1016/S0008-8846\(00\)00327-6](https://doi.org/10.1016/S0008-8846(00)00327-6).
- [19] J.A. Zhou, G.A. Ye, K. van Breugel, Characterization of pore structure in cement-based materials using pressurization-depressurization cycling mercury intrusion porosimetry (PDC-MIP), *Cem. Concr. Res.* 40 (2010) 1120–1128, <https://doi.org/10.1016/j.cemconres.2010.02.011>.
- [20] D.B. Kumarappa, S. Peethamparan, M. Ngami, Autogenous shrinkage of alkali activated slag mortars: basic mechanisms and mitigation methods, *Cem. Concr. Res.* 109 (2018) 1–9, <https://doi.org/10.1016/j.cemconres.2018.04.004>.
- [21] J. Weiss, P. Lura, F. Rajabipour, G. Sant, Performance of shrinkage-reducing admixtures at different humidities and at early ages 638–638, *ACI Mater. J.* 105 (2008), <https://doi.org/10.14359/19977>.
- [22] D.P. Bentz, M.R. Geiker, K.K. Hansen, Shrinkage-reducing admixtures and early-age desiccation in cement pastes and mortars, *Cem. Concr. Res.* 31 (2001) 1075–1085, [https://doi.org/10.1016/S0008-8846\(01\)00519-1](https://doi.org/10.1016/S0008-8846(01)00519-1).
- [23] G. Sant, B. Lothenbach, P. Juilland, G. Le Saout, J. Weiss, K. Scrivener, The origin of early age expansions induced in cementitious materials containing shrinkage reducing admixtures, *Cem. Concr. Res.* 41 (2011) 218–229, <https://doi.org/10.1016/j.cemconres.2010.12.004>.
- [24] S. Chen, H. Zhao, Y. Chen, D. Huang, Y. Chen, X. Chen, Experimental study on interior relative humidity development in early-age concrete mixed with shrinkage-reducing and expansive admixtures, *Constr. Build. Mater.* 232 (2020), <https://doi.org/10.1016/j.conbuildmat.2019.117204>.
- [25] Z.H. He, C.X. Qian, Internal relative humidity and creep of concrete with modified admixtures, *Prog. Nat. Sci.-Mater.* 21 (2011) 426–432, [https://doi.org/10.1016/S1002-0071\(12\)60079-3](https://doi.org/10.1016/S1002-0071(12)60079-3).
- [26] F.H. Wittmann, F. Beltzung, Fundamental aspects of the interaction between hardened cement paste and water applied to improve prediction of shrinkage and creep of concrete: a critical review, *J. Sustain. Cem.-Based* 5 (2016) 106–116, <https://doi.org/10.1080/21650373.2015.1091998>.
- [27] C.J. Shi, R.L. Day, A calorimetric study of early hydration of alkali-slag cements, *Cem. Concr. Res.* 25 (1995) 1333–1346, [https://doi.org/10.1016/0008-8846\(95\)00126-W](https://doi.org/10.1016/0008-8846(95)00126-W).
- [28] A.R. Brough, M. Holloway, J. Sykes, A. Atkinson, Sodium silicate-based alkali-activated slag mortars Part II. The retarding effect of additions of sodium chloride or malic acid, *Cem. Concr. Res.* 30 (2000) 1375–1379, [https://doi.org/10.1016/S0008-8846\(00\)00356-2](https://doi.org/10.1016/S0008-8846(00)00356-2).
- [29] A. Gruskovnjak, B. Lothenbach, L. Holzer, R. Figi, F. Winnefeld, Hydration of alkali-activated slag: comparison with ordinary Portland cement, *Adv. Cem. Res.* 18 (2006) 119–128, <https://doi.org/10.1680/jadcr.2006.18.3.119>.
- [30] A. Fernandez-Jimenez, F. Puertas, I. Sobrados, J. Sanz, Structure of calcium silicate hydrates formed in alkaline-activated slag: influence of the type of alkaline activator, *J. Am. Ceram. Soc.* 86 (2003) 1389–1394, <https://doi.org/10.1111/j.1151-2916.2003.tb03481.x>.
- [31] S. Mindess, J.F. Young, *Concrete*, Prentice-Hall, Englewood Cliffs, N.J., 1981.
- [32] S.P. Shah, M.E. Karaguler, M. Sarigaphuti, Effects of shrinkage-reducing admixtures on restrained shrinkage cracking of concrete, *ACI Mater. J.* 89 (1992) 289–295, <https://doi.org/10.14359/2593>.
- [33] L. Kalina, V. Bilek, E. Bartonickova, J. Krouska, Polypropylene glycols as effective shrinkage-reducing admixtures in alkali-activated materials, *ACI Mater. J.* 115 (2018) 251–256, <https://doi.org/10.14359/51701099>.
- [34] F. Wittmann, H. Splittgerber, K. Ebert, Vanderwaals force at small distances, *Z. Phys.* 245 (1971) 354, <https://doi.org/10.1007/BF01400699>.
- [35] H. Splittgerber, F. Wittmann, Influence of adsorbed water film on vanderwaals forces between quartz glass surfaces, *Surf. Sci.* 41 (1974) 504–514, [https://doi.org/10.1016/0039-6028\(74\)90066-1](https://doi.org/10.1016/0039-6028(74)90066-1).
- [36] K.J. Folliard, N.S. Berke, Properties of high-performance concrete containing shrinkage-reducing admixture, *Cem. Concr. Res.* 27 (1997) 1357–1364, [https://doi.org/10.1016/S0008-8846\(97\)00135-X](https://doi.org/10.1016/S0008-8846(97)00135-X).
- [37] V. Corinaldesi, Combined effect of expansive, shrinkage reducing and hydrophobic admixtures for durable self compacting concrete, *Constr. Build. Mater.* 36 (2012) 758–764, <https://doi.org/10.1016/j.conbuildmat.2012.04.129>.
- [38] V. Bilek, L. Kalina, E. Bartonickova, J. Porizka, Evaluation of the surfactant leaching from alkali-activated slag-based composites using surface-tension measurements, *Mater. Technol.* 53 (2019) 33–38, <https://doi.org/10.17222/mit.2018.148>.
- [39] S. Partyka, S. Zaini, M. Lindheimer, B. Brun, The adsorption of non-ionic surfactants on a silica-gel, *Colloid Surf.* 12 (1984) 255–270, [https://doi.org/10.1016/0166-6622\(84\)80104-3](https://doi.org/10.1016/0166-6622(84)80104-3).
- [40] R. Denoyel, J. Rouquerol, Thermodynamic (including microcalorimetry) study of the adsorption of nonionic and anionic surfactants onto silica, kaolin, and alumina, *J. Colloid Interf. Sci.* 143 (1991) 555–572, [https://doi.org/10.1016/0021-9797\(91\)90287-1](https://doi.org/10.1016/0021-9797(91)90287-1).
- [41] Z.B. Liu, D.A. Edwards, R.G. Luthy, Sorption of nonionic surfactants onto soil, *Water Res.* 26 (1992) 1337–1345, [https://doi.org/10.1016/0043-1354\(92\)90128-0](https://doi.org/10.1016/0043-1354(92)90128-0).
- [42] N. Narkis, B. Bendavid, Adsorption of non-ionic surfactants on activated carbon and mineral clay, *Water Res.* 19 (1985) 815–824, [https://doi.org/10.1016/0043-1354\(85\)90138-1](https://doi.org/10.1016/0043-1354(85)90138-1).
- [43] C. Shi, P.V. Krivenko, D.M. Roy, *Alkali-Activated Cements and Concretes*, Taylor & Francis, London, New York, 2006.
- [44] S.J. Song, H.M. Jennings, Pore solution chemistry of alkali-activated ground granulated blast-furnace slag, *Cem. Concr. Res.* 29 (1999) 159–170, [https://doi.org/10.1016/S0008-8846\(98\)00212-9](https://doi.org/10.1016/S0008-8846(98)00212-9).
- [45] Z. Rajaokarivonyandriambololona, J.H. Thomassin, P. Baillif, J.C. Touray, Experimental Hydration of 2 Synthetic Glassy Blast-Furnace Slags in Water and Alkaline-Solutions (NaOH and KOH.1n) at 40-Degrees-C - Structure, Composition and Origin of the Hydrated Layer, *J. Mater. Sci.* 25 (1990) 2399–2410, <https://doi.org/10.1007/BF00638034>.
- [46] C. Labbez, B. Jonsson, L. Pochard, A. Nonat, B. Cabane, Surface charge density and electrokinetic potential of highly charged minerals: experiments and Monte Carlo simulations on calcium silicate hydrate, *J. Phys. Chem. B* 110 (2006) 9219–9230, <https://doi.org/10.1021/jp057096a>.
- [47] A. Kashani, J.L. Provis, G.G. Qiao, J.S.J. van Deventer, The interrelationship between surface chemistry and rheology in alkali activated slag paste, *Constr. Build. Mater.* 65 (2014) 583–591, <https://doi.org/10.1016/j.conbuildmat.2014.04.127>.
- [48] P. Somasundaran, S. Krishnakumar, Adsorption of surfactants and polymers at the solid-liquid interface, *Colloid Surface A* 123 (1997) 491–513, [https://doi.org/10.1016/S0927-7757\(96\)03829-0](https://doi.org/10.1016/S0927-7757(96)03829-0).
- [49] V. Bilek, L. Kalina, R. Novotny, J. Porizka, O. Opravil, F. Soukal, Effect of alcohol structure on hydration of alkali-activated slag, 10th ACI/RILEM International Conference on Cementitious Materials and Alternative Binders for Sustainable Concrete, 2017.

EFFECT OF AMINO ALCOHOL ADMIXTURES ON  
ALKALI-ACTIVATED MATERIALSVPLIV AMINO-ALKOHOLNIH DODATKOV NA ALKALNO  
AKTIVIRANE MATERIALE

Lukáš Kalina, Vlastimil Bílek Jr., Eva Bartoničková

Brno University of Technology, Faculty of Chemistry, Purkyňova 118, 612 00 Brno, Czech Republic

*Prejem rokopisa – received: .....; sprejem za objavo – accepted for publication: .....*

doi:10.17222/mit. ....

One of the most important technological problems associated with alkali-activated materials (AAM) is large shrinkage. A possible solution to decrease the extensive drying shrinkage of these materials is the use of shrinkage-reducing admixtures (SRAs). The promising group of SRAs, from the perspective of using in AAMs, are amino alcohols. However, the efficiency of reducing the drying shrinkage strongly depends on their chemical structure. Hence, the study is focused on the molecular architecture of amino alcohol surfactants and its relation to the affected properties of alkali-activated blast-furnace slag systems. Selected amino alcohols were tested in terms of the ability to reduce the surface tension of pore solution as well as to influence the drying shrinkage, hydration mechanism and mechanical properties of AAMs. The study confirms that the length and branching of the alkyl chain linked to the amino group play the key role in SRA efficiency. Amino alcohol surfactants with a high-carbon alkyl chain decreased dramatically both the surface tension and the drying shrinkage, but simultaneously negatively affected the process of alkali activation, resulting in a deterioration of the mechanical properties. Conversely, the addition of 0.5 w/ % of the surfactants with a low molecular weight, such as 2-(Methylamino)ethanol, showed a slight improvement of the compressive strength after 7 d and 28 d, and at the same time reduced the drying shrinkage by 30 % compared to the reference sample.

Keywords: amino alcohols, admixture, drying shrinkage, alkali-activated materials

Eden od najpomembnejših tehnoloških problemov, ki se nanaša na alkalno aktivirane materiale (AAM) je njihov skrčec. Možna rešitev za zmanjšanje znatnega krčenja med sušenjem teh materialov je uporaba dodatkov (SRAs) za njegovo zmanjšanje. Obetajoča skupina SRA dodatkov s stališča njihove uporabe za AAM so amino-alkoholi. Vendar je učinkovitost zmanjšanja krčenja med sušenjem močno odvisna od njihove kemijske strukture. Zato so se avtorji tega prispevka osredotočili na študij arhitekture snovi (surfaktantov), ki aktivno vplivajo na površino amino-alkoholov in njihovo povezavo z vzročnimi lastnostmi alkalno aktiviranih sistemov plavžnih žlindrov. Izbrane amino-alkohole so avtorji testirali glede na sposobnost zmanjšanja površinske napetosti porozne (mehurčaste) raztopine, kakor tudi vpliv na krčenje med sušenjem, hidracijske mehanizme in mehanske lastnosti AAM. Študija je potrdila da dolge in razvejane vezi alkalnih verig igrajo ključno vlogo pri dodatkih, ki učinkovito zmanjšujejo krčenje. Amino-alkoholni surfaktanti z visoko vsebnostjo ogljiko-alkilnih vezi močno zmanjšujejo tako površinsko napetost kot tudi krčenje med sušenjem, ki pa žal istočasno negativno vpliva na proces alkalne aktivacije, kar posledično vodi do poslabšanja mehanskih lastnosti. Nasprotno temu pa dodatek 0,5 mas. % površinsko aktivne snovi z majhno molekularno maso kot je 2-(metilamino)etanol kaže rahlo izboljšanje tlačne trdnosti po 7 in 28 dneh in istočasno zmanjšanje skrčka med sušenjem za 30 % v primerjavi z referenčnimi vzorci.

Ključne besede: amino-alkoholi, mešanice, skrčec po sušenju, alkalno aktivirani materiali

## 1 INTRODUCTION

From the general point of view, shrinkage-reducing admixtures (SRAs) are organic surfactants that reduce the surface tension of the pore solution of water films that cover the solid surfaces in cementitious materials.<sup>1</sup> The utilization of SRAs was introduced in 1983 in the study by Sato,<sup>2</sup> where chemical admixtures based on polyoxyalkylene glycol alkyl ether were used. Nowadays, the SRAs are characteristic for their non-ionic nature preventing the adsorption of the additive to the hydration products. The typical chemical compounds used for SRAs belong to the groups of mono-alcohols, glycols, alkylether oxyalkylene glycols and polymeric surfactants or their mutual combination, having a synergic effect in enhancing the shrinkage reduction. The

vast majority of commercial SRAs are designed for ordinary Portland cements (OPCs); therefore, their efficiency in other inorganic binders may vary significantly.

Alkali-activated materials (AAMs) represent a group of inorganic materials characterized by a pore solution with a high pH;<sup>3</sup> therefore, the molecular design of any organic admixture plays a key role. The same applies to SRAs. The searching for a suitable type of SRA designed especially for AAMs turned out to be complicated, despite the fact that shrinkage is one of the most important technological problems related to many alkali-activated systems. Until now, only several studies have been focused on the organic admixtures affecting the shrinkage of AAMs.<sup>4</sup>

Palacios and Puertas<sup>5</sup> studied the effect of polypropylene glycol-based SRA on the shrinkage and other properties of water-glass-activated slag (4 % Na<sub>2</sub>O). At a

\*Corresponding author's e-mail:  
kalina@fch.vut.cz (Lukáš Kalina)

relative humidity of 50 % the drying shrinkage of alkali-activated slag mortars was reduced by approximately 7 % and 35 % for doses of SRA of 1 % and 2 %, respectively, while the shrinkage reduction at the relative humidity of 99 % was considerably greater: about 50 % and 75 % for the same doses. Also, Bilim et al.<sup>6,7</sup> used SRA based on polypropylene glycol to mitigate the shrinkage of alkali-activated slag mortars. Again, the drying shrinkage as well as the shrinkage during the moist curing was significantly reduced (up to about 40 % after 180 days) for either liquid sodium silicate or solid sodium metasilicate. The SRA based on polypropylene glycols with different molecular weights was the subject of an investigation by Kalina et al.<sup>8</sup> as well. The study demonstrated that increasing the length of the polymeric chain decreases the surface tension, but also fundamentally changes the pore size distribution, affecting the total shrinkage of alkali-activated blast-furnace slag. The effect of polyethylene glycols on the drying shrinkage of water-glass-activated slag was studied by Bilek et al.<sup>9</sup> The results showed that the efficiency of the shrinkage reduction increased with the increasing molecular weight of the tested glycols.

It is evident that the research in this area was primarily focused on the surfactants based on alkylene glycols. Another alternative may be amino alcohols. These surfactants provide an essential benefit in comparison with alkylene glycols. One of the important properties regarding the SRA's action is the dispersion of used surfactants within the alkaline solution. Amino alcohols show a high dispersibility range in the pore solution because they contain hydrophilic groups, which increase their hydrophile lipophile balance (HLB) value.<sup>10</sup>

Therefore, this study deals with the efficiency assessment of amino alcohol-based SRAs in alkali-activated blast-furnace slag systems. The molecular structure of the used surfactants is evaluated in terms of affecting the character and properties of the prepared alkali-activated materials.

## 2 EXPERIMENTAL PART

### 2.1 Materials and sample preparation

Blast-furnace slag (BFS) with a Blaine fineness of 400 m<sup>2</sup>/kg and the chemical composition given in **Table 1** was chosen as the primary aluminosilicate material for the preparation of the alkali-activated samples. The XRD analysis determined more than 90 % of amorphous phase with the content of crystals such as melilite, calcite and merwinite. Sodium water-glass with a silicate module of

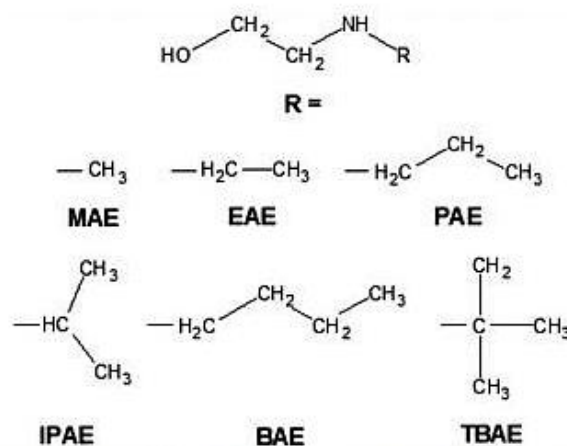


**Figure 1:** Molecular structure of used amino ethanol surfactants (MAE: 2-(Methylamino)ethanol; EAE: 2-(Ethylamino)ethanol; PAE: 2-(Propylamino)ethanol; IPAE: 2-(Isopropylamino)ethanol; BAE: 2-(Isobutylamino)ethanol; TBAE: 2-(*tert*-Butylamino)ethanol)

1.98 was used as the alkaline activator. The Na<sub>2</sub>O/BFS ratio was adjusted to 4 w/%. Amino alcohols with different alkyl chains (summarized in **Figure 1**) were added in the dosage of 0.5 w/% by mass of BFS.

### 2.2 Preparation and physical-mechanical testing of samples

Alkali-activated BFS mortars were prepared as follows. The sand-to-BFS ratio was 3:1 using three different fractions of siliceous sand specified according to the EN-196-1 standard and the water-to-BFS ratio was adjusted to 0.50. The mixing and curing processes were carried out at laboratory temperature (25 °C). Mortar samples with the dimensions of (40 × 40 × 160) mm were cast and further cured under a defined relative humidity (50 %) and then subjected to compressive strength measurements using the strength tester Beton-system Desttest 3310 after 1, 7 and 28 d. The same process of preparation was applied for (25 × 25 × 285) mm samples. These species were subjected to the shrinkage measurements based on ASTM C596 (25 °C; RH = 50 %). The dynamic surface tension of synthetic pore solutions with different amino alcohol admixtures was measured by the tensiometer BPA-800P (KSV Instruments company) using the maximum-bubble-pressure method. The synthetic pore solution was prepared based on the chemical composition of the real pore solution obtained 24 hours after mixing and determined by ICP-OES. It means the same time as the drying shrinkage measurement was started.

**Table 1:** Chemical compositions of blast furnace slag by XRF analysis

raw material	chemical composition / w/%									
	SiO <sub>2</sub>	Al <sub>2</sub> O <sub>3</sub>	CaO	MgO	SO <sub>3</sub>	Na <sub>2</sub> O	K <sub>2</sub> O	TiO <sub>2</sub>	MnO	Fe <sub>2</sub> O <sub>3</sub>
blast furnace slag	34.7	9.1	41.1	10.5	1.4	0.4	0.9	1.0	0.6	0.3

### 2.3 Isothermal calorimetry

The evolution of hydration heat was monitored using the TAM Air isothermal microcalorimeter (TA instruments). The measurements of heat evolution were performed at a constant surrounding temperature of 25 °C. When the thermal equilibrium was achieved, the BFS and alkaline activator with a specific SRA were mixed together by injecting the solution into the 15-mL vial and stirring it for 3 min. The samples were made of alkali-activated paste without the standard sand; however, with the same water/BFS and  $\text{Na}_2\text{O}/\text{BFS}$  mass ratios that were used for the preparation process of the mortars. The heat evolution was recorded as the heat flow immediately after mixing.

### 2.4 Microstructure characterization

Microstructure characterization was performed using scanning electron microscopy (Zeiss EVO LS 10) in secondary-electron mode. The working distance during the observation was 9.5 mm and the accelerating voltage was set to 10 kV. All the samples were sputtered with gold before the measurements.

### 2.5 Mercury-intrusion porosimetry

The total porosity of the samples was determined with a mercury porosimeter (Poremaster Quantachrome Instruments). The working pressure range was from 0.14 MPa to 231 MPa, which covered a pore diameter range from 0.007  $\mu\text{m}$  to 10  $\mu\text{m}$ . The measurements were performed with the following conditions: Hg surface tension was 0.480 N/m, Hg contact angle was 140° and scan mode was chosen to average from 11 points. The intrusion data were normalized by sample weight and volume.

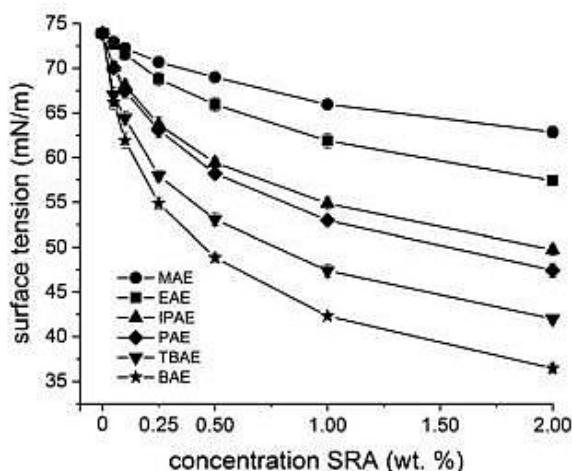


Figure 2: Effect of amino alcohols on the surface tension of the pore solution

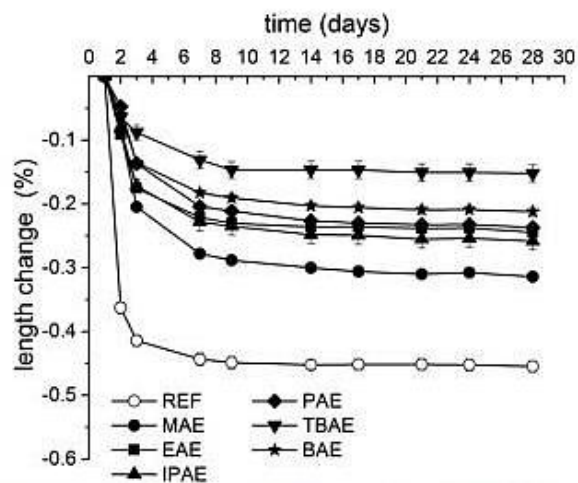


Figure 3: Effect of amino alcohols (0.5 % by weight of BFS) on the drying shrinkage

## 3 RESULTS AND DISCUSSION

The mechanism of action of SRA was introduced in the study of Sato et al.<sup>2</sup> in 1983. They suggested that the decrease of the surface tension of a cement pore solution tends to reduce the shrinkage due to the elimination of capillary forces. Therefore, the effect of quantity and molecular structure of the used amino alcohols on the surface tension of pore solution were tested. Figure 2 shows that the surface tension decreases with both a large amount of surfactant and the presence of long or branched alkyl substituents. Moreover, the surface-tension measurement provides information about the effective bulk concentration of surface-active admixtures in AAM. In terms of a good ability to decrease the surface tension, the addition of 0.5 w/% by mass of BFS was used for the preparation of the mortar samples.

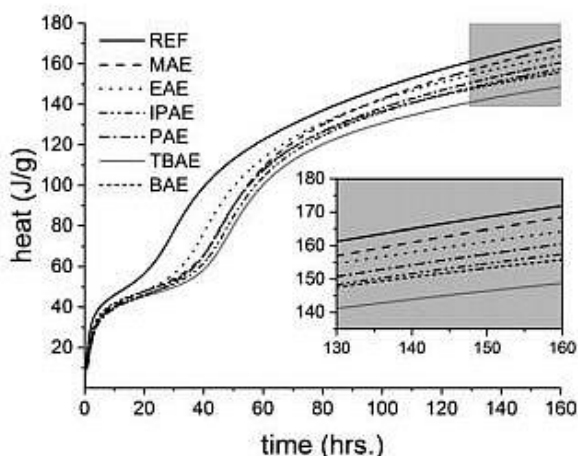


Figure 4: Effect of amino alcohols (0.5 % by weight of BFS) on the total heat evolution

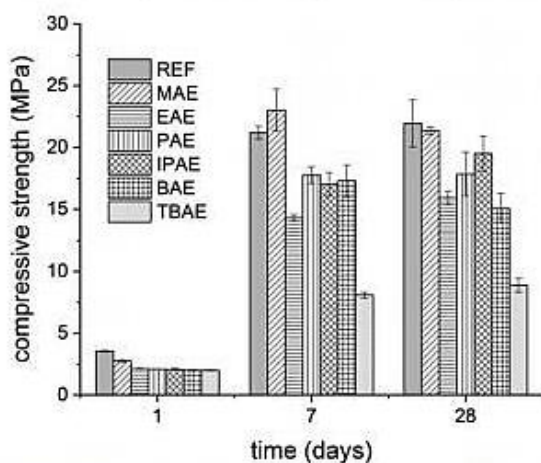


Figure 5: Effect of amino alcohols (0.5 % by weight of BFS) on the compressive-strength development

The effect of amino alcohol SRA on the reduction of the drying shrinkage is clear from Figure 3. It can be seen that the surfactants with a long alkyl chain bonded to the amino group tended to decrease the drying shrinkage. Branched chains of substituents also play an important role. It is evident that 2-(*tert*-Butylamino)alcohol has a higher ability to reduce the drying shrinkage

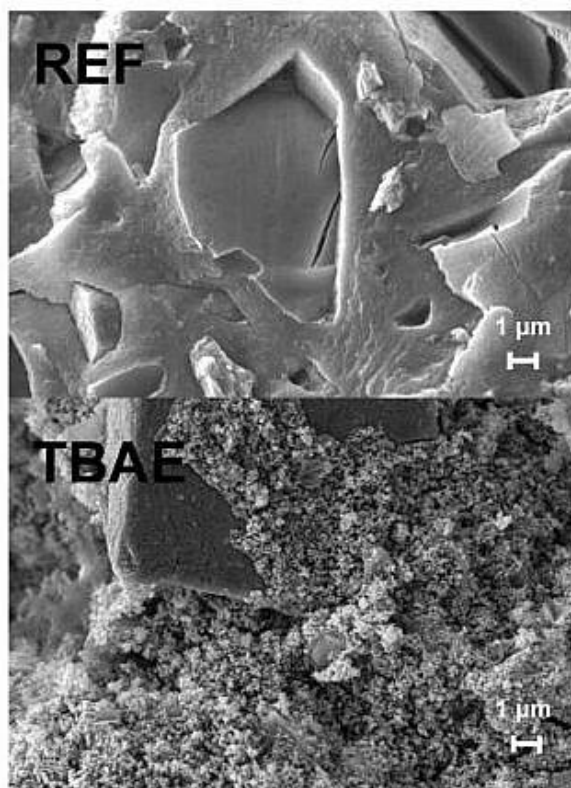


Figure 6: Microstructure of alkali-activated blast-furnace slag without (top) and with 2-(*tert*-Butylamino)alcohol (bottom) after 7 d

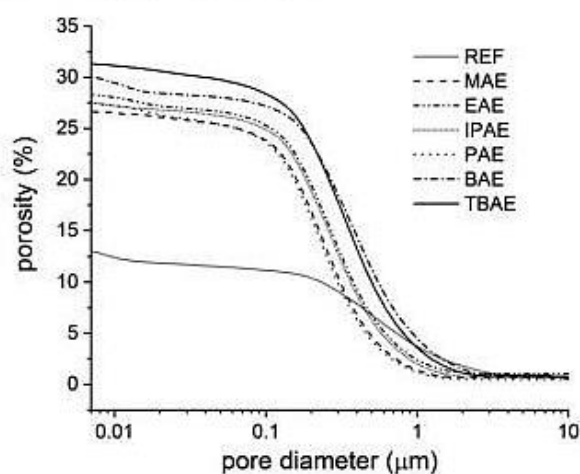


Figure 7: Total porosity measurement of alkali-activated blast-furnace slag with and without amino alcohol admixtures (0.5 % by weight of BFS) after 7 d

compared to 2-(Butylamino)alcohol. However, we can see that the surface-tension measurement does not fully correlate with the drying shrinkage evolution. Therefore, the fundamental question arises. Are these two parameters directly dependent on each other? The answer can be suggested by the monitoring of the hydration process. The measurement of the total heat evolution (Figure 4) during the alkaline activation clearly indicates the negative effect of the SRA content, especially during the early ages of the hydration process. This is also confirmed by the development of compressive strengths (Figure 5). The results from the isothermal calorimetry also show that amino alcohols with a low molecular weight such as 2-(Methylamino)alcohol exhibit almost the same total heat evolution as the reference sample without any admixture after 7 d.

It is well known that the total heat evolution is directly related to the binder phase's formation. CASH (calcium-aluminium-silicate-hydrate) gel is the main hydration product in the systems based on the alkaline activation of BFS, which was confirmed by several studies.<sup>11</sup> The amount of formed CASH gel strongly influences the porosity of the AAM. The materials with higher content of CSH or CASH gels create denser structures with small pores. Such systems contain mainly pores with a diameter lower than 10 nm, which greatly affects the magnitude of the drying shrinkage.<sup>12</sup> Since alkali-activated BFS without SRA has a typical structure, as mentioned above, one would expect the shrinkage strain to be larger than in a material with a coarser microstructure, such as in the case of AAM with TBAE (Figure 6). A similar relationship between the adverse effect of the SRA on the AAM hydration resulting in a lower amount of CASH and a more porous microstructure was also observed in previous studies<sup>8,13</sup> where SRAs-based glycols were used. The changes in total porosity were confirmed by mercury-intrusion porosi-

metry (Figure 7). The samples with the addition of SRA had a significantly higher porosity compared to the reference sample after 7 d. The direct relationship between drying-shrinkage development and the porosity of samples caused by the addition of specific amino alcohol surfactants was clearly observed.

#### 4 CONCLUSIONS

The results suggest that the extent of the drying shrinkage of AAM is mainly controlled by the porosity of the formed structure. In other words, by the quantity of created binder phase, rather than by the decrease of surface tension of the pore solution. Despite the non-ionic character of the used amino alcohol surfactants, the adsorption on the BFS particles, causing the reduction of their solubility in an alkaline environment could be assumed. Promising results indicate the usage of 2-(Methylamino)alcohol. This surface-active admixture in the amount of 0.5 w/% by mass of BFS did not negatively influence the mechanical properties after 7 d and 28 d and reduced the drying shrinkage by 30 % compared to the reference sample.

#### Acknowledgement

This outcome has been achieved with the financial support by the project: GA17-03670S, "Development of shrinkage reducing agents designed for alkali activated systems," with financial support from the Czech science foundation.

#### 5 REFERENCES

- <sup>1</sup> P. C. Aïtcin, R. J. Flatt, *Science and Technology of Concrete Admixtures*, 1<sup>st</sup> ed., Elsevier, Cambridge 2015, 613
- <sup>2</sup> T. Sato, T. Goto, K. Sakai, Mechanism for reducing drying shrinkage of hardened cement by organic additives, *Cement Association of Japan Review*, **1983**, 52–54
- <sup>3</sup> R. R. Lloyd, J. L. Provis, J. S. J. van Deventer, Pore solution composition and alkali diffusion in inorganic polymer cement. *Cement and Concrete Research*, **40** (2010), 1386–1392, doi:10.1016/j.cemconres.2010.04.008
- <sup>4</sup> J. L. Provis, J. S. J. van Deventer, *Alkali Activated Materials*, 1<sup>st</sup> ed., Springer, London 2014, 388, doi:10.1007/978-94-007-7672-2
- <sup>5</sup> M. Palacios, F. Puertas, Effect of shrinkage-reducing admixtures on the properties of alkali-activated slag mortars and pastes, *Cement and Concrete Research*, **37** (2007), 691–702, doi:10.1016/j.cemconres.2006.11.021
- <sup>6</sup> C. Bilim, O. Karahan, C. D. Atis, S. Ilkentapar, Influence of admixtures on the properties of alkali-activated slag mortars subjected to different curing conditions, *Materials & Design*, **44** (2013), 540–547, doi:10.1016/j.matdes.2012.08.049
- <sup>7</sup> C. Bilim, O. Karahan, C. D. Atis, S. Ilkentapar, Effects of chemical admixtures and curing conditions on some properties of alkali-activated cementless slag mixtures, *KSCE Journal of Civil Engineering*, **19** (2015), 733–741, doi:10.1007/s12205-015-0629-0
- <sup>8</sup> L. Kalina, V. Bilek, E. Bartonickova, J. Krouska, Polypropylene Glycols as Effective Shrinkage-Reducing Admixtures in Alkali-Activated Materials, *ACI Materials Journal*, **115** (2018), 251–256, doi:10.14359/51701099
- <sup>9</sup> V. Bilek, L. Kalina, R. Novotny, Polyethylene glycol molecular weight as an important parameter affecting drying shrinkage and hydration of alkali-activated slag mortars and pastes, *Construction and Building Materials*, **166** (2018), 564–571, doi:10.1016/j.conbuildmat.2018.01.176
- <sup>10</sup> X. W. Guo, Z. M. Rong, X. G. Ying, Calculation of hydrophile-lipophile balance for polyethoxylated surfactants by group contribution method, *Journal of Colloid and Interface Science*, **298** (2006), 441–450, doi:10.1016/j.jcis.2005.12.009
- <sup>11</sup> C. Shi, P. V. Krivenko, D. Roy, *Alkali-Activated Cements and Concretes*, 1<sup>st</sup> ed., Taylor&Francis, Oxon 2006, 376.
- <sup>12</sup> S. Mindess, J. F. Young, D. Darwin, *Concrete*, 2<sup>nd</sup> ed., Prentice Hall, NJ 2003, 644
- <sup>13</sup> V. Bilek Jr., L. Kalina, R. Novotný, J. Tkacz, L. Pařízek, Some Issues of Shrinkage-Reducing Admixtures Application in Alkali-Activated Slag Systems, *Materials* **9**, 462 (2016), doi:10.3390/ma9060462

EVALUATION OF THE SURFACTANT LEACHING FROM  
ALKALI-ACTIVATED SLAG-BASED COMPOSITES USING  
SURFACE-TENSION MEASUREMENTSUPORABA MERITEV POVRŠINSKE NAPETOSTI ZA OCENO  
IZLUŽEVANJA POVRŠINSKO AKTIVNE SNOVI IZ KOMPOZITOV  
NA OSNOVI ALKALNO AKTIVIRANE ŽLINDRE

Vlastimil Bílek Jr., Lukáš Kalina, Eva Bartoničková, Jaromír Pořízka

Brno University of Technology, Faculty of Chemistry, Materials Research Centre, Purkyňova 118, 612 00 Brno, Czech Republic

Prejem rokopisa – received: 2018-07-13; sprejem za objavo – accepted for publication: 2018-09-06

doi:10.17222/mit.2018.148

Nowadays, there are many efforts to reduce CO<sub>2</sub> emissions in the building industry, particularly through the use of some alternative binders to those based on Portland cement. One promising group of such binders includes binders based on alkali-activated slag (AAS). However, extensive drying, autogenous shrinkage and the associated cracking prevent AAS from being widely utilized in practice. A possible solution could be the application of shrinkage-reducing admixtures, whose molecules present in the pore solution reduce its surface tension and thus mitigate the AAS shrinkage. However, if AAS comes into contact with water, shrinkage-reducing admixtures can be leached and its effectiveness reduced. This work tries to evaluate the amount of surfactant leached from the AAS-based mortars using a very simple surface-tension (ST) measuring technique. Mortars based on AAS with and without 2 % of PEG varying in molecular weight (MW) were prepared. Waterglass with a SiO<sub>2</sub>-to-Na<sub>2</sub>O ratio equal to 2.0 was used at a dose corresponding to 8 % Na<sub>2</sub>O with respect to the slag weight. Mortar specimens were prepared and sealed for 24 h, 3 d and 7 d. Then they were demolded and immersed in demineralized water, whose ST was monitored over time. During the early stages (from minutes to a few hours) the ST dropped rapidly, while it remained approximately constant after a few days, which indicates that organic molecules are leached from the AAS specimens very quickly. It was observed that a relatively small fraction of PEGs can be leached out, which indicates that organic molecules are rather bound in the matrix, unable to reduce the ST of the pore solution.

Keywords: Alkali-activated slag, polyethylene glycol, leaching, surface tension

Dandanes v gradbeništvu vlagajo velike napore za zmanjšanje emisij CO<sub>2</sub>, še posebej z uporabo nekaterih Portland cementu alternativnih veziv. Ena od takšnih obetajočih skupin so veziva na osnovi alkalno aktiviranih žlindrov (AAS; angl.: alkali-activated slag). Vendar hitro sušenje, avtogeno krčenje, ter s tem povezano pokanje preprečujejo široko uporabo AAS v praksi. Možna rešitev bi lahko bila uporaba dodatkov, ki zmanjšujejo krčenje AAS. Molekule teh dodatkov v porah raztopine zmanjšajo njeno površinsko napetost in tako zmanjšajo krčenje AAS. Če pa je AAS v stiku z vodo, pride do izluževanja dodatkov za zmanjševanje krčenja, pri čemer se zmanjša njihova učinkovitost. V tej raziskavi so avtorji poizkušali oceniti vsebnost izluženega surfaktanta (površinsko aktivne snovi) iz malte na osnovi AAS z uporabo zelo enostavne merilne tehnike merjenja površinske napetosti (ST; angl.: surface tension). Pripravili so malte s spreminjajočo se molekularno maso (MW, angl.: molecular weight) na osnovi AAS brez in z dodatkom 2-% polietilenglikola (PEG). Uporabili so vodno steklo z razmerjem SiO<sub>2</sub>:Na<sub>2</sub>O=2, kar odgovarja vsebnosti 8 % Na<sub>2</sub>O glede na maso žlindre. Pripravili so vzorce malte in jih zaprli za 24 h, 3 d in 7 d zaprti v modele. Nato so modele odprli in malte potopili v destilirano vodo, ter ves čas merili njeno površinsko napetost. V začetnih stadijih opazovanja (nekaj minut do nekaj ur) je površinska napetost vode hitro padala, medtem ko se je po nekaj dneh ustalila, kar pomeni, da so se organske molekule iz vzorcev AAS izlužile zelo hitro. Na osnovi opazovanja so ugotovili, da se lahko izluži le relativno majhen delež PEG. To nakazuje na to, da so organske molekule precej vezane na matrico in niso sposobne zmanjšati površinske napetosti porozne raztopine.

Ključne besede: alkalno aktivirana žlindra, polietilen glikol, izluževanje, površinska napetost

## 1 INTRODUCTION

Alkali-activated materials (AAMs) belong to the group of alternative binders with the potential to enhance the sustainability of the building industry, since they are usually based on secondary raw materials or waste materials, and thus can decrease greenhouse-gas emissions, save energy, etc. The most common sources of aluminosilicate precursors for AAMs are metakaolin, fly ash and granulated blast-furnace slag. The latter, particularly when a waterglass is used for activation, often achieves

excellent mechanical properties, even at room temperature, that are similar or even better compared to those of Portland-cement-based materials.<sup>1</sup> However, extensive drying and autogenous shrinkage, resulting in cracking and deterioration of the material properties in general, limit the use of AAS in practice.

Several possible approaches to reduce AAS shrinkage can be found in literature, e.g., the use of mineral admixtures,<sup>2,3</sup> curing at elevated temperatures<sup>4,5</sup> or internal curing.<sup>6</sup> Also, the use of shrinkage-reducing admixtures (SRAs) or generally surface-active substances was reported as being an effective method for AAS shrinkage reduction.<sup>7-10</sup> In these studies, the beneficial effects of

\*Corresponding author e-mail:  
bilek@fch.vut.cz

SRAs were usually attributed to the changes in pore structure and a reduction of the surface tension, which is, according to capillary-pressure theory, closely related to shrinkage-inducing forces in desiccating (of self-desiccating) material.

These effects can be, in terms of capillary-pressure theory, illustrated by the Young-Laplace equation (Equation (1)), according to which, for the spherical meniscus inside the pore partially filled with liquid, the pressure difference  $\Delta p$  between the liquid and the vapor phase is proportional to the surface tension  $\gamma$  and inversely proportional to the pore radius  $r$ ;  $\cos\theta$  is the wetting angle. Nevertheless, it was summarized<sup>11</sup> that capillary-pressure theory can explain the drying shrinkage only for pores larger than approximately 10 nm and a relative humidity higher than 40–50 %. Some authors<sup>12,13</sup> contest the role of capillary action itself and emphasize that the disjoining pressure is at the origin of the shrinkage. The disjoining pressure is a superposition of attractive van der Waals forces, repulsive electric forces and structural forces.

$$\Delta p = -\frac{2\gamma}{r} \cos\theta \quad (1)$$

It is clear (Equation (1)) that if SRAs would act against AAS shrinkage in accordance with the capillary-pressure theory, they have to be present in a pore solution and able to adsorb at the liquid-air interface to reduce its energy (surface tension). However, this also means that at least part of this portion of the SRAs can be leached either during the water curing or in contact with the surrounding water in practice, and its effectiveness consequently reduced. These issues were widely studied by Eberhardt<sup>14</sup> on Portland-cement-based specimens, who observed that 40 % of the studied SRA was associated with hydration products. Such an immobile fraction of the SRA would only be released with the dissolution of the solid matrix itself. Although it cannot reduce the shrinkage via a reduction of the surface-tension decrease, its beneficial effect on the shrinkage can be explained by the disjoining-pressure theory. On the other hand, the mobile fraction of SRA can be removed from the specimen, particularly by diffusion.

Therefore, the purpose of this paper is to pioneer SRA leaching issues for AAS-based mortars. More specifically, the influence of polyethylene glycol's molecular weight, as well as the time of curing before immersion of the specimens in water, on the leaching extent and rate was investigated. The amount of leached PEG was determined using a dynamic surface-tension measurement. Additionally, this study follows our previous one,<sup>10</sup> where the effect of PEG MW on the drying shrinkage and other properties of AAS mortars and pastes was investigated. In that case, the specimens for drying shrinkage and mechanical properties testing were cured in water for 3 d and thus the study of the impact of leaching on the obtained results is at hand.

## 2 EXPERIMENTAL PART

### 2.1 Materials and mortar composition

Common ground granulated blast-furnace slag from the Czech production (Kotouč Štramberk, spol. s r.o.) with a Blaine fineness of 400 m<sup>2</sup>/kg was activated by sodium waterglass (Vodní sklo, a.s.) with a silicate modulus, i.e., SiO<sub>2</sub>-to-Na<sub>2</sub>O molar ratio, equal to 2.0. Siliceous sand with a maximum grain size of 2 mm was used as a fine aggregate. The Na<sub>2</sub>O (introduced into the system by waterglass) to slag ratio, water-to-slag ratio and sand-to-slag ratio were the same for all the prepared mortars: 0.08, 0.46 and 3.0 by weight, respectively. The mortars differed in the organic admixture used. One mortar type was the reference without any other additive (Ref.), while the other five types were modified by polyethylene glycol in the wide range of MW from monomer (ethylene glycol, EG) up to polyethylene glycol of 35,000 g/mole, namely, PEG400, PEG2000, PEG10000 and PEG35000. Their doses were 2 % with respect to the slag weight.

### 2.2 Specimen preparation and curing

The mixing procedure was the same as that prescribed for Portland-cement testing in EN 196-1. After the mixing, mortars were cast into a polypropylene cylindrical container with a diameter of 33 mm and a height of 70 mm. Then the containers were sealed and kept at 25 °C until the start of the leaching experiments, i.e., 24 h, 3 d or 7 d. After the desired time, the specimens were demolded and immersed in demineralized water for 7 d, during which time the dynamic surface tension of the leachate was measured. After the 7 d of leaching, water was exchanged and the ST of the renewed leachate determined after 24 h. The weight of

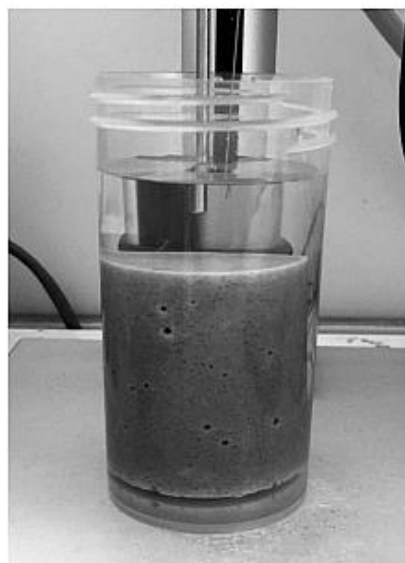


Figure 1: Dynamic surface-tension measurement

water was the same as the weight of the sample in both cases. One or two specimens for the reference mortar and two or three specimens for the PEG-modified mortars were used for each test series.

### 2.3 Dynamic surface-tension measurement

Before the start of the dynamic ST measurement (Figure 1), leachate in a container containing the specimen was homogenized by gentle gyration. The dynamic ST was determined using a bubble pressure tensiometer BPA 800P (KSV Instruments, Ltd.) after (0.5, 2.5, 5 and 24) h of leaching, and during the following days, as was mentioned above. A capillary with a diameter of 0.130 mm was immersed 5 mm under the leachate surface and the bubble life time was set to 0.1 s. For each time of the test, the values of the ST were recorded every 20 s during the several minutes and then averaged. Synthetic leachates (see following section) used for the determination of the amount of leached PEG were tested with the same settings.

### 2.4 Evaluation of the amount of leached PEG

The amount of leached PEG was calculated using calibration curves obtained from the dynamic ST measurement of the synthetic leachates containing various amounts of the desired PEG. The synthetic leachates were prepared on the basis of the silicon and sodium content in the leaching water after the first 7 days of leaching, determined using inductively coupled plasma optical emission spectroscopy (ICP-OES). The presence of other elements was neglected due to their very low content in the leachate. Synthetic leachates were prepared by the dilution of waterglass and sodium hydroxide by demineralized water in a volumetric flask, according to Table 1.

**Table 1:** Average Si and Na contents in the leachates after each curing time and the amounts of waterglass and 50 % NaOH used for the synthetic leachates' preparation

curing series	Si (mg/L)	Na (mg/L)	waterglass (g/L)	50 % NaOH (g/L)
24 h	158.6	4254	1.07	11.28
3 d	126.8	3461	0.857	9.19
7 d	118.2	2845	0.799	7.51

## 3 RESULTS

The development of the ST of the leachates is given in Figure 2. It can be seen that except for their monomer, all the PEGs decreased the dynamic ST rapidly within the first 30 min, while this did not change markedly during the following hours and days. On the other hand, all the leachates after the exchange of water reached the same ST values. To assess the amount of leached PEG, calibration curves were determined using synthetic leachate and known additions of PEG. The obtained

results are in Figure 3. The amount of leached PEG was determined as its concentration (w%) in between the two neighboring points using an interpolation with the assumption that the dependence of ST on the weight concentration is linear between each two measured points and compared with the maximum theoretical PEG concentration (0.42 %). Using this approach, the mass fraction of easily leachable PEG from the total PEG amount was evaluated (Figure 4). It is clear that an

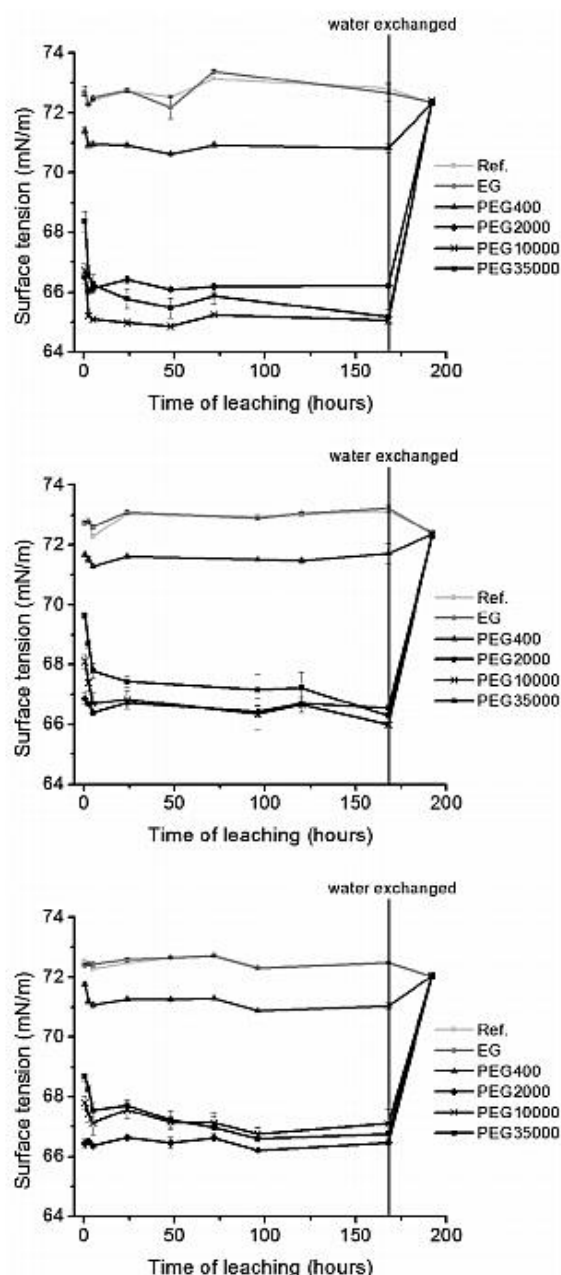


**Figure 2:** Dynamic surface-tension development of the leaching water after 24 h (up), 3 d (in the middle) and 7 d (down) of curing in auto-genous conditions

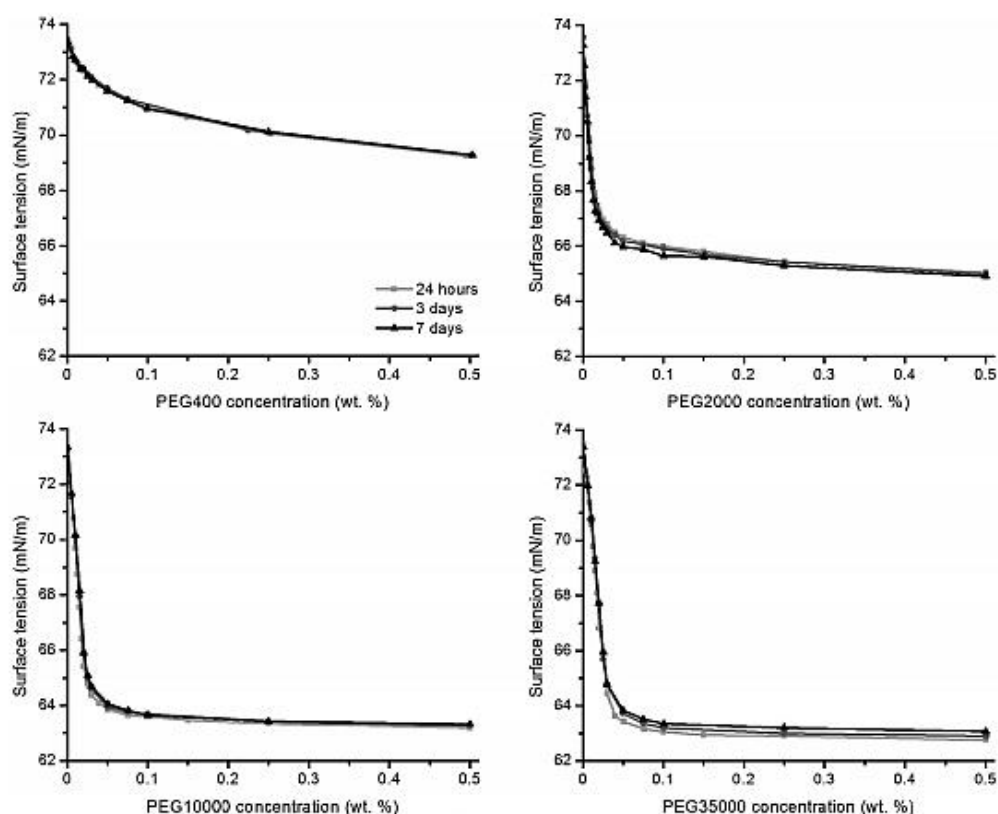


Figure 3: Calibration curves determined using synthetic leachates for each curing time

increase in PEG MW resulted in a decrease of its leachable portion, as it was, e.g., for 24 h of sealed curing calculated to be (28, 14, 5.4 and 6.3) % for PEG400, 2000, 10000 and 35000, respectively. Also, a prolonged time of curing before the leaching experiment, particularly between 24 h and 3 d, resulted in an increased immobilization of the PEGs. The higher leached amount of PEG400 after 7 d compared to 3 d is probably a random error. It also, together with the lengths of the error bars, shows a general disadvantage of the use of ST measurements for a determination of the leached amount of an organic substance. If the ST concentration dependence is flat, i.e., if the substance is not effective in reducing the ST (such as PEG400) or at high surfactant concentrations (above approximately 0.05 % in our cases), even a slight change in the measured ST means a large change in the calculated surfactant concentration. In contrast, the more steep the ST change is, the more precise the results are.

#### 4 DISCUSSION

As is well known and as we also reported earlier,<sup>10</sup> the ST-reducing ability of surfactants depends on their molecular weight. Therefore, it is not possible to estimate the amount of leached PEG only from the ST of the leachate (Figure 2), but the use of calibration curves

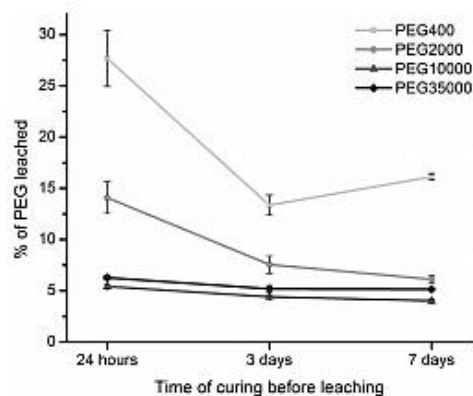


Figure 4: Effect of PEG's molecular weight and time of curing on the amount of PEG leached during the first 7 d of leaching

(Figure 3) is necessary. However, the presence of other ions in the leachate can affect its ST as well as the performance of organic admixtures, and hence synthetic leachates instead of pure water should be used. In our case, the gradual leaching of ions from the specimens, particularly silicon and sodium (Table 1), plays an important role and can also affect the ST's development. This is probably the reason why the ST of the reference and EG leachate rather increased during ongoing leaching and was usually a few tenths higher than those

determined for demineralized water. On the other hand, the ST of the second leachate from the Ref and EG specimens was lower compared to that of the first leachate and very close to that of demineralized water, since most of the Si and Na leached during the first cycle. The same ST values of the second leachates as for the Ref and EG were observed for all the other PEG specimens, regardless of the time of curing before the start of leaching, which indicates that the total or at least the vast majority of the leachable fraction of PEG had already been leached at the end of the first leaching cycle.

Eberhardt<sup>14</sup> summarized that the following three mechanisms of leaching can be distinguished: washing out, diffusion and a dissolution process. The very high rate of leaching during its early stages observed in **Figure 2** suggests that washing out is the dominating factor in our case. The diffusion at later leaching stages cannot be excluded, since there is likely a competition between the leaching of ions like Si or Na and surfactant molecules. Therefore, it can be expected that if the latter is of very limited rate, the former prevails and hence the leaching of the surfactant does not lead to a noticeable ST reduction. To investigate this in more detail, some other methods of organic-matter detection could be used, e.g., chromatography.

According to **Figure 2** and **4**, the molecular weight of the used PEG also affected its leaching rate, as well as the amount of leached PEG. While PEG400 and PEG2000 were mostly leached within the first 30 min or 150 min, the longer PEGs (PEG10000 and PEG35000) gradually decreased the ST up to 5 h. This is likely related to their longer chains, which cannot be transported through the specimen as easily as their shorter analogues. Moreover, the longer molecules are more prone to immobilization in the hydration products, which again contributes to a reduction of their mobile fraction. These issues can also explain the decrease in the amount of mobile fraction with increasing molecular weight and the time of curing before the start of the leaching (**Figure 4**). Slightly higher leached amounts of PEG35000 compared to PEG10000 would probably be due to their lower and slower solubility in water and activating solution and the consequent lower homogeneity of the specimens, despite efforts to dissolve and homogenize them as well as possible before the slag and sand addition.

The presented findings have a significant impact on the shrinkage behavior. As we have already presented,<sup>10</sup> MW plays an important role in the shrinkage-reducing ability since EG did not noticeably reduce the drying shrinkage of the AAS mortar, while a further increase in PEG MW had a beneficial effect, particularly up to a molecular weight of 2000 g/mole. The determination of the amount of SRA that can be leached from the specimen and also the SRA ST-reducing ability allows us to support the discussion from the previous paper and even

distinguish between the dominating mechanisms of shrinkage reduction. For shorter molecules like PEG400, only a slight ST-reducing ability, together with a relatively high leaching extent, indicate that neither the reduction of the ST by the mobile phase nor the reduction of the disjoining pressure by the presence of immobile PEG molecules, particularly when water curing is applied, can explain the quite high shrinkage reduction by PEG400. This supports our findings that the shrinkage-reducing ability of the PEG400 lies rather in the changes of the pore structure. On the other hand, the presence of longer PEG molecules, which cannot be easily leached, can act against shrinking via a disjoining-pressure mechanism and thus can be more effective in practical applications. However, a too high MW would also be impractical due to solubility and miscibility issues. For the case of PEGs, a MW of around 2000 g/mole (and not more than 10,000 g/mole) would be optimal due to the combination of its relatively high shrinkage-reducing ability and good solubility.

## 5 CONCLUSIONS

This paper investigated the leaching issues associated with AAS-based fine-grained composites. The amount of leached PEGs, depending on their molecular weight and time of curing before the start of the leaching, was determined using dynamic ST measurements.

Both the leaching rate and particularly the leaching extent of the PEGs decrease with their increasing molecular weight. This has a significant impact on the AAS shrinkage performance.

The leaching rate and extent also decrease with a prolonged time of curing.

For practical applications, the use of SRAs based on rather longer polymeric surfactants can be recommended, since they are more effective in reducing the ST, which favors shrinkage reduction according to the capillary-pressure theory, while its increased immobile fraction can act against shrinkage in terms of the disjoining-pressure theory. Moreover, a reduced leaching extent is important from the environmental viewpoint. On the other hand, for molecules that are too long, miscibility or solubility issues should also be kept in mind.

## Acknowledgment

This outcome was achieved with the financial support within the project: Materials Research Centre at FCH BUT- Sustainability and Development, REG LO1211, with financial support from the National Program for Sustainability I (Ministry of Education, Youth and Sports) and GA17-03670S "Development of shrinkage reducing agents designed for alkali activated systems", with financial support from the Czech science foundation.

## 6 REFERENCES

- <sup>1</sup> F. G. Collins, J. G. Sanjayan, Workability and mechanical properties of alkali activated slag concrete, *Cem. Concr. Res.*, 29 (1999) 3, 455–458, doi:10.1016/S0008-8846(98)00236-1
- <sup>2</sup> N. K. Lee, J. G. Jang, H. K. Lee, Shrinkage characteristics of alkali-activated fly ash/slag paste and mortar at early ages, *Cem. Concr. Compos.*, 53 (2014), 239–248, doi:10.1016/j.cemconcomp.2014.07.007
- <sup>3</sup> S. Aydın, A ternary optimisation of mineral additives of alkali activated cement mortars, *Constr. Build. Mater.*, 43 (2013), 131–138, doi:10.1016/j.conbuildmat.2013.02.005
- <sup>4</sup> N. Marjanovic, M. Komljenovic, Z. Bascarevic, V. Nikolic, R. Petrovic, Physical-mechanical and microstructural properties of alkali-activated fly ash-blast furnace slag blends, *Ceram. Int.*, 41 (2015) 1, 1421–1435, doi:10.1016/j.ceramint.2014.09.075
- <sup>5</sup> T. Bakharev, J. G. Sanjayan, Y. B. Cheng, Effect of elevated temperature curing on properties of alkali-activated slag concrete, *Cem. Concr. Res.*, 29 (1999) 10, 1619–1625, doi:10.1016/S0008-8846(99)00143-X
- <sup>6</sup> A. R. Sakulich, D. P. Bentz, Mitigation of autogenous shrinkage in alkali activated slag mortars by internal curing, *Mater. Struct.*, 46 (2013) 8, 1355–1367, doi:10.1617/s11527-012-9978-z
- <sup>7</sup> M. Palacios, F. Puertas, Effect of shrinkage-reducing admixtures on the properties of alkali-activated slag mortars and pastes, *Cem. Concr. Res.*, 37 (2007) 5, 691–702, doi:10.1016/j.cemconres.2006.11.021
- <sup>8</sup> C. Bilim, O. Karahan, C. D. Atis, S. Ilkentapar, Influence of admixtures on the properties of alkali-activated slag mortars subjected to different curing conditions, *Mater. Des.*, 44 (2013), 540–547, doi:10.1016/j.matdes.2012.08.049
- <sup>9</sup> L. Kalina, V. Bilek, E. Bartonickova, J. Krouska, Polypropylene glycols as effective shrinkage-reducing admixtures in alkali-activated materials, *ACI Mater. J.*, 115 (2018) 2, 251–256, doi:10.14359/51701099
- <sup>10</sup> V. Bilek, L. Kalina, R. Novotny, Polyethylene glycol molecular weight as an important parameter affecting drying shrinkage and hydration of alkali-activated slag mortars and pastes, *Constr. Build. Mater.*, 166 (2018), 564–671, doi:10.1016/j.conbuildmat.2018.01.176
- <sup>11</sup> P. C. Aitcin, R. J. Flatt, *Science and Technology of Concrete Admixtures*, 1<sup>st</sup> ed., Woodhead Publishing: Sawston, Cambridge, UK 2015
- <sup>12</sup> F. H. Wittman, Heresies on shrinkage and creep mechanisms, *Proc. of the 8<sup>th</sup> Inter. Conf. on Creep, Shrinkage and Durability of Concrete and Concrete Structures, Japan 2009*
- <sup>13</sup> F. Beltzung, F. H. Wittmann, Role of disjoining pressure in cement based materials, *Cem. Concr. Res.*, 35 (2005) 12, 2364–2370, doi:10.1016/j.cemconres.2005.04.004
- <sup>14</sup> A. B. Eberhardt, *On the Mechanisms of Shrinkage Reducing Admixtures in Self Consolidating Mortars and Concretes*, Ph.D. Thesis, Bauhaus Universität Weimar, Weimar, Germany 2011

Article

# Cement Kiln By-Pass Dust: An Effective Alkaline Activator for Pozzolanic Materials

 Lukáš Kalina , Vlastimil Bílek Jr. , Tomáš Kiripolský, Radoslav Novotný and Jiří Másilko

Materials Research Centre, Faculty of Chemistry, Brno University of Technology, Brno 61200, Czech Republic; bilek@fch.vut.cz (V.B.J.); xckiripolsky@fch.vut.cz (T.K.); xcnovotny2@fch.vut.cz (R.N.); masilko@fch.vut.cz (J.M.)

\* Correspondence: kalina@fch.vut.cz; Tel.: +42-054-114-9366

Received: 27 August 2018; Accepted: 18 September 2018; Published: 19 September 2018



**Abstract:** Cement kiln by-pass dust (CKD) is a fine-grained by-product of Portland clinker manufacturing. Its chemical composition is not suitable for returning back into feedstock and, therefore, it has to be discharged. Such an increasing waste production contributes to the high environmental impact of the cement industry. A possible solution for the ecological processing of CKD is its incorporation into alkali-activated blast furnace slag binders. Thanks to high alkaline content, CKD serves as an effective accelerator for latent hydraulic substances which positively affect their mechanical properties. It was found out that CKD in combination with sodium carbonate creates sodium hydroxide in situ which together with sodium water glass content increases the dissolution of blast furnace slag particles and subsequently binder phase formation resulting in better flexural and compressive strength development compared to the sample without it. At the same time, the addition of CKD compensates the autogenous shrinkage of alkali-activated materials reducing the risk of material cracking. On the other hand, this type of inorganic admixture accelerates the hydration process causing rapid loss of workability.

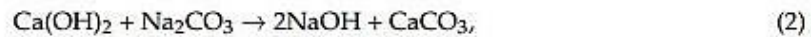
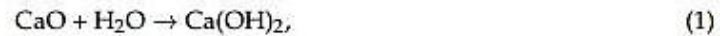
**Keywords:** cement kiln by-pass dust; alkali activation; blast furnace slag; admixture

## 1. Introduction

Worldwide, the material resource consumption increases and consequently large amounts of waste are released into the environment [1]. This phenomenon is also associated with Portland cement production. It is well known that cement production is responsible for approximately 7% of the world's CO<sub>2</sub> emissions [2]. Moreover, the manufacturing of Portland clinker is associated with solid waste production. The cement kiln by-pass dust (CKD), is the typical by-product of the cement clinker burning process [3]. This material contains high concentrations of heavy metals and therefore should be disposed as a hazardous waste [4]. Nevertheless, the economic pressure caused by CKD disposal tends to its re-addition to the final cement product.

A possible way to ecologically process the CKD waste is utilization in alkali-activated materials formed via the reaction of a solid aluminosilicate with highly concentrated alkaline aqueous solution [5]. The alkali activation mechanism includes the destruction of the raw material by breaking the Si–O–Si and Si–O–Al bonds into lower stability structural units, their interaction through the coagulation-condensation process and the precipitation of final reaction products [6]. Thanks to the alkaline contents of CKD, especially due to the free lime, the significance of its usage as an alkaline activator arises. Previous studies [7,8] show that the alkali activation process supported by reactive lime from CKD leads to the creation of calcium silicate binder phases. However, the pH value of alkaline solution with CKD is not high enough for sufficient decomposition of raw materials which in most cases need the addition of a typical alkaline activator such as sodium hydroxide [9,10]. In terms of working with such a caustic chemical compound, one must observe the safety regulations, which

makes it more difficult in practical usage. Therefore, the study is focused on the alkali activation of blast furnace slag with CKD in connection with sodium carbonate resulting in sodium hydroxide according to Equations (1) and (2).



The caustic soda is formed gradually during the hydration process and increases the pH value in the pore solution which promotes the dissolution of aluminosilicate materials and thus positively affects the mechanical properties of the final products.

Thanks to the optimal chemical composition, the CKD seems to be an effective alkaline activator and plays a significant role in autogenous shrinkage mechanism in alkali-activated BFS materials. Therefore, CKD is a promising by-product material, and this paper is focused on its study and its possible utilization in these systems.

## 2. Materials and Methods

### 2.1. Materials and Sample Preparation

The main aluminosilicate material used to produce the alkali-activated mortars was blast furnace slag (BFS) with the Blaine fineness of  $400 \text{ m}^2 \text{ kg}^{-1}$  (ArcelorMittal Ostrava, a.s., Ostrava, Czech Republic). The cement kiln dust (CKD) was collected from the by-pass system of the Horné Srnie cement plant (Cemmac, a.s., Horné Srnie, Slovakia). The chemical composition of raw materials was determined by XRF as shown in Table 1. The XRD analysis of BFS indicated the presence of approximately 90% of amorphous phase determined with the method of internal standard (fluorite). The main minerals identified in BFS were melilite, calcite and merwinite. The CKD was composed of sylvite (KCl), lime (CaO), arcanite ( $\text{K}_2\text{SO}_4$ ), larnite ( $2\text{CaO} \cdot \text{SiO}_2$ ), quartz ( $\text{SiO}_2$ ), portlandite ( $\text{Ca(OH)}_2$ ) and hatrutite ( $3\text{CaO} \cdot \text{SiO}_2$ ). The free lime content determined according to EN 451-1 was 27.2 wt %. The particle size distribution D50 of BFS and CKD determined by laser granulometry in dry state were  $\sim 10 \mu\text{m}$  and  $\sim 4 \mu\text{m}$ , respectively. Anhydrous sodium carbonate (Penta, s.r.o., Prague, Czech Republic) in the form of powder and sodium water glass (Vodní sklo, a.s., Brno, Czech Republic) with the silica modulus of 2.2 were used as the alkaline activators. The pH value of used sodium water glass was 12.48. The  $\text{Na}_2\text{O}/\text{BFS}$  ratio was set to 8 wt %.

**Table 1.** Chemical composition of BFS and CKD as determined by XRF.

Raw Material	Chemical Composition/wt %										
	SiO <sub>2</sub>	Al <sub>2</sub> O <sub>3</sub>	CaO	Na <sub>2</sub> O	K <sub>2</sub> O	MgO	SO <sub>3</sub>	Fe <sub>2</sub> O <sub>3</sub>	TiO <sub>2</sub>	MnO	Cl <sup>-</sup>
BFS	34.7	9.1	41.1	0.4	0.9	10.5	1.4	0.3	1.0	0.6	–
CKD	11.9	4.2	45.7	0.4	16.9	0.9	7.2	2.4	0.3	–	10.1

Alkali-activated BFS mortars with different amount of CKD at the expense of BFS (0; 5; 10; 15; 20; 25 wt %) were prepared. The sand-to-BFS ratio was 3:1 using three different fractions of standard siliceous sand meeting requirements of EN 196-1 and the water-to-BFS ratio was set at 0.46 with respect to the water contained in the sodium water glass. The composition of mortars is shown in Table 2. Mixing and curing processes in molds were carried out at laboratory temperature (25 °C) with RH=99%. After the demolding process (1 day), the specimens were stored in water at 25 °C in the curing chamber. Prepared samples were subjected to compressive, flexural strength determination and length change measurements.

**Table 2.** Composition of alkali-activated mortar samples (wt %).

Mixture Designation	REF	CKD-5	CKD-10	CKD-15	CKD-20	CKD-25
BFS	21.6	20.5	19.4	18.3	17.2	16.1
CKD	–	1.1	2.2	3.3	4.4	5.5
Na <sub>2</sub> CO <sub>3</sub>	2.1	2.1	2.1	2.1	2.1	2.1
Na-water glass	3.5	3.5	3.5	3.5	3.5	3.5
water	8.0	8.0	8.0	8.0	8.0	8.0
standard sand	64.8	64.8	64.8	64.8	64.8	64.8

## 2.2. Physical-Mechanical Measurements

The samples with the dimensions of  $4 \times 4 \times 16$  cm were tested to determine their compressive and flexural strength according to EN 196-1. The strengths were tested at the age of 1, 7 and 28 days. The measurements were carried out by the compressive and bending strength tester Betonsystem Desttest 3310. The length changes for obtaining the shrinkage-expansion evolution were measured in short time intervals using the ASTM C490 apparatus for 28 days. The consistence of fresh alkali-activated mortars was measured based on the mini-cone test procedure in accordance with EN 1015-3. The effect of gradual CKD additions on the pH in water solution with dissolved sodium carbonate was measured using pH-meter S213 SevenCompact Duo (Mettler-Toledo GmbH, Greifensee, Switzerland) until the pH value was constant (approximately 10 min).

## 2.3. Isothermal Calorimetry

The evolution of hydration heat was monitored using the TAM Air isothermal microcalorimeter (TA Instruments, New Castle, DE, USA). The measurements of heat evolution were performed at a constant temperature of 25 °C. When the thermal equilibrium was achieved, the BFS and alkaline activator were mixed together by injecting the solution into the 15 mL vial and stirring it for 3 min. The water/BFS, as well as the Na<sub>2</sub>O/BFS mass ratio, were the same as in the preparation process of mortars. The heat evolution was recorded as the heat flow immediately.

## 2.4. X-ray Diffraction Analysis (XRD)

The X-ray powder diffraction of alkali-activated matrices after 7 days of curing was measured using the PANalytical Empyrean diffractometer with CuK $\alpha$  radiation equipped with a 3D detection system PIXcel3D. The specimens were step scanned from 5° to 40° 2 $\theta$  using vertical high-resolution goniometer with the step size 0.013° 2 $\theta$ . The samples with 0, 10 and 20 wt % of CKD were used for the determination of mineralogical composition after the hydration process, moreover for the verification of reaction mechanism outlined in Equations (1) and (2).

## 2.5. Thermogravimetry (TG)

The behavior of the alkali-activated matrices during the thermal treatment was investigated using 70 mg of the milled sample after 7 days of curing. The thermogravimetric analysis was performed using Q600 analyser (TA Instruments, New Castle, DE, USA) up to 1000 °C with the ramp 5 °C per minute and under the dried air conditions. The samples with 0, 10 and 20 wt % of CKD addition were used for the quantification of the created calcium carbonate, formed according to Equation (2).

## 3. Results and Discussion

The compressive (Figure 1a) and flexural (Figure 1b) strengths development demonstrates a positive effect of CKD on mechanical properties. As observed in Figure 1a, the addition of CKD only slightly increases early compressive strengths after 1 and 7 days. However, a perspicuous improvement was achieved after 28 days, when all samples with the addition of CKD up to 20 wt % indicated higher strengths compared to the reference sample. Conversely, the substitution of 25 wt % BFS by CKD

decreases the compressive strength which is related mainly to very quick loss of workability; this mixture is workable for only several minutes, as is shown in Figure 2. This strongly influences the homogeneity of samples.

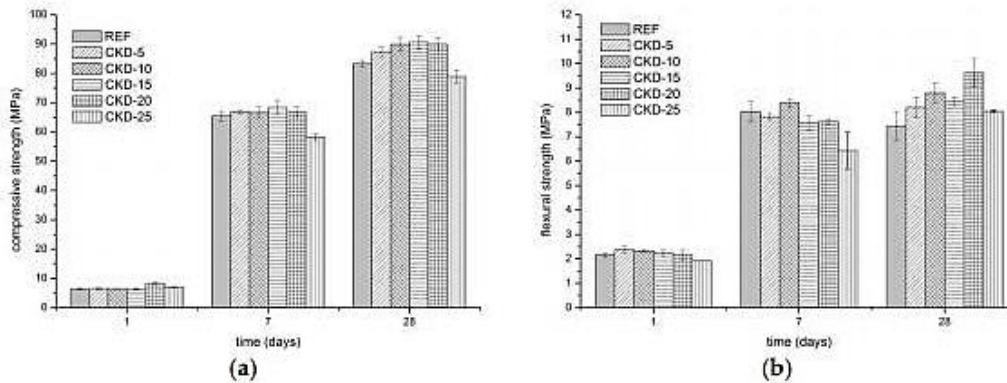


**Figure 1.** Compressive (a) and flexural (b) strengths development of alkali-activated mortars with different amounts of CKD.

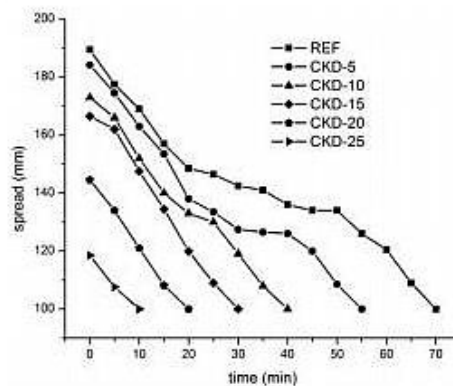


**Figure 2.** Workability over time of fresh alkali-activated mortars with different amount of CKD.

Considering the measurement uncertainty expressed by the error bars in all measurements, the flexural strength development after 7 days suggests a convincing increase in strength compared to 1-day-old samples. However, a significant difference is noticeable after 28 days of curing. Whereas the samples with CKD content show an increase in flexural strengths, the reference sample has the opposite evolution. This phenomenon likely relates to the chemical shrinkage of pure alkali-activated BFS which is described in several studies [11,12]. As a result, the internal stress is present in the material and, therefore, the microcracks in the structure can take place, which negatively influence the flexural strength especially.

The changes of samples length are shown in Figure 3. It is clearly visible that the reference sample exhibits the shrinkage which continues even after 1 day of mixing. This behavior in volume changes of alkali-activated BFS is in contrast with the binders based on ordinary Portland cements (OPC), since these binders cured continuously in water exhibit an increase in volume. This expansion, named as swelling, is connected with the absorption of water by the cement gel where the molecules of water act against cohesive forces and tend to force the gel particles away from each other [13]. On the other hand, the alkali-activated BFS forms CSH gel with the high atomic packing density which prevents water from penetrating into the inner structure during saturated (under water) curing [11] and causes self-desiccation. This process, which takes place in the interior of mortar mass, is known as autogenous volume change [13] and leads to the shrinkage of the whole system. A different situation occurs in the

case of the samples with the CKD additions, the expansion of which depends on the amount of free lime contained therein. Free CaO is very well known as a cheap expansive agent, provided that it is burned at temperatures above 1000 °C resulting in “dead burnt lime” [14]. Such lime is also present in CKD, the collection of which from the Portland cement manufacturing process is carried out at the temperature of about 1100 °C. From the evolution of expansion it is obvious that the complete expansion is achieved in less than 3 days in all samples. This certainly has its advantages in the lower affecting of the curing process as well as in the lower risk of presence of residual un-reacted CaO which could cause later expansion [15].

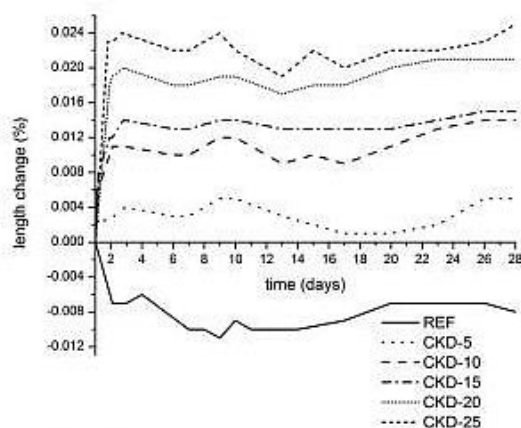


**Figure 3.** Length changes of alkali-activated mortars with different amounts of CKD during saturated (under water) curing.

The increase in mechanical properties of samples with CKD addition is also closely connected with higher dissolution of BFS and subsequent higher formation of binder phases. The dissolution of slag particles strongly depends on the pH of ambient solution [16]. It is obvious that CKD as well as sodium carbonate mixed separately with water indicate lower values of pH in comparison with their joint solution (Figure 4). Thanks to the reaction of lime contained in CKD and sodium carbonate in the water environment, described in Equations (1) and (2), the rise in pH up to the value over 13 occurs and the dissolution of slag particles rapidly increases.

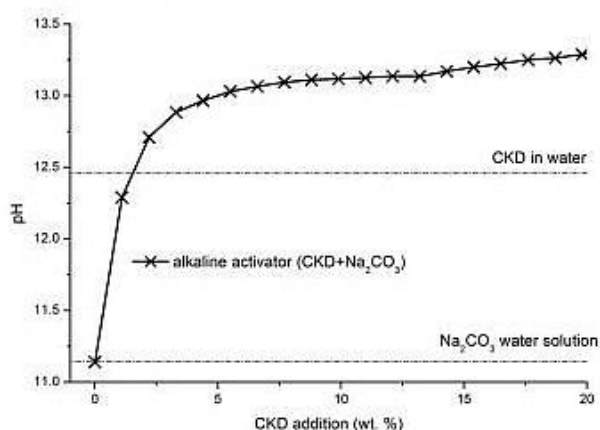


**Figure 4.** Effect of different amounts of CKD additions on the pH of water solution with dissolved sodium carbonate.

The process of dissolution of BFS and the creation of CSH gel was characterized through the isothermal calorimetry as shown in Figure 5. The first peak (Figure 5a), measured during the first

minutes of hydration, is mainly associated with wetting and dissolution of BFS [17]. From the zoomed area it is clear that the samples with the higher content of CKD indicate higher heat flow which would confirm better dissolution of BFS particles. At the same time, the hydration of lime proceeds according Equation (1); therefore, the contribution of heat released by this reaction is also a part of the first peak. After that, the pre-induction band is observed belonging to the formation of primary CSH gel [18] and gaylussite ( $\text{Na}_2\text{Ca}(\text{CO}_3)_2 \cdot 5\text{H}_2\text{O}$ ) which is one of the initial products in  $\text{Na}_2\text{CO}_3$ -activated slag binders [19]. The secondary formation of CSH gel is connected with the peaks from 10 to 40 hours. It is well observed that higher heat flow in this region was measured for the samples with a higher content of CKD. These results suggest that CKDs contribute to a larger formation of binder phase as proven by the measurement of the total amount of heat evolution (Figure 5b), which is particularly associated with the quantity of created CSH gel. The total heat was monitored within 4 days from the beginning of alkaline activation.

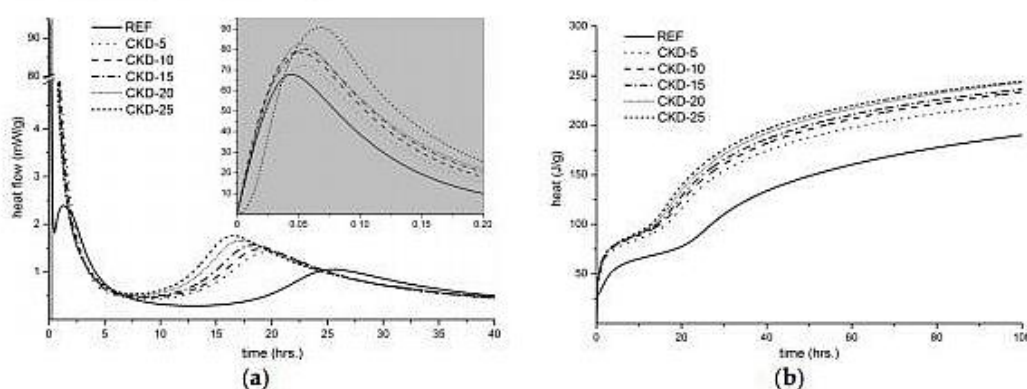


**Figure 5.** Evolution of heat flow (a) and total heat (b) of alkali-activated matrices with different amounts of CKD.

Subsequently, the samples were subjected to XRD analyses (Figure 6). The overlapped diffractograms show the presence of minerals from the raw materials plus gaylussite. The comparison of mineralogical composition among the samples with different amounts of CKD indicates no significant changes except in the formation of calcium carbonate. The samples with higher content of CKD create a considerably higher quantity of calcite, resulting primarily from Equation (2).

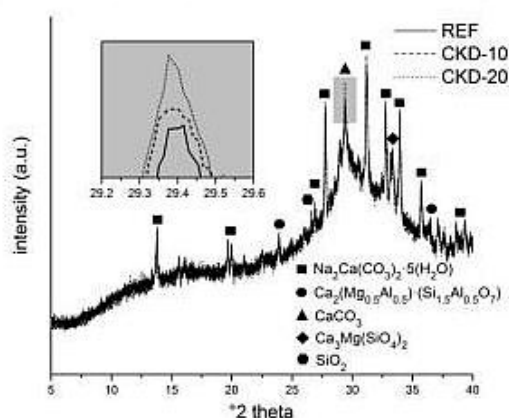


**Figure 6.** XRD of alkali-activated matrices with 0, 10 and 20 wt % of CKD addition.

The detailed quantitative information about the amount of formed calcium carbonate in prepared alkali-activated matrices was given by using of the thermogravimetric analysis. Figure 7 shows that

the mass loss is connected with several ongoing processes during the heating. The first one between 31 and 240 °C can be associated with the loss of physically-bonded water and also the dehydration of chemically-bonded water from the newly formed CSH gel structure. The dehydration of interlayer water bonded in the CSH phase continues up to 600 °C [20]. The next process which appears around 600 to 800 °C can be attributed to the decomposition of carbonates. The first derivative of the TG analysis of the reference sample showed that the two step decomposition of carbonates takes place. The first step is supposed to be associated to the decomposition of gaylussite structure [21] and the second one to the calcite one [22]. The presence of both of them was confirmed by previous XRD analyses. However, it should be emphasized that the decomposition of the carbonate species should be intertwined together. The analyses of the samples with the CKD content shows the slightly different behaviour in this temperature range. It is obvious that the content of the gaylussite decreases with the expense of calcium carbonate, which was proven by the XRD analyses. From the conducted results we can conclude that the content of calcium carbonate increases with the reaction time. This phenomenon should be related with the carbonation process from some minor CO<sub>2</sub> uptake onto the surface between the preparation of samples and TG analysis but it should also be a part of the reaction mechanism described in Equation (2).

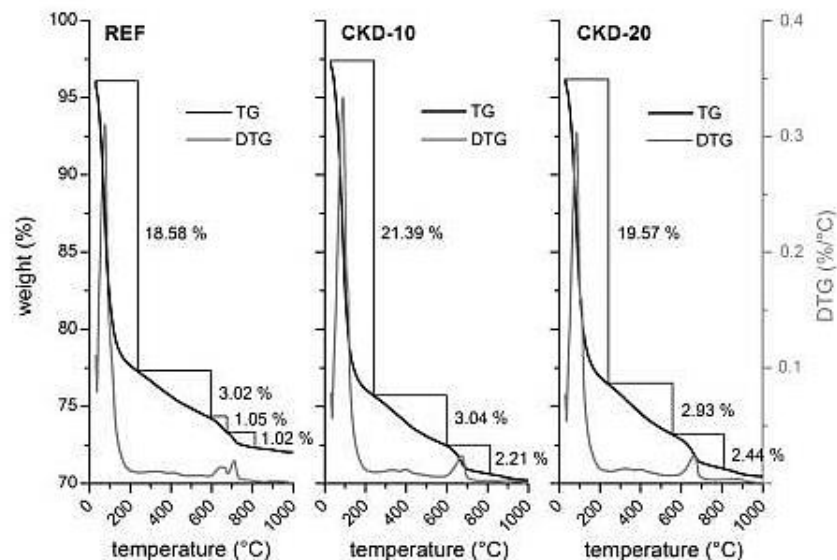


Figure 7. TG, DTG analyses of alkali-activated matrices with 0, 10 and 20 wt % of CKD addition.

#### 4. Conclusions

The results of this study demonstrate that the secondary raw materials such as CKD can be successfully utilized for the alkaline activation of BFS. The following conclusions summarize the experimental part of the work:

1. The combination of CKD and sodium carbonate together with sodium water glass used as alkaline activators leads to the secondary formation of sodium hydroxide causing an increase in the pH of water solution in mixtures which promote the dissolution process of activated aluminosilicate.
2. Higher degree of BFS dissolution influences the hydration process in the sense of higher binder phase creation which positively affects the mechanical properties up to a certain limit.
3. The CKD content in alkali-activated BFS causes a small expansion of the whole system and thereafter the shrinkage cracking connected with the decrease of compressive as well as flexural strengths is reduced.

4. The addition of CKD into the alkali-activated systems decreases the workability due to early hydration of lime resulting in the system inhomogeneity which can strongly influence the mechanical properties.
5. The production of alkali-activated BFS binders with CKD addition depends on its optimum dosage into the system, moreover, the CKD chemical and phase composition must always be taken into account.

**Author Contributions:** L.K. and V.B.J. conceived and designed the experiments; R.N. performed the microcalorimetry measurements; T.K. worked on the experimental parts; J.M. measured the XRD and TG-DTA analysis; L.K. wrote the paper.

**Funding:** This outcome has been achieved with the financial support by the project: Materials Research Centre at FCH BUT—Sustainability and Development, REG LO1211, with financial support from the National Programme for Sustainability I (Ministry of Education, Youth and Sports) and GA17-03670S “Development of shrinkage reducing agents designed for alkali activated systems”, with financial support from the Czech Science Foundation and project of H2020 call—Marie Skłodowska-Curie—Research and Innovation Staff Exchange—GeoDust-734833 financed by European Union funds.

**Conflicts of Interest:** The authors declare no conflict of interest.

## References

1. Blanchard, O. Energy-consumption and modes of industrialization—Four developing-countries. *Energy Policy* **1992**, *20*, 1174–1185. [CrossRef]
2. Mehta, P.K.; Monteiro, P.J.M. *Concrete: Microstructure, Properties, and Materials*; McGraw-Hill Education: New York, NY, USA, 2013.
3. Siddique, R. Utilization of cement kiln dust (CKD) in cement mortar and concrete—An overview. *Resour. Conserv. Recycl.* **2006**, *48*, 315–338. [CrossRef]
4. Eckert, J.O.; Guo, Q.H. Heavy metals in cement and cement kiln dust from kilns co-fired with hazardous waste-derived fuel: Application of EPA leaching and acid-digestion procedures. *J. Hazard. Mater.* **1998**, *59*, 55–93. [CrossRef]
5. Duxson, P.; Fernandez-Jimenez, A.; Provis, J.L.; Lukey, G.C.; Palomo, A.; van Deventer, J.S.J. Geopolymer technology: The current state of the art. *J. Mater. Sci.* **2007**, *42*, 2917–2933. [CrossRef]
6. Palomo, A.; Kavalerova, E.; Fernandez-Jimenez, A.; Krivenko, P.; Garcia-Lodeiro, I.; Maltseva, O. A Review on Alkaline Activation: New Analytical Perspectives. 2015. Available online: <http://digital.csic.es/handle/10261/110274> (accessed on 18 September 2018).
7. Konsta-Gdoutos, M.S.; Shah, S.P. Hydration and properties of novel blended cements based on cement kiln dust and blast furnace slag. *Cem. Concr. Res.* **2003**, *33*, 1269–1276. [CrossRef]
8. Lachemi, M.; Sahmaran, M.; Hossain, K.M.A.; Lotfy, A.; Shehata, M. Properties of controlled low-strength materials incorporating cement kiln dust and slag. *Cem. Concr. Compos.* **2010**, *32*, 623–629. [CrossRef]
9. Kalina, L.; Koplík, J.; Soukal, F.; Masilko, J.; Jaskowiecova, L. Potential uses of geopolymers to immobilize toxic metals from by-products materials. *Environ. Eng. Manag. J.* **2012**, *11*, 579–584. [CrossRef]
10. Wang, K.; Shah, S.P.; Mishulovich, A. Effects of curing temperature and NaOH addition on hydration and strength development of clinker-free CKD-fly ash binders. *Cem. Concr. Res.* **2004**, *34*, 299–309. [CrossRef]
11. Thomas, J.J.; Allen, A.J.; Jennings, H.M. Density and water content of nanoscale solid C-S-H formed in alkali-activated slag (AAS) paste and implications for chemical shrinkage. *Cem. Concr. Res.* **2012**, *42*, 377–383. [CrossRef]
12. Chen, W.; Brouwers, H.J.H. The hydration of slag, part 1: Reaction models for alkali-activated slag. *J. Mater. Sci.* **2007**, *42*, 428–443. [CrossRef]
13. Neville, A.M. *Properties of Concrete*, 5th ed.; Pearson: London, UK, 2011.
14. Troli, R.; Collepardi, M. Shrinkage-compensating concretes for special structures. In Proceedings of the 4th International Conference on Non-Traditional Cement and Concrete, Brno, Czech Republic, 27–30 June 2011; pp. 18–36.
15. Collepardi, M.; Borsoi, A.; Collepardi, S.; Olagot, J.J.O.; Troli, R. Effects of shrinkage reducing admixture in shrinkage compensating concrete under non-wet curing conditions. *Cem. Concr. Compos.* **2005**, *27*, 704–708. [CrossRef]

16. Li, C.; Sun, H.H.; Li, L.T. A review: The comparison between alkali-activated slag (Si + Ca) and metakaolin (Si + Al) cements. *Cem. Concr. Res.* **2010**, *40*, 1341–1349. [CrossRef]
17. Fernandez-Jimenez, A.; Puertas, F.; Arteaga, A. Determination of kinetic equations of alkaline activation of blast furnace slag by means of calorimetric data. *J. Therm. Anal. Calorim.* **1998**, *52*, 945–955. [CrossRef]
18. Shi, C.J.; Day, R.L. A calorimetric study of early hydration of alkali-slag cements. *Cem. Concr. Res.* **1995**, *25*, 1333–1346. [CrossRef]
19. Ke, X.Y.; Bernal, S.A.; Provis, J.L. Controlling the reaction kinetics of sodium carbonate-activated slag cements using calcined layered double hydroxides. *Cem. Concr. Res.* **2016**, *81*, 24–37. [CrossRef]
20. Bernal, S.A.; Rodriguez, E.D.; de Gutierrez, R.M.; Provis, J.L. Performance at High Temperature of Alkali-Activated Slag Pastes Produced with Silica Fume and Rice Husk Ash Based Activators. 2015. Available online: <http://materconstrucc.revistas.csic.es/index.php/materconstrucc/article/view/1689/2071> (accessed on 18 September 2018).
21. Johnson, D.R.; Robb, W.A. Gaylussite—Thermal properties by simultaneous thermal-analysis. *Am. Mineral. J. Earth Planet. Mater.* **1973**, *58*, 778–784.
22. Alarcon-Ruiz, L.; Platret, G.; Massieu, E.; Ehrlicher, A. The use of thermal analysis in assessing the effect of temperature on a cement paste. *Cem. Concr. Res.* **2005**, *35*, 609–613. [CrossRef]



© 2018 by the authors. Licensee MDPI, Basel, Switzerland. This article is an open access article distributed under the terms and conditions of the Creative Commons Attribution (CC BY) license (<http://creativecommons.org/licenses/by/4.0/>).

# Influence of alkali ions on the efficiency of shrinkage reduction by polypropylene glycol in alkali activated systems

**Lukas Kalina**

Senior researcher, Faculty of Chemistry, Materials Research Centre, Brno, Czech Republic (corresponding author: kalina@fch.vut.cz)  
(Orcid:0000-0001-8127-8175)

**Vlastimil Bilek Jr**

Junior researcher, Faculty of Chemistry, Materials Research Centre, Brno, Czech Republic (Orcid:0000-0003-3831-3443)

**Radoslav Novotny**

Junior researcher, Faculty of Chemistry, Materials Research Centre, Brno, Czech Republic (Orcid:0000-0002-1809-5875)

**Alkali-activated materials, especially when activated by water glass, exhibit substantial drying shrinkage that hinders their broader industrial application. The effect of shrinkage-reducing admixtures (SRA), based on polypropylene glycol, on drying shrinkage of alkali-activated blast furnace slag (BFS) mortars was examined. The determination of SRA efficiency and the influence of potassium alkali activators with varying silicate modulus on drying shrinkage characteristics were studied. It was observed that a high amount of alkalis positively affected the effect of SRA. The higher the amount of alkalis was, the lower was the drying shrinkage. The paper further discusses and underlines the role of the amount of alkali ions on the properties of alkali-activated BFS systems.**

## Introduction

High energy consumption and increased emissions along with ageing infrastructure have a harmful impact on the environment. Every year the production of concrete exceeds  $10^{10}$  t, which is more than all other man-made materials combined. Such a huge production results in approximately 5% of the world's total anthropogenic greenhouse gas emissions (Damtoft *et al.*, 2008). Nowadays, this fact brings an even greater need to develop more environmentally friendly materials, which are more durable, highly recyclable and energy efficient.

Alkali-activated materials (AAMs) have become the materials of interest mainly owing to their low environmental impact compared to Portland cement and also because of the possibility of using varieties of industrial waste (Kalina *et al.*, 2012). The utilisation of AAM as an alternative binder instead of ordinary Portland cement (OPC) adds sustainability to concrete by reducing the carbon dioxide ( $\text{CO}_2$ ) emissions compared to cement production. Many scientific studies have revealed that some kinds of AAM are distinguished by superior durability and lower heat of hydration compared to OPC binder, high resistance to aggressive environments (Hossain *et al.*, 2015) and good performance in high temperatures (Bernal *et al.*, 2015). Another advantage could be better behaviour under freeze–thaw cycles (Cai *et al.*, 2013). However, these materials exhibit drying and autogenous shrinkage (Bilek *et al.*, 2016), the subsequent formation of microcracks and higher formation of salt efflorescence, which are the major drawbacks that hinder these materials' broader industrial application.

Only a few authors have studied possible ways of reducing the shrinkage, which could be carried out using shrinkage-reducing admixtures (SRAs), belonging to the group of

surfactants. The effect of SRA has been well investigated in Portland cement systems (Sant *et al.*, 2010); however, only little attention was dedicated to the study of efficiency of SRAs in alkali-activated slag (AAS) systems. It was concluded that the decrease in the surface tension of pore solution caused by SRA brought about smaller internal stress when the water evaporated. This resulted in the capillary stress being much lower than without the admixture. In terms of the drying shrinkage, the content of mesopores also plays a crucial role. According to the capillary pressure theory (Bentz *et al.*, 1995), the system with a higher content of mesopores exhibits higher drying shrinkage (Collins and Sanjayan, 2000). The presence of SRA causes pore size redistribution (Palacios and Puertas, 2007), meaning that SRA decreases the percentage of mesopores in the total porosity of AAMs.

The SRA efficiency is entirely influenced by the nature of the electrolyte solution in which the SRA is located (Bauduin *et al.*, 2004; Morini *et al.*, 2005). There are two effects that have to be taken into account. The 'salting-in' effect initiates the solubilisation or miscibility of the surfactant in an aqueous electrolyte solution. By contrast, the 'salting-out' effect causes a decrease of the critical micelle concentration (CMC), increases the liquid–liquid miscibility gap and enhances the self-organisation. The question is whether the salting-in or the salting-out effect dominates in AAM. A high content of alkali ions in the system would imply that, for the AAM, salting-in may occur. However, the amount and the kind of cations in the pore solution significantly impact the surfactant's behaviour, as the Hofmeister or the lyotropic series suggest (Kunz *et al.*, 2004). To sum up, the present investigation is therefore focused on the role of specific alkali activators with different amounts of alkali ions influencing the shrinkage evolution and other properties of alkali-activated

blast furnace slag (BFS) systems with and without specific SRA based on polypropylene glycol.

## Experiment

### Materials

The aluminosilicate material used for the alkali activation was BFS from ArcelorMittal Ostrava, Inc., Czech Republic, with a specific surface area of 400 m<sup>2</sup>/kg. The chemical composition specified by X-ray fluorescence spectroscopy (XRF) is shown in Table 1. The crystalline composition of BFS determined by X-ray diffraction (XRD) confirmed the presence of merwinite, melilite,  $\beta$ -C<sub>2</sub>S and calcite. The BFS was activated by potassium water glass (Vodní sklo, Inc.) with defined silicate moduli:  $M_s = 1.92$  (4%); 1.29 (6%); 0.97 (8%); 0.78 (10%). The silicate moduli (silicon dioxide to potassium oxide (SiO<sub>2</sub>/K<sub>2</sub>O) molar ratio) correspond to the weight of potassium oxide in the activator, recalculated to the amount of BFS, as is shown in brackets. Three different fractions of standard siliceous sand (ČSN EN 196-1) were used for mortar preparation. The surfactant serving as the SRA was polypropylene glycol (PPG 425) with a specific molar weight,  $M_w = 425$  (Sigma Aldrich, Ltd.). The amount of PPG 425 added into the alkali-activated mixture was determined as 0.5 wt%, recalculated to the amount of BFS.

### Methods

#### Pore solution characterisation

The pore solutions were extracted from samples activated by water glass with different silicate moduli after 24 h using the hydraulic press BS-3000 (manufactured by BetonSystem company). After 24 h, the chemical composition of the pore solution did not change substantially and this time also indicates the beginning of drying shrinkage measurement. One hundred microlitres of pore solution were placed into a 100 ml volumetric flask and filled with water. The samples were then analysed by inductively coupled plasma optical emission spectrometry Horiba Ultima 2 (Horiba Scientific). The concentrations obtained were then used for synthetic preparation of pore solutions, which were further used for the surface tension measurement.

#### Surface tension testing

The surface tension of prepared samples was measured by the tensiometer BPA-800P (KSV Instruments) using the maximum bubble pressure method. The measurement was carried out in standard mode under the laboratory temperature (21°C). The pore solution was weighed out into plastic flasks, one

containing the reference sample and the others containing PPG 425 in the mass concentrations of 0.05, 0.10, 0.25, 0.50, 1.00 and 2.00 wt% related to the mass of BFS, the amount of which corresponded to the amount of activator used that was necessary for alkali activation.

#### Drying shrinkage measurement

The mortar specimens were prepared according to ČSN EN 196-1 (ČSN, 2016) standard with the dimensions of 25 × 25 × 285 mm and were subjected to the drying shrinkage tests according to ASTM C596 (ASTM, 2017b). After 24 h the specimens were removed from molds and kept in the n humidity chamber at approximately 50% RH until the age of 28 d. During this period, the relative length changes were measured almost every workday at the beginning and then usually every 3 d using the ASTM C490 (ASTM, 2017a) dilatometer.

#### Isothermal calorimetry measurement

All calorimetric measurements were performed using TAMAir isothermal conduction calorimeter by TA Instruments at the temperature of 25°C. For each measurement, 4 g of BFS and adequate amount of alkali activator were used. Slag was placed into 15 ml glass flask and alkali activator was dosed into admix vial. BFS and the activator were inserted into the calorimeter and tempered separately (for approximately 3 h), then mixed together and stirred for 2 min with a teflon stirrer. A siliceous sand was used as a reference sample. The amount of reference was chosen so that it had similar heat capacity as the sample, in this case being 15.5 g of reference.

#### Compressive strength testing

For the compressive strength measurement, the testing mortar samples with the diameters of 40 × 40 × 160 mm were prepared according to ČSN EN 196-1 standard. Each value in compressive strength development was supported by the average of four measurements. The tests were performed at the ages of 24 h, 7 d and 28 d after the specimen preparation. The press BS-300 (BetonSystem) was used for the compressive strength measurement.

## Results and discussion

First, the most suitable PPG 425 concentration for the test of drying shrinkage was determined. The dependence of surface tension of pore solutions on PPG 425 concentration is represented in Figure 1. Each pore solution extracted from samples activated by water glass of specific silicate moduli contained a

Table 1. Chemical composition of BFS according to XRF

Raw material	Chemical composition: wt%									
	Silicon dioxide (SiO <sub>2</sub> )	Aluminium oxide (Al <sub>2</sub> O <sub>3</sub> )	Calcium oxide (CaO)	Sodium oxide (Na <sub>2</sub> O)	Potassium oxide (K <sub>2</sub> O)	Magnesium oxide (MgO)	Sulfur trioxide (SO <sub>3</sub> )	Iron (III) oxide (Fe <sub>2</sub> O <sub>3</sub> )	Titanium dioxide (TiO <sub>2</sub> )	Manganese oxide (MnO)
BFS	34.7	9.1	41.1	0.4	0.9	10.5	1.4	0.3	1.0	0.6

different amount of potassium ions. Even a small addition of surfactant led to a steep drop of surface tension. This effect was also supported by the presence of alkalis. Generally, the more alkalis that were present in the solution, the lower was the surface tension, and thus they positively influenced the effect of admixture. This is in a good agreement with the Hofmeister series and salting-in effect. This dependence was observed for all pore solutions. Nevertheless, the surface tension values of pore solutions with  $M_s = 0.78$  and  $0.97$  were basically the same within the deviation values. It can also be concluded that after a sudden decrease of surface tension the values did not change further but, on the contrary, they remained more or less constant for almost all solutions. This phenomenon occurred at the moment when the concentration of PPG 425 was  $0.5$  wt%, meaning that the surfactant reached its critical micelle concentration (CMC) ( $45\text{--}55$  mJ/m<sup>2</sup>). As a consequence, it was concluded that  $0.5$  wt % of PPG 425 should have been further added to the samples for the following measurements.

The efficiency of PPG 425 on the drying shrinkage development of potassium alkali-activated mortars is shown in Figure 2. The dependence of the drying shrinkage decrease on decreasing silicate modulus of the alkali activator is evident. This phenomenon is probably related to the formation of different amounts of calcium silicate hydrate (C-S-H) gel. A higher amount of C-S-H gel causes a more compact structure, which leads to lower evaporation of water from the capillary menisci (Figure 3) and, therefore, the drying shrinkage is consequently smaller. Nevertheless, within the same silicate modulus of alkali activator, higher weight losses of mortars with PPG 425 were observed, compared to those without it. This could be explained by the lower liquid saturation induced by SRA as previously described (Aïtcin and Flatt, 2015). Moreover, the amount of alkalis has a significant influence on drying shrinkage. Comparing the samples with

PPG 425 and the reference samples, the effect of added surfactant is evident. Thanks to the higher content of alkaline ions, the efficiency of PPG 425 increases. It is obvious that the samples activated by water glass with low silicate modulus ( $0.78$ ;  $0.97$ ) show a greater difference between the reference and the surfactant-containing samples in drying shrinkage evolution. This phenomenon is in a good agreement with previous results presented in Figure 1 and confirms the importance of the amount of alkali ions for the PPG 425 efficiency affecting the reduction of surface tension of the pore solution and the drying shrinkage.

The hydration mechanism was studied based on the calorimetry measurement. Figure 4 presents slag pastes activated by

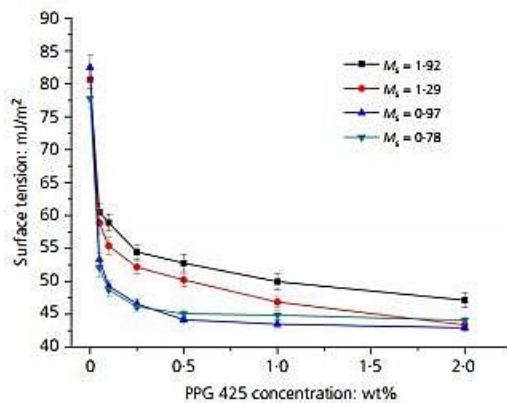


Figure 1. Surface tension of pore solutions with different silicate moduli of potassium water glass depending on the PPG 425 concentration

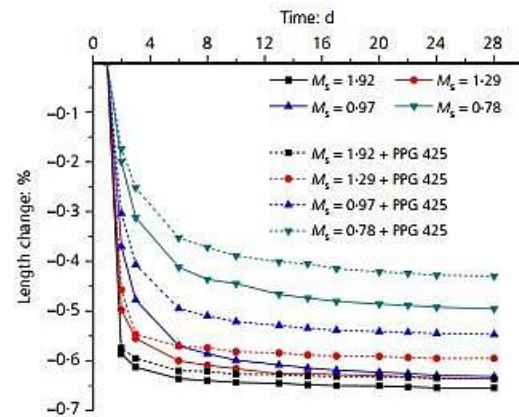


Figure 2. Effect of PPG 425 on drying shrinkage evolution of samples activated by potassium water glass with different silicate moduli

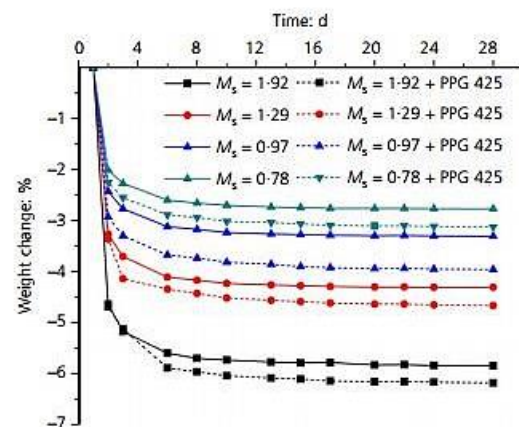


Figure 3. Effect of PPG 425 on weight changes of samples activated by potassium water glass with different silicate moduli

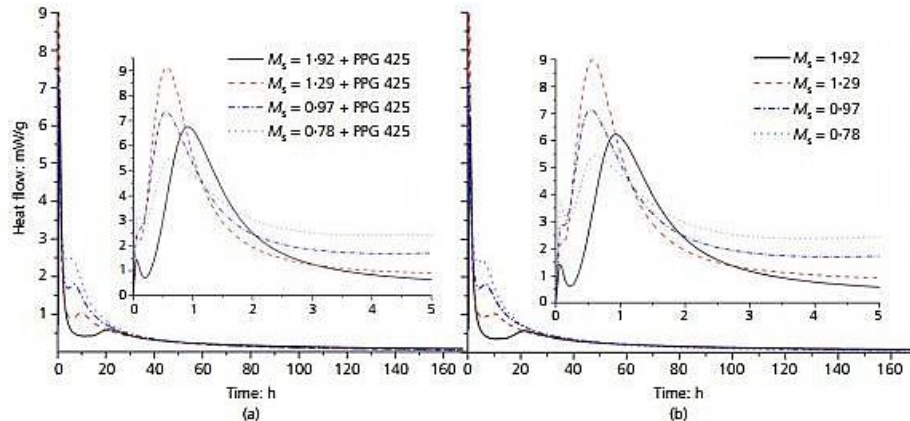


Figure 4. Heat evolution rate of slag pastes activated by potassium water glass with different silicate moduli: (a) with the addition of PPG 425 and (b) without it

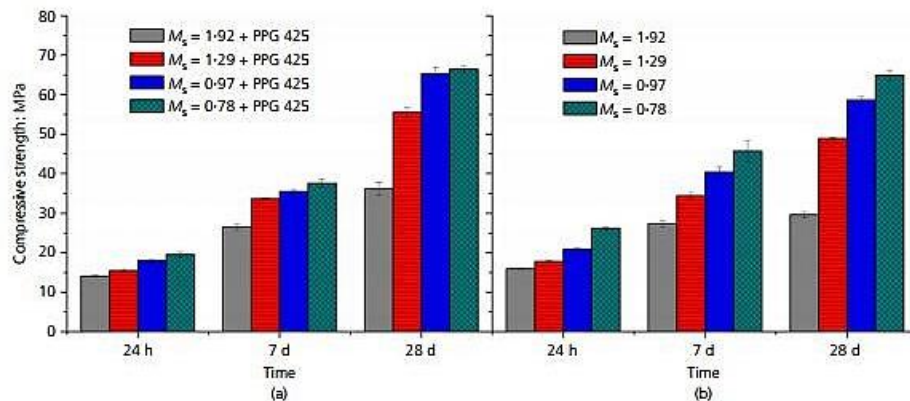


Figure 5. Effect of PPG 425 on the compressive strength development of samples activated by potassium water glass with different silicate moduli: (a) with the addition of PPG 425 and (b) without it

potassium water glass with varying silicate moduli ( $M_s = 1.92, 1.29, 0.97, 0.78$ ). Figure 4(a) shows the heat flow evolution for the mixtures with added PPG 425, whereas Figure 4(b) demonstrates the curves for the mixtures without it. The amount of PPG 425 was always 0.5 wt% of BFS. Particular peaks capture various stages of the slag activation process. The first initial peak is always associated with particle wetting and slag dissolution and the second additional peak corresponds to primary C-S-H gel formation, both during the so-called pre-induction period (Shi and Day, 1995). Then the process is followed by the precipitation of the secondary C-S-H gel, and therefore the third peak was recorded. It was observed that the heat flow evolution remained the same for the mixtures with PPG 425 as well as without it. However, it was found that the samples activated

by potassium water glass with various silicate moduli differed significantly in the third peak. Higher silicate modulus caused the delay of secondary C-S-H gel formation, and moreover decreased its heat flow release, which influenced the compressive strength development. When the mortars activated by potassium water glass were prepared, it was confirmed that the compressive strength was higher with decreasing value of silicate modulus of alkali activator (Figure 5). This trend is evident both in the samples with the addition of PPG 425 (Figure 5(a)) and in the reference samples (Figure 5(b)). The results are consistent with the calorimetry measurement, where it was proved that the samples activated by water glass with higher silicate modulus showed less formation of binder phase. It is also obvious that the addition of surfactant influences the compressive strength

development. In the early stages of the alkali activation process (1–7 d), the compressive strength of samples with PPG 425 is lower compared to the reference samples. After 1 d, the compressive strength of samples with PPG 425 achieved only 87% of the reference samples' values in cases of  $M_s = 1.92$ , 1.29, 0.97 and just 75% for samples activated by potassium water glass with silicate modulus  $M_s = 0.78$ . This decrease could be related to possible adsorption of surfactant to the BFS particles, which slows down the process of alkali activation, as previously described (Partyka *et al.*, 1984). After 7 d, the equalisation of compressive strengths of samples with surfactant and without it occurred, with respect to the error bars. However, the role of surfactant in preventing the drying shrinkage is visible after 28 d. The samples with PPG 425 did not show any visible cracks on their surface, which positively affected the compressive strengths results; see, for example, the samples activated by water glass with  $M_s = 0.78$ . While the compressive strength of the reference sample between 7 and 28 d has been augmented by 30%, the strength of samples with PPG 425 added has improved by more than 40%. A similar trend was also observed in other cases.

### Conclusions

On the basis of the results obtained, it can be stated that polypropylene glycol with the molecular weight 425 plays a critical role in drying shrinkage development. Its efficiency is highly enhanced by the amount of alkalis in the activator. The addition of the surfactant used slightly decreases the compressive strength in the early stages of the hydration process (1–7 d), but after 28 d it gives better results compared to samples without it. These pieces of knowledge point out the importance of using suitable SRAs to improve the properties of AAMs and consequently increase the potential for their broader industrial application.

### Acknowledgements

This outcome has been achieved with financial support by the project: Materials Research Centre at Faculty of Chemistry, Brno University of Technology – Sustainability and Development, REG LO1211, with financial support from the National Programme for Sustainability I (Ministry of Education, Youth and Sports) and GA17-03670S 'Development of shrinkage reducing agents designed for alkali activated systems', and with the financial support from the Czech science foundation.

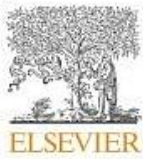
### REFERENCES

- Altın PC and Flatt RJ (2015) *Science and Technology of Concrete Admixtures*. Woodhead Publishing, Sawston, UK.
- ASTM (2017a) C490/C490M-17: Standard practice for use of apparatus for the determination of length change of hardened cement paste, mortar, and concrete. ASTM International, West Conshohocken, PA, USA.
- ASTM (2017b) C596-09: Standard test method for drying shrinkage of mortar containing hydraulic cement. ASTM International, West Conshohocken, PA, USA.
- Baudouin P, Wattebled L, Touraud D and Kunz W (2004) Hofmeister ion effects on the phase diagrams of water-propylene glycol propyl ethers. *International Journal of Research in Physical Chemistry & Chemical Physics* **218**(6): 631–641.

- Bentz DP, Quenard DA, Baroghelbouny V, Garboczi EJ and Jennings HM (1995) Modeling drying shrinkage of cement paste and mortar. I. Structural models from nanometers to millimeters. *Materials and Structures* **28**(182): 450–458.
- Bernal SA, Rodriguez ED, de Gutierrez RM and Provis JL (2015) Performance at high temperature of alkali-activated slag pastes produced with silica fume and rice husk ash based activators. *Materiales de Construcción* **65**(318): 1–10.
- Bilek V, Kalina L, Novotny R, Tkacz J and Parizek L (2016) Some issues of shrinkage-reducing admixtures application in alkali-activated slag systems. *Materials* **9**(6): 1–12.
- Cai LC, Wang HF and Fu YW (2013) Freeze–thaw resistance of alkali-slag concrete based on response surface methodology. *Construction and Building Materials* **49**: 70–76, <https://doi.org/10.1016/j.conbuildmat.2013.07.045>.
- Collins F and Sanjayan JG (2000) Effect of pore size distribution on drying shrinkage of alkali-activated slag concrete. *Cement and Concrete Research* **30**(9): 1401–1406.
- ČSN (Czech Technical Standard) (2016) EN 196-1: Methods of testing cement – Part 1: Determination of strength. Czech Office for Standards, Metrology and Testing, Prague, Czech Republic.
- Damtoft JS, Lukasik J, Hertfort D, Sorrentino D and Gartner EM (2008) Sustainable development and climate change initiatives. *Cement and Concrete Research* **38**(2): 115–127.
- Hossain MM, Karim MR, Hossain MK, Islam MN and Zain MFM (2015) Durability of mortar and concrete containing alkali-activated binder with pozzolans: a review. *Construction and Building Materials* **93**: 95–109, <https://doi.org/10.1016/j.conbuildmat.2015.05.094>.
- Kalina L, Koplík J, Soukal F, Masilko J and Jaskowicova L (2012) Potential uses of geopolymers to immobilize toxic metals from by-products materials. *Environmental Engineering and Management Journal* **11**(3): 579–584.
- Kunz W, Henle J and Ninham BW (2004) 'Zur Lehre von der Wirkung der Salze' (about the science of the effect of salts): Franz Hofmeister's historical papers. *Current Opinion in Colloid & Interface Science* **9**(1–2): 19–37.
- Morini MA, Messina PV and Schulz PC (2005) The interaction of electrolytes with non-ionic surfactant micelles. *Colloid and Polymer Science* **283**(11): 1206–1218.
- Palacios M and Puertas F (2007) Effect of shrinkage-reducing admixtures on the properties of alkali-activated slag mortars and pastes. *Cement and Concrete Research* **37**(5): 691–702.
- Partyka S, Zaini S, Lindheimer M and Brun B (1984) The adsorption of non-ionic surfactants on a silica-gel. *Colloids and Surfaces* **12**(3–4): 255–270.
- Sant G, Eberhardt A, Bentz D and Weiss J (2010) Influence of shrinkage-reducing admixtures on moisture absorption in cementitious materials at early ages. *Journal of Materials in Civil Engineering* **22**(3): 277–286.
- Shi CJ and Day RL (1995) A calorimetric study of early hydration of alkali-slag cements. *Cement and Concrete Research* **25**(6): 1333–1346.

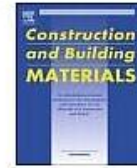
### How can you contribute?

To discuss this paper, please submit up to 500 words to the editor at [journals@ice.org.uk](mailto:journals@ice.org.uk). Your contribution will be forwarded to the author(s) for a reply and, if considered appropriate by the editorial board, it will be published as a discussion in a future issue of the journal.



Contents lists available at ScienceDirect

## Construction and Building Materials

journal homepage: [www.elsevier.com/locate/conbuildmat](http://www.elsevier.com/locate/conbuildmat)

## Polyethylene glycol molecular weight as an important parameter affecting drying shrinkage and hydration of alkali-activated slag mortars and pastes

Vlastimil Bílek Jr. <sup>\*</sup>, Lukáš Kalina, Radoslav Novotný

Brno University of Technology, Faculty of Chemistry, Materials Research Centre, Purkyňova 464/118, Brno CZ-612 00, Czech Republic

## HIGHLIGHTS

- Increasing glycol dose had minor effect on strength while significant on shrinkage.
- Longer molecules reduced drying shrinkage of AAS more than short molecules.
- Shrinkage was reduced thanks to surface tension decrease and porosity changes.
- Ethylene glycol reduced both 2nd and 3rd peaks of AAS calorimetric curve.
- 3rd AAS calorimetric peak reduction increased with increasing molecular weight.

## ARTICLE INFO

## Article history:

Received 8 August 2017

Received in revised form 26 January 2018

Accepted 29 January 2018

## Keywords:

Alkali-activated slag  
Polyethylene glycol  
Molecular weight  
Shrinkage  
Hydration  
Strength  
Porosity  
Surface tension

## ABSTRACT

The aim of this study was to explore the influence of ethylene glycol in a wide range of polymerization degree, i.e. from monomer (EG) up to polyethylene glycol (PEG) with molecular weight of about 35,000, on properties of alkali-activated slag mortars. Changes in molecular weight and dose of all tested glycols had only minor effect on compressive strength, while drying shrinkage was significantly affected by both these factors. EG had negligible impact on drying shrinkage, but other tested glycols reduced it significantly with PEG2000 and PEG10000 being the most effective. Such different shrinkage behavior was attributed to the changes in surface tension and pore structure. All tested glycols reduced the total heat released during the hydration and interestingly modified the heat flow depending on their molecular weight.

© 2018 Elsevier Ltd. All rights reserved.

## 1. Introduction

Materials based on alkali activated slag (AAS) can achieve excellent mechanical properties and durability, but their wider utilization is limited by significant drying and autogenous shrinkage, the values of which are usually considerably higher compared to those of OPC-based materials [1]. Therefore, many different approaches focused on the shrinkage reduction have been published. From possible solutions, partial replacement of slag by other materials such as fly ash or silica fume [2], prolonged the

curing period [3], heat curing [4], and the use of expanding [5] or shrinkage reducing admixtures [6–9] can be depicted.

Shrinkage reducing admixtures (SRAs) were introduced in 1980s to mitigate the drying shrinkage of OPC concretes [10]. Although several products are available on market, only rare studies dealing with their application in AAS systems have been published. Palacios and Puertas [6] studied the effect of SRA based on polypropylene glycol (PPG) on the properties of slag activated by waterglass with the silicate modulus of 1.0–1.2 and the dose of 4% Na<sub>2</sub>O by mass of slag. SRA had rather beneficial effect on the flexural strength and little or no effect on the compressive strength, it also slightly retarded the hydration of slag, but later the precipitation of CSH was more intense in pastes containing SRA. SRA based on PPG also reduced the drying shrinkage of AAS after 180 days at 50% relative humidity (RH) by 7 and 35% for 1

<sup>\*</sup> Corresponding author.

E-mail addresses: [bilek@fch.vut.cz](mailto:bilek@fch.vut.cz) (V. Bílek Jr.), [kalina@fch.vut.cz](mailto:kalina@fch.vut.cz) (L. Kalina), [xcnovotny2@fch.vut.cz](mailto:xcnovotny2@fch.vut.cz) (R. Novotný).

<https://doi.org/10.1016/j.conbuildmat.2018.01.176>  
0950-0618/© 2018 Elsevier Ltd. All rights reserved.

and 2% of SRA, respectively. The same doses of SRA were markedly more efficient at 99% RH, where the shrinkage reduction was 50 and 80%, respectively. Eberhardt [10], who studied OPC-based mortars, explained different efficiency of SRA depending on RH as the consequence of an increase of interfacial area during the drying, on which SRA molecules have to act.

The action of SRA based on PPG in AAS was studied also by Bilim et al. [7]. The silicate modulus of waterglass and sodium hydroxide mixture was 0.75 and 1.0, while its dose was 5.4 and 8.1% Na<sub>2</sub>O by mass of slag and the dose of SRA was 1.0%. Regardless the type of curing and the dose and modulus of activator, the long-term drying shrinkage was reduced generally by 15–30%, although during first few days of drying, the shrinkage reduction was significantly higher, particularly for the specimens which were heat cured in water before exposing to the atmospheric conditions. Similar shrinkage performance of AAS, at least from the long term point of view, was also reported for the activation by solid sodium silicate [8]. Generally, SRA did not have significant effect on the strength and setting time of AAS, but some exceptions like prolonged setting time in the case of mixtures with lower activator dose could be found.

Besides SRAs, other organic admixtures are also able to modify the shrinkage behavior of AAS. Slight shrinkage reduction was reported for the set retarding and water reducing admixture by Bilim et al. [7,8]. Bakharev et al. [9] reduced the long-term drying shrinkage of AAS concrete by 30% with lignosulphonate plasticizer and even by 75% with alkyl aryl sulphonate-based air entraining agent, while an unspecified SRA reduced the drying shrinkage by 67%. On the other hand, the application of superplasticizer based on modified naphthalene formaldehyde polymers resulted in the shrinkage increase by more than 100% after seven days and by almost 40% after 224 days.

Based on this brief review, we can conclude that SRAs and other chemical admixtures can lead to significant decrease in shrinkage of AAS-based materials. However, its values are still higher compared to those of OPC without SRAs in most cases. Moreover, some studies [11,12] revealed that common commercially available SRAs can retard the hydration of AAS by several days even at relatively low doses (1%) and, in this case, it is likely that observed shrinkage reduction was caused by coarser pore structure, which resulted from the retardation of slag hydration. SRAs are generally based on lower monoalcohols and diols, while promising results were obtained for SRA based on polymers (polypropylene glycol), as was discussed above. Therefore, it was our interest to investigate the effect of molecular weight of such organic compounds, e.g. polyethylene glycol which was used in this study.

## 2. Materials and experimental procedures

### 2.1. Materials and sample preparation

Ground granulated blast furnace slag with specific surface area of about 400 m<sup>2</sup>/kg was used as an aluminosilicate precursor for alkaline activation by liquid sodium silicate with SiO<sub>2</sub>-to-Na<sub>2</sub>O molar ratio of 2.1 at the dose expressed as 8% Na<sub>2</sub>O by slag weight. Ethylene glycol (EG) and polyethylene glycol with molecular weight of about 400 (PEG400), 2000 (PEG2000), 10,000 (PEG10000) and 35,000 (PEG35000) were used in amounts corresponding to 1.0 and 2.0% of slag weight. The type and amount of these chemicals was also used for the designation of prepared mortars and pastes, and those, which contained no additive, were marked as Ref. The water-to-slag ratio (w/s) was adjusted to 0.35 for pastes and to 0.42 for mortars. The siliceous sand with the maximum grain size of 2 mm was used as a fine aggregate in the

amount three times higher than the weight of slag for the mortars preparation.

At the beginning of the mixing procedure, all the liquid components were mixed together. EG and PEG400 are liquids at laboratory conditions, while longer PEGs are solids; therefore they were dissolved in water before combining it with activator. The longer the PEG was the more time was needed for its dissolution with PEG10000 and particularly PEG35000 being time consuming. After combining aqueous solution of PEG with waterglass, the immiscibility of all PEGs and activating solution was observed. The mixing procedure was performed in accordance with the EN 196-1 standard, fresh mortar properties were determined (see Section 2.2) and the mortar was cast into the molds with dimensions of 25 mm × 25 mm × 285 mm for the drying shrinkage and strength testing. After 24 h of moist curing, the specimens were demolded and cured according to specific testing procedure.

### 2.2. Fresh mortar properties

Mortar consistency was determined using flow table test. After the lifting the steel truncated cone with a lower diameter of 100 mm mortar diameter after consequent spread as well as after 15 table strokes was measured. Mortar density and air content were determined using FORM + TEST Seidner & Co., Ltd. air content tester with a vessel volume of 1 dm<sup>3</sup>.

### 2.3. Drying shrinkage tests

The drying shrinkage was evaluated as the average of length changes of three mortar bars for each mixture measured with the ASTM C490 apparatus. Unlike the specimens for the strength testing, the drying shrinkage specimens were removed from water after three days and stored at the laboratory conditions (approximately 50% relative humidity and 23 °C). Their length changes during drying were measured until the age of 28 days.

### 2.4. Compressive strength tests

Compressive strengths were tested on the same type of specimens as were used for drying shrinkage tests, i.e. with dimensions of 25 mm × 25 mm × 285 mm. Unlike the shrinkage tests, specimens for compressive strength testing were cured immersed in water until their testing. Compressive strength values were obtained after 1, 7 and 28 days on the broken parts of mortar bars on which the flexural strength tests were done.

### 2.5. Isothermal conduction calorimetry

The effect of EG and PEGs on the hydration of AAS at 25 °C was studied by means of isothermal conduction calorimetry. For each measurement, 4.0 g of slag were used and the dose of activating solution was adjusted to w/s ratio of 0.35 and 8% Na<sub>2</sub>O. The admixtures were added together with the activating solution. Slag and the mixture of liquid components were tempered separately inside the TAM Air (TA Instruments) calorimeter. The measurement started immediately after the addition of the mixture of liquids to slag. The paste was homogenized by mechanical stirring during the first three minutes of measurement.

### 2.6. Mercury intrusion porosimetry

Mercury intrusion porosimetry (MIP) tests were carried out using paste bars with dimensions of approximately 5 mm × 5 mm × 12 mm. These small bars were prepared from larger ones by sand paper abrading at the age of four days after the same curing regime as was used for mortar bars on which shrinkage was

measured. To stop hydration just after their preparation small bars for MIP measurements were immersed in isopropyl alcohol whose original batch was exchanged after 24 h. Two to three specimens of each composition were tested by porosimeter able to reach pressures up to 225 MPa. Wetting angle and surface tension of mercury were assumed to be 140° and 480 mN/m, respectively. Therefore, the finest pores which were possible to detect had diameter of about 6.5 nm.

2.7. Surface tension measurements

Effect of increasing concentration of used glycols from 0.01 to 2.0 wt% in demineralized water on surface tension (ST) was determined using bubble pressure tensiometer BPA 800P (KSV Instruments, Ltd.). Water was selected for simplicity instead of pore solution whose composition at the beginning of drying process was not known. It was assumed that thanks to dilution of pore

solution by curing water the behavior of glycols is similar to behavior in pure water.

3. Results

Density, air content and workability of the prepared mortars are given in Fig. 1. Although the differences in both these properties are not very significant for the various glycol type and dose, the results suggest that increased glycol dose as well as its increasing polymerization degree led to increase in entrained air and decrease in mortar density. These results correspond with the workability of the mortars which was slightly improved by EG, but significantly decreased for all tested PEGs.

The effect of EG and PEGs on the compressive strength is shown in Fig. 2. It can be seen that obtained results are similar for all admixtures, i.e. minor or no decrease in the compressive strength with increasing glycol dose. After 24 h, the compressive strengths

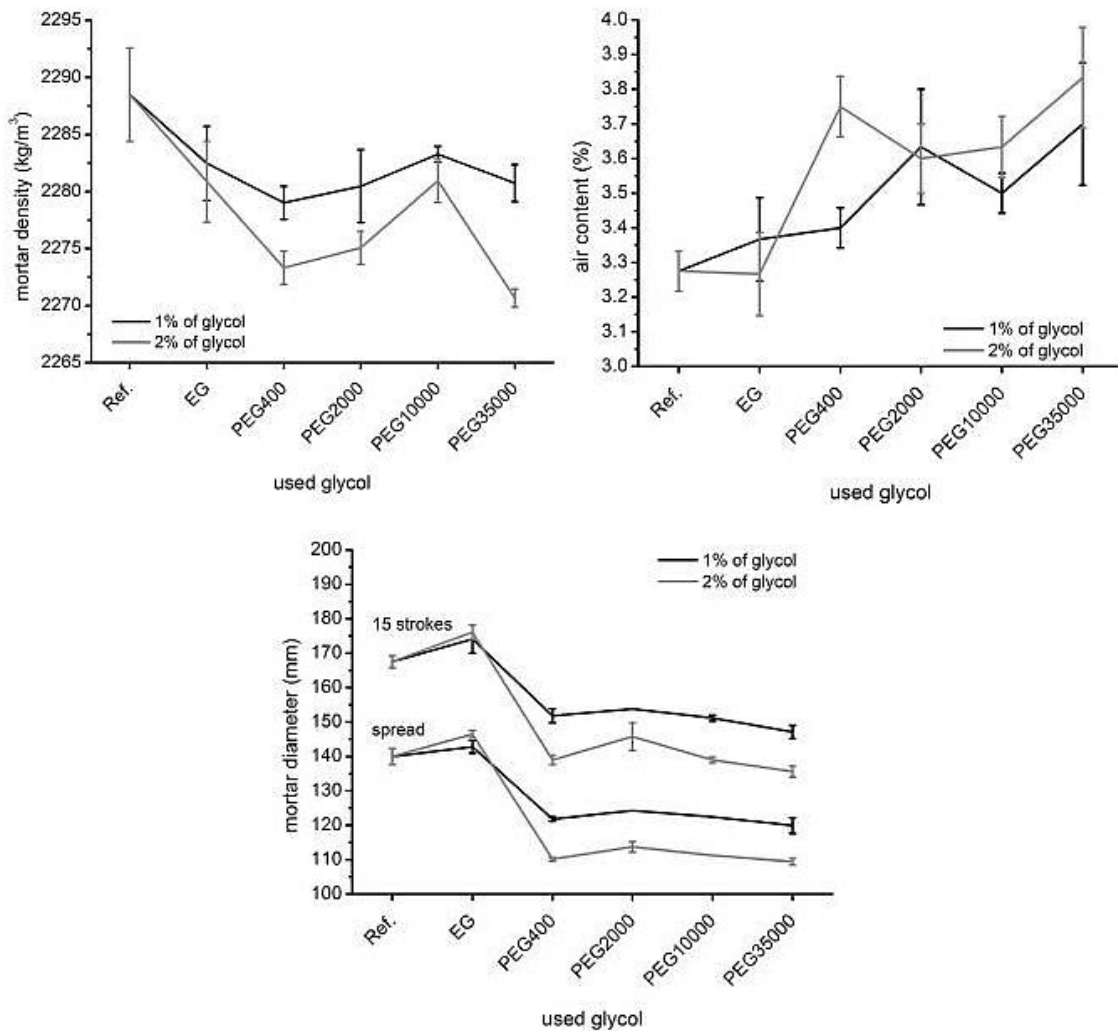


Fig. 1. Effect of used glycols on fresh properties of AAS mortars.

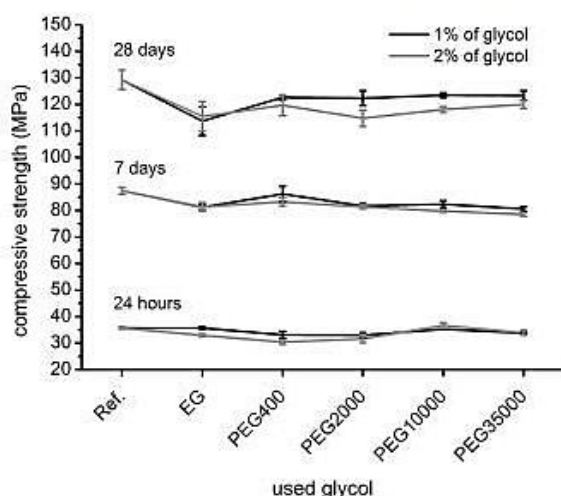


Fig. 2. Effect of used glycols on compressive strength of AAS mortars.

around 35 MPa were recorded and their values gradually increased during the testing period up to about 130 MPa after 28 days.

The shrinkage results (Fig. 3) showed that higher drying shrinkage reduction was observed for polymeric species compared to monomeric EG. While EG did not markedly reduce the drying shrinkage, as the differences in obtained values of all tested mortars are in the range of reproducibility of the measurement, PEG400 and PEG2000 gradually decreased the drying shrinkage with their increasing doses and molecular weight. PEG10000 had similar shrinkage reducing efficiency to PEG2000, while PEG35000 reduced shrinkage somewhat lower compared to these two PEGs. The most effective PEGs (PEG2000 and PEG10000) reduced the drying shrinkage of tested mortars at the age of 28 days by around 25% at the dose of 2%, respectively. Efficiency of all PEGs was much higher during the first days of drying: For example after first 24 h shrinkage was reduced by 25% and 53% using PEG2000 at the dose of 1% and 2%.

To shed more light on the role of used PEGs on shrinkage behavior of AAS mortars MIP measurements as well as ST measurements were carried out. Complete MIP curves are given in Fig. 4. According to Collins and Sajayan [13] capillary tensile forces inducing drying shrinkage of AAS are the most severe in mesopores, pores ranging from 1.25 to 25 nm, and therefore the portion of mesopores (or more specifically portion of pores in the range of 6.5–25 nm due to limits of the measuring device) from all detected pore sizes was calculated and summarized (Fig. 5). The highest mesopore portion was found in the reference and EG containing pastes while by far the lowest mesopore portion was detected in PEG400 paste. Mesopore content of PEG2000 paste was among the Ref. and PEG400 pastes and pastes with longer PEGs had similar mesopore fraction as the reference one. Surface tension measurements (Fig. 6) showed very different ability of tested glycols to reduce surface tension depending on their molecular weight: ST reducing effect sharply increased with increasing molecular weight of tested glycols, particularly up to molecular weight of 2000.

The results from the calorimetric experiments are given in Fig. 7 and Fig. 8. All tested chemicals reduced the total heat released during the testing period and modified the heat release rate curve, which comprised two peaks during the pre-induction period and one small peak or rather a shoulder after the induction period.

#### 4. Discussion

All tested chemicals glycols affected the compressive strength of AAS mortar in a similar manner. Their increasing dose had no or slightly negative effect. Similar results were achieved by other researchers [6–8], while another commercially available SRA greatly reduced both, the compressive and the flexural strength of AAS, particularly during the early ages [11]. Unlike the compressive strength, the shrinkage behavior and workability of studied mortars differed for EG compared to all tested PEGs. As was shown in Fig. 1 increasing dose of monomeric EG led to a gradual workability improvement, which can be explained by increased volume of the liquid phase, as the dose of water was kept constant for all mortars. Despite this fact, workability markedly decreased when PEGs were used. Possible explanation would be the simultaneous adsorption of one PEG molecule onto the two or more slag particles and thus increased yield stress. Such a bridging mechanism was proposed by Kashani et al. [14] for superplasticizer molecules.

Molecular weight played an important role also in the AAS drying shrinkage development. As can be found in literature, few theories explaining shrinking of the cementitious materials during their drying have been developed. Probably the most common and widely accepted is capillary pressure theory, according to which liquid-vapor interface in the form of menisci is formed in the capillaries partially filled with pore fluid. The pressure difference between liquid phase  $p_l$  and vapor phase  $p_v$  is called capillary pressure  $p_c$ . It can be expressed also through the radius of curvature  $\kappa$  of the menisci and surface tension  $\gamma$  [15] and further simplified for spherical shape of meniscus and good wetting of the pore walls (wetting angle close to zero) to include pore radius  $r$ , which is expressed by Eq. (1).

$$p_c = p_l - p_v = \kappa\gamma = -2\gamma/r \quad (1)$$

It is generally agreed [16] that capillary suction is the main driving force for drying shrinkage when the pores are larger than approximately 10 nm. Nevertheless, some authors [17,18] contested capillary pressure importance and presented disjoining pressure to be the principle mechanism for drying shrinkage. Theory of disjoining pressure can be applied through the whole range of humidity and particularly for very fine pores. This theory is based on the balance of attractive and repulsive forces among the two surfaces close to each other. Attractive forces are mainly represented by van der Waals forces whose magnitude depends on the thickness of the adsorbed water layer among the surfaces. Thus, with increasing relative humidity water layer thickness also increases, attractive forces are weakened, surfaces can be separated and material swells. For more details see e.g. [17,18].

Different shrinkage reducing ability of used PEGs can be explained by both these theories: According to the capillary pressure theory, capillary suction which induces shrinkage is proportional to surface tension (Eq. 1) and therefore the lower the surface tension of the pore fluid the lower the shrinkage of the mortar. In sense of disjoining pressure theory shrinkage reducing effect of glycols can be explained by their presence in fine pores which would weaken attractive forces among them and sterically hinder shrinkage. It would also be expected that longer molecules are more capable to act in such manner compared to shorter molecules. Moreover, one can expect that longer organic molecules are more resistant to leaching during the water curing which would also contribute to increasing shrinkage-reducing ability of glycols with increasing molecular weight. Furthermore, it was observed that PEGs increased air content in the mortars which also contributed to their shrinkage reducing effect together with the changes of the pore structure, i.e. decrease in mesopore fraction

## Příloha VI

568

*V. Bílek Jr. et al. / Construction and Building Materials 166 (2018) 564–571*

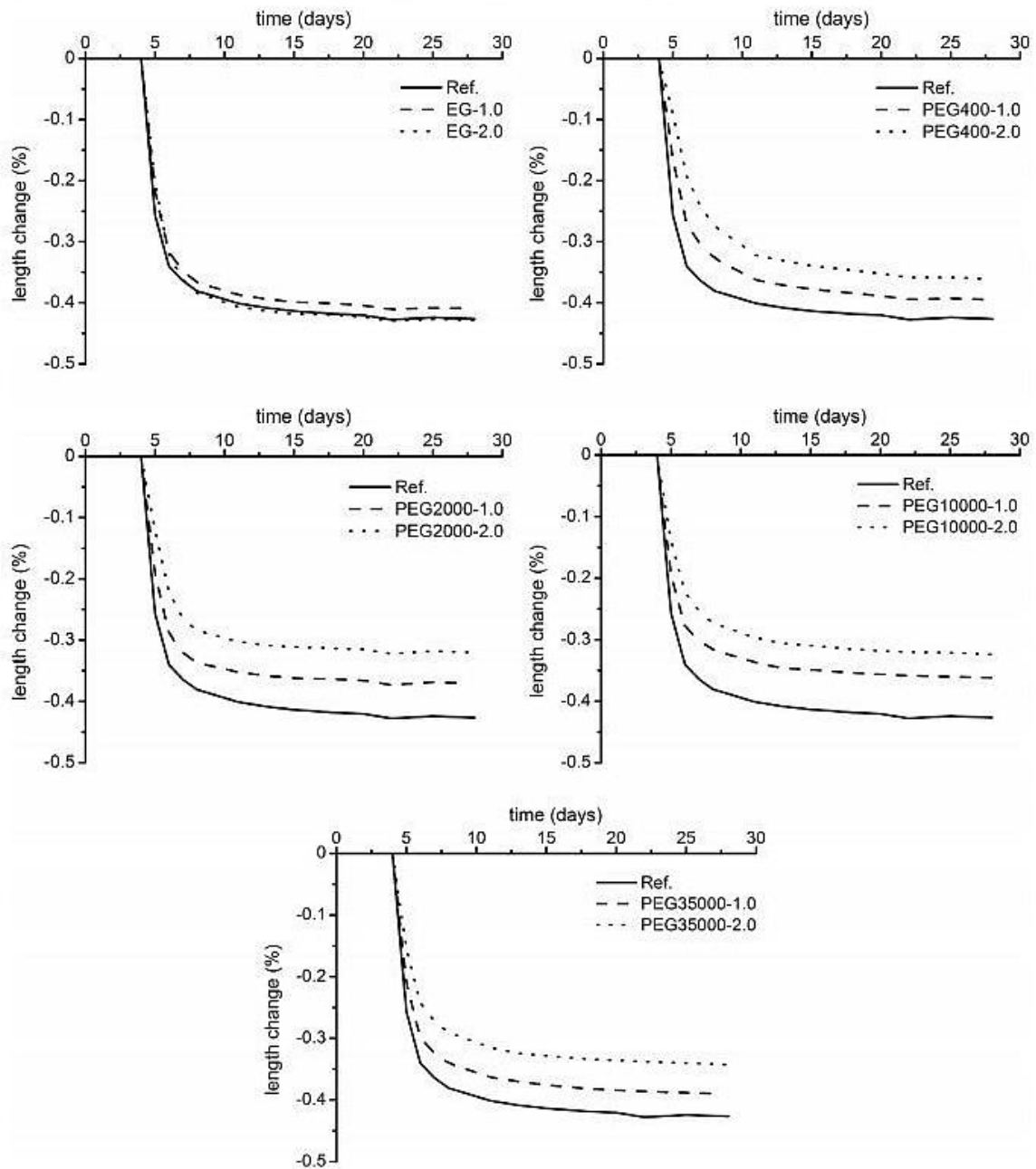


Fig. 3. Effect of used glycols on drying shrinkage of AAS mortars.

(Fig. 5). Therefore, it is clear that several factors contribute to overall shrinkage reducing efficiency of glycols, particularly their impact on pore structure of the material and surface tension of the pore fluid: Since EG did not reduce mesopore content nor surface tension it is not surprising that it did not reduce shrinkage of AAS mortars while PEGs did, because the longer the chain the sharper the surface tension decrease. Although PEG400 was not so

effective in surface tension reducing as longer PEGs it was able to reduce shrinkage markedly thanks to reduction of mesopore content. Similar shrinkage behavior of mortars with PEG2000 and PEG10000 also corresponds well with both their similar mesopore content and similar surface tension reducing ability. Only PEG35000 reduced shrinkage somewhat lower than could be expected from the comparison with PEG2000 and PEG10000. It

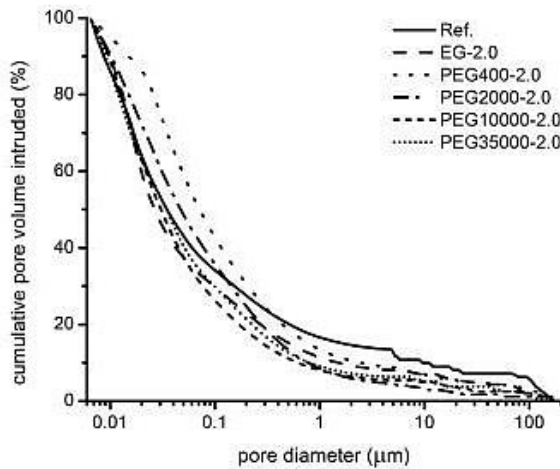


Fig. 4. Effect of 2% addition of used glycols on MIP curves of AAS pastes (one representative curve for each mixture was selected for clarity).

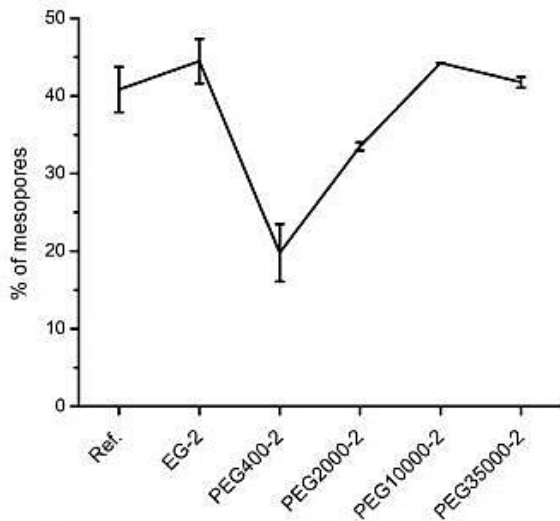


Fig. 5. Effect of 2% addition of used glycols on fraction of pores with diameter of 6.5–25 nm as calculated from MIP data.

should be noted that PEG35000 was not soluble directly in activating solution (mixture of water and waterglass), but it was possible to dissolve in water alone before waterglass addition. This solubility issue could be a reason for its limited shrinkage reducing efficiency.

Comparing the shrinkage results obtained in present study for both PEGs and those from other studies, we can see similar trends. These chemicals or admixtures are able to reduce the drying shrinkage by a few tens of percent from the long-term point of view, but during the first days of drying their efficiency can be even around 60–80%. According to Eberhardts [10] observations of reduced SRA efficiency at intermediate relative humidity, the decrease in the shrinkage reduction during ongoing drying process could be the result of increasing interfacial area on which the surfactant molecules have to act.

It is generally emphasized that the miscibility of SRAs with water or with pore solution is a limiting factor for the shrinkage

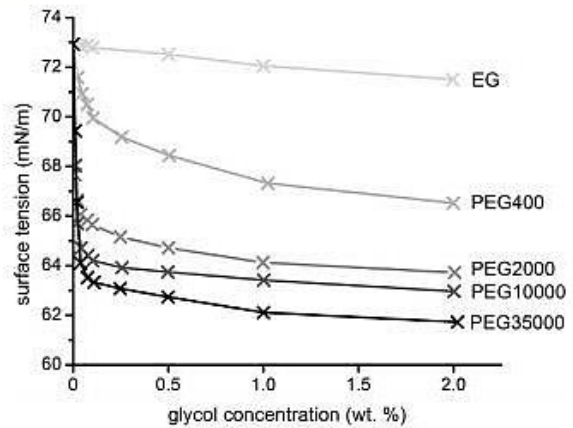


Fig. 6. Effect of used glycols on surface tension of water.

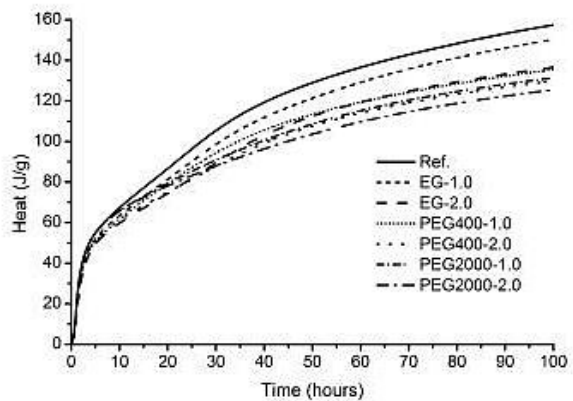


Fig. 7. Effect of EG, PEG400 and PEG2000 on total heat released during the first 100 h of AAS hydration.

reduction, because beyond the critical SRA concentration, further decrease in surface tension with increasing dose of SRA is very low [10,15,19]. However, according to obtained results, the drying shrinkage was reduced by all tested PEGs, despite they were not miscible with the waterglass solution (Fig. 9). A possible explanation could be that the SRA molecules are expelled to the liquid-vapor interface, where they can act as an interphase between the pore solution and ambient vapor phase, and thus reduce the surface tension and shrinkage. Another and perhaps more likely explanation of the shrinkage reduction could be that the SRA miscibility with pore solution increases during the alkaline activation as the consequence of consuming silicate species introduced into the system with sodium silicate activator, particularly during the primary C-S-H gel formation. Unfortunately, there is no information about the miscibility of SRAs with activating solution in the literature focused on their influence on AAS [6–8], which does not allow further discussion. Nevertheless, as was already mentioned, the trend of the shrinkage development of AAS with and without SRAs in these studies is similar compared to present work, i.e. decreasing efficiency of SRAs during the drying process. It thus seems that the SRA behavior in these systems is comparable, although waterglass with higher silicate modulus (2.1 vs. 0.75–1.2) and higher dose of activator in most cases (8% Na<sub>2</sub>O vs. 4.0,

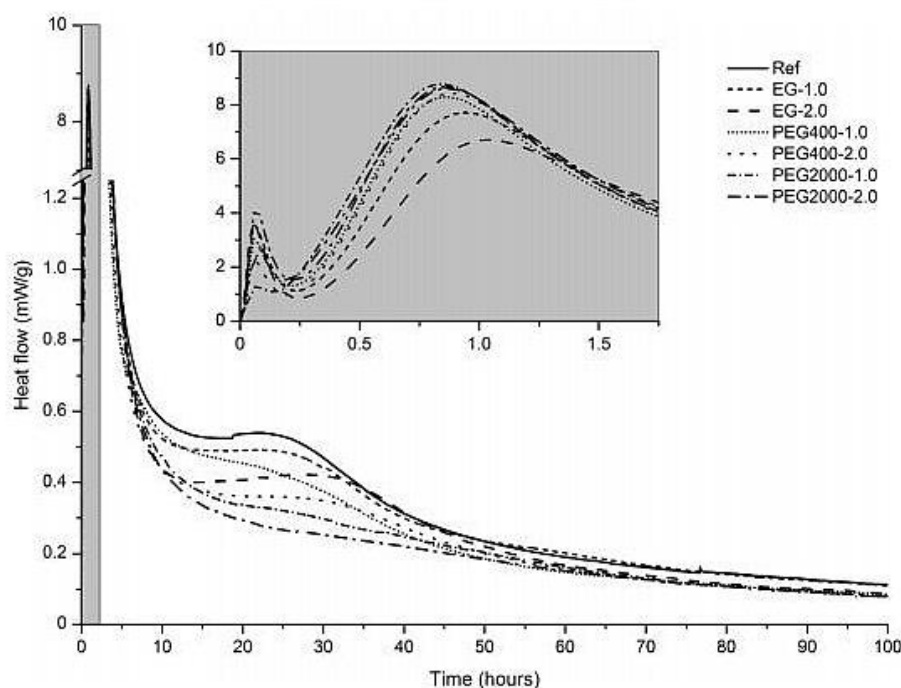


Fig. 8. Effect of EG, PEG400 and PEG2000 on heat evolution rate during the AAS hydration.



Fig. 9. Miscibility and color change of used glycols in activating solution of the same composition as for pastes with 2% addition of glycol after 14 days.

5.4 or 8.1%  $\text{Na}_2\text{O}$ , respectively) was used in present study, as well as different curing regime before the start of drying.

Besides the miscibility, the chemical stability of the organic compounds in highly alkaline environment of AAS is another issue to be considered. Palacios and Puertas [20] observed the structural alteration of polycarboxylate-, vinyl copolymer- and melamine-based superplasticizers in NaOH and waterglass solutions. On the other hand, SRA based on PPG was stable in both alkaline solutions. In present study, the chemical stability of PEGs was not investigated in a detail, but as the structure of their molecule resembles the structure of PPG molecule, similar chemical stability can be expected. From tested glycols, EG was suspected being the most reactive in alkaline condition since it is known to polymerize in alkaline environment. Nevertheless, it was macroscopically stable in the concentrated activating solution used for paste preparation even for 14 days (Fig. 9). Unlike in used activating solution it readily reacted in 50% sodium hydroxide solution to form white solid. Therefore, pH of used waterglass is not high enough to assure macroscopically observable EG polymerization or other chemical changes. Surprisingly, it should be noted that PEG400 and

PEG35000 changed color few hours after mixing. The former turned yellow while the latter turned orange, which could be due to some degradation of these chemicals, while all other PEGs remained colorless. This unexpected feature could also be a topic for further study.

This work was also focused on the effect of EG and PEGs on the hydration process of AAS by means of isothermal calorimetry. All pastes, which contained glycols, released less heat than the reference paste (Fig. 7). Such an influence of organic admixtures (superplasticizers) was observed by Jang et al. [21]. Of course, the differences in the hydration process are more obvious from the heat release rate curves (Fig. 8). These curves were similar to those described for waterglass-activated slag by Shi [22]. The first peak occurring within the first 10 min was related mainly to the dissolution of slag particles [22]. This peak was reduced in presence of glycols in most cases, but it should be noted that the reproducibility of this peak is not good. However, further behavior of AAS with and without chemicals was even more interesting. It was observed that the changes in calorimetric curves were dependent on increasing molecular weight of PEG: The second peak with maximum between 45 and 60 min depending on glycol type was associated with primary C-S-H formation through the reaction of silicon ions mainly from waterglass and calcium ions released during the slag dissolution. This peak was strongly reduced and its maximum delayed by increasing dose of EG, while PEG400 and particularly PEG2000 did not influence it significantly. On the other hand, roughly inverse effect of increasing molecular weight on the third peak was recorded, i.e. its intensity decreased with increasing molecular weight. Increased dose of chemicals resulted in the decrease of this peak too, and, at least increasing dose of EG, slightly delayed this peak. Comparing Figs. 7 with 8 it can be seen, that the influence of EG and PEGs on the third peak is the main reason for the total heat released reduction in the presence of these chemicals.

The calorimetric results suggest, that short EG molecules could interact with the AAS system during the first tens of minutes or hours, while longer PEG molecules are able to affect further hydration stages more extensively. This is probably the consequence of higher concentration of hydroxyl groups of EG than in the same mass unit of PEGs and also EG molecules can be expected being more mobile. Glycols belong to the group of nonionic surfactants [15] which means that only a few of many EG molecules can deprotonate. However, in highly alkaline conditions deprotonation could be intensified which would open wide range of interactions with ionic species in the pore solution as well as with hydration products.

The decreasing intensity of the third peak in the presence of glycols can partially explain lower compressive strength of corresponding mortars as the consequence of reduced formation of hydration products (C-S-H gel). Also higher air content in the PEGs containing mortars contributed to slight strength decrease. However, despite these factors, compressive strength of all the tested mortars was almost the same as for the reference one.

## 5. Conclusions

This paper studied the effect of EG and PEG with different molecular weight on drying shrinkage and other properties of the waterglass-activated slag. The obtained results showed that while the compressive strength was influenced by all tested chemicals in a similar manner, the drying shrinkage gradually decreased with increasing molecular weight up to 2000. PEG2000 and PEG10000 were found to be the most effective in shrinkage reduction. This suggests that polyethylene glycols or polyalkylene glycols in general are suitable for AAS systems compared to those with low molecular weight. Different efficiency in shrinkage mitigation of PEGs was attributed to their more effective surface tension reduction and changes in pore structure. The polymerization degree of EG also played an important role during the hydration process of AAS, where monomeric EG affected more its initial stages of hydration, while the action of its polymeric forms was more obvious after several hours.

## Acknowledgments

This outcome was achieved with the financial support within the project: Materials Research Centre at FCH BUT- Sustainability and Development, REG LO1211, with financial support from the National Programme for Sustainability I (Ministry of Education, Youth and Sports) and GA17-03670S "Development of shrinkage reducing agents designed for alkali activated systems", with financial support from the Czech science foundation.

## References

- [1] A.A. Melo Neto, M.A. Cincotto, W. Repette, Drying and autogenous shrinkage of pastes and mortars with activated slag cement, *Cem. Concr. Res.* 38 (4) (2008) 565–574, <https://doi.org/10.1016/j.cemconres.2007.11.002>.
- [2] S. Aydın, A ternary optimisation of mineral additives of alkali activated cement mortars, *Constr. Build. Mater.* 43 (2013) 131–138, <https://doi.org/10.1016/j.conbuildmat.2013.02.005>.
- [3] J.L. Provis, J.S.J. van Deventer, *Alkali Activated Materials: State-of-the-Art Report*, RILEM TC 224-AAM, Springer, 2014.
- [4] S. Aydın, B. Baradan, Mechanical and microstructural properties of heat cured alkali-activated slag mortars, *Mater. Des.* 35 (2012) 374–383, <https://doi.org/10.1016/j.matdes.2011.10.005>.
- [5] X.-H. Yuan, W. Chen, Z.-A. Lu, H. Chen, Shrinkage compensation of alkali-activated slag concrete and microstructural analysis, *Constr. Build. Mater.* 66 (2014) 422–428, <https://doi.org/10.1016/j.conbuildmat.2014.05.085>.
- [6] M. Palacios, F. Puertas, Effect of shrinkage-reducing admixtures on the properties of alkali-activated slag mortars and pastes, *Cem. Concr. Res.* 37 (5) (2007) 691–702, <https://doi.org/10.1016/j.cemconres.2006.11.021>.
- [7] C. Bilim, O. Karahan, C.D. Atiş, S. İlkentapar, Influence of admixtures on the properties of alkali-activated slag mortars subjected to different curing conditions, *Mater. Des.* 44 (2013) 540–547, <https://doi.org/10.1016/j.matdes.2012.08.049>.
- [8] C. Bilim, O. Karahan, C.D. Atiş, S. İlkentapar, Effects of chemical admixtures and curing conditions on some properties of alkali-activated cementless slag mixtures, *KSCE J. Civ. Eng.* 19 (3) (2015) 733–741, <https://doi.org/10.1007/s12205-015-0629-0>.
- [9] T. Bakharev, J.G. Sanjayan, Y.B. Cheng, Effect of admixtures on properties of alkali-activated slag concrete, *Cem. Concr. Res.* 30 (9) (2000) 1367–1374, [https://doi.org/10.1016/S0008-8846\(00\)00349-5](https://doi.org/10.1016/S0008-8846(00)00349-5).
- [10] A.B. Eberhardt, On the Mechanisms of Shrinkage Reducing Admixtures in Self Consolidating Mortars and Concretes (Ph.D. Thesis), Bauhaus Universität Weimar, Weimar, Germany, 2011.
- [11] V. Bílek, L. Kalina, R. Novotný, J. Tkacz, L. Pařízek, Some issues of shrinkage-reducing admixtures application in alkali-activated slag systems, *Materials* 9 (6) (2016) 462, <https://doi.org/10.3390/ma9060462>.
- [12] V. Bílek, L. Kalina, J. Koplik, M. Mončeková, R. Novotný, Effect of a combination of fly ash and shrinkage-reducing additives on the properties of alkali-activated slag-based mortars, *Mater. Technol.* 50 (5) (2016) 813–817, <https://doi.org/10.17222/mit.2015.133>.
- [13] F. Collins, J.G. Sanjayan, Effect of pore size distribution on drying shrinkage of alkali-activated slag concrete, *Cem. Concr. Res.* 30 (9) (2000) 1401–1406, [https://doi.org/10.1016/S0008-8846\(00\)00327-6](https://doi.org/10.1016/S0008-8846(00)00327-6).
- [14] A. Kashani, J.L. Provis, J. Xu, A.R. Kilcullen, G.G. Qiao, J.S.J. van Deventer, Effect of molecular architecture of polycarboxylate ethers on plasticizing performance in alkali-activated slag paste, *J. Mater. Sci.* 49 (7) (2014) 2761–2772, <https://doi.org/10.1007/s10853-013-7979-0>.
- [15] P.C. Aitcin, R.J. Flatt, *Science and Technology of Concrete Admixtures*, Elsevier Science, 2015.
- [16] G.W. Scherer, Drying, shrinkage, and cracking of cementitious materials, *Transp. Porous Media* 110 (2) (2015) 311–331, <https://doi.org/10.1007/s11242-015-0518-5>.
- [17] F. Beltzung, F.H. Wittmann, Role of disjoining pressure in cement based materials, *Cem. Concr. Res.* 35 (12) (2005) 2364–2370, <https://doi.org/10.1016/j.cemconres.2005.04.004>.
- [18] F.H. Wittmann, Heresies on shrinkage and creep mechanisms, in: T.-A. Tanabe, K. Sakata, H. Mihashi, R. Sato, K. Maekawa, H. Nakamura (Eds.), *Creep, Shrinkage and Durability Mechanics of Concrete and Concrete Structures*, CRC Press, Taylor & Francis Group, Japan, 2009.
- [19] F. Rajabipour, G. Sant, J. Weiss, Interactions between shrinkage reducing admixtures (SRA) and cement paste's pore solution, *Cem. Concr. Res.* 38 (5) (2008) 606–615, <https://doi.org/10.1016/j.cemconres.2007.12.005>.
- [20] M. Palacios, F. Puertas, Effect of superplasticizer and shrinkage-reducing admixtures on alkali-activated slag pastes and mortars, *Cem. Concr. Res.* 35 (7) (2005) 1358–1367, <https://doi.org/10.1016/j.cemconres.2004.10.014>.
- [21] J.G. Jang, N.K. Lee, H.K. Lee, Fresh and hardened properties of alkali-activated fly ash/slag pastes with superplasticizers, *Constr. Build. Mater.* 50 (2014) 169–176, <https://doi.org/10.1016/j.conbuildmat.2013.09.048>.
- [22] C. Shi, R.L. Day, A calorimetric study of early hydration of alkali-slag cements, *Cem. Concr. Res.* 25 (6) (1995) 1333–1346, [https://doi.org/10.1016/0008-8846\(95\)00126-W](https://doi.org/10.1016/0008-8846(95)00126-W).

MS No. M-2017-122.R1

## Polypropylene Glycols as Effective Shrinkage-Reducing Admixtures in Alkali-Activated Materials

by Lukáš Kalina, Vlastimil Bílek Jr., Eva Bartoníčková, and Jitka Krouská

*In recent years, the use of various non-traditional cements and composites has increased. Alkali-activated materials, especially those based on alkali activation of blast-furnace slag, have considerable potential in construction industry. However, alkali-activated slag binders exhibit significant shrinkage, in some circumstances several times greater than portland cement-based materials, which hinders wider use of these materials in numerous applications. Therefore, the use of specific admixtures suitable for alkali-activated systems is necessary. This paper is consequently focused on testing the efficiency of shrinkage-reducing additives based on polypropylene glycols, as well as their influence on the hydration mechanism and mechanical properties of prepared alkali-activated materials.*

**Keywords:** alkali-activated materials; chemical admixtures; shrinkage reduction.

### INTRODUCTION

Either 50 years ago or nowadays, concrete based on ordinary portland cement (OPC) has been by far the most widely used construction material around the world. It is versatile and durable, but also widely available and cheap.<sup>1</sup> Nevertheless, the process of OPC production is associated with a high rate of carbon dioxide emissions, alterations of the landscape due to the exploitation of quarries, and high energy consumption required for the clinkerization process.<sup>2</sup> Because concrete production continuously increases, it is necessary to search for some alternative non-clinker binders. Alkali-activated materials is a field of a wider mosaic towards sustainable solutions.

From the wide group of these materials, alkali-activated slag (AAS) is probably the most prospective for construction purposes because it generates superior mechanical performance even at room temperature, particularly when it is activated by waterglass.<sup>3</sup> This phenomenon is a consequence of the presence of dissolved silicates in waterglass, which lead to the formation of calcium silicate hydrate (CSH) with a lower Ca/Si ratio and a more cross-linked structure.<sup>4</sup> Last but not least, AAS was reported to be equal or even better than portland cement in terms of durability in aggressive environments,<sup>5</sup> behavior at elevated temperatures,<sup>6</sup> and interfacial transition zone.<sup>7</sup>

On the other hand, AAS has some disadvantages considerably limiting its practical application, particularly its rapid set time<sup>8</sup> and high autogenous and drying shrinkage.<sup>9</sup> The significantly higher shrinkage of AAS compared to portland cement is attributed to its more refined pore structure,<sup>10</sup> the formation of shrinkage-prone silicate gel,<sup>11</sup> and lower creep modulus of its solid skeleton.<sup>12</sup> Previous studies suggest<sup>13-15</sup>

that the extensive shrinkage could be solved with the addition of shrinkage reducing admixtures (SRAs) commonly used in concrete technology. For more than 30 years, SRAs have been used to reduce shrinkage of cementitious systems. They generally belong to group of organic compounds called surfactants, which are chemical species with amphiphilic character; that is, they are composed of a hydrophilic head and hydrophobic chain. The main effect in shrinkage reduction consists of a decrease in pore solution surface tension.<sup>16</sup> Due to the very distinct chemistry of the alkali activation process compared with the hydration of portland cement, the efficiency of common SRAs differs. Bílek et al.<sup>17</sup> found that one of the typical chemical compounds (2-methyl-2,4-pentandiol) used in SRAs designed for OPC binders reduces shrinkage only with a high dosage, which negatively influences the mechanical properties of AAS concretes. Very similar results were published by Kalina et al.<sup>18</sup> when they tested commercial SRA based on oxyalkylene glycols. The shrinkage was considerably reduced by half with 1.25 wt.% addition of SRA; however, the same reduction was obtained in compressive strength development. From the wide range of non-ionic surfactants, the SRAs with the structure of polymeric glycols show promising results for their use in alkali-activated materials. Palacios and Puertas<sup>14</sup> reported that SRAs based on polypropylene glycol reduced both autogenous and drying shrinkage significantly. Moreover, the mechanical properties of the specimens with admixture were even better in comparison with reference AAS samples. Therefore, the effect of different polypropylene glycols in terms of chemical structure on the shrinkage behavior, hydration process, and mechanical properties of AAS samples is essential to study.

### RESEARCH SIGNIFICANCE

The main obstacle for wider practical use of alkali-activated materials is its significant autogenous and drying shrinkage, which may cause cracks, resulting in decrease of mechanical properties and durability. The use of SRAs has been suggested to reduce both drying and autogenous shrinkage. Unfortunately, these admixtures are designed mainly for binders based on OPC. Therefore, the authors believe that the research focused on the specific chemical

*ACI Materials Journal*, V. 115, No. 2, March 2018.

MS No. M-2017-122.R1, doi: 10.14359/51701099, was received April 24, 2017, and reviewed under Institute publication policies. Copyright © 2018, American Concrete Institute. All rights reserved, including the making of copies unless permission is obtained from the copyright proprietors. Pertinent discussion including author's closure, if any, will be published ten months from this journal's date if the discussion is received within four months of the paper's print publication.

additives designed especially for alkali-activated systems could be very helpful for their potential practical applications.

### EXPERIMENTAL INVESTIGATION

Alkali-activated blast-furnace slag (BFS) mortars with different kinds of chemical admixtures (polypropylene glycols) and three different fractions of siliceous sand were prepared based on ČSN EN 196-1 standard. The mass ratio between sand and binder was set as 3:1, while the water-BFS ratio was calculated to be 0.40. The amount of sodium water-glass was adjusted to maintain the mass ratio  $\text{Na}_2\text{O}/\text{BFS}$  at 0.04. Mixing and curing processes were carried out at a laboratory temperature 77°F (25°C) and the specimens were then stored in the curing chamber with defined relative humidity (50%). Thus, prepared samples were subjected to compressive strength determination and shrinkage measurements.

### Materials

The main material used for alkali activation was blast-furnace slag with Blaine fineness of 1953 ft<sup>2</sup>/lb (400 m<sup>2</sup>/kg). The XRD analysis of BFS indicated the presence of a great amount of amorphous phase. The main mineral phases identified in BFS were melilite and merwinite. The chemical composition of slag determined by X-ray fluorescence (XRF) is given in Table 1. The particle size distribution D50 of BFS determined by laser granulometry in dry state was  $2.8 \times 10^{-4}$  in. (~7.0 μm). BFS was activated by sodium waterglass with a silica modulus of 1.93. The surfactants used as SRAs were propylene (PG) and polypropylene glycols (PPG) with different molar weights (PPG 200; PPG 425; PPG 725; PPG 1000) in addition to 0.5% by weight of BFS.

### Specimens

For the compressive strength development, specimens of dimension 1.57 x 1.57 x 6.30 in. (40 x 40 x 160 mm), based on ČSN EN 196-1 standard, were prepared. Each value was supported by the average of four measurements. The shrinkage evolution was determined based on ASTM C596. Three mortar bars 0.98 x 0.98 x 11.22 in. (25 x 25 x 285 mm) of each mixture were prepared and measured until the age of 28 days. Each value was supported by the average of three measurements.

### Items of investigation

At the age of 1, 7, and 28 days, specimens were tested for mechanical properties through the compressive and bending strength tester Betonsystem Desttset 3310. Length changes for obtaining the shrinkage evolution were measured in short time intervals using the ASTM C490 apparatus. Evolution of hydration heat was monitored by using of TAM Air isothermal microcalorimeter (TA instruments). Measurements of heat evolution were performed at constant temperature of  $77 \pm 0.02^\circ\text{F}$  ( $25 \pm 0.04^\circ\text{C}$ ). When thermal equilibrium was achieved, the BFS and the alkali liquid created by waterglass, water, and SRA were mixed together by injecting the solution into the  $5.3 \times 10^{-4}$  ft<sup>3</sup> (15 mL) vial and stirred for 3 minutes. The water/BFS, as well as the mass  $\text{Na}_2\text{O}/\text{BFS}$ , were the same as in the preparation process of the mortars. The heat evolution was recorded as heat flow immediately.

**Table 1—Physical and chemical compositions of blast-furnace slag**

	BFS
Specific gravity	2.95
Blaine fineness, ft <sup>2</sup> /lb	1953
SiO <sub>2</sub> , %	34.7
Al <sub>2</sub> O <sub>3</sub> , %	9.1
CaO, %	41.1
MgO, %	10.5
SO <sub>3</sub> , %	1.4
Na <sub>2</sub> O, %	0.4
K <sub>2</sub> O, %	0.9
TiO <sub>2</sub> , %	1.0
MnO, %	0.6
Fe <sub>2</sub> O <sub>3</sub> , %	0.3

The total porosity and pore size distribution was determined by mercury porosimeter Poremaster (Quantachrome Instruments, USA). The working pressure range was from 0.2 to 33 000 psi (0.14 to 231 MPa) which covered a pore diameter range from  $2.56 \times 10^{-7}$  to  $3.94 \times 10^{-5}$  in. (6.5 to 1000 nm). The measurements were performed with the following conditions: Hg surface tension was  $2.74 \times 10^{-3}$  lbf/in. (0.480 N/m); Hg contact angle was 140; and scan mode was chosen to average from 11 points. Obtained intrusion data were normalized by sample weight and volume.

### ANALYTICAL INVESTIGATION

It was previously stated that the beneficial effect of SRAs on shrinkage lies in the reduction of surface tension at the pore solution/air interface. The surface tension arises thanks to the aqueous character of the pore solution, where the molecules interact mutually through the hydrogen bonds and form a loose three-dimensional network. Molecules at the surface cannot achieve the same level of molecular interactions compared to the molecules in the bulk and therefore have an energy excess. The consequence of this effect is that the liquid squeezes itself together to minimize surface area. This process is termed surface tension ( $\gamma$ ) and was determined through a bubble pressure tensiometer. This analytical instrument measures the maximum internal pressure of a gas bubble which is formed in a liquid. According to the Young-Laplace equation, the internal pressure ( $p$ ) of a spherical gas bubble depends on the radius of curvature ( $r$ ) and surface tension

$$p = \frac{2\gamma}{r} \quad (\text{Pa}) \quad (1)$$

When a gas bubble is produced in a liquid at the tip of a capillary, the maximum internal pressure ( $p_{max}$ ) is measured. This greatest pressure occurs when the radius of a gas bubble is equal to the radius of the capillary ( $r_c$ ). As the capillary is immersed in the liquid, the hydrostatic pressure ( $p_0$ ) resulting from the immersion depth and the density of the

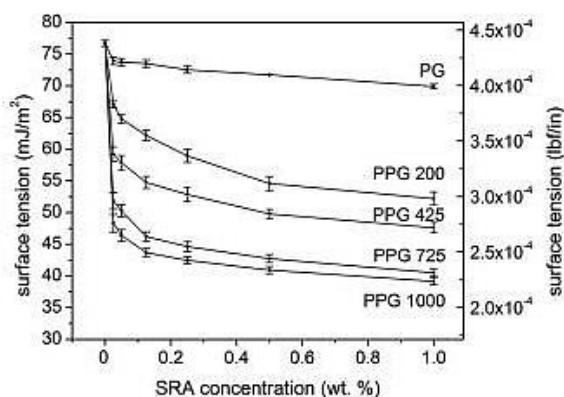


Fig. 1—Effect of surfactants on surface tension of pore solution (PG is propylene glycol; PPG is polypropylene glycol).

liquid must be subtracted from the measured pressure. The resulting surface tension is then calculated

$$\gamma = \frac{(p_{max} - p_0) \cdot r_c}{2} \quad (\text{mJ/m}^2) \quad (2)$$

### COMPARISON OF PREDICTIONS AND EXPERIMENTAL RESULTS

According to the theoretical background, the analytical calculations predict the relationship between the tail length of surfactants and surface tension.<sup>19</sup> The molecular dynamic simulation clearly demonstrates that increasing the chain length makes the surfactants more effective. This model is also supported by the study of Szleifer et al.,<sup>20</sup> which supposed dependence of lateral pressure among hydrophobic chains and their length. The theory could be simplified and explained as follows. If the chain length is increased, the lateral pressure arises and therefore the surface tension decreases, which is described in the following equation

$$\gamma = \int (p_n - p_l(z)) dz \quad (3)$$

The surface is oriented in the  $z$ -direction, where  $p_n$  is the normal pressure and  $p_l(z)$  is the lateral pressure.<sup>21</sup>

The experimental data show (Fig. 1) that the surfactants with higher molar weight, consequently with a longer hydrophobic chain, generally show a higher efficiency at low concentrations. Therefore, a smaller amount of surfactants is needed to achieve the same reduction of surface tension. The measured data are completely in agreement with presented theoretical predictions.

### EXPERIMENTAL RESULTS AND DISCUSSION

#### Surface tension of pore solution

The action of a specific surfactant depends strongly on the chemical composition of the solution in which it is situated. In the other words, the aqueous solution may contain ions that promote the solubilisation and miscibility of surfactants or decrease critical micellation concentration (CMC). This phenomenon describes Hofmeister series relating in

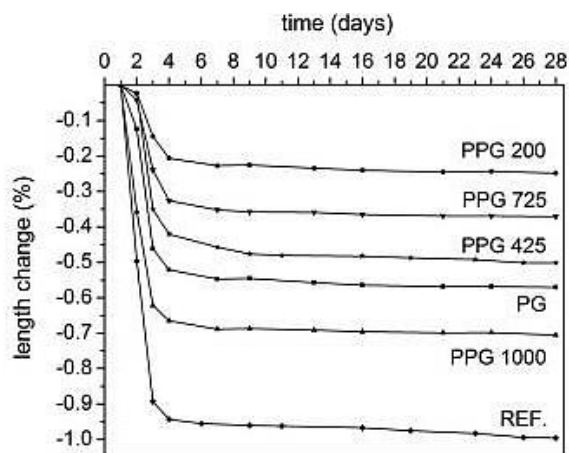


Fig. 2—Effect of surfactant addition (0.5% by weight of BFS) on shrinkage evolution.

the ability of ions to increase or decrease the solubility of non-ionic surfactants in electrolyte solution.<sup>22</sup> Therefore, the nature of a pore solution of alkali-activated BFS is crucial for SRA efficiency. Its chemical composition was obtained by ICP-OES 24 hours after from mixing, thus the same time as shrinkage measurement was started.

The surface tension of synthetic pore solutions with different glycols is shown in Fig. 1. The higher content of surfactants in the solution causes a decrease in surface tension until reaching a plateau. In the case of polypropylene glycols, the critical micellation concentrations correspond to surface tension in the range of  $2.28 \times 10^{-4}$  to  $3.14 \times 10^{-4}$  lbf/in. ( $40$  to  $55$  mJ/m<sup>2</sup>). The presented results suggest that the surfactant PPG 1000 reduces the surface tension the most because its molecular weight is the highest. The other glycols achieved worse results in surface tension reduction as was expected, based on the theoretical background.

#### Factors affecting shrinkage evolution

Figure 2 shows that all the used surfactants, dosed at 0.5% by weight of BFS, are more effective in decreasing shrinkage evolution compared with the reference sample. However, the molecular character of the used glycols does play a significant role on the drying shrinkage evolution. Surprisingly, the length change measurements demonstrate the highest shrinkage reduction using PPG 200 and the lowest in the case of PPG 1000. These results clearly indicate that the ability to effectively decreasing the surface tension may not be correlated to the shrinkage reduction. There are other factors that must be taken into consideration.

One of the important things is the miscibility of used surfactants with aqueous alkali solution, because it is generally accepted that the critical surfactant concentrations are formed from the surfactant molecules' adsorption on interfaces and thus, further surface tension reduction is negligible.<sup>23</sup> In the case of glycols, the micellation related to total miscibility is controlled by molecular weight, as reported by Seguin et al.<sup>24</sup> Higher effective volume of micelles causes irregular distribution of surfactant in the pore solution, thus



Fig. 3—Miscibility of surfactants in alkali activator solution (sodium waterglass).

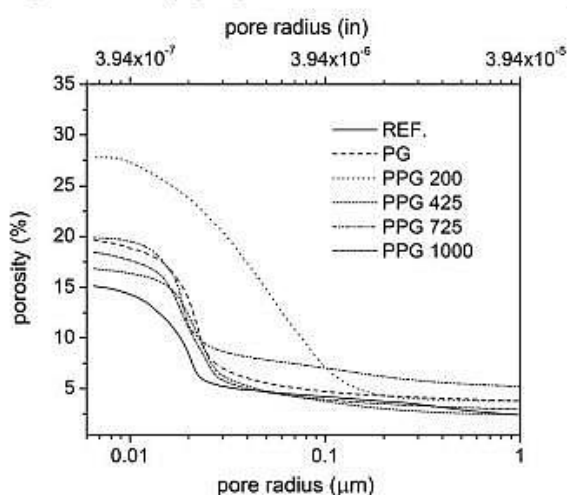


Fig. 4—Pore size distribution of alkali-activated samples.

resulting in higher shrinkage in certain areas of the alkali activated system. Figure 3 shows the 0.5 wt.% addition of used surfactants in alkali activator (sodium waterglass with a silica modulus of 1.93), where the higher molecular weight tends to increase the segregation of polypropylene glycols. To highlight this effect, a drop of phenolphthalein was added to the solutions. However, during the AAS hydration especially, silicate ions from activating solution are consumed to form CSH phase, which leads to increased miscibility of longer PPGs with pore solution, making them more effective in pore fluid surface tension reduction as was shown in Fig. 1.

Another impact of SRA is the ability to change the pore size distribution, which can significantly influence the drying shrinkage. During the ongoing drying process of AAS, the diameter of the pores partially filled with water (that is, with the presence of menisci) decreases until the equilibrium for a given relative humidity is reached, and thus capillary stress according to the Young-Laplace equation (Eq. (1)) increases, which results in higher shrinkage. The magnitude of drying shrinkage strongly depends on the loss of water from small ( $9.84 \times 10^{-8}$  to  $3.93 \times 10^{-7}$  in. [2.5 to 10 nm]) and medium ( $3.93 \times 10^{-7}$  to  $1.97 \times 10^{-6}$  in. [10 to 50 nm]) capillaries.<sup>25</sup> Previous studies<sup>10,26</sup> suggest that the alkali-activated BFS binders contain mainly pores in

Table 2—Porosity of alkali-activated samples

Sample (0.5% surfactant by weight of BFS)	Total porosity, %	Pores in small and medium capillaries, %
REF.*	15.08	69.89
PG	19.59	73.10
PPG 200	27.81	54.36
PPG 425	16.83	73.02
PPG 725	19.80	61.26
PPG 1000	18.43	76.18

\*Reference sample (REF.) did not contain any surfactant.

the mentioned regions, which is probably one of the main reasons for higher shrinkage of AAS compared to OPC.

Bílek et al.<sup>17</sup> showed that some surfactants strongly retard the hydration of AAS, which leads to its increased porosity and coarser the pore size distribution. Similar results were also observed in the case of the tested glycols (Fig. 4). The samples with surfactants indicated higher porosity in comparison with the reference sample, particularly in the case of PPG 200 sample, which was the most porous and had a coarser pore structure as a consequence of the strong retardation of hydration. The essential factor for the drying shrinkage behavior is the content of small and medium capillaries in the total porosity of materials. Table 2 summarizes the percentage portion of pore sizes within the critical  $2.56 \times 10^{-7}$  to  $1.97 \times 10^{-6}$  in. (6.5 to 50 nm) range. If the samples are ordered according to increasing content of pores in that region, the following dependence will be achieved: PPG 200 < PPG 725 < REF. < PPG 425 < PG < PPG 1000. This trend is similar with the extent of shrinkage of measured samples (Fig. 2) except the reference sample, which did not contain any admixture reducing surface tension of pore solution. It can be said that PPG additions influence surface tension reduction and also possibility their air-entraining effects, which could contribute to the increased total porosity of PPG containing mixtures.

From the presented shrinkage evolution results follow that the surfactant action influencing surface tension, pore size distribution, and miscibility, plays a crucial role in final shrinkage reduction.

#### Hydration process

The hydration process of alkali-activated systems with different kinds of glycols was measured using isothermal

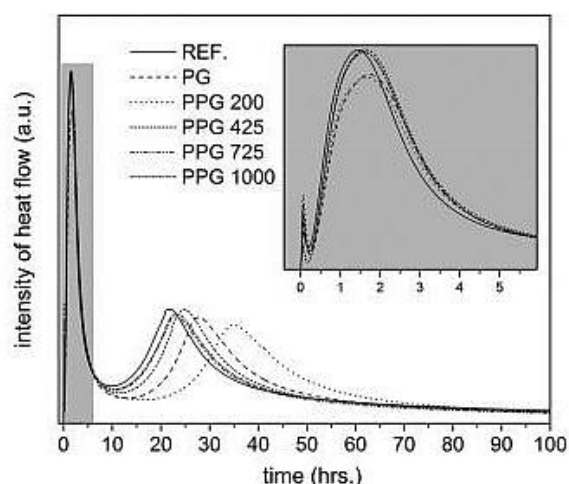


Fig. 5—Effect of surfactant addition (0.5% by weight of BFS) on hydration process.

microcalorimetry (Fig. 5). Typical calorimetric curves for waterglass-activated slag with three peaks as described by Shi and Day<sup>27</sup> were observed. The first peak occurring during the first 10 minutes of hydration is always associated with wetting and dissolution of BFS. From the zoomed area, it is clear that the second peak, starting after 15 minutes, which is connected with the gelation of dissolved silica to formation of primary CSH gel,<sup>28</sup> is reduced with the use of propylene (PG) and polypropylene (PPG 200) glycols, respectively. The slowing of hydration in case of these glycols is also well observed on the third peak, associated with the secondary formation of CSH gel. For the reference sample, the maximum of this peak occurred after 22 hours of hydration, but in presence of 0.5% of PG and PPG 200, was delayed by 6 and 14 hours, respectively. The other surfactants did not affect the alkali activation process significantly. These results suggest that the polypropylene glycols with a shorter chain length (for example, PPG 200) are responsible for the lower binder phase creation and create a smaller amount of capillary pores, resulting in shrinkage reduction. However, this effect leads to the deterioration of mechanical properties, which is further discussed.

### Mechanical properties

Compressive strength evolution of samples with different kinds of surfactants is shown in Fig. 6. The measured data are fully in accordance with previous calorimetry measurements. After 24 hours, there is a decrease in the compressive strength of samples with the addition of PG and PPG 200. This difference is enhanced after 7 days of curing. The noticeable negative influence of PG and PPG 200 on compressive strength is probably related to the combination of their retardation effect and drying after the demolding process, followed by exposure to dry conditions (50% relative humidity). This influence started after 24 hours of hydration—that is, beyond the maximum of the reference main hydration peak, but significantly earlier than its maximum

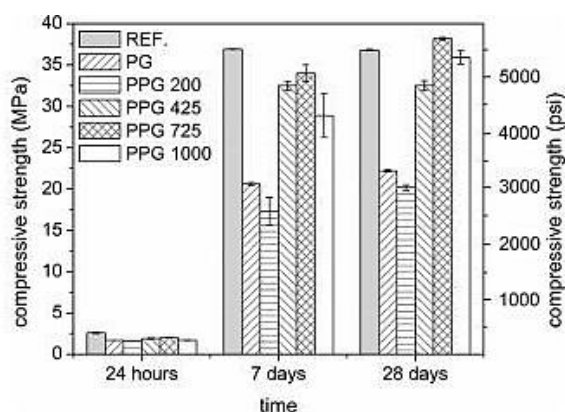


Fig. 6—Effect of surfactants (0.5% by weight of BFS) on compressive strength evolution.

for PG and PPG 200 occurred, as can be seen from Fig. 5. Due to drying, further hydration was limited and thus, the hydration degree was lower in these mortars compared to those without significant retardation effect. The question about the efficiency of shrinkage reducing admixtures is well answered after 28 days. Similar to the reference specimens, the compressive strength of PG and PPG 425 samples remained almost the same between 7 and 28 days. On the other hand, the specimens with PPG 200, PPG 725, and surprisingly in the case of PPG 1000 showed a progressive increase in strength. Additionally, the surface of reference samples without any glycols was covered with small visible cracks, which only confirm the importance of the surfactants usage.

### FURTHER RESEARCH

The presented results show that the effect of surfactants in alkali-activated binders depends on various factors. Therefore, further research will be focused on the detailed study of microstructure with different kinds of SRAs. Moreover, the effort to enhance their efficiency through the synthesis of specific organic groups into polymeric structure will be another possible solution. Long-term testing (months and years) of alkali-activated materials with SRAs within the meaning of mechanical properties and durability will also take place.

### CONCLUSIONS

In general, polypropylene glycols significantly reduce surface tension and seem to be suitable for SRAs. The measured data connected several factors which must be taken into account:

1. The significant reduction of surface tension leads not only to effective reduction of shrinkage. Other factors play an important role, such as the effect of surfactants on the pore size distribution and miscibility of used shrinkage reducing admixtures in the alkali activator solution.
2. The microcalorimetry results demonstrate that surfactants with low molecular weight (for example, PG and PPG 200) delay the hydration of BFS, which negatively influence their compressive strength development.

3. The behavior of polypropylene glycols investigated in this study greatly affects shrinkage reduction as well as compressive strength development.

The presented results suggest that the most usable polypropylene surfactant is PPG 725, which exhibits good ability to reduce shrinkage, does not affect negatively the alkali activation process, and increases the 28 days compressive strength compared with reference sample.

#### AUTHOR BIOS

**Lukáš Kalina** is a Senior Researcher at the Materials Research Centre, Faculty of Chemistry, Brno University of Technology, Brno, Czech Republic. He received his MS and PhD in chemistry and materials technology. His interests include inorganic binders, especially alkali-activated materials.

**Vlastimil Bilek Jr.** is a Junior Researcher at Materials Research Centre, Faculty of Chemistry, Brno University of Technology. He received his MS in chemistry and materials technology. His research interests include alkali-activated materials and cementitious admixtures.

**Eva Bartoničková** is a Senior Researcher at Materials Research Centre, Faculty of Chemistry, Brno University of Technology. She received her PhD from the Institute of Physical and Applied Chemistry at Brno University of Technology. Her research interests include ceramic materials.

**Jitka Krouská** is a Junior Researcher at Materials Research Centre, Brno University of Technology, Faculty of Chemistry. She received her PhD from the Institute of Physical and Applied Chemistry. Her research interests include colloid chemistry.

#### ACKNOWLEDGMENTS

This outcome has been achieved with the financial support by the project: Materials Research Centre at FCH BUT- Sustainability and Development, REG LO1211, with financial support from the National Programme for Sustainability I (Ministry of Education, Youth and Sports) and GA17-03670S, "Development of shrinkage reducing agents designed for alkali activated systems," with financial support from the Czech science foundation.

#### REFERENCES

1. Mehta, P. K., and Monteiro, P. J. M., *Concrete: Microstructure, Properties, and Materials*, McGraw-Hill Education, New York, 2013, 704 pp.
2. Puertas, F.; Gutiérrez, R.; Fernández-Jiménez, A.; Delvasto, S.; and Maldonado, J., "Alkaline Cement Mortars. Chemical Resistance to Sulfate and Seawater Attack," *Materiales de Construcción*, V. 52, No. 267, 2002, pp. 55-71. (in Spanish) doi: 10.3989/mc.2002.v52.i267.326
3. Fernández-Jiménez, A.; Palomo, J. G.; and Puertas, F., "Alkali-Activated Slag Mortars," *Cement and Concrete Research*, V. 29, No. 8, 1999, pp. 1313-1321. doi: 10.1016/S0008-8846(99)00154-4
4. Fernández-Jiménez, A.; Puertas, F.; Sobrados, L.; and Sanz, J., "Structure of Calcium Silicate Hydrates Formed in Alkaline-Activated Slag: Influence of the Type of Alkaline Activator," *Journal of the American Ceramic Society*, V. 86, No. 8, 2003, pp. 1389-1394. doi: 10.1111/j.1151-2916.2003.tb03481.x
5. Bernal, S. A., and Provis, J. L., "Durability of Alkali-Activated Materials: Progress and Perspectives," *Journal of the American Ceramic Society*, V. 97, No. 4, 2014, pp. 997-1008. doi: 10.1111/jace.12831
6. Wang, W. C.; Wang, H. Y.; and Lo, M. H., "The Engineering Properties of Alkali-Activated Slag Pastes Exposed to High Temperatures," *Construction & Building Materials*, V. 68, 2014, pp. 409-415. doi: 10.1016/j.conbuildmat.2014.06.016
7. San Nicolas, R.; Bernal, S. A.; Mejía de Gutiérrez, R.; van Deventer, J. S. J.; and Provis, J. L., "Distinctive Microstructural Features of Aged Sodium Silicate-Activated Slag Concretes," *Cement and Concrete Research*, V. 65, Nov, 2014, pp. 41-51. doi: 10.1016/j.cemconres.2014.07.008
8. Kalina, L.; Bilek, V.; Novotny, R.; Moncekova, M.; Masilko, J.; and Koplík, J., "Effect of Na<sub>3</sub>PO<sub>4</sub> on the Hydration Process of Alkali-Activated

Blast Furnace Slag," *Materials (Basel)*, V. 9, No. 12, 2016, p. 395 doi: 10.3390/ma9050395

9. Melo Neto, A. A.; Cincotto, M. A.; and Repette, W., "Drying and Autogenous Shrinkage of Pastes and Mortars with Activated Slag Cement," *Cement and Concrete Research*, V. 38, No. 4, 2008, pp. 565-574. doi: 10.1016/j.cemconres.2007.11.002

10. Collins, F., and Sanjayan, J. G., "Effect of Pore Size Distribution on Drying Shrinkage of Alkali-Activated Slag Concrete," *Cement and Concrete Research*, V. 30, No. 9, 2000, pp. 1401-1406. doi: 10.1016/S0008-8846(00)00327-6

11. Krizan, D., and Zivanovic, B., "Effects of Dosage and Modulus of Water Glass on Early Hydration of Alkali-Slag Cements," *Cement and Concrete Research*, V. 32, No. 8, 2002, pp. 1181-1188. doi: 10.1016/S0008-8846(01)00717-7

12. Ye, H. L.; Cartwright, C.; Rajabipour, F.; and Radlinska, A., "Understanding the Drying Shrinkage Performance of Alkali-Activated Slag Mortars," *Cement and Concrete Composites*, V. 76, Feb, 2017, pp. 13-24. doi: 10.1016/j.cemconcomp.2016.11.010

13. Bakharev, T.; Sanjayan, J. G.; and Cheng, Y. B., "Effect of Admixtures on Properties of Alkali-Activated Slag Concrete," *Cement and Concrete Research*, V. 30, No. 9, 2000, pp. 1367-1374. doi: 10.1016/S0008-8846(00)00349-5

14. Palacios, M., and Puertas, F., "Effect of Shrinkage-Reducing Admixtures on the Properties of Alkali-Activated Slag Mortars and Pastes," *Cement and Concrete Research*, V. 37, No. 5, 2007, pp. 691-702. doi: 10.1016/j.cemconres.2006.11.021

15. Bilim, C.; Karahan, O.; Atis, C. D.; and Ilkعتapar, S., "Effects of Chemical Admixtures and Curing Conditions on Some Properties of Alkali-Activated Cementless Slag Mixtures," *KSCCE Journal of Civil Engineering*, V. 19, No. 3, 2015, pp. 733-741. doi: 10.1007/s12205-015-0629-0

16. Aïcin, P. C., and Flatt, R. J., *Science and Technology of Concrete Admixtures*, Elsevier Science, Amsterdam, the Netherlands, 2015, 666 pp.

17. Bilek, V.; Kalina, L.; Novotny, R.; Tkacz, J.; and Parizek, L., "Some Issues of Shrinkage-Reducing Admixtures Application in Alkali-Activated Slag Systems," *Materials (Basel)*, V. 9, No. 12, 2016, p. 462 doi: 10.3390/ma9060462

18. Kalina, L.; Bilek, V.; Šoukal, F.; and Opravil, T., "Recycling of Waste Technological Sludge in Alkali-Activated Concretes," *Recycling of Waste Technological Sludge in Alkali-Activated Concretes*, fédération internationale du béton, Lausanne, Switzerland, 2016, 635 pp.

19. Smit, B.; Schlijper, A. G.; Rupert, L. A. M.; and Vanos, N. M., "Effects of Chain-Length of Surfactants on the Interfacial-Tension—Molecular Dynamics Simulations and Experiments," *Journal of Physical Chemistry*, V. 94, No. 18, 1990, pp. 6933-6935. doi: 10.1021/j100381a003

20. Szeifer, I.; Benschaul, A.; and Gelbart, W. M., "Chain Packing Statistics and Thermodynamics of Amphiphile Monolayers," *Journal of Physical Chemistry*, V. 94, No. 12, 1990, pp. 5081-5089. doi: 10.1021/j100375a060

21. Lundberg, L., and Edholm, O., "Dispersion Corrections to the Surface Tension at Planar Surfaces," *Journal of Chemical Theory and Computation*, V. 12, No. 8, 2016, pp. 4025-4032. doi: 10.1021/acs.jctc.6b00182

22. Kunz, W.; Henle, J.; and Ninham, B. W., "Zur Lehre von der Wirkung der Salze (About the Science of the Effect of Salts): Franz Hofmeister's Historical Papers," *Current Opinion in Colloid & Interface Science*, V. 9, No. 1-2, 2004, pp. 19-37. doi: 10.1016/j.cocis.2004.05.005

23. Rajabipour, F.; Sant, G.; and Weiss, J., "Interactions between Shrinkage Reducing Admixtures (SRA) and Cement Paste's Pore Solution," *Cement and Concrete Research*, V. 38, No. 5, 2008, pp. 606-615. doi: 10.1016/j.cemconres.2007.12.005

24. Seguin, C.; Eastoe, J.; Clapperton, R.; Heenan, R. K.; and Grillo, L., "Alternative Non-Aqueous Water-Miscible Solvents for Surfactants," *Colloids and Surfaces a-Physicochemical and Engineering Aspects*, V. 282, July 2006, pp. 134-142.

25. Mindess, S., and Young, J. F., *Concrete*, Prentice-Hall, Upper Saddle River, NJ, 1981, 671 pp.

26. Shi, C. J.; Day, R. L.; Wu, X. Q.; and Tang, M. S., "Uptake of Metal Ions by Autoclaved Cement Pastes," *Advanced Cementitious Systems: Mechanisms and Properties*, V. 245, 1992, pp. 141-149.

27. Shi, C. J., and Day, R. L., "A Calorimetric Study of Early Hydration of Alkali-Slag Cements," *Cement and Concrete Research*, V. 25, No. 6, 1995, pp. 1333-1346. doi: 10.1016/0008-8846(95)00126-W

28. Brough, A. R., and Atkinson, A., "Sodium Silicate-Based, Alkali-Activated Slag Mortars," *Cement and Concrete Research*, V. 32, No. 6, 2002, pp. 865-879. doi: 10.1016/S0008-8846(02)00717-2

## Research Article

# Influence of Pb Dosage on Immobilization Characteristics of Different Types of Alkali-Activated Mixtures and Mortars

Jan Koplík , Jaromír Pořízka, Lukáš Kalina, Jiří Másilko, and Matěj Březina

Faculty of Chemistry, Materials Research Centre, Brno University of Technology, Purkyňova 118, 612 00 Brno, Czech Republic

Correspondence should be addressed to Jan Koplík; [koplík@fch.vutbr.cz](mailto:koplík@fch.vutbr.cz)

Received 9 June 2017; Revised 31 October 2017; Accepted 28 November 2017; Published 11 January 2018

Academic Editor: Kedsarin Pimraksa

Copyright © 2018 Jan Koplík et al. This is an open access article distributed under the Creative Commons Attribution License, which permits unrestricted use, distribution, and reproduction in any medium, provided the original work is properly cited.

Alkali-activated matrices are suitable materials for the immobilization of hazardous materials such as heavy metals. This paper is focused on the comparison of immobilization characteristics of various inorganic composite materials based on blast furnace slag and on the influence of various dosages of the heavy metal Pb on the mechanical properties and fixation ability of prepared matrices. Blast furnace slag (BFS), fly ash, and standard sand were used as raw materials, and sodium water glass was used as an alkaline activator.  $\text{Pb}(\text{NO}_3)_2$  served as a source of heavy metal and was added in various dosages in solid state or as aqueous solution. The immobilization characteristics were determined by leaching tests, and the content of Pb in the eluate was measured by inductively coupled plasma optical emission spectroscopy (ICP-OES). The microstructure of matrices and distribution of Pb within the matrix were determined by scanning electron microscopy (SEM) equipped with energy dispersive X-ray spectroscopy (EDS). Increasing the dosage of the heavy metal had negative impacts on the mechanical properties of prepared matrices. The leaching tests confirmed the ability of alkali-activated materials to immobilize heavy metals. With increasing addition of Pb, its content in eluates increased.

## 1. Introduction

Heavy metals such as Pb belong to hazardous materials, which are harmful to the human beings. Lead is highly toxic element, which attacks mainly the nervous system. Lead exposure mostly occurs through the ingestion of contaminated water or food. Therefore, it is important to prevent its leakage into the environment by stabilization or solidification of waste materials before their deposition into the landfill [1]. A possible way on how to immobilize heavy metals is using alkali-activated materials (AAMs). AAMs present a broad range of materials (geopolymers, activated blast furnace slag, etc.), but all of them are activated by high pH during their preparation. The AAMs can be divided into two big groups: high-calcium alkali-activated materials (HCAAMs) and low-calcium alkali-activated materials (LCAAMs). HCAAMs are represented mainly by activated BFS, and LCAAMs are represented mainly by activated fly ash or metakaolin. The structure of HCAAMs consists of the C-A-S-H gel as

a major hydration product. This gel has a similar structure as the C-S-H gel in hydrated ordinary Portland cement and is made up of tetrahedrally coordinated silicate chains, where aluminium is located in the bridging position instead of silicon. The structure and composition of the C-A-S-H gel depend on the nature and concentration of the used activator. AFm-type phases (NaOH-activated binders), hydrotalcite (BFS with high content of MgO), and zeolites (binders with high content of  $\text{Al}_2\text{O}_3$ ) are usually formed as secondary hydration products [2–4].

Heavy metals can be immobilized by two types of fixation—physical and chemical. Mostly, both types of immobilization occur together. Physical fixation is linked with mechanical properties and porosity of the matrix. Chemical fixation means that there is a chemical bond between the heavy metal and the matrix. Heavy metals can be inhibited by transformation into a less soluble form as well. After alkali activation, the heavy metals usually occur in the form of silicate or hydroxide [5–7]. The

TABLE 1: Particle size distribution of raw materials.

	$x$ (10%) $\mu\text{m}$	$x$ (50%) $\mu\text{m}$	$x$ (90%) $\mu\text{m}$	$x$ (99%) $\mu\text{m}$
BFS	0.88	10.73	33.97	59.57
Fly ash	4.18	44.56	236.89	486.20

TABLE 2: The nomenclature of samples.

Mixture	Mixture name
BFS; 1% Pb added as solid	S1
BFS; 2.5% Pb added as solid	S2
BFS; 5% Pb added as solid	S5
BFS + sand; 1% Pb added as solid	M1
BFS + sand; 2.5% Pb added as solid	M2
BFS + sand; 5% Pb added as solid	M5
BFS + fly ash; 1% Pb added as solid	P1
BFS + fly ash; 2.5% Pb added as solid	P2
BFS + fly ash; 5% Pb added as solid	P5
BFS; 1% Pb added as liquid	SR1
BFS; 2.5% Pb added as liquid	SR2
BFS + sand; 1% Pb added as liquid	MR1
BFS + sand; 2.5% Pb added as liquid	MR2
BFS + fly ash; 1% Pb added as liquid	PR1
BFS + fly ash; 2.5% Pb added as liquid	PR2

TABLE 3: The mixture design of prepared matrices.

	BFS matrices	Matrices with sand	Matrices with fly ash
BFS	100 wt.%	25 wt.%	50 wt.%
Fly ash	—	—	50 wt.%
Sand	—	75 wt.%	—
Activator/binder	8%	8%	8%
Water/binder	0.33	0.42	0.33

immobilization of heavy metals within AAMs can be influenced by various factors, such as the composition of the matrix, the type of alkaline activator, the immobilized heavy metal, and the leaching medium [8, 9]. Previous researches proved that Pb reached high efficiency of immobilization in AAMs, but there is only little information about the influence of Pb dosage on immobilization characteristics of AAMs [10–13].

The aim of this work was to compare the ability of three different alkali-activated matrices based on BFS to immobilize Pb within their structure. The influence of different Pb dosages on the immobilization efficiency was also investigated.

## 2. Materials and Methods

**2.1. Materials, Sample Preparation, and Leaching Tests.** BFS and high-temperature fly ash were used as raw materials. The particle size distribution of both raw materials is listed in Table 1. Liquid sodium silicate with the  $\text{SiO}_2/\text{Na}_2\text{O}$  ratio of

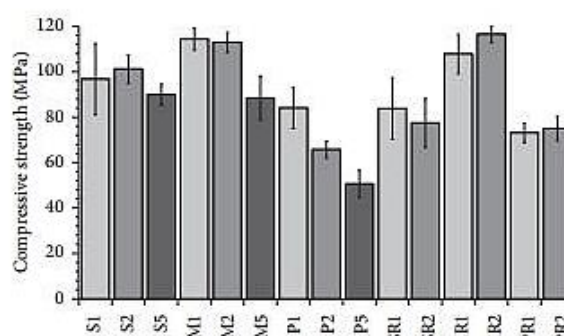


FIGURE 1: Compressive strength of prepared matrices (28 days).

1.85 served as an alkaline activator. As fine aggregates, three different fractions of siliceous Czech standard sand complying with ČSN EN 196-1 were used (the mass ratio of the fractions was 1 : 1 : 1). Pb was used in the form of  $\text{Pb}(\text{NO}_3)_2$ .

Three types of matrices were prepared. The first one was based only on BFS. In the second one, 50 wt.% of BFS was replaced by fly ash. And the third one consisted of BFS and standard sand. The sample nomenclature and the mixture designs are listed in Tables 2 and 3, respectively. Pb was added in the dosages of 1, 2.5, and 5 wt.% to binder mass and was added in two ways: as a solution and as a solid. In both cases, the water-to-binder ratios were the same.

The whole mixing procedure took four minutes. In the beginning, all materials without aggregates were put together and sand, if needed, was added after 30 s of mixing. The samples were cast in steel molds measuring  $20 \times 20 \times 100$  mm. All analyses were performed after 28 days of moist curing (98% relative humidity) at laboratory temperature ( $23 \pm 2^\circ\text{C}$ ).

The leaching tests were based on ČSN EN 12457-4. The demineralized water served as leaching agent. The solid/liquid ratio was 1 : 10, and the mixture was agitated for 24 hours. After the leaching time ended, the mixture was filtered by a membrane filter with the pore size of  $0.45 \mu\text{m}$ , and the concentration of Pb in solution was determined by ICP-OES.

**2.2. Methods.** The compressive strength was measured according to the ČSN EN 196-1 using Betonsystem Desttest 3310. To determine the porosity, prepared matrices were investigated by mercury intrusion porosimetry using Quantachrome instrument PoreMaster 33. The surface tension of mercury was  $480 \text{ mN/m}$ , and the contact angle was  $140^\circ$  based on the recommendation. The pore sizes were determined in the range from over  $170 \mu\text{m}$  to  $0.0064 \mu\text{m}$ . The ICP-OES data were obtained using Horiba Jobin Yvon Ultima II Spectrometer. The parameters of measurement were as follows: RF power,  $1350 \text{ W}$ ; gas, argon; plasma gas,  $13 \text{ L}\cdot\text{min}^{-1}$ ; auxiliary gas,  $0.1 \text{ L}\cdot\text{min}^{-1}$ ; nebuliser gas,  $0.85 \text{ L}\cdot\text{min}^{-1}$ ; plasma view, radial; nebuliser, Meinhard; and nebuliser pressure, 3 bar. The scanning electron microscopy (SEM) and the energy dispersive X-ray spectroscopy (EDS)

TABLE 4: Compressive strength of prepared matrices (7 days).

Mixture	S1	S2	S5	M1	M2	M5	P1	P2
MPa	62.3	61.8	58.3	75.0	74.8	59.7	56.7	49.7
Mixture	P5	SR1	SR2	MR1	MR2	PR1	PR2	—
MPa	40.1	55.4	53.2	70.5	76.3	50.3	52.7	—

TABLE 5: The porosity of matrices.

Total intruded volume (cm <sup>3</sup> /g)	P1	P5	PR1	M1	M5	MR1	S1	S5	SR1
	0.130	1.312	0.117	0.034	0.050	0.036	0.022	0.035	0.023

analyses were performed using Zeiss EVO LS 10 equipped with an Oxford X-Max 80 mm<sup>2</sup> detector in the backscattering mode. The working distance for all samples was 12 mm and the accelerate voltage was 30 kV. All samples were sputtered by carbon to obtain good surface conductivity.

### 3. Results and Discussion

**3.1. Compressive Strength.** The compressive strength of prepared matrices is shown in Figure 1 and Table 4. Following the results, the type of matrix had the highest influence on the compressive strength. The highest values had the matrix with aggregates, and the lowest values reached the matrix with fly ash. The results correspond with the findings in literature that, by replacing BFS with fly ash, the compressive strength decreases [2]. No clear behavior correlation was observed between the Pb dosage amount and mechanical properties. Increasing the dosage of Pb from 1 up to 2.5 wt.% led, in some cases, to the compressive strength increase and in some cases to the strength decrease. The addition of 5 wt.% of Pb caused the decrease of compressive strength in all types of matrices.

**3.2. Porosity.** The porosity of the prepared materials depended mainly on the type of the matrix. The total porosity of chosen samples is listed in Table 5. The matrix with fly ash showed the highest porosity. High-temperature fly ash consists of spherical particles, which can be filled in with similar smaller particles or can be hollow. Hence, partially reacted fly ash particles increased the porosity. The lowest porosity was observed in the matrix based on BFS. It is due to a very compact microstructure of this matrix, which was confirmed by SEM analysis (Figure 2). The dosage of Pb influenced the porosity of matrices too. The total porosity of matrices increased with increasing Pb content. As can be seen in Figure 3, around the areas, where Pb was cumulated, the matrix was not compact and the cracks and pores were formed. This caused the increase in porosity. The state of Pb addition—liquid/solid—did not affect the porosity.

**3.3. Leaching Tests.** To determine the efficiency of Pb immobilization, the leaching test based on ČSN EN 12457-4

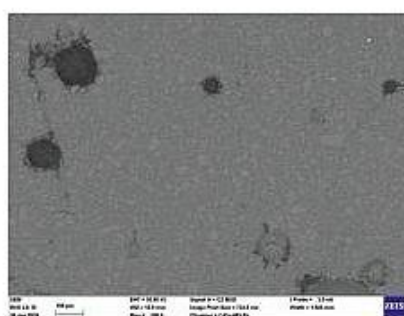


FIGURE 2: The microstructure of SR2 matrix.

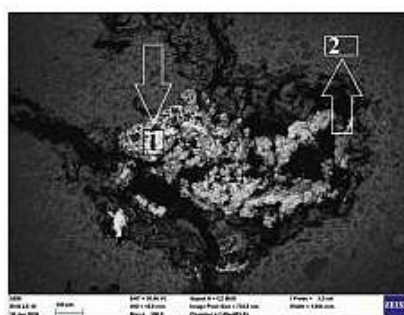


FIGURE 3: The microstructure of S2 matrix.

was performed. This test serves to determine whether the material is suitable for landfilling and whether it does not represent any hazard for the environment. Figure 4 shows the concentration of Pb in eluates from the prepared matrices. The immobilization of Pb in all matrices was very high and reached up to 99%. The results correspond with previous research and correlate with the total porosity of the matrices [11]. The highest Pb release occurred from matrices with fly ash, which also had the highest porosity and the lowest mechanical properties. The dosage of Pb had the influence on immobilization too. With increasing Pb addition, the content of Pb released into the leaching medium increased as well. It should be taken into consideration that when the Pb addition rose five times, the release increased only maximally three times. The efficiency of Pb immobilization was better with higher dosages of Pb.

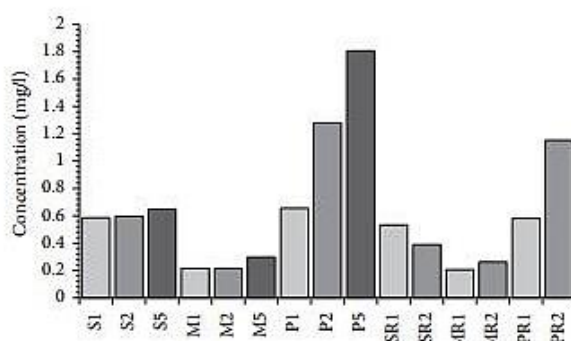


FIGURE 4: Concentration of Pb in eluates from matrices.

TABLE 6: The pH of eluates from matrices.

Mixture	S1	S2	S5	M1	M2	M5	P1	P2
pH	11.92	11.89	11.77	11.32	11.29	11.15	11.63	11.60
Mixture	P5	SR1	SR2	MR1	MR2	PR1	PR2	—
pH	11.51	11.89	11.88	11.31	11.31	11.63	11.58	—

TABLE 7: EDS analysis of S2 matrix.

Area 1											
Element	O	Na	Mg	Al	Si	Ca	Pb	—	—	—	—
Atomic (%)	57.85	3.29	0.76	0.95	12.32	1.64	23.20	—	—	—	—
Area 2											
Element	O	Na	Mg	Al	Si	Ca	Pb	S	K	Ti	Mn
Atomic (%)	58.13	4.62	3.93	3.00	15.23	12.80	0.97	0.88	0.19	0.07	0.18

TABLE 8: EDS analysis of P2 matrix.

Area 3										
Element	O	Si	Ca	Al	Pb	—	—	—	—	—
Atomic (%)	81.61	3.95	3.61	1.03	9.79	—	—	—	—	—
Area 4										
Element	O	Si	Ca	Al	Pb	Na	Mg	K	Ti	Fe
Atomic (%)	59.10	18.91	5.96	7.57	0.12	4.89	1.86	0.57	0.30	0.72

The pH of eluates is listed in Table 6. The matrices with sand reached the lowest pH, because they contained the smallest amount of the binder. The presence of fly ash led to the decrease of pH. The highest dosage of Pb (5 wt.%) caused the decrease of pH as well.

**3.4. SEM.** The SEM analysis showed three different microstructures depending on the type of matrix. The samples S2, P2, M2, and SR2 were investigated. The matrix based on BFS had a compact structure with unreacted particles of BFS and hydration products between them (Figure 3, Area 2; Table 7). A similar structure was observed in the matrix containing fly ash, but moreover, unreacted particles of fly ash were identified. The addition of fly ash led to the increase in the content of Si and Al and the decrease in the

content of Ca (Table 8). A quite different microstructure occurred in the matrix with aggregates. The unreacted aggregates filled the major area of the sample and in between them there was the matrix with the same composition as observed in the S2 sample (Figure 5, Table 9, and Area 6). The aggregates were composed of quartz (Table 9 and Area 7).

When Pb was added as a solid, it behaved in the same manner in all types of matrices. Pb was cumulated in pores and formed specific structures (Figures 3, 5, and 6). These structures consisted mainly of Pb and O. It can be assumed that Pb transformed into its insoluble salt  $Pb(OH)_2$  after the alkali activation. These findings correspond to previous research [14]. Minor amount of Pb was dispersed throughout the matrix. A quite different situation came up with the addition of Pb as a solution. Pb was dispersed



salt. There was a difference in Pb behavior when added either as a solid or as a solution. In the case of solution, Pb was dispersed throughout the matrix equally, but when added as a solid, it formed specific structures, which cumulated in pores.

### Conflicts of Interest

The authors declare that there are no conflicts of interest regarding the publication of this paper.

### Acknowledgments

This outcome has been achieved with the financial support by the project Materials Research Centre at FCH BUT-Sustainability and Development (REG LO1211), National Programme for Sustainability I (Ministry of Education, Youth and Sports), and "Development of shrinkage reducing agents designed for alkali activated systems" (GA17-03670S, Czech Science Foundation).

### References

- [1] J. M. Stellman, *Encyclopaedia of Occupational Health and Safety*, International Labour Office, Geneva, Switzerland, 4th edition, 1998.
- [2] J. L. Provis and J. S. J. van Deventer, *Alkali Activated Materials: State-of-the-Art Report*, Springer, Dordrecht, Netherlands, 2014.
- [3] L. Chao, S. Henghu, and L. Longtu, "A review: the comparison between alkali-activated slag (Si + Ca) and metakaolin (Si + Al) cements," *Cement and Concrete Research*, vol. 40, no. 9, pp. 1341–1349, 2010.
- [4] F. Puertas, M. Palacios, H. Manzano, J. S. Dolado, A. Rico, and J. Rodríguez, "A model for the C-A-S-H gel formed in alkali-activated slag cements," *Journal of the European Ceramic Society*, vol. 31, no. 12, pp. 2043–2056, 2011.
- [5] J. G. S. van Jaarsveld, J. S. J. van Deventer, and L. Lorenzen, "Factor affecting the immobilization of metals in geopolymerized fly ash," *Metallurgical and Materials Transactions B*, vol. 29, no. 1, pp. 283–291, 1998.
- [6] J. W. Phair and J. S. J. van Deventer, "Effect of silicate activator pH on the leaching and material characteristic of waste-based inorganic polymer," *Minerals Engineering*, vol. 14, no. 3, pp. 289–304, 2001.
- [7] A. Palomo and M. Palacios, "Alkali-activated cementitious materials: alternative matrices for the immobilisation of hazardous wastes part II. Stabilisation of chromium and lead," *Cement and Concrete Research*, vol. 33, no. 2, pp. 289–295, 2003.
- [8] J. W. Phair, J. S. J. van Deventer, and J. D. Smith, "Effect of Al source and alkali activation on Pb and Cu immobilisation in fly-ash based "geopolymers"," *Applied Geochemistry*, vol. 19, no. 3, pp. 423–434, 2004.
- [9] L. Zheng, W. Wang, and Y. Shi, "The effects of alkaline dosage and Si/Al ratio on the immobilization of heavy metals in municipal solid waste incineration fly ash-based geopolymer," *Chemosphere*, vol. 79, no. 6, pp. 665–671, 2010.
- [10] J. Zhang, J. L. Provis, D. Feng, and J. S. J. van Deventer, "Geopolymers for immobilization of Cr<sup>6+</sup>, Cd<sup>2+</sup> and Pb<sup>2+</sup>," *Journal of Hazardous Materials*, vol. 157, no. 2-3, pp. 587–598, 2008.
- [11] J. Deja, "Immobilization of Cr<sup>6+</sup>, Cd<sup>2+</sup>, Zn<sup>2+</sup> and Pb<sup>2+</sup> in alkali-activated slag binders," *Cement and Concrete Research*, vol. 32, no. 12, pp. 1971–1979, 2002.
- [12] J. G. S. van Jaarsveld and J. S. J. van Deventer, "The effect of metal contaminants on the formation and properties of waste-based geopolymers," *Cement and Concrete Research*, vol. 29, no. 8, pp. 1189–1200, 1999.
- [13] L. Kalina, J. Koplík, F. Šoukal, J. Másilko, and L. Jaskowicová, "Potential uses of geopolymers to immobilize toxic metals from by-products material," *Environmental Engineering and Management Journal*, vol. 11, no. 3, pp. 579–584, 2012.
- [14] J. Koplík, L. Kalina, J. Másilko, and F. Šoukal, "The characterization of fixation of Ba, Pb, and Cu in alkali-activated fly ash/blast furnace slag matrix," *Materials*, vol. 9, no. 7, p. 533, 2016.

Article

# The Characterization of Fixation of Ba, Pb, and Cu in Alkali-Activated Fly Ash/Blast Furnace Slag Matrix

Jan Koplík \*, Lukáš Kalina, Jiří Másilko and František Šoukal

Materials Research Centre, Faculty of Chemistry, Brno University of Technology, Purkyňova 118, Brno 61200, Czech Republic; kalina@fch.vut.cz (L.K.); masilko@fch.vut.cz (J.M.); soukal@fch.vut.cz (F.Š.)

\* Correspondence: koplík@fch.vut.cz; Tel.: +420-541-149-426

Academic Editor: Claudio Ferone

Received: 13 April 2016; Accepted: 24 June 2016; Published: 30 June 2016

**Abstract:** The fixation of heavy metals (Ba, Cu, Pb) in an alkali-activated matrix was investigated. The matrix consisted of fly ash and blast furnace slag (BFS). The mixture of NaOH and Na-silicate was used as alkaline activator. Three analytical techniques were used to describe the fixation of heavy metals—X-ray photoelectron spectroscopy (XPS), scanning electron microscopy (SEM) equipped with energy dispersive X-ray spectroscopy (EDS), and X-ray powder diffraction (XRD). All heavy metals formed insoluble salts after alkaline activation. Ba was fixed as BaSO<sub>4</sub>, and only this product was crystalline. EDS mapping showed that Ba was cumulated in some regions and formed clusters. Pb was present in the form of Pb(OH)<sub>2</sub> and was dispersed throughout the matrix on the edges of BFS grains. Cu was fixed as Cu(OH)<sub>2</sub> and also was cumulated in some regions and formed clusters. Cu was present in two different chemical states; apart from Cu(OH)<sub>2</sub>, a Cu–O bond was also identified.

**Keywords:** fixation; alkali-activated materials; X-ray photoelectron spectroscopy; heavy metals

## 1. Introduction

Heavy metals are a significant part of various industrial and chemical waste materials, which can be a serious environmental threat. Waste materials with heavy metal content are processed by the set of procedures called stabilization/solidification. During these procedures, many different materials such as concrete and glass are used. In the past few decades, a new material for the inhibition of hazardous materials was used—alkali-activated material (AAM) [1,2].

The history of AAMs began in 1940s, when Kühl [3] and later Purdon [4] used an alkali activator for the activation of blast furnace slag. Nowadays, AAMs include broad types of materials—blast furnace slag, metakaolin, fly ash, etc. However, AAMs can vary in chemical or phase composition, and an alkali activator (high pH) is always used during the preparation of them. The main difference among AAMs is the content of calcium. AAMs can be divided into the groups of high-calcium alkali-activated materials (HCAAMs) and low-calcium alkali-activated materials (LCAAMs). HCAAMs are represented by alkali-activated blast furnace slag (BFS) or other types of slag (steel, phosphorus, copper, nickel, etc.). The C–S–H and C–A–S–H gels are assumed to be the main hydration products of alkali activation of HCAAMs. This gel has a similar structure like disordered tobermorite-like C–S–H(I) type and AlO<sub>4</sub> tetrahedra enable the extension or crosslinking of the silicon chains. The secondary hydration products are formed depending on the composition of blast furnace slag and used activator. AFm type phases were identified when using NaOH as the activator, hydrotalcite was identified in activated slags with a high amount of MgO, and zeolites were identified in BFS with a high amount of Al<sub>2</sub>O<sub>3</sub> [5–10]. A considerably different structure is present after the alkali activation of LCAAMs. The structure can be described as a disordered cross-linked aluminosilicate network, which consists of SiO<sub>4</sub> and AlO<sub>4</sub> tetrahedra linked by oxygen atoms. The negative charge of AlO<sub>4</sub> is balanced by the presence of a positive ion in the structure. Usually Na<sup>+</sup> or K<sup>+</sup> serve as

the charge-balancing ions, but  $\text{Ca}^{2+}$ ,  $\text{Ba}^{2+}$ ,  $\text{Mg}^{2+}$ , and  $\text{NH}_4^+$  can also occur. In fact, the structure of LCAAMs is very similar to the structure of zeolites [5,11,12]. The main reaction product of the alkali activation of the mixture of both types of AAMs (BFS and fly ash) is the N–A–S–H type gel. The gel is actually of a C–S–H type with a high concentration of tetrahedrally coordinated Al and an interlayer of Na ions incorporated into its structure [13].

The ability of AAMs to immobilize heavy metals and other hazardous materials in their structure has been investigated since the second half of the last century. The efficiency of the inhibition of heavy metals and other hazardous materials within AAMs depends on more factors including the type of immobilized material, its dosage, the type of matrix, the nature of alkaline activator, and its concentration. In general, Pb, Zn, Cr, and B reach a high efficiency of immobilization in AAMs, as opposed to Cu, Cd, and As, which have worse inhibition results. There are two different ways of how to fix heavy metals in the matrix—physical and chemical. Often, both of these types occur at the same time. The physical immobilization of heavy metals is the same in AAMs as in other binders (e.g., ordinary Portland cement). The physical immobilization is linked with the mechanical properties of matrix and its porosity. The chemical fixation means bonding with newly formed aluminosilicate phases. Some metals are fixed by forming insoluble salts, mainly hydroxides or silicates [14–29].

The aim of this study was to describe, how heavy metals (Ba, Pb, Cu) are fixed within the matrix based on the alkali-activated mixture of fly ash and BFS, what their chemical state is, and how they are distributed in the matrix. The description of form and chemical state of heavy metals after the activation was enabled by using a modern analytical method—X-ray photoelectron spectroscopy.

## 2. Materials and Methods

### 2.1. Sample Preparation

Blast furnace slag and high-temperature fly ash were used as raw materials. Their chemical composition is shown in Table 1. The mixture of NaOH and Na-silicate (weight ratio  $\text{SiO}_2:\text{Na}_2\text{O}$ —3.1; wt %  $\text{SiO}_2$ —27.3) was used as the alkaline activator. Heavy metals were used in the form of  $\text{Ba}(\text{NO}_3)_2$  p. a.,  $\text{Pb}(\text{NO}_3)_2$  p. a., and  $\text{CuCl}_2 \cdot 2\text{H}_2\text{O}$  p. a. They were added as solids in the dosage of 2.5 wt % of binder. Finally, three matrices with added heavy metals were prepared—one matrix for each heavy metal. Demineralized water was used throughout. The composition of matrices is listed in Table 2. The preparation of the matrix started with the mixture of all solid compounds together for 5 min, followed by the adding of the alkaline activator and mixing for another 5 min. After mixing, the samples were cast in steel molds measuring  $20 \times 20 \times 100 \text{ mm}^3$  and vibrated for 90 s. All analyses were performed after 28 days of open curing at ambient conditions.

Table 1. Chemical composition of fly ash and BFS (wt %).

Fly Ash									
$\text{SiO}_2$	$\text{Al}_2\text{O}_3$	CaO	$\text{Na}_2\text{O}$	$\text{K}_2\text{O}$	MgO	$\text{SO}_3$	$\text{Fe}_2\text{O}_3$	$\text{TiO}_2$	$\text{P}_2\text{O}_5$
50.30	27.70	3.84	0.76	2.67	1.15	0.87	10.40	1.45	0.28
Blast Furnace Slag									
$\text{SiO}_2$	$\text{Al}_2\text{O}_3$	CaO	$\text{Na}_2\text{O}$	$\text{K}_2\text{O}$	MgO	$\text{SO}_3$	$\text{Fe}_2\text{O}_3$	$\text{TiO}_2$	MnO
34.70	9.05	41.1	0.41	0.90	10.5	1.46	0.25	0.96	0.55

Table 2. Composition of matrices (wt %).

Slag	Fly ash	NaOH	$\text{Na}_2\text{O} \cdot \text{SiO}_2$	Water	Ba, Pb, Cu
15.6	57.4	6.1	6.2	12.2	2.5

## 2.2. Methods

The X-ray photoelectron spectroscopy (XPS) analyses were carried out with an Axis Ultra DLD spectrometer (Kratos Analytical Ltd., Manchester, UK) using a monochromatic Al K $\alpha$  ( $h\nu = 1486.7$  eV) X-ray source operating at 150 W (10 mA, 15 kV). The spectra were obtained using the analysis area of  $\sim 300 \times 700$   $\mu\text{m}$ . The Kratos charge neutralizer system was used for all analyses. The high-resolution spectra were measured with the step size of 0.1 eV and 20 eV pass energy. The instrument base pressure was  $2 \times 10^{-8}$  Pa. The spectra were analyzed using the CasaXPS software (version 2.3.15) (Casa Software Ltd., Teignmouth, UK) and were charge-corrected to the main line of the carbon C 1s spectral component (C–C, C–H) set to 284.80 eV. Standard Shirley background was used for all sample spectra.

The scanning electron microscopy (SEM) and energy dispersive X-ray spectroscopy (EDS) analyses were performed using a JEOL JSM-7600F (JEOL Ltd., Tokyo, Japan) scanning electron microscope equipped with X-Max 80 mm<sup>2</sup> SDD detector in back-scattering mode. The working distance for all samples was 15 mm, the accelerate voltage was 15 kV, and the probe current was 1 nA. Prior to the SEM analysis, all samples were polished for 6 h by a cross-section polisher JEOL (JEOL Ltd., Tokyo, Japan). All samples were sputtered by gold to obtain good surface conductivity.

The X-ray powder diffraction (XRD) data were obtained using a PANanalytical Empyrean (PANanalytical B.V., Almelo, The Netherlands) diffractometer with CuK $\alpha$  radiation (1.54 Å) operating at the voltage of 40 kV, and the current of 30 mA and equipped with 3D detection system PIXcel3D (PANanalytical B.V., Almelo, The Netherlands). All samples were step-scanned from 5° to 90° 2 $\theta$  using vertical high-resolution goniometer with a step size of 0.013° 2 $\theta$ . Time per step was 96 s. The variable slits with an irradiated length of 10 mm were used. Presented X-ray patterns have an original background that has not been subtracted.

## 3. Results and Discussion

### 3.1. XPS

The XPS results show the chemical state of examined elements (Pb, Ba, Cu). In the case of lead, the high-resolution spectrum gives the binding energy of 138.6 eV for Pb 4f<sub>7/2</sub> line (Figure 1), typical for Pb(OH)<sub>2</sub>. The conversion of primary phase Pb(NO<sub>3</sub>)<sub>2</sub> to hydroxide will probably take place in the same way as in the hydration of Portland cement. This salt forms insoluble hydroxide in an alkaline solution and may form a coating on the cement (blast furnace slag) particles, which can be observed in Figure 6. There is no evidence that the lead compound creates highly insoluble Pb<sub>3</sub>SiO<sub>5</sub> as in the system of alkali-activated fly ash in Palomo et al.'s study [29].

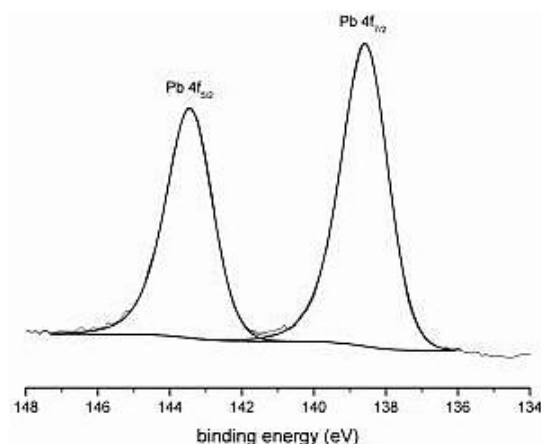


Figure 1. X-ray photoelectron spectroscopy (XPS) spectrum of Pb.

The Ba 4d spectrum (Figure 2) demonstrates the creation of BaSO<sub>4</sub> with a binding energy of Ba 3d<sub>5/2</sub> of 780.0 eV, which is consistent with the EDS analysis.

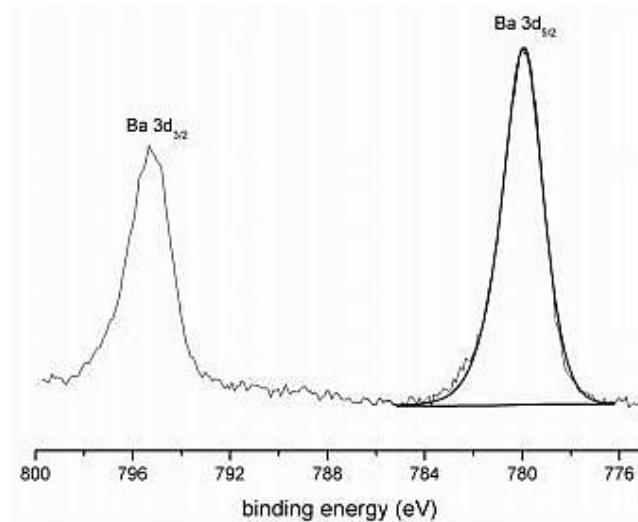


Figure 2. XPS spectrum of Ba.

Finally, the XPS spectrum of Cu 2p (Figure 3) shows two different chemical states. The first Cu 2p<sub>3/2</sub> component at 934.8 eV with a strong shake-up satellite belongs to Cu(OH)<sub>2</sub>. Shake-up peaks may occur when the outgoing photoelectron simultaneously interacts with a valence electron and excites it to a higher-energy level. The kinetic energy of the shaken-up core electron is then slightly reduced giving the satellite structure a few eV below (higher on the calculated binding energy scale) the core level position [30]. It should be noted that the determination of Cu(OH)<sub>2</sub> also depends on the peak shape and main peak to shake up peak separation. The second Cu 2p<sub>3/2</sub> peak at 932.7 eV represents the bond of Cu with O. That can be interpreted as the formation of copper oxide or the formation of the bond with the matrix.

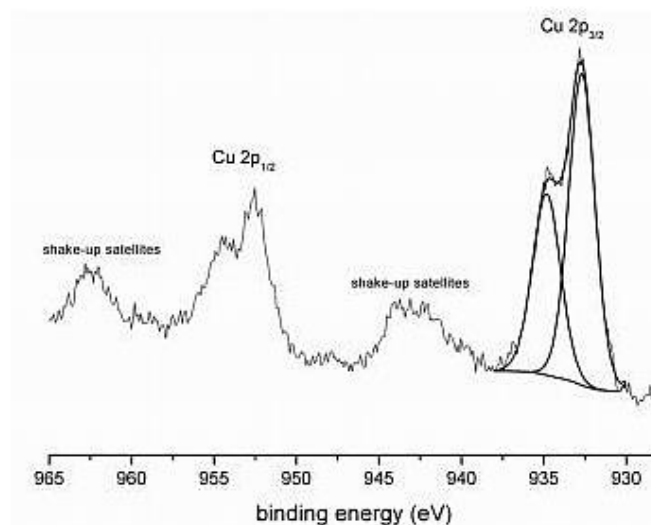


Figure 3. XPS spectrum of Cu.

### 3.2. SEM

The microstructure of prepared matrices with heavy metals was characterized by the SEM analysis. The regions containing heavy metals were investigated with EDS analysis. In all images, remaining particles of fly ash and grains of BFS are evident. High-temperature fly ash consists of spherical particles of various sizes. Some of them can be hollow, and smaller particles are encapsulated in bigger ones in many cases. BFS is represented by grains of irregular shape. The remaining space is filled by aluminosilicate gel.

Figure 4 shows the SEM image of the prepared matrix. The light structure in the middle of the image represents the area with a high amount of barium. Performed EDS analysis determined barium, sulfur, and oxygen as the main components of the structure (Table 3). Their molar ratio of 1:1:4 responds to  $\text{BaSO}_4$ . These results correspond with the XPS analysis.  $\text{BaSO}_4$  was also identified by the XRD analysis. Subsequently, the mapping of chemical elements within the matrix was performed. The mapping (Figure 7) showed that Ba cumulated in some bigger areas such as  $\text{BaSO}_4$ , rather than being dispersed uniformly throughout the matrix. Unlike Cu and Pb, Ba did not form hydroxide because of the good solubility of  $\text{Ba}(\text{OH})_2$ . The sulfates originated from raw materials due to the fact that the chemical composition of both fly ash and blast furnace slag contained a sufficient amount of sulphur to form  $\text{BaSO}_4$ .

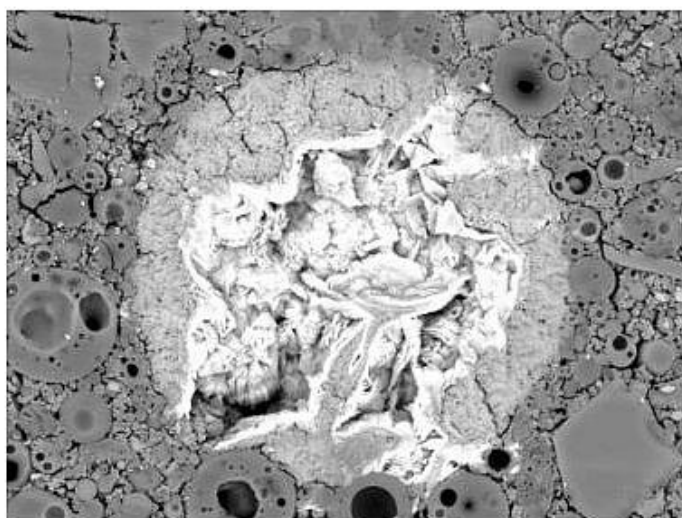


Figure 4. Scanning electron microscopy (SEM) image of the region with fixed barium, magnitude 2000 $\times$ .

Table 3. Energy dispersive X-ray spectroscopy (EDS) analysis of the Ba cluster (atom %).

O	Na	Si	S	Cl	K	Ca	Fe	Ba
62.86	0.59	1.96	14.44	1.76	1.12	0.32	0.59	16.36

In Figure 5, the SEM image of the area with cumulated Cu is displayed. It can be seen as “foggy” lighter structure of irregular shape in the central part of image. The prevailing components are Cu and O (Table 4). The molar ratio of 1:1.6 shows  $\text{Cu}(\text{OH})_2$  as a possible reaction product of Cu. This assumption was proved by the XPS analysis. No  $\text{Cu}(\text{OH})_2$  was identified by the XRD analysis. It indicates a non-crystalline character of  $\text{Cu}(\text{OH})_2$ . The mapping showed similar results as in the case of barium. Cu tends to cumulate in small areas of  $\text{Cu}(\text{OH})_2$  rather than being dispersed throughout the matrix. The difference of distribution between barium and copper is that copper forms a higher number of smaller clusters.

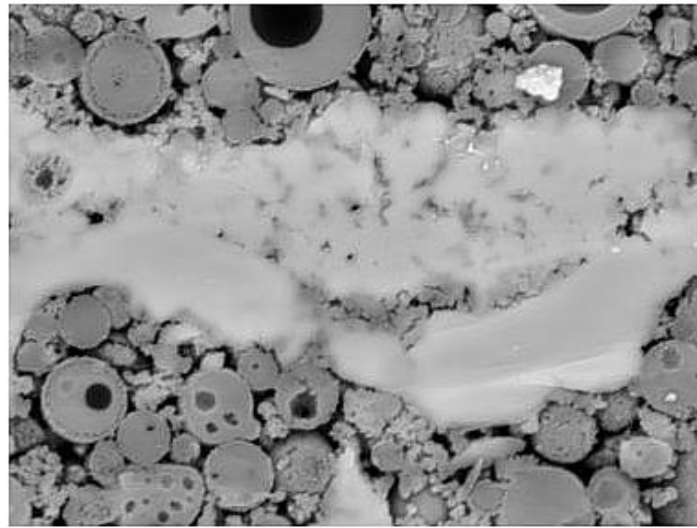


Figure 5. SEM image of region with fixed Cu, magnitude 7000×.

Table 4. EDS analysis of the Cu cluster (atom %)

O	Al	Si	Cl	Ca	Fe	Cu	Pb
55.8	0.87	6.91	1.31	0.34	0.28	33.79	0.38

Figure 6 shows the detail of a grain of BFS. A coating of small particles are visible on the edges of the grain. The EDS analysis proved that the coating contained Pb (Table 5). The particles are supposed to be formed of  $\text{Pb}(\text{OH})_2$  according to XPS analysis. Unlike both previous elements, Pb did not cumulate in larger clusters of  $\text{Pb}(\text{OH})_2$ , but it seems to be dispersed throughout the matrix (Figure 7). The reason that Pb did not form bigger clusters could be caused by the smaller amount of Pb atoms in the matrix. All metals were added in wt %, so the amount of Pb atoms in the matrix is the lowest, because of its superlative molar weight.

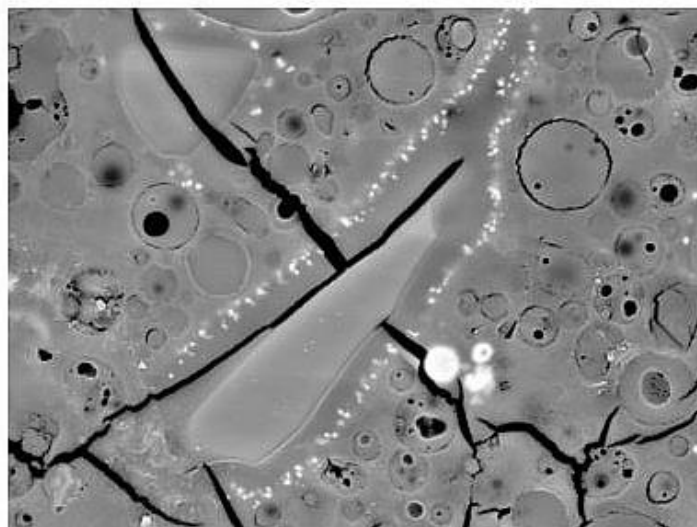


Figure 6. SEM image of Pb coating on the BFS grain, magnitude 4000×.

Table 5. EDS analysis of the Pb coating (atom %).

O	Mg	Al	Si	S	K	Ca	Ti	Fe	Cu	Pb
58.36	5.48	5.64	20.08	0.58	3.29	4.25	0.28	0.57	0.42	1.04

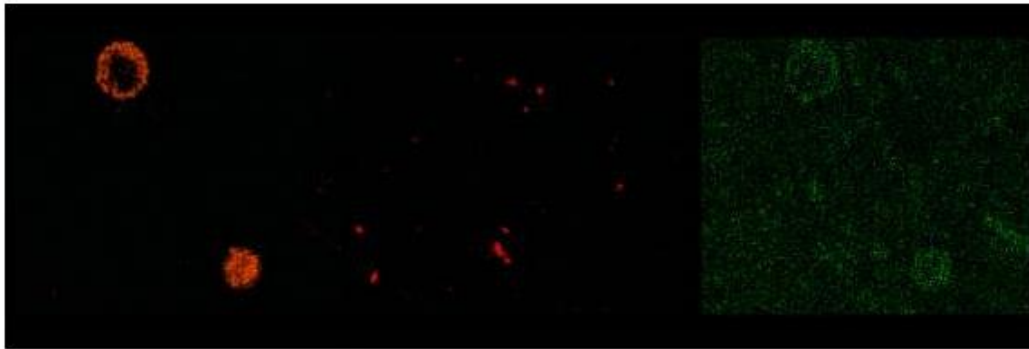


Figure 7. EDS mapping of Ba, Cu, and Pb in the matrix.

### 3.3. XRD

The XRD analysis identified only one crystalline compound of fixed heavy metals—BaSO<sub>4</sub>. The XRD patterns of the alkali-activated matrix are shown in Figure 8. The patterns of BaSO<sub>4</sub> are described, the rest of the patterns belongs to the phases of the matrix (quartz, mullite, merwinite, calcite, magnetite) and to NaCl. No compounds of Pb and Cu were identified by XRD, since they are fixed in the amorphous phases.

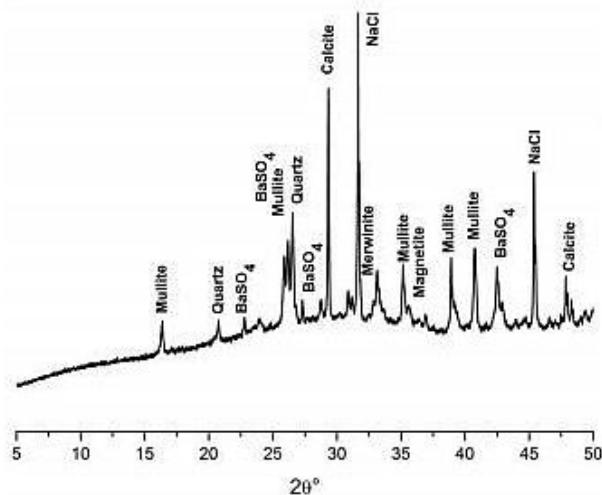


Figure 8. X-ray powder diffraction (XRD) patterns of the alkali-activated material (AAM) matrix with heavy metals.

## 4. Conclusions

The fixation of three heavy metals—Ba, Pb, and Cu—in alkali-activated matrices based on blast furnace slag and fly ash was examined. The XPS analyses proved that all metals formed insoluble salts—BaSO<sub>4</sub>, Pb(OH)<sub>2</sub> and Cu(OH)<sub>2</sub>—after alkaline activation. Only Cu was present in matrices in two different chemical states; apart from Cu(OH)<sub>2</sub>, a Cu–O bond was also identified. Both Pb(OH)<sub>2</sub>

and  $\text{Cu}(\text{OH})_2$  were present in an amorphous or semicrystalline form, which could not be identified by XRD. The distribution of heavy metals within the matrices was quite different. Ba and Cu were not dispersed throughout the matrix evenly and were cumulated in some regions. On the other hand, EDS mapping showed that Pb did not form clusters and was present as a coating on the edges of grains of the blast furnace slag in the whole matrix. The results show that the metals were fixed mainly by encapsulation in the matrix and forming insoluble salts. Only in the case of Cu can the formation of some chemical bond with newly formed phases after alkali activation be assumed.

**Acknowledgments:** This work was financially supported by the project “Materials Research Centre at FCH BUT”—Sustainability and Development, REG LO1211—with financial support from National Programme for Sustainability I (Ministry of Education, Youth and Sports).

**Author Contributions:** Jan Koplík and František Šoukal conceived and designed the experiments; Jan Koplík performed the experiments; Jiří Másilko and Lukáš Kalina performed the analysis; Jan Koplík wrote the paper.

**Conflicts of Interest:** The authors declare no conflict of interest.

### Abbreviations

The following abbreviations are used in this manuscript:

BFS	blast furnace slag
XPS	X-ray photoelectron spectroscopy
SEM	scanning electron microscopy
EDS	energy dispersive X-ray spectroscopy
XRD	X-ray powder diffraction
AAM	alkali-activated material
HCAAMs	high-calcium alkali-activated materials
LCAAMs	low-calcium alkali-activated materials

### References

1. Shi, C.; Fernández-Jiménez, A. Stabilization/solidification of hazardous and radioactive wastes with alkali-activated cements. *J. Hazard. Mater.* **2006**, *B137*, 1656–1663. [CrossRef] [PubMed]
2. Chang, H.O. *Hazardous and Radioactive Waste Treatment Technologies Handbook*; CRC Press LLC: Boca Raton, FL, USA, 2001.
3. Shi, C.; Krivenko, P.V.; Roy, D. *Alkali-Activated Cements and Concretes*; Taylor & Francis: New York, NY, USA, 2006.
4. Purdon, A.O. The action of alkalis on blast-furnace slag. *J. Soc. Chem. Ind.* **1940**, *59*, 191–202.
5. Provis, J.L.; van Deventer, J.S.J. *Alkali Activated Materials: State-of-the Art-Report*; Springer: Dordrecht, The Netherlands, 2014.
6. Fernández-Jiménez, A.; Palomo, A.; Revuelta, D. Alkali activation of industrial by-products to develop new earth-friendly cements. In Proceedings of the 11th International Conference on Non-Conventional Materials and Technologies, Bath, UK, 6–9 September 2009; pp. 1–15.
7. Myers, R.J.; Bernal, S.A.; San Nicolas, R.; Provis, J.L. Generalized structural description of calcium-sodium aluminosilicate hydrate gels: The cross linked substituted tobermorite model. *Langmuir* **2013**, *29*, 5294–5306. [CrossRef] [PubMed]
8. Bernal, S.A.; Provis, J.L.; de Mejía Gutierrez, R.; Rose, V. Evolution of binder structure in sodium silicate-activated slag-metakaolin blends. *Cem. Concr. Compos.* **2011**, *33*, 46–54. [CrossRef]
9. Escalante-García, J.; Fuentes, A.F.; Gorokhovskiy, A.; Fraire-Luna, P.E.; Mendoza-Suarez, G. Hydration products and reactivity of blast-furnace slag activated by various alkalis. *J. Am. Ceram. Soc.* **2003**, *86*, 2148–2153. [CrossRef]
10. Ben Haha, M.; Lothenbach, B.; Le Saout, G.; Winnefeld, F. Influence of slag chemistry on the hydration of alkali-activated blast-furnace slag—Part I: Effect of MgO. *Cem. Concr. Res.* **2011**, *41*, 955–963. [CrossRef]
11. Komnitsas, K.; Zaharaki, D. Geopolymerisation: A review and prospects for the minerals industry. *Min. Eng.* **2007**, *20*, 1261–1277. [CrossRef]
12. Provis, J.L.; Lukey, G.C.; van Deventer, J.S.J. Do geopolymers actually contain zeolites? A reexamination of existing results. *Chem. Mater.* **2005**, *17*, 3075–3085. [CrossRef]

13. Puertas, F.; Martínez-ramírez, S.; Alonso, S.; Vázquez, T. Alkali-activated fly ash/slag cement. Strength behavior and hydration products. *Cem. Concr. Res.* **2000**, *30*, 1625–1632. [CrossRef]
14. Van Jaarsveld, J.G.S.; van Deventer, J.S.J.; Lorenzen, L. Factor affecting the immobilization of metals in geopolymerized fly ash. *Metall. Mater. Trans.* **1998**, *29B*, 283–291. [CrossRef]
15. Phair, J.W.; van Deventer, J.S.J.; Smith, J.D. Effect of Al source and alkali activation on Pb and Cu immobilization in fly-ash based “geopolymers”. *App. Geochem.* **2004**, *19*, 423–434. [CrossRef]
16. Xu, J.Z.; Zhou, Y.L.; Chang, Q.; Qu, H.Q. Study on the factors affecting the immobilization of heavy metals in fly ash-based geopolymers. *Mater. Lett.* **2006**, *60*, 820–822. [CrossRef]
17. Palomo, A.; de la Fuente, J.I.L. Alkali-activated cementitious materials: Alternative matrices for the immobilization of hazardous wastes Part I. Stabilization of boron. *Cem. Concr. Res.* **2003**, *33*, 281–288. [CrossRef]
18. Zhang, J.; Provis, J.L.; Feng, S.; van Deventer, J.S.J. Geopolymers for immobilization of Cr<sup>6+</sup>, Cd<sup>2+</sup>, and Pb<sup>2+</sup>. *J. Hazard. Mater.* **2008**, *157*, 587–598. [CrossRef] [PubMed]
19. Fernández-Jiménez, A.; Palomo, A.; Macphee, D.E.; Lachowski, E.E. Fixing arsenic in alkali-activated cementitious matrices. *J. Am. Ceram. Soc.* **2005**, *88*, 1122–1126. [CrossRef]
20. Phair, J.W.; van Deventer, J.S.J. Effect of silicate activator pH on the leaching and material characteristic of waste-based inorganic polymers. *Min. Eng.* **2001**, *14*, 289–304. [CrossRef]
21. Zhang, Y.; Sun, W.; Chen, Q.; Chen, L. Synthesis and heavy metal immobilization behaviors of slag based geopolymer. *J. Hazard. Mater.* **2007**, *143*, 206–213.
22. Deja, J. Immobilization of Cr<sup>6+</sup>, Cd<sup>2+</sup>, Zn<sup>2+</sup> and Pb<sup>2+</sup> in alkali-activated slag binders. *Cem. Concr. Res.* **2002**, *32*, 1971–1979. [CrossRef]
23. Škvára, F.; Kopecký, L.; Šmilauer, V.; Bittnar, Z. Material and structural characterization of alkali activated low-calcium brown coal fly ash. *J. Hazard. Mater.* **2009**, *168*, 711–720. [CrossRef] [PubMed]
24. Zhang, J.; Provis, J.L.; Feng, D.; van Deventer, J.S.J. The role of sulfide in the immobilization of Cr(VI) in fly ash geopolymers. *Cem. Concr. Res.* **2008**, *38*, 681–688. [CrossRef]
25. Bankowski, P.; Zhou, L.; Hodges, R. Using inorganic polymer to reduce leach rates of metals from brown coal fly ash. *Min. Eng.* **2004**, *17*, 159–166. [CrossRef]
26. Álvarez-Ayuso, E.; Querol, X.; Plana, F.; Alastuey, A.; Moreno, N.; Izquierdo, M.; Font, O.; Moreno, T.; Díez, S.; Vázquez, E.; et al. Environmental, physical and structural characterization of geopolymer matrixes synthesized from coal (co-)combustion fly ash. *J. Hazard. Mater.* **2008**, *154*, 175–183. [CrossRef] [PubMed]
27. Fernández Pereira, C.; Luna, Y.; Querol, X.; Antenucci, D.; Vale, J. Waste stabilization/solidification of an electric arc furnace dust using fly ash-based geopolymers. *Fuel* **2009**, *88*, 1185–1193. [CrossRef]
28. Li, F.; Li, Q.; Zhai, J.; Sheng, G. Effect of zeolitization of CFBC fly ash on immobilization of Cu, Pb and Cr. *Ind. Eng. Chem. Res.* **2007**, *46*, 7087–7095. [CrossRef]
29. Palomo, A.; Palacios, M. Alkali-activated matrices for the immobilization of hazardous waste Part II. *Cem. Concr. Res.* **2003**, *33*, 289–295. [CrossRef]
30. Watts, J.F.; Wolstenholme, J. *An Introduction to Surface Analysis by XPS and AES*; John Wiley & Sons: Chichester, UK, 2005.



© 2016 by the authors; licensee MDPI, Basel, Switzerland. This article is an open access article distributed under the terms and conditions of the Creative Commons Attribution (CC-BY) license (<http://creativecommons.org/licenses/by/4.0/>).

Article

## Some Issues of Shrinkage-Reducing Admixtures Application in Alkali-Activated Slag Systems

Vlastimil Bílek Jr. \*, Lukáš Kalina, Radoslav Novotný, Jakub Tkacz and Ladislav Pařízek

Materials Research Centre, Faculty of Chemistry, Brno University of Technology, Brno 612 00, Czech Republic; kalina@fch.vut.cz (L.K.); xcnovotny2@fch.vut.cz (R.N.); tkacz@fch.vut.cz (J.T.); xcpařízekl@fch.vut.cz (L.P.)

\* Correspondence: bilek@fch.vut.cz; Tel.: +420-54-114-9426

Academic Editor: Claudio Ferone

Received: 9 June 2016; Accepted: 6 June 2016; Published: 10 June 2016

**Abstract:** Significant drying shrinkage is one of the main limitations for the wider utilization of alkali-activated slag (AAS). Few previous works revealed that it is possible to reduce AAS drying shrinkage by the use of shrinkage-reducing admixtures (SRAs). However, these studies were mainly focused on SRA based on polypropylene glycol, while as it is shown in this paper, the behavior of SRA based on 2-methyl-2,4-pentanediol can be significantly different. While 0.25% and 0.50% had only a minor effect on the AAS properties, 1.0% of this SRA reduced the drying shrinkage of waterglass-activated slag mortar by more than 80%, but it greatly reduced early strengths simultaneously. This feature was further studied by isothermal calorimetry, mercury intrusion porosimetry (MIP) and scanning electron microscopy (SEM). Calorimetric experiments showed that 1% of SRA modified the second peak of the pre-induction period and delayed the maximum of the main hydration peak by several days, which corresponds well with observed strength development as well as with the MIP and SEM results. These observations proved the certain incompatibility of SRA with the studied AAS system, because the drying shrinkage reduction was induced by the strong retardation of hydration, resulting in a coarsening of the pore structure rather than the proper function of the SRA.

**Keywords:** alkali activated slag; shrinkage reducing admixture; shrinkage; hydration; microstructure; retardation

### 1. Introduction

Ordinary Portland clinker or cement (OPC)-based binders are probably the most common in concrete production. OPC is a traditional and versatile binder but, on the other hand, its manufacturing consumes great amounts of energy and significantly contributes to the global emissions of greenhouse gases. Approximately one ton of CO<sub>2</sub> is released per one ton of cement produced [1]. Therefore, it is necessary to search for some alternative binders such as calcium aluminate cements, calcium sulfoaluminate cements or supersulfated cements [2]. Another possible way is the formulation of alkali-activated binders, usually based on blast furnace slag (BFS), fly ash (FA) or metakaolin [3]. According to Duxson *et al.* [4], geopolymers can provide approximately 80% reduction of CO<sub>2</sub> emissions compared to OPC.

AAS-based materials seem to be promising for practical applications. Naturally, their properties are often compared to those of OPC-based materials. In general, AAS can be equal to or even better than OPC in terms of mechanical strength [5], durability in aggressive environments [6–8], behavior at elevated temperatures [9–11] and interfacial transition zone [12]. However, AAS-based materials also have some drawbacks, especially their complicated workability improvement by conventional superplasticizers designed for OPC [13,14], rapid setting [15] and high shrinkage [15,16].

Shrinkage of AAS can be classified into drying shrinkage, autogenous shrinkage and carbonation shrinkage [17]. The considerably higher shrinkage of AAS compared to that of OPC is mostly attributed to the significantly higher mesopore content in AAS binders [18] and the different nature of C–S–H or C–S–A–H gel [19]. Autogenous shrinkage can be regarded as the macroscopic result of the effects of chemical shrinkage and self-desiccation [20]. Lee *et al.* [21] stated that self-desiccation is the main reason for the autogenous shrinkage of AABFS/FA. Shrinkage during drying originates from the two mechanisms of capillary suction and disjoining pressure. The former dominates for pore diameters higher than 10 nm, while the latter becomes more important for a very fine porosity [22].

Recently, many various efforts to reduce the shrinkage of AAS were made, such as the partial replacement of BFS by mineral additives such as FA [21,23–25] and silica fume [23] or a combination of these [23], initial curing at elevated temperature [26–29], internal curing [30], use of fibers [31–33] and utilization of some expanding admixtures [34–36]. The most effective seem to be the partial replacement of slag by silica fume and heat curing prior to dry air exposure. However, heat curing means additional energy consumption and is restricted mostly to the precast production. Moreover, volume changes during the heat curing stage are not always measured, despite the fact that they can noticeably contribute to the total shrinkage, particularly under sealed conditions.

Another possibility of shrinkage mitigation is provided by SRAs. The use of these admixtures in order to reduce both autogenous and drying shrinkage of OPC-based matrices is relatively well established [37–41] and such admixtures are commercially available. The beneficial effect of SRAs is attributed mainly to the decline of the surface tension of the pore water. Only a few studies investigating the influence of these admixtures, designed originally for OPC systems, on properties of AAS were reported: Puertas and Palacios [42] reduced both autogenous and drying shrinkage of AAS by using SRA based on polypropylene glycol. Significantly higher shrinkage reduction was observed at 99% relative humidity than at 50% relative humidity. Better results for moist curing than for dry curing were reported by Bilim *et al.* [43], also using SRA based on polypropylene glycol. Bakharev *et al.* [44] significantly reduced shrinkage by using some nonstandard SRA and then reduced it even more by using an air-entraining admixture, which was recommended for use in AAS concrete, as it greatly improved workability.

Despite the great effort and promising results mentioned above, shrinkage is still regarded as the main limiting factor for the practical use of AAS. The aim of this paper is to investigate the effect of different types of SRAs from those mentioned above not only on the shrinkage of AAS, but also on its other properties such as microstructural and strength development.

## 2. Materials and Methods

### 2.1. Materials and Sample Preparation

BFS from the Czech production with a volume mean diameter of about 12  $\mu\text{m}$  was used as a solid precursor for the reference binder.

The prevailing amount of amorphous phase was determined by X-ray diffraction as well as the presence of melilite, merwinite and traces of  $\beta\text{-C}_2\text{S}$  and calcite. The chemical composition of slag determined by X-ray fluorescence is given in Table 1.

**Table 1.** Chemical composition of BFS as determined by XRF.

Raw Material	Chemical Composition wt. %									
BFS	SiO <sub>2</sub>	Al <sub>2</sub> O <sub>3</sub>	CaO	Na <sub>2</sub> O	K <sub>2</sub> O	MgO	SO <sub>3</sub>	Fe <sub>2</sub> O <sub>3</sub>	TiO <sub>2</sub>	MnO
	34.7	9.1	41.1	0.4	0.9	10.5	1.4	0.3	1.0	0.6

BFS was activated by waterglass with a silica modulus of 1.85 provided by Vodní sklo, a.s. The amount of waterglass was adjusted to maintain the mass ratio Na<sub>2</sub>O/slag of 0.04. Commercially available SRA based on 2-methyl-2,4-pentanediol originally designed for OPC systems was used to

test its effect on the properties of AAS in amounts of 0.25, 0.50 and 1.0 wt. % of slag. Corresponding mortars and pastes were marked as SRA0.25, SRA0.50 and SRA1.0, respectively. SRA was mixed with activating solution just before the slag addition. Specimens with no SRA were also prepared as a reference (R). The mixture of SRA with activating solution quickly separated into two layers.

Based on the composition described above, both AAS pastes and mortars were prepared. In the case of the mortars, three different fractions of siliceous Czech standard sand (complying with ČSN EN 196-1) were used as a fine aggregate. The sand-to-binder ratio was 2:1. The water-to-binder ratio (w/b) was 0.35 for the pastes and 0.40 for the mortars. After the mixing, fresh material was cast into the steel molds and moist-cured for 24 h. After that, specimens were demolded and water- and/or air-cured until the time of testing (see following sections). Both mixing and curing was performed at laboratory temperature.

### 2.2. Drying Shrinkage Tests

Drying shrinkage tests were based on ASTM C596. After three days of water curing, mortar bars with dimensions of 25 mm × 25 mm × 285 mm were removed from water and air-cured at laboratory conditions, *i.e.*, relative humidity of approximately 50% and temperature of 23–25 °C, until the age of 28 days. During this period, relative length changes were measured almost every workday using the ASTM C490 apparatus. Three samples of each mixture were measured. For comparison, mortars with 0% and 1% of SRA were also water-cured until the age of 28 days and then the relative length changes during air-curing were measured.

### 2.3. Mechanical Strength Testing

Flexural strengths were tested on the mortar specimens with dimensions of 20 mm × 20 mm × 100 mm. Compressive strength tests were performed on the broken parts after the flexural strength tests. Only water-cured samples were used for the mechanical strength tests. These tests were performed at the age of 24 h, seven days and 28 days. Three prisms were used for every flexural strength test.

### 2.4. Isothermal Calorimetry

Influence of SRA on AAS hydration at 25 °C was investigated through isothermal conduction calorimetry. Slag and mixture of liquid components of the AAS paste were tempered separately inside the calorimeter, mixed together and mechanically stirred for three minutes. This *in situ* mixing enabled an immediate heat flow measurement.

### 2.5. Mercury Intrusion Porosimetry

MIP measurements were conducted on the paste samples containing 0% and 1% of SRA at the age of one, seven, 28 and 56 days. These pastes were moist-cured during the first 24 h and then cured immersed in water. Before the MIP testing, thin plates with dimensions of approximately 10 mm × 30 mm × 3 mm were sawed from inner parts of the 20 mm × 20 mm × 100 mm prisms and put into acetone in order to stop hydration until their drying and start of MIP measurement. Three such plates were used together for one measurement. Pore diameter in the range of 7 nm to 100 μm was calculated according to the Washburn equation [45] from the pressure required to intrude pores of a certain diameter. The contact angle between mercury and a pore wall was assumed to be 140° and the surface tension of mercury was assumed to be 480 mN/m.

### 2.6. Scanning Electron Microscopy

For the SEM observations in the secondary electron mode the same paste prisms with the same curing conditions as for the MIP measurements were prepared, but unlike the MIP measurements, SEM observations were performed on the fracture surfaces. An accelerating voltage of 10 kV was used. Broken parts of hardened pastes were immersed in acetone in order to stop hydration until the

time of testing. Then the samples were stuck on a carbon tape and the exposed fracture surfaces were sputter-coated with gold. SEM tests were performed at the age of 24 h, three, 14 and 28 days.

### 3. Results and Discussion

#### 3.1. Drying Shrinkage and Weight Loss

The drying shrinkage development depending on the mortar composition and the age of the samples at the end of water curing (four or 28 days) is presented in Figure 1a. It can be seen that SRA at the dosages of 0.25% and 0.50% did not markedly affect the drying shrinkage of the plain mortar (R), but when 1% of SRA was used, shrinkage was reduced by more than 80%. When more mature mortars were exposed to the atmospheric conditions, there was no difference between the drying shrinkage of the plain (R-28d) mortar and that containing 1% of SRA (SRA1.0-28d). This indicated that the beneficial effect of SRA on shrinkage diminished as the time of water curing increased. This may be related to the leaching of the SRA molecules during the water curing. The leaching phenomenon of SRA in OPC-based materials was widely studied by Eberhardt [46], where the vanishing of the beneficial effect of the SRA mobile fraction in the capillary range of humidity was observed. Also, the differences in microstructural development could be an issue, as will be discussed in Sections 3.4 and 3.5. A decrease in shrinkage of the reference mortar with a prolonged time of curing is in agreement with data summarized in [3] and is probably attributed to the maturity of the binder phase.

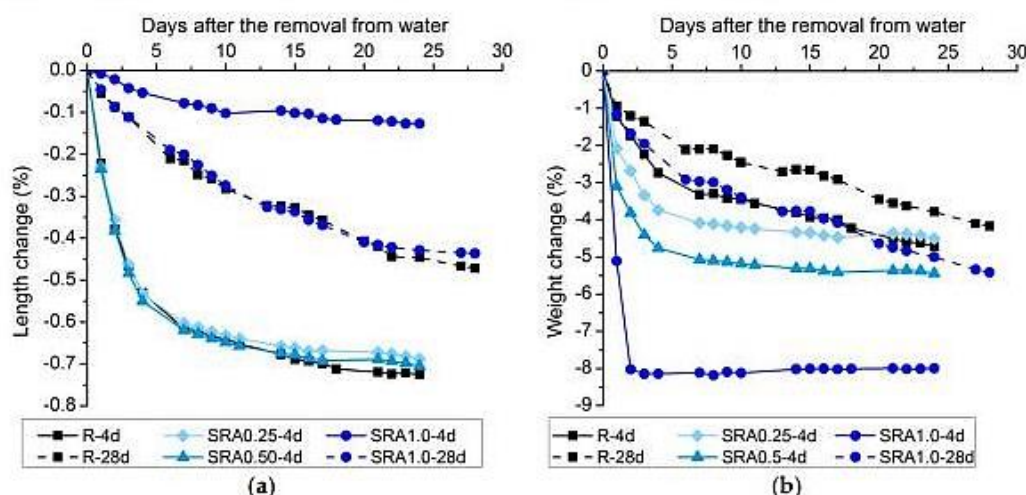


**Figure 1.** Effect of SRA on (a) drying shrinkage development and (b) weight loss development during drying of AAS mortars.

Figure 1b shows the effect of SRA on weight changes during drying. The increasing amount of SRA resulted in an increase in weight loss, especially during the initial stages of drying. When the length of water curing was increased, a lower weight loss was recorded for both the plain and the SRA mortar. The reason is a decrease in porosity and more water incorporated in a binder phase as a result of the proceeding hydration reactions. However, unlike similar shrinkage of these mortars after prolonged curing, the weight loss values of S1.0-28d mortar were significantly higher than those of the R-28d mortar. Higher weight losses of mortars with SRA than those without were observed also for OPC-based materials and this was explained by the lower liquid saturation for the same relative humidity induced by the SRA [47]. Contrary to this, Saliba *et al.* [38] observed lower mass loss during the drying of concrete with SRA compared to the concrete without, at least during the first 24 h. Unfortunately, there is a lack of information about the effect of SRAs on the weight loss of AAS in the literature to compare the obtained results. Nevertheless, as the chemical admixtures are usually

consumed during the proceeding hydration reactions, it is more likely that the difference after 28 days of water curing is a consequence of the different porosity of the binder phase. This is also in agreement with the decrease in strength and the increased volume of the intruding mercury for specimens with SRA, as will be shown further.

### 3.2. Flexural and Compressive Strength

The flexural strength development of the water-cured mortars is shown in Figure 2a. It is clear that even a low amount of SRA resulted in a significant decrease in the flexural strength. This effect increased with the increasing SRA dosage, especially at early ages. At the age of 28 days, all three SRA-containing mixtures showed similar flexural strengths whose values were about 30% lower than that of the reference mortar. For more precise results, more than three specimens of each series should be tested.

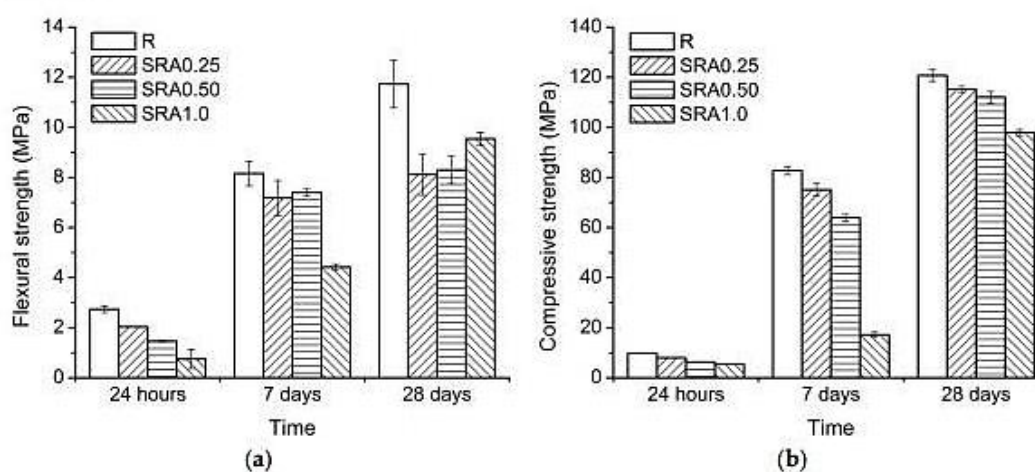


Figure 2. Effect of SRA on (a) flexural strength and (b) compressive strength development of AAS-based mortars; error bars correspond to a standard error of the mean.

As can be seen from Figure 2b, compressive strength values showed a similar trend as to what was observed for flexural strength development, *i.e.*, with an increasing amount of SRA the compressive strength decreased. This was recorded for all the tested series. While compressive strength development for the mortars with 0.25% and 0.50% of SRA had a comparable shape to the reference mortar, the SRA1.0 mortar showed a different rate of strength gain. For up to seven days, the SRA1.0 mortar had a very low compressive strength, but beyond this age, it had the highest strength gain of all the tested mortars, which may indicate that SRA caused some retardation during the hydration processes. We observed a similar effect on the compressive strength development of AABFS/FA mortars for the three different commercially available SRAs based on modified alcohols [48]. In order to investigate this feature, additional experimental methods, namely isothermal calorimetry, MIP and SEM, were applied.

### 3.3. Isothermal Calorimetry

The heat flow evolution curves for the plain and SRA-containing mortars are shown in Figure 3. Especially in the case of the plain slag paste curve, the typical shape for waterglass-activated slag was observed, as was schematically introduced by Shi and Day [49], *i.e.*, the initial peak was related to the particle wetting and slag dissolution as well as the additional initial peak was mainly associated with the primary C-S-H gel formation, both during the pre-induction period. Then several hours of the induction period followed, after which the acceleration/deceleration stage occurred, where massive

precipitation of the reaction products took place. In the presence of SRA, similar curves with some differences were recorded.

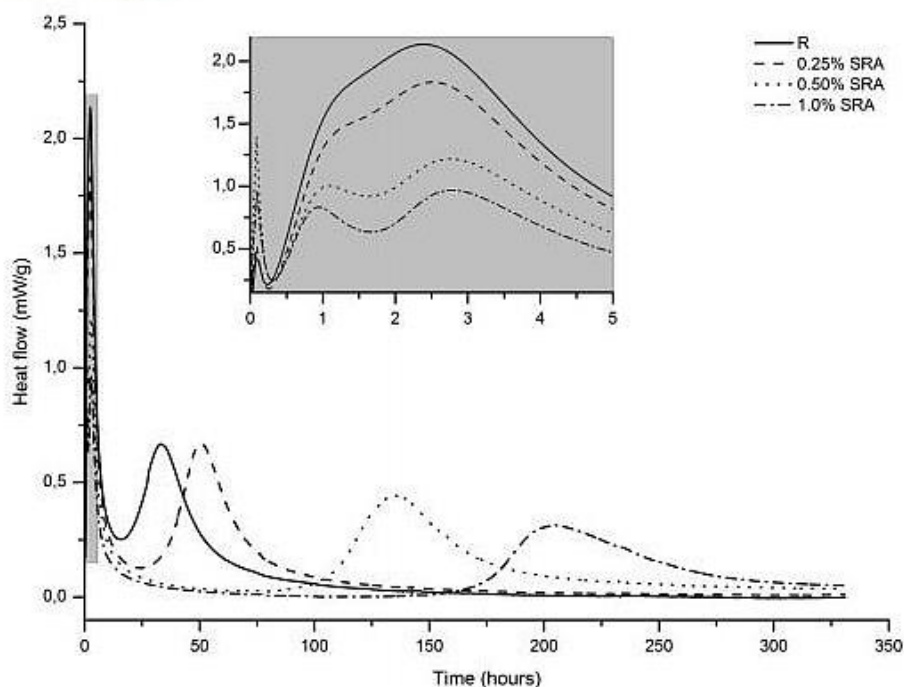


Figure 3. Effect of SRA on hydration heat evolution of AAS pastes.

Firstly, the initial peak seems to be more intense when the SRA is added, which might be caused by the interactions of the SRA molecules with the AAS system, e.g., the adsorption of SRA molecules onto the slag particles. However, the reproducibility of this peak is generally poor, which makes its interpretation uncertain. This is also probably the reason why the most intense peak was recorded for the paste with 0.5% of SRA.

Secondly, significant changes of the additional initial peak were observed. With the increasing SRA content, the overall intensity of this peak decreased, but what is even more interesting is that this peak was split into two partially mutually overlapping peaks with its maximums just before 1 and 3 h, respectively. For the plain slag paste curve, these peaks were merged into one peak, but even in this case two parts with different slopes of the increasing heat evolution rate are distinguishable. This could imply that the formation of the primary C–A–S–H gel proceeded in two steps, or some additional process occurred. Increasing the amount of SRA in the pastes made this observation more obvious and led even to the splitting of this peak into two partially separated peaks. To the best knowledge of the authors, this has not been reported yet and deserves further study.

Thirdly, the occurrence of the peak of the acceleration/deceleration stage is strongly affected by the dose of SRA. The higher the SRA portion, the more delayed this peak, which indicates a retardation effect of SRA on the AAS hydration. Moreover, the peak was wider and lower in magnitude when the dose of the SRA was increased, which could be due to the more developed surface layer of the reaction products on the slag grains and, consequently, the slower diffusion of pore solution species. A similar effect, although much less intense, was reported for slag systems activated with an increasing modulus of waterglass [50], *i.e.*, a decreasing alkalinity of the activating solution, but such a long induction period as in this case cannot be explained only by the very slight neutralization and therefore by the increase of the silicate modulus of the activating solution by the SRA (pH approx. 6.5). The reason for this could be some process occurring in the pre-induction period during or just after the mixing,

because further calorimetric response is significantly affected, the formation of the primary C–A–S–H gel is suppressed and the formation of the secondary C–A–S–H gel is delayed. The exact retardation mechanism deserves further study. A certain retardation effect of SRA based on polypropylene glycol on the hydration of waterglass-activated slag was reported Palacios and Puertas [42], but unlike the SRA used in the present study, their SRA delayed the main hydration peak only by several hours. It also seems that increasing the dose of their SRA resulted in the more intense second peak in the pre-induction period, while in the present study SRA had the opposite effect. Therefore, two different SRAs may affect AAS hydration in a completely different manner.

The retardation effect of SRA on AAS hydration is also evident from Figure 4, which shows the cumulative heat release of the evaluated pastes. Although during the first days of hydration the highest amount of the heat released was recorded for the pure slag paste, the total heat release increased in the presence of the SRA. This indicates that after the retardation, hydration reactions can continue to an even greater extent than for the pure slag paste. Nevertheless, the strengths measured up to 28 days of hydration were still significantly lower when SRA was added to the slag paste.

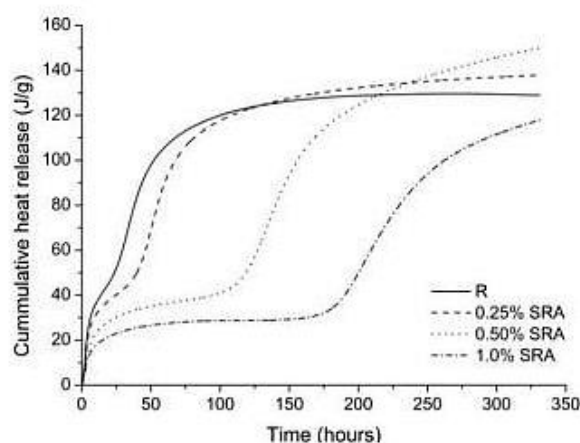


**Figure 4.** Effect of SRA on the total heat released during the hydration of AAS pastes.

The action of chemical admixtures can be negatively affected by the high pH in AAS, as was proved by Palacios and Puertas [13], particularly for superplasticizers. On the other hand, this was not the case for the SRA in their study. Also, the SRA used in this study would be stable in a highly alkaline environment, but the deprotonation of its hydroxyl groups as a consequence of high pH can be expected, despite the glycols belonging to the non-ionic surfactants [47]. Therefore, one cannot exclude the adverse effect of SRA on AAS properties resulting from either possible adsorption on solid particles or interactions with the dissolved species present in AAS pore solution.

### 3.4. Mercury Intrusion Porosimetry

Since there are serious limiting factors in cementitious systems for the use of the Washburn equation adopted for the pore size distribution calculations, particularly the inaccessibility of all the pores for mercury, MIP cannot provide realistic pore size distribution determination [51]. However, it can give us interesting information about the size of the pores (threshold diameter), which interconnect larger pores throughout the matrix. The threshold pore diameter is related to the permeability and diffusion characteristics of the material and thus may affect its durability [52].

Differential intrusion curves obtained for the reference paste and the paste containing 1% of SRA after the different hydration times are shown in Figure 5. A great difference between the pore structures of these two mortars can be observed, particularly at the early ages: the threshold diameter of the reference paste after 24 h (approx. 70 nm) was much lower than that of the SRA

paste (more than 1  $\mu\text{m}$ ). Similarly, after seven days the SRA paste still exhibited the net of relatively large pores, while significant mercury intrusion into the pure slag paste was recorded only for pores corresponding to a pore diameter lower than 20 nm. At later ages, the reference and SRA pastes' intrusion curves resemble each other more. This could be a consequence of the proceeding of retarded hydration reactions as was shown in the previous section and also of the gradual leaching of SRA, as the specimens were cured in water. For both pastes no intrusion was observed after the 56 days, indicating pore system refinement beyond the measurability range of MIP. Also pore blockage, as a consequence of the hydration products' growth, may affect the volume of the intruded mercury.

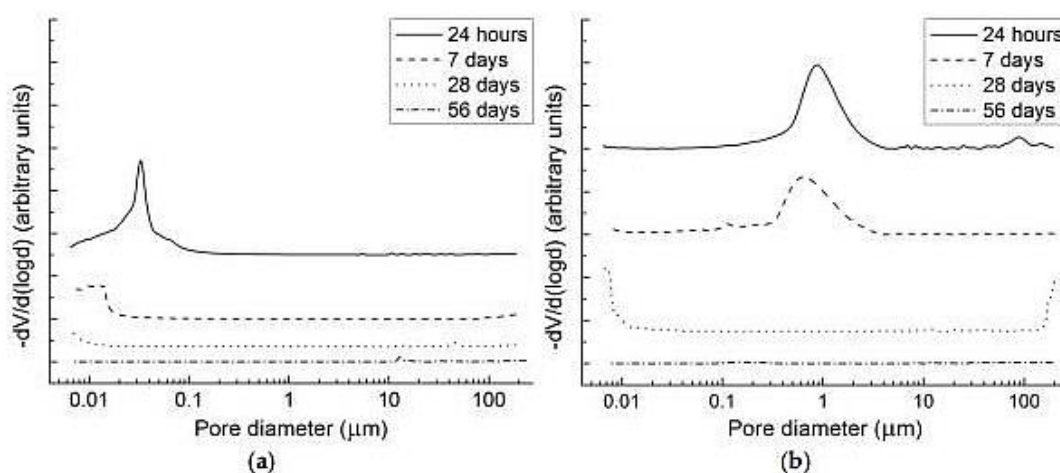


**Figure 5.** MIP curves showing the effect of SRA on pore structure development: (a) pure AAS paste; (b) AAS paste with 1% of SRA.

Such high differences between the intrusion curves of the studied pastes during the first several days of hydration proved that the presence of 1% SRA caused the retardation of the hydration products' formation and thus slowed down the pore structure refinement. Therefore, if these pastes or mortars are exposed to dry ambient conditions without sufficient length of the curing stage, they start to dry rapidly and are not able to fully hydrate. This is the main reason for such an intense weight loss of SRA1.0 mortar during drying as presented in Section 3.1. The coarser pore structure of SRA1.0 specimens compared to those without SRA led to a modified weight loss development, with accelerated weight loss rate during the first days of drying. A slight increase in weight beyond the third day of dry air exposure is probably caused by the intense carbonation which was, together with the relatively low strengths of these air-stored specimens, presented in [53]. The importance of the pore size distribution for drying shrinkage was emphasized by Collins and Sanjayan [18] and it can thus be concluded that the great reduction of drying shrinkage induced by 1% of SRA is attributed to coarser pores, where the shrinkage forces are not so high. Puertas and Palacios [42] also explained the beneficial effect of SRA based on polypropylene glycol on shrinkage with the pore structure redistribution, but as they stated, it was "due to the decrease of the capillary stress of the water that SRA induces during the mixing process". This is the difference between their study and the present one, where the SRA induced changes in the pore structure primarily by the retardation of hydration.

### 3.5. Scanning Electron Microscopy

The data obtained from the previously described methods are in a good agreement with the results from SEM presented in Figure 6. Microstructural development of the pastes with 0% and 1% of SRA was investigated. After the 24 h of hydration, the reference mortar showed a relatively dense matrix surrounding the slag grains, while in the case of SRA-containing paste only surface reacted

separate slag grains were observed. After three days, the situation was very similar to that after 24 h, *i.e.*, dense C–A–S–H gel formed in the plain paste in contrast with the porous structure and practically unreacted slag grains. The situation of the SRA paste at the ages of 14 and 28 days was completely different, where its microstructure was the same as that of the paste with no SRA addition. This agrees well with the experimental data either from the strength testing or calorimetry or MIP measurements.

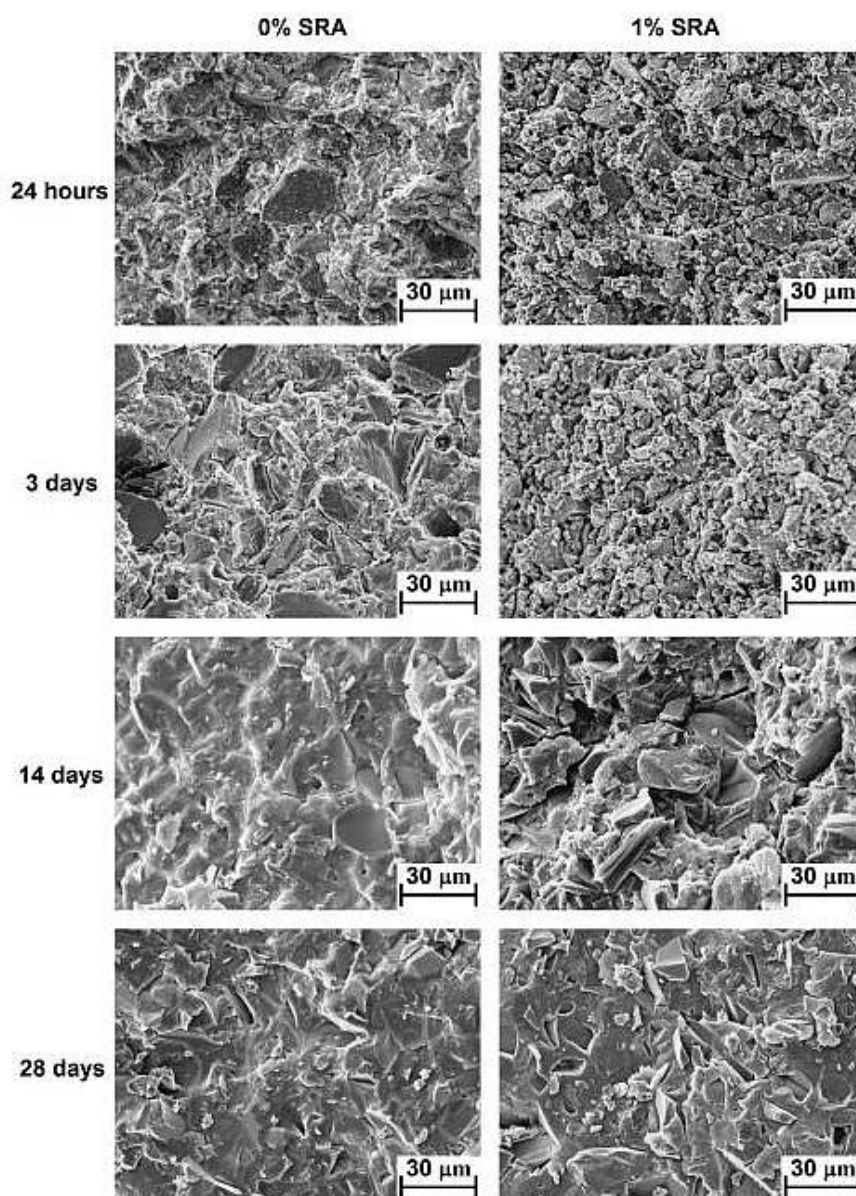


Figure 6. SEM image showing the effect of SRA on the microstructure development of AAS paste.

#### 4. Conclusions

This study investigated the effect of SRA based on 2-methy-2,4-pentanediol on the mechanical properties, drying shrinkage and microstructure development of waterglass-activated slag ( $M_s = 1.85$ ,  $Na_2O/slag = 0.04$ ).

It was found that the SRA greatly influenced the course of hydration of the studied AAS system. An increase of the SRA content resulted in a reduction and bisection of the second peak on the calorimetric curve and also in a delayed occurrence of the main hydration peak.

This was observed as flexural and compressive strength reduction, increased weight loss during drying and coarser porosity of mixtures with the SRA when compared to the mixtures without the SRA, particularly during the first several days of hydration. This is also probably the main reason for such a high shrinkage reduction recorded for mortar with 1% of SRA exposed to the dry environment four days after mixing, *i.e.*, before reaching the proper degree of hydration.

**Acknowledgments:** This work was financially supported by the project: Materials Research Centre at FCH BUT- Sustainability and Development, REG LO1211, with financial support from the National Programme for Sustainability I (Ministry of Education, Youth and Sports).

**Author Contributions:** Vlastimil Bílek Jr. and Lukáš Kalina conceived and designed the experiments; Vlastimil Bílek Jr. performed the strength and shrinkage tests; Radoslav Novotný performed the calorimetry experiments; Jakub Tkacz performed the SEM observations; Ladislav Pařezek provided MIP experiments; Vlastimil Bílek Jr. wrote the paper.

**Conflicts of Interest:** The authors declare no conflict of interest.

## Abbreviations

The following abbreviations are used in this manuscript:

AAS	Alkali activated slag
AABFS/FA	alkali activated blend of BFS and FA
BFS	Blast furnace slag
C-S-H	Calcium-silicate-hydrate
C-A-S-H	Calcium-aluminate-silicate-hydrate
FA	Fly ash
MIP	Mercury intrusion porosimetry
OPC	Ordinary Portland cement
SRA	Shrinkage reducing admixture
SEM	Scanning electron microscopy

## References

1. Aitcin, P.-C.; Mindess, S. *Sustainability of Concrete*; Spon Press: New York, NY, USA, 2011.
2. Juenger, M.; Winnefeld, F.; Provis, J.L.; Ideker, J. Advances in alternative cementitious binders. *Cem. Concr. Res.* **2011**, *41*, 1232–1243. [CrossRef]
3. Provis, J.L.; van Deventer, J.S.J. *Alkali Activated Materials*; Springer: Dordrecht, The Netherlands, 2014.
4. Duxson, P.; Provis, J.L.; Lukey, G.C.; van Deventer, J.S. The role of inorganic polymer technology in the development of 'green concrete'. *Cem. Concr. Res.* **2007**, *37*, 1590–1597. [CrossRef]
5. Collins, F.; Sanjayan, J. Workability and mechanical properties of alkali activated slag concrete. *Cem. Concr. Res.* **1999**, *29*, 455–458. [CrossRef]
6. Bakharev, T.; Sanjayan, J.; Cheng, Y.-B. Resistance of alkali-activated slag concrete to acid attack. *Cem. Concr. Res.* **2003**, *33*, 1607–1611. [CrossRef]
7. Bakharev, T.; Sanjayan, J.; Cheng, Y.-B. Sulfate attack on alkali-activated slag concrete. *Cem. Concr. Res.* **2002**, *32*, 211–216. [CrossRef]
8. Bernal, S.A.; Rodríguez, E.D.; de Gutiérrez, R.M.; Provis, J.L. Performance of alkali-activated slag mortars exposed to acids. *J. Sustain. Cem. Based Mater.* **2012**, *1*, 138–151. [CrossRef]
9. Wang, W.-C.; Wang, H.-Y.; Lo, M.-H. The engineering properties of alkali-activated slag pastes exposed to high temperatures. *Constr. Build. Mater.* **2014**, *68*, 409–415. [CrossRef]
10. Guerrieri, M.; Sanjayan, J.; Collins, F. Residual compressive behavior of alkali-activated concrete exposed to elevated temperatures. *Fire Mater.* **2009**, *33*, 51–62. [CrossRef]
11. Guerrieri, M.; Sanjayan, J.; Collins, F. Residual strength properties of sodium silicate alkali activated slag paste exposed to elevated temperatures. *Mater. Struct.* **2010**, *43*, 765–773. [CrossRef]
12. San Nicolas, R.; Bernal, S.A.; de Gutiérrez, R.M.; van Deventer, J.S.; Provis, J.L. Distinctive microstructural features of aged sodium silicate-activated slag concretes. *Cem. Concr. Res.* **2014**, *65*, 41–51. [CrossRef]

13. Palacios, M.; Puertas, F. Effect of superplasticizer and shrinkage-reducing admixtures on alkali-activated slag pastes and mortars. *Cem. Concr. Res.* **2005**, *35*, 1358–1367. [CrossRef]
14. Kashani, A.; Provis, J.L.; Xu, J.; Kilcullen, A.R.; Qiao, G.G.; van Deventer, J.S. Effect of molecular architecture of polycarboxylate ethers on plasticizing performance in alkali-activated slag paste. *J. Mater. Sci.* **2014**, *49*, 2761–2772. [CrossRef]
15. Palacios, M.; Puertas, F. Effectiveness of mixing time on hardened properties of waterglass-activated slag pastes and mortars. *ACI Mater. J.* **2011**, *108*, 73.
16. Collins, F.; Sanjayan, J. Cracking tendency of alkali-activated slag concrete subjected to restrained shrinkage. *Cem. Concr. Res.* **2000**, *30*, 791–798. [CrossRef]
17. Shi, C.; Krivenko, P.V.; Roy, D. *Alkali-Activated Cements and Concretes*; Taylor & Francis: London, UK, 2006.
18. Collins, F.; Sanjayan, J. Effect of pore size distribution on drying shrinking of alkali-activated slag concrete. *Cem. Concr. Res.* **2000**, *30*, 1401–1406. [CrossRef]
19. Krizan, D.; Zivanovic, B. Effects of dosage and modulus of water glass on early hydration of alkali-slag cements. *Cem. Concr. Res.* **2002**, *32*, 1181–1188. [CrossRef]
20. Neto, A.A.M.; Cincotto, M.A.; Repette, W. Drying and autogenous shrinkage of pastes and mortars with activated slag cement. *Cem. Concr. Res.* **2008**, *38*, 565–574. [CrossRef]
21. Lee, N.; Jang, J.; Lee, H. Shrinkage characteristics of alkali-activated fly ash/slag paste and mortar at early ages. *Cem. Concr. Compos.* **2014**, *53*, 239–248. [CrossRef]
22. Scherer, G.W. Drying, shrinkage, and cracking of cementitious materials. *Transp. Porous Media* **2015**, *110*, 311–331. [CrossRef]
23. Aydin, S. A ternary optimisation of mineral additives of alkali activated cement mortars. *Constr. Build. Mater.* **2013**, *43*, 131–138. [CrossRef]
24. Bilek, V.; Parizek, L.; Kalina, L. Effect of the by-pass cement kiln dust and fluidized bed combustion fly ash on properties of fine-grained alkali-activated slag-based composites. *Mater. Tehnol.* **2015**, *49*, 549–552. [CrossRef]
25. Chi, M.; Huang, R. Binding mechanism and properties of alkali-activated fly ash/slag mortars. *Constr. Build. Mater.* **2013**, *40*, 291–298. [CrossRef]
26. Marjanović, N.; Komljenović, M.; Bašćarević, Z.; Nikolić, V.; Petrović, R. Physical-mechanical and microstructural properties of alkali-activated fly ash-blast furnace slag blends. *Ceram. Int.* **2015**, *41*, 1421–1435. [CrossRef]
27. Bakharev, T.; Sanjayan, J.; Cheng, Y.-B. Effect of elevated temperature curing on properties of alkali-activated slag concrete. *Cem. Concr. Res.* **1999**, *29*, 1619–1625. [CrossRef]
28. Aydin, S.; Baradan, B. Mechanical and microstructural properties of heat cured alkali-activated slag mortars. *Mater. Des.* **2012**, *35*, 374–383. [CrossRef]
29. Chi, M. Effects of dosage of alkali-activated solution and curing conditions on the properties and durability of alkali-activated slag concrete. *Constr. Build. Mater.* **2012**, *35*, 240–245. [CrossRef]
30. Sakulich, A.; Bentz, D. Mitigation of autogenous shrinkage in alkali activated slag mortars by internal curing. *Mater. Struct.* **2013**, *46*, 1355–1367. [CrossRef]
31. Aydin, S.; Baradan, B. The effect of fiber properties on high performance alkali-activated slag/silica fume mortars. *Compos. Part B Eng.* **2013**, *45*, 63–69. [CrossRef]
32. Alcaide, J.; Alcocel, E.; Puertas, F.; Lapuente, R.; Garcés, P. Carbon fibre-reinforced, alkali-activated slag mortars. *Mater. Constr.* **2007**, *57*, 33–48.
33. Puertas, F.; Gil-Maroto, A.; Palacios, M.; Amat, T. Alkali-activated slag mortars reinforced with ar glassfibre. Performance and properties. *Mater. Constr.* **2006**, *56*, 79–90.
34. Shen, W.G.; Wang, Y.H.; Zhang, T.; Zhou, M.K.; Li, J.S.; Cui, X.Y. Magnesia modification of alkali-activated slag fly ash cement. *J. Wuhan Univ. Technol. Mater. Sci. Ed.* **2011**, *26*, 121–125. [CrossRef]
35. Yuan, X.-H.; Chen, W.; Lu, Z.-A.; Chen, H. Shrinkage compensation of alkali-activated slag concrete and microstructural analysis. *Constr. Build. Mater.* **2014**, *66*, 422–428. [CrossRef]
36. Chang, J.J.; Yeih, W.; Hung, C.C. Effects of gypsum and phosphoric acid on the properties of sodium silicate-based alkali-activated slag pastes. *Cem. Concr. Compos.* **2005**, *27*, 85–91. [CrossRef]
37. Rajabipour, F.; Sant, G.; Weiss, J. Interactions between shrinkage reducing admixtures (sra) and cement paste's pore solution. *Cem. Concr. Res.* **2008**, *38*, 606–615. [CrossRef]

38. Saliba, J.; Roziere, E.; Grondin, F.; Loukili, A. Influence of shrinkage-reducing admixtures on plastic and long-term shrinkage. *Cem. Concr. Compos.* **2011**, *33*, 209–217. [CrossRef]
39. Bian, R.; Jian, S. Synthesis and evaluation of shrinkage-reducing admixture for cementitious materials. *Cem. Concr. Res.* **2005**, *35*, 445–448.
40. Folliard, K.J.; Berke, N.S. Properties of high-performance concrete containing shrinkage-reducing admixture. *Cem. Concr. Res.* **1997**, *27*, 1357–1364. [CrossRef]
41. Sant, G.; Lothenbach, B.; Juilland, P.; Le Saout, G.; Weiss, J.; Scrivener, K. The origin of early age expansions induced in cementitious materials containing shrinkage reducing admixtures. *Cem. Concr. Res.* **2011**, *41*, 218–229. [CrossRef]
42. Palacios, M.; Puertas, F. Effect of shrinkage-reducing admixtures on the properties of alkali-activated slag mortars and pastes. *Cem. Concr. Res.* **2007**, *37*, 691–702. [CrossRef]
43. Bilim, C.; Karahan, O.; Atis, C.D.; Ilkentapar, S. Influence of admixtures on the properties of alkali-activated slag mortars subjected to different curing conditions. *Mater. Des.* **2013**, *44*, 540–547. [CrossRef]
44. Bakharev, T.; Sanjayan, J.G.; Cheng, Y.B. Effect of admixtures on properties of alkali-activated slag concrete. *Cem. Concr. Res.* **2000**, *30*, 1367–1374. [CrossRef]
45. Abell, A.B.; Willis, K.L.; Lange, D.A. Mercury intrusion porosimetry and image analysis of cement-based materials. *J. Colloid Interface Sci.* **1999**, *211*, 39–44. [CrossRef] [PubMed]
46. Eberhardt, A.B. On the Mechanisms of Shrinkage Reducing Admixtures in Self Consolidating Mortars and Concretes. Ph.D. Thesis, Bauhaus Universität Weimar, Weimar, Germany, 2011.
47. Aïtcin, P.C.; Flatt, R.J. *Science and Technology of Concrete Admixtures*; Woodhead Publishing: Sawston, Cambridge, UK, 2015.
48. Bílek, V., Jr.; Kalina, L.; Koplík, J.; Hajdúchová, M.; Radoslav, N. Effect of combination of fly ash and shrinkage reducing additives on properties of alkali activated slag based mortars. *Mater. Tehnol.* **2016**. in press.
49. Shi, C.J.; Day, R.L. A calorimetric study of early hydration of alkali-slag cements. *Cem. Concr. Res.* **1995**, *25*, 1333–1346. [CrossRef]
50. Ravikumar, D.; Neithalath, N. Reaction kinetics in sodium silicate powder and liquid activated slag binders evaluated using isothermal calorimetry. *Thermochim. Acta* **2012**, *546*, 32–43. [CrossRef]
51. Diamond, S. Mercury porosimetry—an inappropriate method for the measurement of pore size distributions in cement-based materials. *Cem. Concr. Res.* **2000**, *30*, 1517–1525. [CrossRef]
52. Cook, R.A.; Hover, K.C. Mercury porosimetry of hardened cement pastes. *Cem. Concr. Res.* **1999**, *29*, 933–943. [CrossRef]
53. Bulejko, P.; Bílek, V., Jr. Influence of chemical additives and curing conditions on mechanical properties and carbonation resistance of alkali-activated slag composites. *Mater. Tehnol.* **2017**. in press.



© 2016 by the authors; licensee MDPI, Basel, Switzerland. This article is an open access article distributed under the terms and conditions of the Creative Commons Attribution (CC-BY) license (<http://creativecommons.org/licenses/by/4.0/>).

Article

## Effect of Na<sub>3</sub>PO<sub>4</sub> on the Hydration Process of Alkali-Activated Blast Furnace Slag

Lukáš Kalina \*, Vlastimil Bílek Jr., Radoslav Novotný, Miroslava Mončeková, Jiří Másilko and Jan Koplík

Materials Research Centre, Faculty of Chemistry, Brno University of Technology, Brno 612 00, Czech Republic; bilek@fch.vut.cz (V.B.J.); xcnovotny2@fch.vut.cz (R.N.); xcmoncekova@fch.vut.cz (M.M.); masilko@fch.vut.cz (J.M.); koplík@fch.vut.cz (J.K.)

\* Correspondence: kalina@fch.vutbr.cz; Tel.: +420-54-114-9366

Academic Editor: Claudio Ferone

Received: 13 April 2016; Accepted: 17 May 2016; Published: 20 May 2016

**Abstract:** In recent years, the utilization of different non-traditional cements and composites has been increasing. Alkali-activated cementitious materials, especially those based on the alkali activation of blast furnace slag, have considerable potential for utilization in the building industry. However, alkali-slag cements exhibit very rapid setting times, which are too short in some circumstances, and these materials cannot be used for some applications. Therefore, it is necessary to find a suitable retarding admixture. It was shown that the sodium phosphate additive has a strong effect on the heat evolution during alkali activation and effectively retards the hydration reaction of alkali-activated blast furnace slag. The aim of the work is the suggestion of a reaction mechanism of retardation mainly based on Raman and X-ray photoelectron spectroscopy.

**Keywords:** alkali activated cement; granulated blast furnace slag; retardation

### 1. Introduction

In recent years, a diverse selection of admixtures has been used to retard the setting in alkali-activated cements, although their activity varies substantially [1]. The research was initially focused on the retardants commonly used for Portland cement. Wu *et al.* [2] observed that potassium or sodium tartrate did not show any effect on the initial setting time, but slightly shortened the final setting time. The use of borates as retardants for Portland cement is also very well known. However, Nicholson *et al.* [3] reported that borates added to alkali-activated fly ash (class C) did not influence the setting behavior; conversely, the strength of the binders was negatively affected by a high amount of borates. Some admixtures used as setting accelerators in Portland cement systems have the opposite effect when used in alkali-activated materials. Brought *et al.* [4] investigated that the addition of NaCl significantly retarded both setting and strength development at high levels, but at low addition levels, *i.e.*, 4% or less by weight of slag, NaCl acted as an accelerator. Another possibility is the usage of phosphoric acid or its salts. Chang *et al.* [5] concluded that using solely phosphoric acid increased the setting time, but reduced the compressive strength at an early age. Gong and Yang [6] observed the strong retardant effect of sodium phosphate on alkali-activated red mud slag cementitious material. However, Shi and Li [7] found no retardation effect of Na<sub>3</sub>PO<sub>4</sub> on alkali-activated phosphorus slag. From the published studies it is thus apparent that the nature and dosage of added admixtures and also the types of activated raw materials have a significant effect on the retardation of the setting process of the alkali-activated materials.

Unfortunately, the reaction mechanism of the retarding admixtures has not fully been explained [1]. Lee and Deventer [8] tried to suggest the hydration kinetics of PO<sub>4</sub><sup>3-</sup> in fly ash-based alkali-activated materials. They assumed that phosphate anions have strong affinities to Ca<sup>2+</sup> cations. The value of the

solubility product equilibrium constant for  $\text{Ca}(\text{OH})_2$  is very low ( $\text{p}K_{\text{sp}} = 5.26$ ); therefore, dissolved calcium cations from fly ash precipitated as  $\text{Ca}_{10}(\text{PO}_4)_6(\text{OH})_2$  (hydroxyapatite) instead of  $\text{Ca}(\text{OH})_2$ . On the other hand, Shi and Day indicate a different reaction mechanism [9] in alkali-activated blast furnace slag. From their study it seems that the formation of  $\text{Ca}_3(\text{PO}_4)_2$  retards the activation of slag as usually observed during the hydration of Portland cement. It is obvious that the final reaction products from the retardation process depend on used raw materials but the detailed action of phosphate in alkali-activated systems remains unclear.

The current study presents the possibilities of using sodium phosphate as an effective retardant for alkali-activated blast furnace slag-based materials and clearly explains the retarding effect which is described in more detail compared to the other published reaction mechanisms.

## 2. Materials and Methods

### 2.1. Materials and Sample Preparation

Blast furnace slag (BFS) obtained from ArcelorMittal Ostrava, Inc. (Ostrava, Czech Republic) ironworks was used as the raw material. The chemical composition of BFS determined by X-ray fluorescence spectroscopy (XRF) is given in Table 1. The phase composition of BFS measured by powder X-ray diffraction (XRD) revealed the presence of merwinite, melilite,  $\beta\text{-C}_2\text{S}$  and calcite. Water glass (molar ratio of  $\text{SiO}_2/\text{Na}_2\text{O} = 2.00$ ) used as an alkali activator was produced by Vodní Sklo, Inc. (Brno, Czech Republic). Sodium phosphate (SP) additive was obtained from Sigma-Aldrich (St. Louis, MO, USA).

Table 1. Chemical composition of used BFS as determined by XRF.

Raw Material	Chemical Composition wt %									
BFS	$\text{SiO}_2$	$\text{Al}_2\text{O}_3$	$\text{CaO}$	$\text{Na}_2\text{O}$	$\text{K}_2\text{O}$	$\text{MgO}$	$\text{SO}_3$	$\text{Fe}_2\text{O}_3$	$\text{TiO}_2$	$\text{MnO}$
	34.7	9.1	41.1	0.4	0.9	10.5	1.4	0.3	1.0	0.6

Alkali-activated samples were made by mixing water and water glass solution with the mixture of BFS and specific addition of sodium phosphate (recalculated to wt % of  $\text{P}_2\text{O}_5$  contained in SP) for three minutes to produce homogenous pastes. Individual additions of SP were 0.5, 1.0, 2.5 and 5.0 wt % of  $\text{P}_2\text{O}_5$  in sodium phosphate calculated on BFS content. The water glass solution and BFS ratio was set to 0.25 for all samples and the additional water was always mixed with water glass in the constant weight ratio 1:1. These pastes were cast into the polystyrene crucibles covered with teflon foil to prevent drying of the system. The specific quantity of the samples with the addition of SP was then taken in times defined by the microcalorimeter results, the hydration was then quenched by acetone and subsequently subjected to Raman and XPS spectroscopy. Due to the high amount of amorphous phase in the samples the usage of powder X-ray diffraction as common silicate analytical technique was not satisfactory.

### 2.2. Physical-Mechanical Tests

Initial setting time was determined according to the standard procedure ČSN EN 196-3 using Vicat's device. Compressive strength tests were based on ČSN EN 196-1 and were carried out by means of compressive and bending strength on tester Desttest 3310 (Betonsystem Ltd., Brno, Czech Republic). The strengths were tested at the age of one, seven and 28 days. The workability of fresh mortars was measured using a flow table spread test (ČSN EN 1015-3). The diameter was measured in four directions after 15 blows with the jolting table. The final value was the arithmetic mean of these measurements.

### 2.3. Heat Evolution Rates Measurement

The evolution of hydration heat was monitored by means of TAM Air isothermal calorimeter (TA instruments, Wetzlar, Germany). The test samples of BFS and sodium phosphate were weighted and uniformly distributed to the glass-closed ampules (15 mL). The solution of water and alkali activator was weighted in a syringe. The water ratio was the same as in the preparation process of pastes and the mass of slag was 4 g. The measurements of heat evolution were performed at constant temperature of  $25\text{ °C} \pm 0.02\text{ °C}$ . The samples with BFS and SP as well as the syringe with the activator and water were heated to testing temperature prior to mixing in the admix ampule directly in the calorimeter. When the thermal equilibrium was achieved, BFS with SP and alkali activator were mixed by injecting the solution into the ampule. The time of mixing was three minutes. The heat evolution was recorded as the heat flow (mW/g).

### 2.4. Raman Spectroscopy

Raman scattering measurements were performed using Nanofinder S micro-Raman spectrometer (SOL instruments, Minsk, Belarus) equipped with a confocal microscope (Nikon, Amsterdam, The Netherlands). The Raman scattering spectra were excited by 633 nm with 10 mW power. The system was calibrated on silicon ( $518.2\text{ cm}^{-1}$ ). The beam was focused on the samples with a  $20\times$  microscope objective with a numerical aperture of 0.45. The exposure time was 100 s and 600 grating with  $2.7\text{ cm}^{-1}$  resolution. All measurements were performed at room temperature in ambient atmosphere.

### 2.5. X-ray Photoelectron Spectroscopy

X-ray photoelectron spectroscopy (XPS) were carried out with Axis Ultra DLD spectrometer (Kratos Analytical Ltd., Manchester, UK) using a monochromatic Al  $K\alpha$  ( $h\nu = 1486.7\text{ eV}$ ) X-ray source operating at 150 W (10 mA, 15 kV). The spectra were obtained using an analysis area of  $\sim 300 \times 700\text{ }\mu\text{m}$ . The Kratos charge neutralizer system (Kratos Analytical Ltd., Manchester, UK) was used for all analyses. High resolution spectra were measured with the step size 0.1 eV and 20 eV pass energy. Instrument base pressure was  $2 \cdot 10^{-8}\text{ Pa}$ . The spectra were analyzed using CasaXPS software (version 2.3.15) and charge corrected to the main line of the carbon C 1s spectral component (C–C, C–H) set to 284.80 eV. A standard Shirley background was used for all sample spectra.

## 3. Results and Discussion

### 3.1. Physical-Mechanical Properties

The influence of different additions of sodium phosphate is shown in Figure 1. Both initial and final setting time were prolonged with the sodium phosphate content but only to a certain limit of  $\text{P}_2\text{O}_5$  content (Figure 1a). The maximum of retardation is observed for the content of 2.5 wt % of  $\text{P}_2\text{O}_5$ ; above that value, the time of setting is shortened, and therefore this content was chosen for further study of the reaction mechanism via Raman and XPS analyses. In general, the addition of SP considerably delays the initial time of setting which has been already verified in previous studies [5–8].

The workability determination of the flow table spread test is shown in Figure 1b. The workability gradually decreased with the higher content of SP. With respect to the initial and final setting time measurement, the reason of the workability decline is not related to the formation of the binder phase but is caused by the loss of mixing water which is very quickly bonded to the created phosphate hydrates, as verified by Raman spectroscopy.

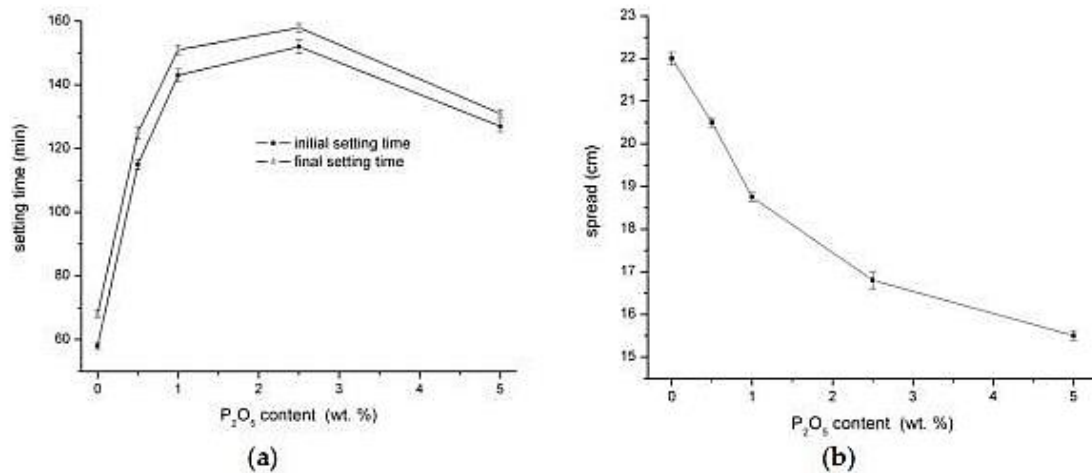


**Figure 1.** Influence of  $Na_3PO_4$  on the initial and final setting time (a) and workability (b) of alkali-activated BFS.

The compressive strength development is shown in the Figure 2. The early strengths of samples with the addition of SP are slightly lower compared to the reference sample. This effect is probably connected to the secondary formation of CSH gel. The formation of secondary CSH gel in the reference sample starts to increase earlier, which positively affects the mechanical properties after one day (Figure 3). After seven days, the obvious trend of lower compressive strength with the greater addition of SP is observed. The addition of SP decreases the secondary formation of CSH gel which is well correlated with the heat evolution in Figure 3. However, after 28 days, the samples with a lower addition of SP (0.5 and 1.0 wt %) showed higher compressive strength compared to the reference sample. This beneficial strength development could play an important role in the production of alkali-activated materials, because the lower SP content (up to 1.0 wt %) significantly retards the initial and final setting time, and it also slightly worsens the workability but improves the final mechanical properties.

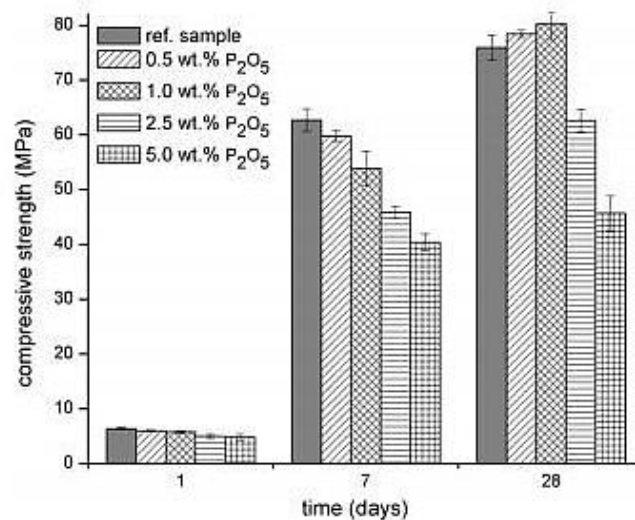


**Figure 2.** Influence of  $Na_3PO_4$  on the compressive strength development of alkali-activated BFS.

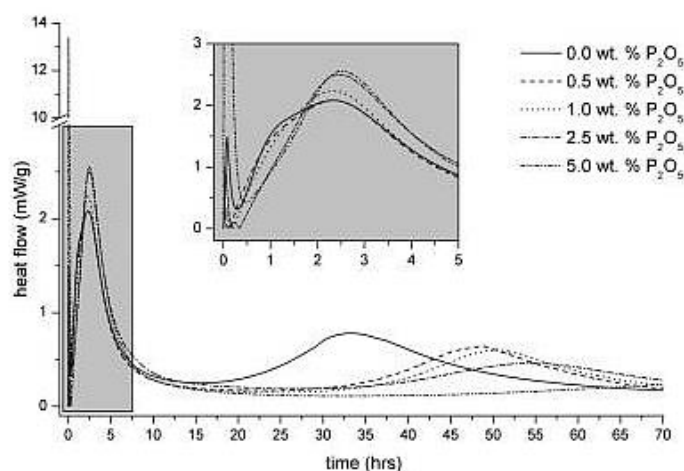


Figure 3. Influence of  $\text{Na}_3\text{PO}_4$  on the initial setting of alkali-activated BFS.

### 3.2. Heat Evolution

The hydration heat evolution of alkali activated BFS without or with the specific addition of  $\text{P}_2\text{O}_5$  contained in SP is shown in Figure 3. The first peak is associated with wetting and dissolution of slag and phosphates particles as well as with the formation of sodium phosphate hydrates. The second peak is mainly connected with the formation of primary CSH gel through the reaction of  $\text{SiO}_4^{4-}$  from water glass and  $\text{Ca}^{2+}$  dissolved from the surface of slag grains. In this hydration period, the effect of the added sodium phosphate is also reflected. The total heat evolution values corresponding to the second peak increase with the greater addition of SP, which can be attributed to the formation of new hydrogen phosphate phases as discussed further. Finally, the third peak belongs to the secondary formation of CSH gel. It is evident that the hydration reactions start earlier in pure alkali-activated BFS systems than in the case of alkali-activated slag with a retardant admixture. The calorimetry results clearly show that the heat evolution changes with the addition of sodium phosphates. Unfortunately, it is not possible to explain the reaction mechanism only from thermocalorimetric curves because the released heats connected with the formation of different phases (CSH gel, calcium phosphates and phosphate hydrates) are overlapped. Therefore, the employment of suitable testing methods, such as the combination of Raman spectroscopy and X-ray photoelectron spectroscopy, is needed. Due to the high amount of amorphous phase in the samples, these methods are most appropriate for the study of the reaction mechanism of the phosphate additive in alkali-activated binders.

### 3.3. Raman Spectroscopy

The Raman investigations show five spectra at various times of alkali activation (Figure 4). The first spectrum, 30 min after mixing, reveals the characteristic band at  $930\text{ cm}^{-1}$  corresponding to the symmetric stretching vibration  $\nu_1(\text{A}_1)$  of tetrahedral  $\text{PO}_4^{3-}$  [10,11]. All spectra show the presence of  $\text{Na}_3\text{PO}_4$  hydrates. This hydration process of  $\text{Na}_3\text{PO}_4 \cdot x\text{H}_2\text{O}$  is connected with the decrease in the asymmetric stretching mode around  $1078\text{ cm}^{-1}$   $\nu_3(\text{F}_2)$ , which presents the distortion of symmetry of  $\text{PO}_4^{3-}$  in the crystal structure. The shoulder at  $\sim 900\text{ cm}^{-1}$  indicates the changes in the symmetry site of the  $\text{PO}_4^{3-}$  characteristic of the hydrated form of  $\text{Na}_3\text{PO}_4 \cdot 7\text{H}_2\text{O}$  [12]. After 0.5 h from the beginning of the hydration process, two bands at  $993$  and  $1062\text{ cm}^{-1}$  appear and they are attributed to the P–O symmetric stretching vibration  $\nu_1(\text{A}_1)$  and both P–O, P–OH asymmetric stretching vibrations  $\nu_3(\text{F}_2)$  in the  $\text{H}_2\text{PO}_4^-$  unit, respectively [13]. After one hour, the hydration process of  $\text{Na}_3\text{PO}_4 \cdot x\text{H}_2\text{O}$  continues, and it is connected with the shift of the band position from  $930$  to  $940\text{ cm}^{-1}$  [12]. As could be seen from the spectra, the phase with the  $\text{H}_2\text{PO}_4^-$  unit completely disappears and the new band at  $965\text{ cm}^{-1}$  of the symmetric stretching vibration of  $\nu_1(\text{A}_1)$ , typical for  $\text{HOPO}_3^{2-}$ , is observed [13]. This band does

not remain in the system for long and it completely diminishes over time at around 32 h. However, after 75 h, the band at  $965\text{ cm}^{-1}$  arises again. In this case, the very strong band is typical for the calcium hydroxyapatite  $\text{Ca}_x(\text{PO}_4)_y(\text{OH})_z$  structure which also corresponds to the growth of the weak bands at  $1057$ ,  $1030$  and  $1005\text{ cm}^{-1}$  assigned to the asymmetric stretching modes  $\nu_3(\text{F}_2)$  of the P–O bond in the tetrahedral  $\text{PO}_4^{3-}$  group [14,15]. The suggested mechanism of created phosphate phases is further discussed in XPS measurements.

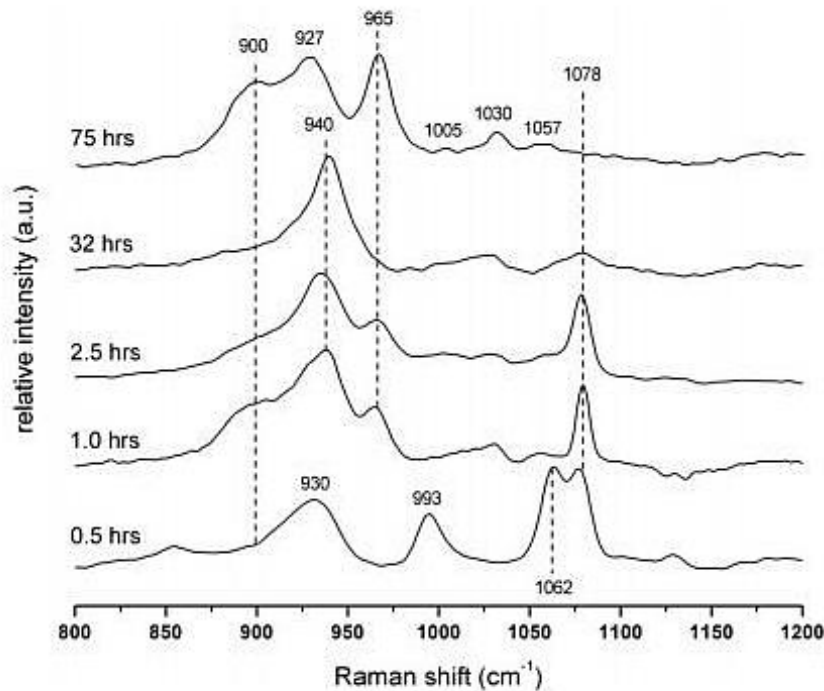


**Figure 4.** Raman spectra of alkali-activated BFS with  $\text{Na}_3\text{PO}_4$  recalculated to the 2.5 wt % addition of  $\text{P}_2\text{O}_5$ .

### 3.4. X-ray Photoelectron Spectroscopy

The core level  $\text{P } 2p_{3/2}$  positions of samples subjected to measurements are summarized in Table 2 and provide an insight into the binding of the phosphate in the system. The high resolution spectra of samples quenched at the same times as in the case of the Raman spectroscopy are presented in Figure 5.

**Table 2.** The binding energies and peak widths (FWHM) of  $\text{P } 2p_{3/2}$  components.

Component	Binding Energy (FWHM)/eV		
	$\text{Na}_3\text{PO}_4$	0.5 h	1.0 h
$\text{P } 2p_{3/2}$	132.2 (1.4)	132.2 (1.4)	132.2 (1.4)
		133.9 (1.4)	133.5 (1.4)
	2.5 h	32 h	75 h
	132.2 (1.4)	132.2 (1.4)	132.4 (1.4)
	133.5 (1.4)		

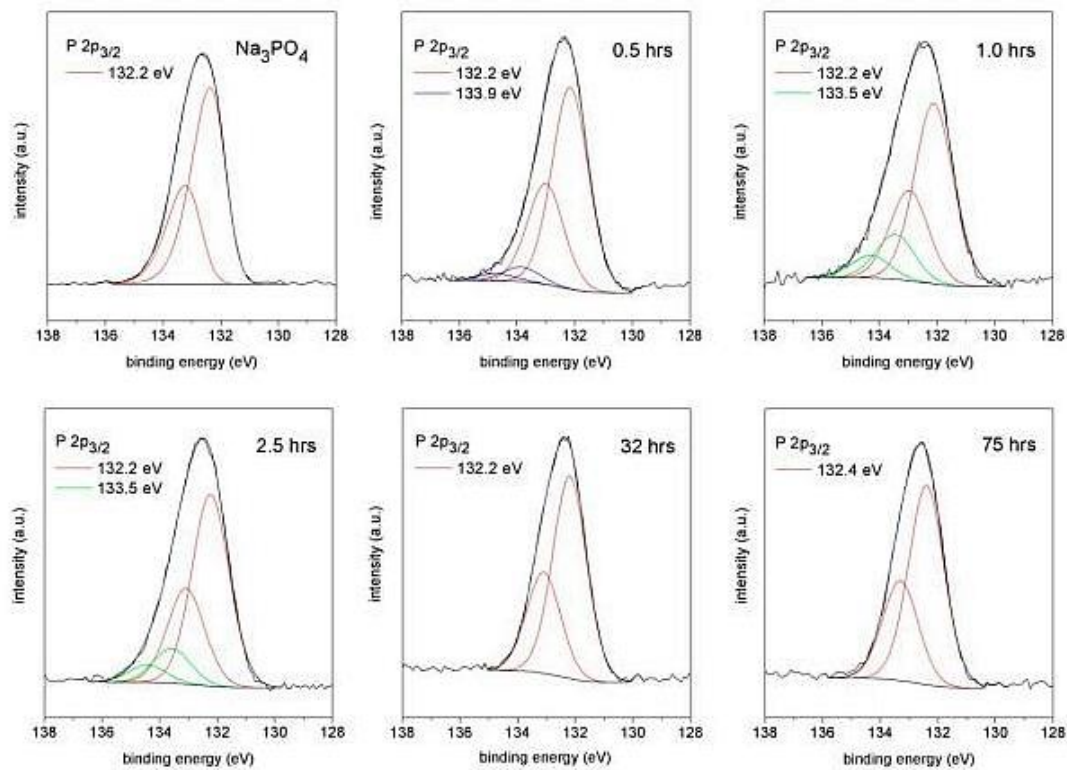


**Figure 5.** XPS spectra of alkali-activated BFS with  $\text{Na}_3\text{PO}_4$  recalculated to the 2.5 wt % addition of  $\text{P}_2\text{O}_5$ . (The energy separations for the P  $2p_{3/2}$  and P  $2p_{1/2}$  lines were fixed at 0.80 eV.)

The first P 2p spectrum represents a pure  $\text{Na}_3\text{PO}_4$  compound with a typical binding energy (BE) of  $\text{PO}_4^{3-}$  equal to 132.2 eV. Strong peaks with this BE appear in each spectrum, which indicates the presence of the  $\text{Na}_3\text{PO}_4$  phase at any time during the alkali activation. However, other components representing different chemical states of phosphorus are detected. According to the previous experimental measurements, the phosphate anions of the  $[\text{PO}_n(\text{OH})_m]^{y-}$  type generally follow a systematic rule. The contribution of covalently bonded OH ligands ( $m$ ) to “free” O ligands ( $n$ ) increases together with the binding energy of P 2p. The stepwise increase from  $\text{PO}_4^{3-}$  up to  $\text{H}_3\text{PO}_4$  is typically about 1 eV in every OH ligand presented in the structure [16,17]. Therefore, the P  $2p_{3/2}$  component with BE at 133.9 eV in 30 minutes of alkali activation belongs to the  $\text{H}_2\text{PO}_4^-$  units verified with Raman spectroscopy as well (993 and  $1062\text{ cm}^{-1}$  bands). The P 2p spectra at 1.0 and 2.5 h indicate the increase of BE to 133.5 eV, which corresponds to phosphate with only one hydroxyl unit. The results of Raman spectroscopy together with the XPS investigations revealed the existence of  $\text{HOPO}_3^{2-}$ . XPS measurements also correspond to the Raman spectroscopy concerning the disappearance of this phase 32 h after mixing, which comes just before the secondary formation of the CSH gel (Figure 3). The calcium ions bonded so far in the hydrogen phosphate structure likely move into the solution and incorporate the created phases with the always higher value of the negative logarithms of the solubility product equilibrium constant  $\text{pK}_{\text{sp}}$  such as secondary CSH gel ( $\text{pK}_{\text{sp}} = 8.16$  for CSH gel with low C/S ratio [18]) and calcium hydroxyapatites ( $\text{pK}_{\text{sp}} = 115.50$  for  $\text{Ca}_{10}(\text{PO}_4)_6(\text{OH})_2$  [19]). The P  $2p_{3/2}$  component in the spectrum of 75 h with BE at 132.4 eV does not show any hydrogen phosphate forms, which is also in good agreement with the Raman investigations. The shift in the BE compared to the pure  $\text{Na}_3\text{PO}_4$  P 2p spectrum could be attributed to sodium phosphates with a small addition of stable calcium hydroxyapatite of which the binding energy is slightly higher [16,20]. The peak positions of both phases are considerably overlapped and should not be deconvoluted.

#### 4. Conclusions

The results from Raman and XPS analyses combined with microcalorimetry measurements were beneficially used to clarify the mechanism of retardation in alkali-activated materials with the addition of sodium phosphate. It was assessed that  $\text{Ca}^{2+}$  ions formed after the dissolution of alkali-activated blast furnace slag in a highly alkaline environment bond to the phosphate anion from the retardant agent ( $\text{Na}_3\text{PO}_4$ ). The formation of calcium dihydrogen, later hydrogen phosphate structures, arises. The deficiency of calcium ions in the solution causes the nucleation and the growth of the CSH phase to be poisoned and the initial setting time is prolonged. Their formation, nevertheless, also strongly affects the delayed formation of secondary CSH gel compared to the system without the retarding agent, which may affect the mechanical properties of alkali-activated materials at an early age. The stability of the created calcium hydrogen phosphate phase in the system is temporary, which leads to its dissolution and the formation of less soluble phases such as secondary CSH gel and calcium hydroxyapatite.

**Acknowledgments:** This work was financially supported by the project: Materials Research Centre at FCH BUT-Sustainability and Development, REG LO1211, with financial support from the National Programme for Sustainability I (Ministry of Education, Youth and Sports).

**Author Contributions:** Lukáš Kalina and Vlastimil Bílek Jr. conceived and designed the experiments; Radoslav Novotný performed the microcalorimetry measurements; Miroslava Mončeková provided Raman analyses results; Lukáš Kalina measured and determined the XPS spectra; Jiří Másilko and Jan Koplík performed the XRD and XRF analysis; Lukáš Kalina wrote the paper.

**Conflicts of Interest:** The authors declare no conflict of interest.

#### Abbreviations

The following abbreviations are used in this manuscript:

$K_{sp}$	solubility product constant
BFS	blast furnace slag
XRF	X-ray fluorescence
XRD	X-ray diffraction
$\beta\text{-C}_2\text{S}$	$\beta$ -dicalcium silicate
SP	sodium phosphate
XPS	X-ray photoelectron spectroscopy
CSH gel	calcium-silicate-hydrate gel
FWHM	full width at half maximum
BE	binding energy
$\nu_1(\text{A}_1)$	symmetric stretching vibration
$\nu_3(\text{F}_2)$	asymmetric stretching vibration

#### References

1. Provis, J.L.; van Deventer, J.S.J. *Alkali Activated Materials*; Springer: Houten, The Netherlands, 2014; p. 388.
2. Wu, C.; Zhang, Y.; Hu, Z. Properties and application of alkali-slag cement. *J. Chin. Ceram. Soc.* **1993**, *21*, 175–181.
3. Nicholson, C.L.; Murray, B.J.; Fletcher, R.A.; Brew, D.; Mackenzie, K.J.; Schmücker, M. Novel Geopolymer Materials Containing Borate Structural Units. In Proceedings of the World Congress Geopolymer, Perth, Australia, September 2005; pp. 31–33.
4. Brough, A.; Holloway, M.; Sykes, J.; Atkinson, A. Sodium silicate-based alkali-activated slag mortars: Part II. The retarding effect of additions of sodium chloride or malic acid. *Cem. Concr. Res.* **2000**, *30*, 1375–1379. [CrossRef]
5. Chang, J.J.; Yeih, W.; Hung, C.C. Effects of gypsum and phosphoric acid on the properties of sodium silicate-based alkali-activated slag pastes. *Cem. Concr. Compos.* **2005**, *27*, 85–91. [CrossRef]
6. Gong, C.; Yang, N. Effect of phosphate on the hydration of alkali-activated red mud–slag cementitious material. *Cem. Concr. Res.* **2000**, *30*, 1013–1016. [CrossRef]
7. Shi, C.; Li, Y. Investigation on some factors affecting the characteristics of alkali-phosphorus slag cement. *Cem. Concr. Res.* **1989**, *19*, 527–533.

8. Lee, W.; van Deventer, J.J. Effects of anions on the formation of aluminosilicate gel in geopolymers. *Ind. Eng. Chem. Res.* **2002**, *41*, 4550–4558. [CrossRef]
9. Shi, C.; Day, R.L. A calorimetric study of early hydration of alkali-slag cements. *Cem. Concr. Res.* **1995**, *25*, 1333–1346. [CrossRef]
10. Ghule, A.; Baskaran, N.; Murugan, R.; Chang, H. Phase transformation studies of  $\text{Na}_3\text{PO}_4$  by thermo-raman and conductivity measurements. *Solid State Ion.* **2003**, *161*, 291–299. [CrossRef]
11. McAfee, L. Infrared and raman spectra of inorganic and coordination compounds. Part A: Theory and applications in inorganic chemistry; part B: Application in coordination, organometallic, and bioinorganic chemistry, (Nakamoto, Kazuo). *J. Chem. Educ.* **2000**, *77*, 1122. [CrossRef]
12. Ghule, A.; Murugan, R.; Chang, H. Thermo-raman studies on dehydration of  $\text{Na}_3\text{PO}_4 \cdot 12\text{H}_2\text{O}$ . *Thermochim. Acta* **2001**, *371*, 127–135. [CrossRef]
13. Frost, R.L.; López, A.; Xi, Y.; Scholz, R. Vibrational spectroscopic characterization of the phosphate mineral althausite  $\text{Mg}_2(\text{PO}_4)(\text{OH},\text{F},\text{O})$ —Implications for the molecular structure. *Spectrochim. Acta Part A Mol. Biomol. Spectrosc.* **2014**, *120*, 252–256. [CrossRef] [PubMed]
14. Taddei, P.; Tinti, A.; Gandolfi, M.G.; Rossi, P.L.; Prati, C. Ageing of calcium silicate cements for endodontic use in simulated body fluids: A micro-raman study. *J. Raman Spectrosc.* **2009**, *40*, 1858–1866. [CrossRef]
15. Koutsopoulos, S. Synthesis and characterization of hydroxyapatite crystals: A review study on the analytical methods. *J. Biomed. Mater. Res.* **2002**, *62*, 600–612. [CrossRef] [PubMed]
16. Moulder, J.F.; Chastain, J. *Handbook of X-ray Photoelectron Spectroscopy: A Reference Book of Standard Spectra for Identification and Interpretation of XPS Data*; Physical Electronics Division, Perkin-Elmer Corporation: Eden Prairie, MN, USA, 1995; pp. 84–85.
17. Textor, M.; Ruiz, L.; Hofer, R.; Rossi, A.; Feldman, K.; Hähner, G.; Spencer, N.D. Structural chemistry of self-assembled monolayers of octadecylphosphoric acid on tantalum oxide surfaces. *Langmuir* **2000**, *16*, 3257–3271. [CrossRef]
18. Berner, U.R. Modelling of incongruent dissolution of hydrated cement minerals. *Radiochim. Acta* **1988**, *44/45*, 387–393. [CrossRef]
19. Moreno, E.C.; Gregory, T.M.; Brown, W.E. Preparation and solubility of hydroxyapatite. *Phys. Chem.* **1968**, *72A*, 773–782. [CrossRef]
20. Shin, H.-Y.; Jung, J.-Y.; Kim, S.-W.; Lee, W.-K. XPS analysis on chemical properties of calcium phosphate thin films and osteoblastic cell responses. *J. Ind. Eng. Chem.* **2006**, *12*, 476–483.



© 2016 by the authors; licensee MDPI, Basel, Switzerland. This article is an open access article distributed under the terms and conditions of the Creative Commons Attribution (CC-BY) license (<http://creativecommons.org/licenses/by/4.0/>).

EFFECT OF THE BY-PASS CEMENT-KILN DUST AND  
FLUIDIZED-BED-COMBUSTION FLY ASH ON THE PROPERTIES  
OF FINE-GRAINED ALKALI-ACTIVATED SLAG-BASED  
COMPOSITESVPLIV PRAHU IZ PEČI ZA CEMENT IN LETEČEGA PEPELA IZ  
VRTINČASTE PLASTI NA LASTNOSTI DROBNOZRNATEGA,  
Z ALKALIJAMI AKTIVIRANEGA KOMPOZITA NA OSNOVI  
ŽLINDRE

Vlastimil Bílek Jr., Ladislav Pařízek, Lukáš Kalina

Brno University of Technology, Faculty of Chemistry, Materials Research Centre, Purkyňova 118, 612 00 Brno, Czech Republic  
xcbilekv@fch.vutbr.cz

Prejem rokopisa – received: 2014-08-01; sprejem za objavo – accepted for publication: 2014-09-23

doi:10.17222/mit.2014.162

The aim of this work is to investigate the influence of the by-pass cement-kiln dust (CKD) and two types of the fluidized-bed-combustion (FBC) fly ash on the workability, shrinkage and mechanical properties (compressive and flexural strengths) of the water-glass-activated slag. The utilization of CKD and FBC is very problematic. One of the main reasons for this is a high lime and sulfate content in these wastes, which can lead to the formation of expansive hydration products and, consequently, to the cracking of ordinary Portland-cement (OPC) materials. On the other hand, these products might act against the high shrinkage of the alkali-activated slag (AAS). In order to investigate this assumption and the influence of these admixtures on the other properties mentioned above, fine-grained AAS-based composites were prepared. A ground, granulated blast-furnace slag (the reference binder) was partially replaced (0–50 %) by one type of CKD and two types of the FBC fly ash. A significant reduction in the shrinkage was observed on the samples containing an even lower amount of fly ash, while the composites with CKD did not show any notable shrinkage reduction. When using higher dosages of these admixtures the mechanical properties were reduced, but lower dosages did not have such effects, especially as regards the compressive strength. The workability was also strongly dependent on the admixture dosage. Its improvement was observed especially in the case when slag was replaced by up to 30 % of CKD.

Keywords: alkali-activated slag, by-pass cement-kiln dust, FBC fly ash, workability, strength, shrinkage

Namen tega dela je preiskati vpliv prahu iz peči za cement (CKD) in dveh vrst letečega pepela (FBC) iz zgorovanja v vrtinčasti plasti na obdelovalnost, krčenje in mehanske lastnosti (tlačna in upogibna trdnost) žlindre, aktivirane z vodnim steklom. Uporaba CKD in FBC je zelo problematična. Eden od glavnih razlogov za to je visoka vsebnost apna in sulfatov v teh odpadkih, kar lahko povzroči nastanek ekspanzijskih hidracijskih produktov in posledično pokažanje portlandskih cementnih materialov (OPC). Po drugi strani pa ti produkti lahko zavirajo veliko krčenje žlindre, aktivirane z alkalijami (AAS). Da bi preverili te predpostavke in vpliv teh dodatkov na druge, zgoraj omenjene lastnosti, so bili pripravljene na osnovi AAS drobnozrnati kompoziti. Grobozrnata plavžna žindra (referenčno vezivo) je bila delno nadomeščena (0–50 %) z eno vrsto CKD in dvema vrstama FBC letečega pepela. Opazeno je bilo občutno zmanjšanje krčenja pri vzorcih s celo majhnim deležem letečega pepela, medtem ko kompozit s CKD ni pokazal opaznega zmanjšanja krčenja. Pri uporabi večjih deležev obeh dodatkov so se poslabšale mehanske lastnosti, pri majhnem dodatku pa ni bilo takega vpliva na tlačno trdnost. Obdelovalnost je bila močno odvisna od količine dodatkov. Njeno izboljšanje je bilo posebno opazno v primeru, ko je bila žindra nadomeščena z do 30 % CKD.

Ključne besede: z alkalijami aktivirana žindra, prah iz peči za cement, FBC leteči pepel, obdelovalnost, trdnost, krčenje

## 1 INTRODUCTION

The binders based on AAS are considered as an ecological alternative to the OPC-based binders, which are most common in the concrete production. AAS, in comparison with Portland cement, can have a better durability, a lower hydration heat, a better resistance to elevated temperatures and an aggregate-matrix interphase and other benefits.<sup>1</sup> On the other hand, the main disadvantages of AAS are a very high shrinkage and a poor rheology, especially with respect to a relatively rapid setting in the case of a water-glass activation.<sup>2</sup>

CKD is a by-product of cement manufacturing with a highly variable composition, but it usually contains

significant amounts of alkali, chloride, sulfate and free lime.<sup>3</sup> Several works investigating the CKD use in the mortar and concrete production were published. It is usually concluded that a replacement of OPC higher than 5–10 % has an adverse effect on the compressive and tensile strengths.<sup>4</sup> FBC technology has many advantages in comparison with pulverized coal combustion,<sup>5</sup> but the ashes from FBC are very porous and they contain high amounts of very reactive free lime and anhydrite, which lead, on the one hand, to their self-cementing properties, but, on the other hand, to the problems with the workability and volume stability due to the formation of expansive-hydration products.<sup>6</sup>

## 2 EXPERIMENTAL WORK

### 2.1 Materials and sample preparation

A ground, granulated blast-furnace slag with a specific surface of 380 m<sup>2</sup>/kg was used as the reference binder (R). The slag was partially replaced (0–50 %) by one type of the by-pass CKD and two types of the FBC fly ash. The phase compositions of CKD and fly ashes were determined with X-ray diffraction (XRD). CKD mainly consisted of KCl, K<sub>2</sub>SO<sub>4</sub>, CaO and C<sub>2</sub>S. The main phases found in both fly ashes were anhydrite, quartz, glassy phase, free lime, portlandite and calcite. The fly ash designed as P contained more anhydrite, quartz and free lime, while the fly ash designed as L contained a higher amount of the glassy phase. The water glass with the silicate modulus equal to 1.85 was used as the alkaline activator. The weight ratio of Na<sub>2</sub>O/binder was kept constant at 0.042. The mass ratio of the Czech standard sand (three different fractions according to standard ČSN EN 196) to the binder was 2 : 1. The water-to-binder ratio (*w/b*) was kept constant at 0.40, only in the case of the mixtures with fly ash L, *w/b* had to be increased due to a very low workability. The binder compositions of the mortars prepared are shown in **Table 1**.

After approximately four minutes of mixing the workability of the mortar was measured using the flow-table spread test and then the mortar was cast into the molds. Prisms with the dimensions of 20 mm × 20 mm × 100 mm were prepared for the compressive- and flexural-strength tests and prisms with the dimensions of 25 mm × 25 mm × 285 mm and stainless-steel gauge studs in their front walls were prepared for the shrinkage tests.

### 2.2 Compressive- and flexural-strength testing

The prisms for the strength testing were demolded after 24 h and moist cured at a 99 % relative humidity and (23 ± 2) °C. Compressive strengths were tested at the ages of (1, 7 and 28) d. Three prisms were used for the flexural testing (three-point bending) of each mixture at each age and broken parts from these tests were used for the compressive-strength testing.

### 2.3 Shrinkage tests

The shrinkage tests were based on ASTM C596. After 24 h of moist curing the specimens were demolded, a comparator reading was taken and the speci-

mens were immersed for three days in tap water. Then the bars were removed from the water, their surfaces were dried with a wet towel and a zero reading was performed. After that the bars were stored in laboratory conditions ((45 ± 5) % relative humidity, (23 ± 2) °C) for 56 d and their length changes were measured. These shrinkage tests were rather tentative because only two samples of each mixture were measured.

## 3 RESULTS AND DISCUSSION

The average values of compressive  $f_c$  and flexural strength  $f_t$  for different ages with the standard errors of the mean are listed in **Table 2**. There are also the results of the workability testing expressed as the average values of the diameters of the mortar spread  $d$  in the same table. The data for the mortars designed as P10, L30 and L50 are not included because these mortars did not harden even after three days.

**Table 2:** Flexural  $f_t$  and compressive  $f_c$  strength development, standard errors of the mean (in parenthesis) and workability of the prepared composites

**Tabela 2:** Spreminjanje upogibne  $f_t$  in tlačne  $f_c$  trdnosti, povprečje standardne napake (v oklepaju) in obdelovalnost pripravljenih kompozitov

Mortar	$f_t$ /MPa			$f_c$ /MPa			$d$ /mm
	24 h	7 d	28 d	24 h	7 d	28 d	
R	2.5 (0.1)	7.3 (0.7)	11.7 (0.4)	10.0 (0.2)	72.7 (1.7)	107.4 (3.6)	190
CKD10	2.0 (0.1)	2.4 (0.3)	8.8 (0.1)	10.0 (0.2)	62.0 (1.0)	115.1 (2.8)	220
CKD20	1.3 (0.3)	4.1 (0.7)	7.6 (0.7)	6.0 (0.1)	46.5 (1.1)	99.4 (0.9)	240
CKD30	1.0 (0.0)	3.9 (0.4)	7.5 (0.4)	3.0 (0.1)	35.8 (0.6)	72.0 (2.9)	225
CKD40	1.0 (0.0)	3.9 (0.2)	5.9 (0.1)	2.6 (0.1)	33.9 (0.9)	50.2 (1.9)	170
CKD50	0.0 (0.0)	2.6 (0.4)	4.5 (0.2)	0.0 (0.0)	21.3 (0.4)	26.3 (1.8)	120
P2.5	1.6 (0.1)	6.1 (0.1)	8.4 (0.0)	6.6 (0.1)	67.6 (1.5)	104.3 (2.2)	155
P5	1.5 (0.0)	6.0 (0.2)	7.4 (0.3)	5.8 (0.1)	60.2 (1.7)	102.2 (1.1)	115
L10	1.2 (0.1)	2.4 (0.1)	7.4 (0.5)	4.8 (0.1)	11.1 (0.1)	66.3 (2.4)	215*

\*  $w/b = 0.48$

Except for some cases of the CKD10 mixtures, the highest strengths were observed for the reference mortar.

**Table 1:** Binder compositions of the prepared composites in mass fractions, *w*%

**Tabela 1:** Sestava veziv pripravljenih kompozitov v masnih deležih, *w*%

Mixture designation	R	CKD10	CKD20	CKD30	CKD40	CKD50
Slag	100	90	80	70	60	50
Cement kiln dust	0	10	20	30	40	50
Mixture designation	P2.5	P5	P10	L10	L30	L50
Slag	97.5	95	90	90	70	50
FBC fly ash P	2.5	5	10	0	0	0
FBC fly ash L	0	0	0	10	30	50

However, a significant strength gain was observed between 24 h and 7 d and also between 7 d and 28 d in the case of replacing the slag with up to 40 % of CKD and up to 5–10 % of the FBC fly ash. Higher dosages of these admixtures had a fatal effect on the mechanical properties of AAS, especially in the case of the FBC fly ash.

Both compressive and flexural strengths gradually decreased with the increasing slag replacement at all the ages. The strength reduction was the most severe at the early ages and in the case of the flexural strength. The strength reduction in the presence of CKD could have been caused not only by the decrease in the slag content, but also by a possible formation of chloro and sulfoaluminate phases, leading to a softening and an increased porosity.<sup>7</sup> Another reason can be the increase in the real *w/b* ratio if taking into account the CKD composition, which can also be a reason for the workability improvement at the replacement levels of up to 30 %. When more than 30 % of CKD was used, the workability became reduced, which can be attributed to the fast setting. The setting time was not measured but it was observed that these mortars set very soon after the filling of the molds. A shortening of the setting time was also observed with the increasing FBC-fly-ash dosages. The reason for this can be the formation of the primary CSH through the reaction between  $[\text{SiO}_4]^-$  from the water glass and  $\text{Ca}^{2+}$  released from the free lime present in the fly ash. The precipitation of portlandite is probably suppressed due to its higher solubility in comparison with CSH.<sup>8</sup> Anyway, the hydration of the alkali-activated slag in the presence of the FBC fly ash needs further investigation to explain the problems with the hardening of the mortars with the replacements of the slag by the FBC fly ash higher than 5–10 %. Perhaps most of  $[\text{SiO}_4]^-$  from the activator is consumed during the first minutes to form some type of calcium silicate which is cannot contribute to the strength gain or which suppresses further hydration.

On the other hand, at the later ages, especially the compressive strength grew faster in the case of the appropriately blended composites in comparison with the reference composites. From this point of view, it could be interesting to study the strength development over a longer period. This strength increase might be associated with the  $\text{C}_2\text{S}$  hydration and the pozzolanic reactions of the slag in the presence of the lime contained in CKD. The strength increase of the L10 mortar at the later ages might be due to the pozzolanic reactions of its glassy phase.

The shrinkage development is outlined in Table 3. The highest shrinkage rate was observed during the first three days after taking the specimens out of the water. After 14 d, only slight length changes were recorded.

When using CKD at a different replacement level, no clear trend in the shrinkage development was observed. Some mortars showed a slightly lower shrinkage than the

reference mortar, but the shrinkage values of the other mortars were higher. From the data obtained, CKD does not seem to affect the shrinkage reduction. However, the situation with both fly ashes is considerably different: in the case of a 2.5 % replacement of the slag by FBC fly ash P, the shrinkage of the reference mortar was reduced by more than 20 % and if 10 % of fly ash L was used, the shrinkage was reduced even by more than 70 %. Unfortunately, both P5 specimens were broken during demolding, so the data for them were not obtained. These preliminary results showed that the FBC fly ashes can be beneficial for the suppressing of the AAS shrinkage, but attention must be paid to the preservation of the other properties. Additional investigations through instrumental methods like scanning electron microscopy, calorimetry or XRD are planned for the future to clarify the role of the FBC fly ash in the AAS systems.

Table 3: Shrinkage development of the prepared composites

Tabela 3: Spreminjanje krčenja pripravljenih kompozitov

Compo- site	Days after water curing					
	1	3	7	14	28	56
R	0.52	0.74	0.81	0.83	0.85	0.86
CKD10	0.58	0.81	0.88	0.89	0.90	0.91
CKD20	0.52	0.84	0.84	0.84	0.84	0.84
CKD30	0.36	0.77	0.78	0.78	0.78	0.78
CKD40	0.40	0.75	0.81	0.81	0.81	0.81
CKD50	0.40	0.78	0.90	0.91	0.91	0.91
P2.5	0.32	0.55	0.61	0.66	0.67	0.67
L10	0.05	0.13	0.15	0.18	0.22	0.24

#### 4 CONCLUSIONS

This pilot study investigated the effect of a partial replacement of the water-glass-activated blast-furnace slag with the CKD and FBC fly ashes on the workability, mechanical properties and the shrinkage. It was observed that CKD, in proper dosages, improved the workability, while the FBC fly ashes reduced it dramatically even at a low content. On the other hand, unlike CKD, the FBC fly ashes significantly reduced the shrinkage. Both these admixtures, at low replacement levels, had no or little adverse effect on the compressive strength, especially at later ages. In contrast, the flexural strength was affected more negatively. The FBC fly ashes at the dosages higher than 5–10 % had a fatal impact on the strength development.

#### Acknowledgement

This outcome was achieved with the financial support of the junior specific research program at the Brno University of Technology, project No. FAST/FCH-J-14-2371.

## Příloha XII

V. BÍLEK et al.: EFFECT OF THE BY-PASS CEMENT-KILN DUST AND FLUIDIZED-BED-COMBUSTION FLY ASH ...

### 5 REFERENCES

- <sup>1</sup> J. L. Provis, J. S. J. van Deventer (Eds.), *Alkali Activated Materials: State-of-the-art report*, RILEM TC 224-AAM, vol. 13, Springer, Dordrecht 2014, doi:10.1007/978-94-007-7672-2
- <sup>2</sup> M. Palacios, F. Puertas, *ACI Materials Journal*, 108 (2011), 73–78, doi:10.14359/51664218
- <sup>3</sup> P. Chaunsali, S. Peethamparan, *ACI Materials Journal*, 110 (2013), 297–304, doi:10.14359/51685663
- <sup>4</sup> R. Siddique, *Resources, Conservation and Recycling*, 48 (2006), 315–338, doi:10.1016/j.resconrec.2006.03.010
- <sup>5</sup> J. Koornneef, M. Junginger, A. Faaij, *Progress in Energy and Combustion Science*, 33 (2007), 19–55, doi:10.1016/j.pecs.2006.07.001
- <sup>6</sup> G. Sheng, J. Zhai, Q. Li, F. Li, *Fuel*, 86 (2007), 2625–2631, doi:10.1016/j.fuel.2007.02.018
- <sup>7</sup> R. Kunal, R. Siddique, A. Rajor, *Resources, Conservation and Recycling*, 61 (2012), 59–68, doi:10.1016/j.resconrec.2012.01.006
- <sup>8</sup> C. Shi, R. Day, *Cement and Concrete Research*, 25 (1995), 64–105, doi:10.1016/0008-8846(95)00126-W



Contents lists available at ScienceDirect

Cement and Concrete Research

journal homepage: <http://ees.elsevier.com/CEMCON/default.asp>

## XPS characterization of polymer–monocalcium aluminate interface



Lukáš Kalina\*, Jiří Másilko, Jan Koplík, František Šoukal

Brno University of Technology, Faculty of Chemistry, Materials Research Centre, Purkyňova 464/118, Brno CZ-612 00, Czech Republic

## ARTICLE INFO

## Article history:

Received 23 January 2014

Accepted 30 July 2014

Available online 17 August 2014

## Keywords:

Characterization

Composite

X-ray photoelectron spectroscopy

## ABSTRACT

The aim of this paper is the introduction of a sophisticated testing method, X-ray photoelectron spectroscopy (XPS), used to study the interface between the hydrated cement phase and polymer after mechanochemical activation, which is fundamental for the creation of macro-defect-free (MDF) composites. The XPS results clearly explain the hypothesis of a chemical reaction mechanism in the interphase regions affecting the final properties of the MDF materials.

© 2014 Elsevier Ltd. All rights reserved.

## Contents

1. Introduction	110
2. Experimental program	111
2.1. Preparation process	111
2.2. Test methods	111
2.2.1. X-ray diffraction analysis (XRD)	111
2.2.2. X-ray photoelectron spectroscopy	111
3. Results and discussion	111
4. Conclusion	112
Acknowledgments	113
References	113

## 1. Introduction

MDF cements were developed following the work by the research group led by Birchall at ICI during the late 1970s and early 1980s [1]. The 'MDF' signification, which stands for 'macro-defect-free', refers to the material's structure, which is without relatively large voids or defects normally present in ordinary cement pastes [2]. MDF materials represent a potentially attractive range of materials whose properties lie between those of conventional cements and ceramics. They are examples of alternative technological approaches to obtain low-porosity and very high-strength products. These materials are made with a cement paste with a very low w/c ratio, containing up to 7% by mass of a water soluble plasticizing agent, such as hydrolyzed polyvinyl acetate, hydroxypropyl-methyl cellulose, polyacrylamide or sodium polyphosphate. Glycerol is often added to improve the processing

[2–4]. Many studies have defined the different variable roles of polymer varying during the production process. Initially, the polymer acts as a rheological aid, significantly improves the workability of normally dry cement paste and reduces friction of particles during mixing and especially high shear-mixing process. Moreover, polymer also fills the space between the unreacted cement grains and allows them to join together in a tightly packed compact structure during compaction [5–7]. However, studies on the chemistry and the microstructure of the calcium aluminate MDF materials have attributed to the significant improvements of the mechanical properties of these materials and also to the chemical reactions occurring between the PVA polymer (the polyvinyl alcohol arising from the PVAc hydrolysis) and the inorganic ions produced when the cement constituents dissolve in water [8]. The bonding forces formed in this way are quite strong, and thus the failure of MDF material tends to occur within the polymer phase or clinker grains rather than at the interface [9].

In the preparation process of MDF materials the high-shear mixing is an important step [10]. The crumbly mixture of cement, polymer and water is subjected to the twin roll mixer which rapidly produces

\* Corresponding author. Tel.: +420 541 149 426; fax: +420 541 149 361.  
E-mail address: kalina@fch.vutbr.cz (L. Kalina).

rubbery, cohesive dough usable for further processing. The high-shear mixing intensity could be well controlled by gap and speed of two rollers [11]. At the beginning, researchers supposed that the high-shear mixing is used only to eliminate macrodefects (large pores and air voids) from the paste, but further development confirmed, that the high-shear mixing also induces chemical interactions between the polymer and the inorganic cement [12]. It was also recognized that much of the mechanical strength of these materials is due to the mechanically induced chemical changes [9]. However, the shear rate cannot be increased above a certain limit, because with an increasing rate of mixing the amount of heat is generated, which may cause the material to become stiff before the processing is completed [2].

The key role plays the interphase region that influences the mechanical behavior of the MDF materials. The interphase region is a very complicated system that was subject to a number of different techniques to understand the chemical structure of this amorphous system. It has been suggested that the cement grains are dissolved in high pH environment,  $\text{Ca}^{2+}$  ions will be present as  $\text{Ca}(\text{OH})_2$  and  $\text{Al}^{3+}$  ions in a  $[\text{Al}(\text{OH})_4]^-$  complex unit. Calcium can form a hemihydrate calcium acetate following interaction with the polymer and the presence of aluminum led to the suggestion of the existence of a cross-linking of the PVA chains by Al ions where Al is bonded to the O atoms of two different PVA chains with O–Al–O bonds [13,14]. The proposed chemical reaction mechanism is illustrated in Fig. 1 [9,11]. The irreversible confirmation of these bonds is the main objective of this study.

## 2. Experimental program

### 2.1. Preparation process

Due to the high sensitive nature of XPS the use of pure constituents of both polymer and cement is required. The synthesis of major phase  $\text{CaAl}_2\text{O}_4$  was prepared by repeated sintering at 1450 °C for 10 h using  $\text{Al}_2\text{O}_3$  (p.a.) and  $\text{CaO}$  (p.a.). The quality of the created monocalcium aluminate phase was controlled using an XRD analysis (Fig. 2). The results demonstrated the creation of almost pure CA phase with approximately 2.6 wt.% of grossite, calculated through the Rietveld method.

The mechanochemical activation was applied into the interface between the surface of sintered  $\text{CaAl}_2\text{O}_4$  and the tablet of pressed PVA (Gohsenol GH 17 s, Nippon Chemicals). The PVA tablet of 13 mm diameter was stuck with epoxy glue to the bottom of a glass dish. The tablet of sintered  $\text{CaAl}_2\text{O}_4$  of 25 mm diameter was stuck also with epoxy glue to

the steel shaft in the center of the tablet. The shaft was fixed to the controlled electric motor and the tablet was rotated by 300  $\text{min}^{-1}$  speed. The PVA tablet was over-layered with distilled water and the rotating  $\text{CaAl}_2\text{O}_4$  tablet was pressed to the top of the PVA tablet. The shear between the surfaces was decreased by the formation of a gel layer at the surface of PVA. The rotation was stopped after 300 s and the surfaces of tablets were quickly rinsed with distilled water and then dried at 60 °C. To get the effect of mechanochemical activation the experiment was repeated without the rotation of a  $\text{CaAl}_2\text{O}_4$  tablet. The supposed chemical reaction at the interface was able to proceed but no mechanical energy was applied. Such a way prepared surfaces of  $\text{CaAl}_2\text{O}_4$  and PVA was subjected to further investigation.

### 2.2. Test methods

#### 2.2.1. X-ray diffraction analysis (XRD)

X-ray powder diffraction data were obtained using a PANanalytical Empyrean diffractometer with  $\text{CuK}\alpha$  radiation equipped with the detection system PIXcel<sup>3D</sup>. Specimens were step scanned from 5° to 60°  $2\theta$  using a vertical high-resolution goniometer with a step size of 0.013°  $2\theta$ .

#### 2.2.2. X-ray photoelectron spectroscopy

XPS analyses were carried out with Axis Ultra DLD spectrometer using a monochromatic  $\text{Al K}\alpha$  ( $h\nu = 1486.7$  eV) X-ray source operating at 150 W (10 mA, 15 kV). The spectra were obtained using an analysis area of  $\sim 300 \times 700$   $\mu\text{m}$ . The Kratos charge neutralizer system was used for all analyses. The high resolution spectra were measured with the step size 0.1 eV and a pass energy of 20 eV. Instrument base pressure was  $2 \cdot 10^{-8}$  Pa. Spectra were analyzed using CasaXPS software (version 2.3.15) and have been charge corrected to the main line of the carbon C 1s spectral component (C–C, C–H) set to 284.80 eV. A standard Shirley background is used for all sample spectra.

## 3. Results and discussion

The main objective of the study was the investigation of chemical reactions that might be occurring between monocalcium aluminate (main phase of alumina cement) and polyvinyl alcohol/acetate co-polymer (PVA) after mechanochemical activation. The X-ray photoelectron spectroscopy (XPS) is the technique well suited to examining possible interactions on inorganic–organic interphase. The binding energies and peak widths (FWHM) of primary and activated samples are given in Table 1.

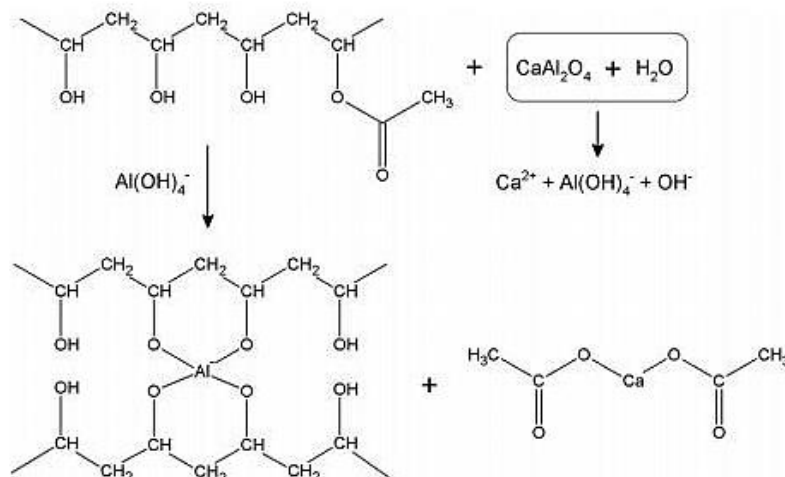


Fig. 1. Proposed chemical reaction in the formation of MDF composite.

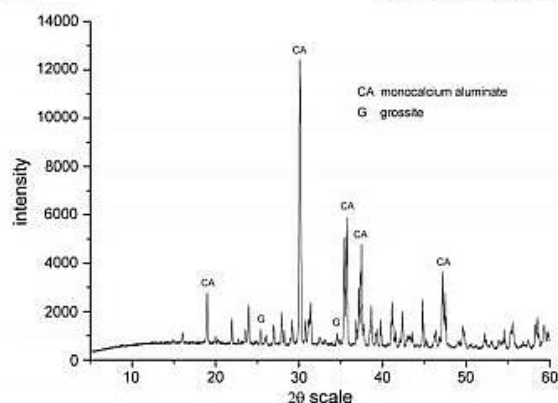


Fig. 2. XRD spectrum of the primary monocalcium aluminate phase.

For the first time, the chemical state of calcium and alumina in the primary phase of monocalcium aluminate (CA) phase was measured. All XPS spectra are shown in Fig. 3. A certain amount of carbon, belonging to the organic contaminants, was detected on the surface of the sample. A single peak (Gaussian 70%–Lorentzian 30%), ascribed to alkyl type carbon, was fitted to the main peak of the C 1s spectrum for adventitious carbon (284.80 eV). A second peak (286.10 eV), with a higher value of FWHM to the main peak, is attributed to alcohol functionalities. Further high binding energy component (289.18 eV) can be added to the O–C=O functional group [15]. The spectrum of calcium shows two different chemical states. The ratio between the components was calculated to 2:1, which is in accordance with the expected  $\beta$ -tridymite structure. There are two calcium cations (347.16 eV) in the distorted octahedral and the one (347.96 eV) that is coordinated with nine  $O^{2-}$  ions to form a trigonal antiprism with six oxygens and a triangular formation with the other three [16]. Binding energy of alumina (73.47 eV) is typical for  $AlO_4$  tetrahedra with sharing corners creating the three-dimensional framework. All alumina high resolution spectra were fitted by an asymmetric form  $A(a,b,n)GL(p)$ . The parameters  $a$  and  $b$  allow the asymptotic form of the alumina asymmetric tail while the third parameter  $n$  defines the width of Gaussian used to convolute the basic shape of the profile. The best mixture of Gaussian–Lorentzian components is controlled by the parameter  $p$ , which is dependent on the instrument and resolution (pass energy) settings used as well as the natural line width of the specific core hole [17].

**Table 1**  
The binding energies and peak widths (FWHM) of the primary phases and after mechanochemical activation.

	Binding energy (FWHM)/eV			
	Primary phases		Mechanochemical activation	
	CA	PVA	CA	PVA
C 1s	284.80 (1.33)	284.80 (1.23)	284.80 (1.11)	284.80 (1.01)
	286.10 (2.09)	286.20 (1.53)	286.23 (1.41)	286.26 (1.25)
	289.18 (2.41)	289.24 (1.26)	287.76 (1.02)	288.16 (0.84)
Ca 2p <sub>3/2</sub>	347.16 (1.32)		347.13 (1.21)	347.45 (1.39)
	347.96 (1.37)		347.75 (1.30)	
			73.50 (1.25)	
Al 2p <sub>3/2</sub>	73.47 (1.22)		74.30 (1.33)	

The energy separations for the 2p<sub>3/2</sub> and 2p<sub>1/2</sub> lines were fixed at 0.42 and 3.50 eV for aluminum and calcium, respectively. Values in italics were assigned to new created phases formed after mechanochemical activation.

The C 1s spectrum of primary PVA phase shows the presence of three carbon environments with 92.3% of the peak area contributing to C–C; C–H (284.80 eV) and C–OH (286.2 eV) groups. The remaining 7.8% of the C 1s region is derived from non-hydrolyzed acetate groups (289.24 eV), which increased the surface activity of the material.

The different chemical situation of monocalcium aluminate phase arises after the mechanochemical process with PVA. The surface of the CA sample was covered mainly with PVA, but the C 1s spectrum was not the same as for the pure polyvinyl alcohol phase. Not only the expected chemical states of carbon were measured, which have been described above, but also another component at 287.76 eV was detected. According to the Handbook of X-ray Photoelectron Spectroscopy [18], this binding energy is typical of carbon–oxygen chemical bonding. More explanation provided Al 2p spectrum. The first peak at 73.50 eV belongs to alumina in tetrahedral coordination as well as in the CA phase, but the second peak at 74.30 eV characterizes C–O–Al connection presented in many studies [19–21]. It proves the chemical interaction between the monocalcium aluminate and polymer. According to the main hypothesis of reaction mechanisms, the hydroxyl groups of PVA are crosslinked with the aluminate ions ( $Al(OH)_4^-$ ) released during the hydration reaction of the CA phase [22–24], which also explains the slight decrease in C–OH contribution compared to the primary PVA. The Ca 2p spectrum of activated CA shows two different kinds of calcium. The chemical state of the first one is the same as in the primary phase (347.13 eV), but the second one is characterized by shift to a lower value of binding energy (347.75 eV). This could mean the creation of new calcium aluminate hydrates, such as  $CAH_{10}$  or  $C_2AH_6$ , where hydroxyl functional groups are incorporated into the structure, which causes the decrease in binding energy of calcium. The expected formation of  $C_2AH_6$  is inhibited by the presence of PVA [14].

On the surface of PVA sample, only carbon and a small amount of calcium were detected. The C 1s spectrum indicates the decrease of the C–OH group and at the same time the creation of another carboxyl functionality (288.16 eV), which can be ascribed to carbon of ester in calcium acetate. In the polyvinyl alcohol/acetate co-polymer a hydrolysis of the acetate groups takes place. The liberated acetate groups react with  $Ca^{2+}$  cations in the liquid phase resulting in calcium acetate precipitation, Ca 2p<sub>3/2</sub> spectrum with component at 347.45 eV, which is consistent with the expected reaction mechanism [9,11]. The NIST database [25] unfortunately does not include the measured spectra of calcium acetate, but only of calcium(II) formate with binding energy of Ca 2p<sub>3/2</sub> at 347.40 eV. However, it can be expected that the Ca 2p<sub>3/2</sub> binding energies of these compounds will be very close.

The effect of mechanochemical activation is well observed, when the whole process was repeated without rotation. Both CA and PVA surfaces were covered of a thin layer of polyvinyl alcohol/acetate with a small amount of the created calcium acetate. The C 1s and Ca 2p spectra contained the same features as the PVA activated sample (Fig. 3). The surface of monocalcium aluminate tablet additionally comprises the alumina with binding energy of Al 2p<sub>3/2</sub> at 74.01 eV belonging to gibbsite –  $Al(OH)_3$  [25], which is the hydration product of the CA phase. The experiment without mechanochemical activation clearly shows that there is no crosslinking via C–O–Al connection characterized with specific chemical states of C 1s (287.76 eV), respectively Al 2p<sub>3/2</sub> (74.30 eV).

#### 4. Conclusion

The XPS analysis provides a very successful method for the study of the composition and interphase structure of surface layers at the molecular level. It was found out that the mechanochemical activation of monocalcium aluminate and polyvinyl alcohol causes the creation of new C–O–Al chemical bonds. The appearance of this connection is evidence of a chemical reaction between the hydrated inorganic phase and PVA chains.

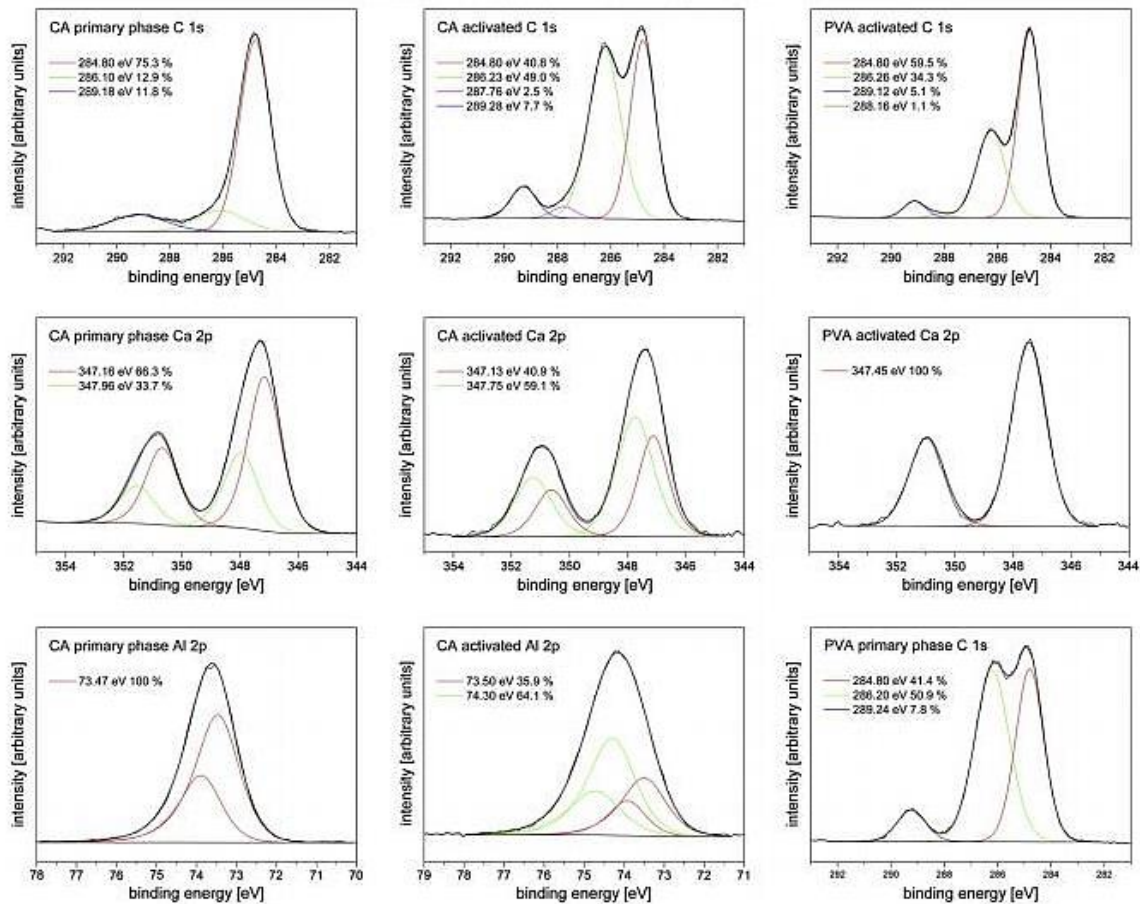


Fig. 3. Curve fitted XPS spectra of the primary and mechanochemical activated phases.

### Acknowledgments

This work was financially supported by the project: Materials Research Centre at FCH BUT – Sustainability and Development, REG LO1211, with financial support from the National Programme for Sustainability I (Ministry of Education, Youth and Sports).

### References

- [1] J.D. Birchall, A.J. Howard, K. Kendall, Flexural strength and porosity of cement, *Nature* 289 (1981) 388–390.
- [2] I. Odler, *Special Inorganic Cements*, 1st ed. E & F.N. Spon, London, New York, 2000.
- [3] M. Drábik, P. Billik, L. Gálíková, Macro defect free materials; The challenge of mechanochemical activation, *Ceram. Silik.* 56 (2012) 396–401.
- [4] M. Drábik, L. Gálíková, P. Billik, G. Maier, B. Kosednar-Legenstein, Macro defect free materials; Mechanochemical activation of raw mixes as the intensifying tool of the entire MDF synthesis, *Ceram. Silik.* 57 (2013) 120–125.
- [5] N. Alford, J.D. Birchall, Properties and potential applications of macro-defect free cement, *Mater. Res. Symp. Proc.* 42 (1985) 265–276.
- [6] D.M. Roy, *Advanced cement systems, including CBC, DSP, MDF*, 9th ICCI, New Delhi, 1992, pp. 357–380.
- [7] A.A. Bonapasta, F. Buda, P. Colombet, G. Guerrini, Cross-linking of poly(vinyl alcohol) chains by Ca ions in macro-defect-free cements, *Chem. Mater.* 14 (2002) 1016–1022.
- [8] A.A. Bonapasta, F. Buda, P. Colombet, Cross-linking of poly(vinyl alcohol) chains by Al ions in macro-defect-free cements: a theoretical study, *Chem. Mater.* 12 (2000) 738–743.
- [9] M. Drábik, Contribution of materials chemistry to the knowledge of macro-defect-free (MDF) materials, *Pure Appl. Chem.* 81 (2009) 1413–1421.
- [10] F. Šoukal, P. Ptáček, J. Másičko, T. Opravil, J. Havlica, M. Drdlová, High temperature properties of MDF composite based on calcium aluminate cement and polyvinyl alcohol, *J. Therm. Anal. Calorim.* 115 (2014) 1245–1252.
- [11] O. Ekinocoglu, M.H. Ozkul, L.J. Struble, S. Patachia, Optimization of material characteristics of macro-defect free cement, *Cem. Concr. Compos.* 34 (2012) 556–565.
- [12] S.A. Rodger, High strength cement pastes, *J. Mater. Sci.* 20 (1986) 2853–2860.
- [13] L.S. Tan, Evolution of mechano-chemistry and microstructure of a calcium aluminate-polymer component. Part II. Mixing rate effect, *J. Mater. Res.* 11 (1996) 1739–1747.
- [14] S. Donatello, M. Tyrer, C.R. Cheeseman, Recent developments in macro-defect-free (MDF) cements, *Constr. Build. Mater.* 23 (2009) 1761–1767.
- [15] M.C. Biesinger, L.W.M. Lau, A.R. Gerson, R.S.C. Smart, The role of the Auger parameters in XPS studies of nickel metal, halides and oxides, *Phys. Chem. Chem. Phys.* 14 (2012) 2434–2442.
- [16] W. Hörkner, H. Müller-Buschbaum, Zur kristallstruktur von  $\text{CaAl}_2\text{O}_4$ , *J. Inorg. Nucl. Chem.* 38 (1976) 983.
- [17] M.C. Biesinger, B.P. Payne, A.P. Grosvenor, L.W.M. Lau, A.R. Gerson, R.S.C. Smart, Resolving surface chemical states in XPS analysis of first row transition metals oxides and hydroxides: Cr, Mn, Fe, Co and Ni, *Appl. Surf. Sci.* 257 (2011) 2717–2730.
- [18] J.F. Moulder, W.F. Stickle, P.E. Sobol, K.D. Bomben, in: J. Chastain (Ed.), *Handbook of X-ray Photoelectron Spectra—A Reference Book of Standard Spectra for Identification and Interpretation of XPS Data*, Perkin-Elmer, Eden Prairie, Minnesota, 1992, p. 41.
- [19] L. Sandrin, E. Sacher, X-ray photoelectron spectroscopy studies of the evaporated aluminum/corona-treated polyethylene terephthalate interface, *Appl. Surf. Sci.* 135 (1998) 339–349.
- [20] M. Bou, J.M. Martin, T. Le Monge, Chemistry of the interface between aluminium and polyethyleneterephthalate by XPS, *Appl. Surf. Sci.* 47 (1991) 149–161.
- [21] S. Akhrer, X.L. Zhou, J.M. White, XPS study of polymer/organometallic interaction: trimethyl aluminum on polyvinyl alcohol polymer, *Appl. Surf. Sci.* 37 (1989) 201–216.

## Příloha XIII

114

L. Kalina et al. / *Cement and Concrete Research* 66 (2014) 110–114

- [22] S.A. Rodger, W. Sinclair, G.W. Groves, S.A. Brooks, D.D. Double, in: J.F. Young (Ed.), *Reactions in the setting of high strength cement pastes*, Proceedings of the Materials Research Society Symposia, Boston, Massachusetts, USA, vol. 42, 1984, pp. 45–51.
- [23] S.A. Rodger, S.A. Brooks, W. Sinclair, G.W. Groves, D.D. Double, High strength cement pastes. Part 2: reactions during setting, *J. Mater. Sci.*, 20 (1985) 2853–2860.
- [24] O.G. Popoola, W.M. Kriven, J.F. Young, Microstructural and microchemical characterization of a calcium aluminate-polymer composite (MDF cement), *J. Am. Ceram. Soc.* 74 (1991) 1928–1933.
- [25] A.V. Naumkin, A. Kraut-Vass, W. Gaarenstroom, C.J. Powell, NIST standard reference database 20, version 4.1, (web version) <http://srdata.nist.gov/xps/> 2012.



"Gheorghe Asachi" Technical University of Iasi, Romania



## POTENTIAL USES OF GEOPOLYMERS TO IMMOBILIZE TOXIC METALS FROM BY-PRODUCTS MATERIALS

Lukáš Kalina\*, Jan Koplík, František Šoukal, Jiří Másilko, Lenka Jaskowiczová

Brno University of Technology, Faculty of Chemistry, Centre for Materials Research CZ.1.05/2.1.00/01.0012,  
Purkyňova 464/118, Brno, CZ-61200, Czech Republic

### Abstract

Portland cement-based products are the most commonly used building materials. Worldwide production accounted for about 2.5 billion metric tons. However, it is well known that the production of Ordinary Portland Cement (OPC) is associated with generating of by-product materials. Cement kiln dust is one of secondary material of cement manufacturing process. Purpose of this work is to use this undesirable material for development of new cementitious material similar to Portland cement-based concrete, which is convenient in terms of energy and is environmental-friendly at once. This article presents preparation and composition of new alkali activated material, called geopolymer, synthesized from blast furnace slag and fly ash activated by sodium hydroxide and cement kiln dust as well as the potential to immobilize heavy metals in its structure. Study was mainly based on SEM-EDX, XRD and ICP-MS analyses.

*Key words:* alkali activation, cement kiln dust, environmental-friendly material, immobilization

*Received:* September, 2011; *Revised final:* February, 2012; *Accepted:* March, 2012

### 1. Introduction

Throughout the world, millions of tones of waste materials are generated each year. Often these materials contain heavy metals which adversely affect environment. Currently is an effort to utilization of waste materials in order to avert the increasing contamination of the planet with toxic substances (Brandštetr, 2004). A large proportion of waste products are still stored in landfills or in surface, underground mines. Therefore there is a necessity to find new technology which will be focused on cheap and simple processing of large amount of these materials. Economic factors also increasingly dictate that industry should look towards recycling or value addition to waste materials as opposed to landfilling and discarding (Fu et al., 2011; Xu et al., 2005).

Another reason for usage of the industrial by-product is a considerable increase in production of construction materials which causes that the consumption of Ordinary Portland cement (OPC) is

still growing. Portland cement-based products are the most often used building materials. Currently, the cement industry produces 1.5 billion tons of OPC each year. However, it is well known that the production of OPC not only consumes a significant amount of natural resources and energy but also releases high quantity of carbon dioxide (CO<sub>2</sub>) to the atmosphere. In the manufacture of cement the CO<sub>2</sub> is emitted from the calcination process of limestone, from combustion of fuels in the kiln as well as from the power generation. Carbon dioxide emissions are the largest source of greenhouse gases associated with global warming. During cement manufacturing 0.498 metric ton of CO<sub>2</sub> is released from each ton of cement production, therefore is cement production the third largest cause of man-made carbon dioxide emissions (Davidovits, 1991).

One of the possibilities how to produce more environmentally friendly concrete is to replace the OPC with aluminosilicate polymer, called **geopolymer**, synthesized by alkali activation of

\* Author to whom all correspondence should be addressed: e-mail: kalina@fch.vutbr.cz

by-products materials such as fly ash, slag and another sources rich in silicon and aluminum (Sumajouw et al., 2006).

Geopolymers are formed by dissolution (Fig. 1) of solid aluminosilicate particles at high pH which quickly create a supersaturated aluminosilicate solution. Result is the formation of large network by condensation. Chemical structure can be described by  $M_n\{-(Si-O)_z-Al-O\}_n \cdot wH_2O$  where "M" is a cation such as potassium, sodium or calcium; "n" is a degree of polymerization; and "z" is ratio of  $SiO_2$  and  $Al_2O_3$ . The network is configured of  $SiO_4$  and  $AlO_4$  tetrahedrons united together by oxygen bridges. The fact that aluminum is four coordinated with respect to oxygen creates a negative charge imbalance and therefore the presence of cations such as  $K^+$  and  $Na^+$  is essential to maintain electric neutrality in the matrix (Davidovits, 1994; Harja et al., 2009).

The chemical stability of geopolymer materials is proved as well as a tendency to drastically decrease the mobility of most heavy metal ions contained in large quantity of industrial by-products. Another important consideration in connection with concrete is the price of final products. The alkali activators used for geopolymerization are mainly sodium or potassium hydroxides that are very expensive. The aim of this work is to develop inexpensive geopolymer concrete activated by another secondary material – cement kiln dust (CKD).

Cement kiln dust is created in the kiln during the production of cement clinker. The dust is a particulate mixture of partially calcined and unreacted raw feed, clinker dust and ash, enriched with alkali sulfates, halides and other volatiles. These particulates are captured by the exhaust gases and collected in electrostatic precipitators (Adaska et al., 2008). They are vary in composition, but most of them contain silica, calcium carbonate and calcium oxide ("free lime"); many also contain alkali sulfates and chlorides and sometimes other minor components. The presence of free-lime (CaO), the high alkali content and high fineness of CKD also makes them an excellent activator for pozzolanic materials such as blast furnace slag and fly ash (Peethamparan et al., 2008).

The objective of the work is to understand the interaction of CKD with slag/fly ash mixture in order to explore the feasibility and the approaches to development of new inorganic binder.

It is expected that the high free lime content of CKD will improve the hydration process by accelerating hydration. Hydrated lime ( $Ca(OH)_2$ ) is the most common used soil stabilizer. The hydration products may significantly affect CKD's soil stabilization potential. The characterization process of CKD's alkali activated matrix, leading to better understanding of stabilization mechanisms, is based on chemical analysis such as XRD, SEM-EDX analysis. The ability to inhibit hazardous material is determined by leaching tests and identified by using ICP-MS method.

## 2. Experimental

### 2.1. Materials and specimens preparation

In this research, low calcium fly ash (LCFA) obtained from Czech power plant, blast furnace slag (BFS) and cement kiln dust (CKD) were used as the base materials. Chemical composition of by-products materials is given in Table 1. XRD analysis of blast furnace slag and fly ash indicate the presence of a great deal of amorphous phase. The main crystal minerals identified in BFS were merwinite, melilite and calcite. The major crystal phases detected in LCFA include mullite, quartz, hematite and magnetite. Through the use of the Rietveld method for XRD quantitative analysis of CKD were determined 50.0 % sylvite (KCl), 23.8 % free lime (CaO), 16.5 % arcanite ( $K_2SO_4$ ) and 9.8 % larnite ( $2CaO \cdot SiO_2$ ). Alkali activator used in this study was sodium hydroxide in flake form dissolved in water to create 4M water solution.

The hydroxide solution was then poured into a solid fly ash/slag/CKD mixture. Time of the mixing takes 3 minutes. The paste was elaborated into steel molds of  $2 \times 2 \times 10$  cm. Specimens were cured at laboratory temperature for 24 hours.

### 2.2. Test methods

#### 2.2.1. X-ray diffraction analysis (XRD)

X-ray powder diffraction data were obtained using a PANalytical Empyrean diffractometer with  $CuK\alpha$  radiation equipped with a 3D detection system PIXcel<sup>3D</sup>. Specimens were step scanned from  $5^\circ$  to  $90^\circ 2\theta$  using vertical high-resolution goniometer with step size  $0.013^\circ 2\theta$ .

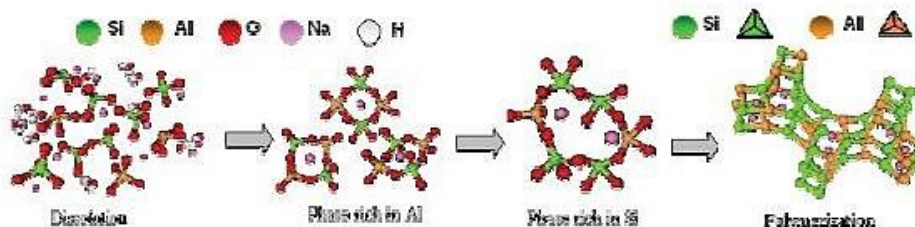


Fig. 1. Conceptual model for geopolymerization (Fenández-Jiménez et al., 2009)

## Příloha XIV

*The potential use of geopolymers to immobilize toxic metals from by-products materials*

**Table 1.** Mineralogical composition of used materials

<i>Content (%)</i>	<i>BFS</i>	<i>CKD</i>	<i>LCFA</i>
SiO <sub>2</sub>	34.7	4.1	40.3
Al <sub>2</sub> O <sub>3</sub>	9.1	–	29.8
Fe <sub>2</sub> O <sub>3</sub>	0.3	1.3	19.2
CaO	41.1	19.3	4.3
Na <sub>2</sub> O	0.4	–	0.9
K <sub>2</sub> O	0.9	36.2	1.5
MgO	10.5	–	1.3
SO <sub>3</sub>	1.5	5.1	1.1
TiO <sub>2</sub>	1.0	–	1.4
P <sub>2</sub> O <sub>5</sub>	–	–	0.3
PbO	–	1.8	–
Cl	–	31.8	–

### 2.2.2. Scanning electron microscopy (SEM-EDX)

Scanning electron microscopy was used to examine the fractured specimen surfaces in the backscatter mode using JEOL JSM-7600F and ZEISS EVO LS10 electron microscopes. The surface was polished using JEOL Cross section CP Polisher for 5 hours. The specimens were stick on carbon tape and the exposed fractured surfaces were sputter-coated with gold. Energy dispersive X-ray (EDX) results and EDS mapping of sample surface were obtained at selected locations using an Oxford AZtec System.

### 2.2.3. Leaching analysis

Leaching analyses were occurred after 28 days. The samples were stirred using the special shakers for 24 hours at ambient temperature according to ČSN EN 12457-4 norm. The sample solutions were filtered using a 0.45 μm membrane filters and analyzed by Thermo X Series II ICP-MS.

## 3. Results and Discussions

### 3.1. Mineralogical and microstructure of CKD-BFS-LCFA binder

The mineralogical characterization was determined using TG-DTA-EGA and XRD analyses. The XRD result (Fig. 2) of CKD-BFS-LCFA paste identified the presence of new crystalline phases such as hydroxalcalite and carbonates. The sample indicates the presence of great deal of amorphous phase (hump from 20 to 40 °2θ). The microscopic appearance of alkali activated binder was examined by scanning electron microscope imaged in the backscatter mode using EDX analysis. The main objective was the determination of binder phases responsible for mechanical properties of material. The Fig. 3 shows fracture area of 28 days old hydrated CKD-BFS-LCFA binder composed of spherical

particles of LCFA (place 1) and longitudinal grains of BFS (place 2). The EDX spectrum collected from fly ash particles had the main peaks for Al, Si and O revealed the presence of mullite and quartz. Some particles contained also high amount of Fe probably in Fe<sub>2</sub>O<sub>3</sub> or Fe<sub>3</sub>O<sub>4</sub> phases. Blast furnace slag grains were rich in O, Si, Ca, Mg and Al associated with presence of merwinite, melilite and calcite, as well as with amorphous calcium aluminosilicate glass. In the alkali activation process of slag, two layers are formed at the slag grain surface. The inner layer contains a constant thickness of a hydroxalcalite-type composition (place 3) and the outer product belongs to binder CSH phase (place 4). EDX analysis of binder phase indicates CSH gel with the Ca/Si ratio ~ 1.1. This ratio is almost same as in hydrated blended Portland cement, but it differs by the presence of distinct amounts of aluminum (Al/Ca ~ 0.2) and alkali ions in its structure. Aluminum substitutes for silicon in the bridging tetrahedron of dreierketten chains constituting the CASH phase (Richardson, 2004).

The second type of binder phase is created around and inside of fly ash particles (place 5). The chemical composition differs from previous phase. The main difference is the low value of Ca/Si ~ 0.6, conversely the high content of alumina. The ratio Al/Ca ~ 1.1 suggests the creation of phase related to zeolite (Ca-faujasite) as confirms XRD analysis (Fig. 4). As shown Fig. 3, the chemical attack via alkali activators can be observed on fly ash particle. The reaction product is generated both inside and outside of fly ash particles until the particle is completely or almost completely consumed. When alkaline solution penetrates inside the particles, the interior space is filled up with reaction product forming a dense matrix (Fernández-Jiménez et al., 2005). The results from EDX analysis are summarized in Table 2.

**Table 2.** EDX results at selected locations

<i>Place/at. [%]</i>	<i>O</i>	<i>Na</i>	<i>Mg</i>	<i>Al</i>	<i>Si</i>	<i>Cl</i>	<i>K</i>	<i>Ca</i>	<i>C</i>
1	54.5	–	0.8	18.9	23.4	–	1.1	0.7	–
2	51.3	0.5	8.8	7.7	16.2	–	–	15.6	–
3	57.7	3.0	15.8	7.2	6.1	–	–	4.7	4.8
4	38.3	3.2	1.7	4.6	20.4	4.5	4.5	22.7	–
5	47.0	4.5	1.6	12.3	18.3	1.5	3.7	11.3	–

## Příloha XIV

Kalina et al./Environmental Engineering and Management Journal 11 (2012), 3, 579-584

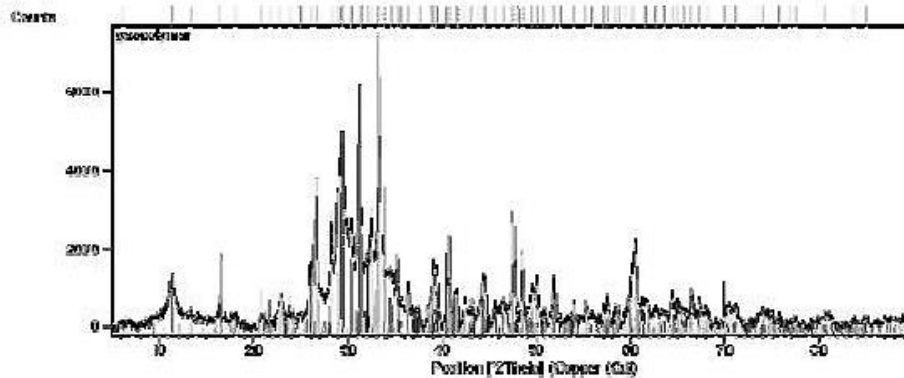


Fig. 2. XRD diffractogram of CKD-BFS-LCFA binder

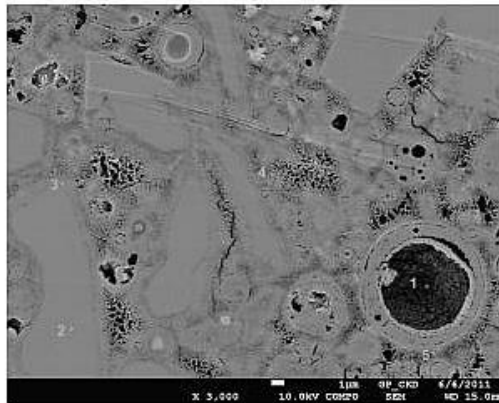


Fig. 3. SEM picture of CKD-BFS-LCFA binder

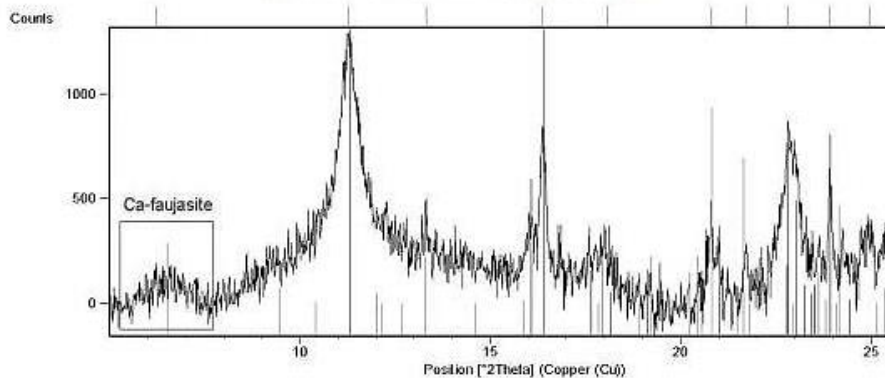


Fig. 4. Detail of XRD diffractogram of CKD-BFS-LCFA binder

The technology of geopolymerization can be also applied to solidify with the resultant immobilization of toxic materials. The example, how the immobilization process works is shown in case of lead (Pb) in Fig.5.

The particles of blast furnace slag were surrounded by round shining particles that were identified as Pb by EDX analysis. In this case are

possible two different explanations. Lead can be incorporated within the hydration products of the blast furnace slag mainly into the C-S-H gel. This corresponds with the fact that Pb was concentrated near the particles of the blast furnace slag. Pb could substitute Ca in the structure. At the place 1 was conducted EDX analysis (Table 3).

## Příloha XIV

*The potential use of geopolymers to immobilize toxic metals from by-products materials*

**Table 3.** EDX results at selected location

place/at.[%]	O	Pb	Mg	Al	Si	S	K	Cu	C
1	52.5	1.8	5.4	5.4	16.2	1.0	10.8	4.0	2.9

**Table 4.** The concentrations of hazardous elements leached from secondary industrial by-products materials [µg/l]

Materials/ elements	As	Ba	Cr	Cu	Ni	Pb	Sr	Zn
LCFA	9.97	143.00	5.91	603.90	303.70	7.85	1095.00	1019.00
BFS	0.62	185.70	2.11	1.60	1.98	0.02	279.80	0.55
CKD	153.60	65.93	82.43	0.21	4.23	4954.00	118.50	99.50
Matrix	86.56	20.53	7.97	2.29	142.10	6.90	39.30	3.64

It was found that elemental composition was dominated by Si, K and important was also occurrence of Al. According to this EDX analysis Pb is rather incorporated within geopolymer aluminosilicate matrix. Possibly  $Pb_3SiO_5$  can be formed (Palomo, 2003).

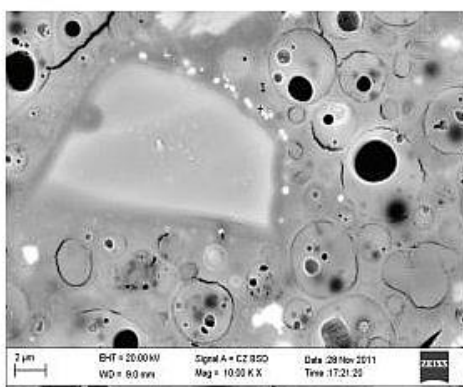


**Fig. 5.** SEM picture of geopolymer matrix with Pb particles

### 3.2. Immobilization

The technology of geopolymerization can be also applied to solidify with the resultant immobilization of toxic materials.

The exact mechanism of inhibition of hazardous elements hasn't been found out yet, but there are two possible types of mechanism. The first one is physical encapsulation. Elements are fixed within the matrix after setting only by physical forces. This mechanism is linked with mechanical properties of matrix mainly with compressive strength.

The other one is chemical fixation. Alkali metals like Cs, Ba, Sr can replace charged balancing cation and can be incorporated into the geopolymer network. Other elements such as Pb can be bonded in new created aluminosilicate phases, which are formed after the alkali activation. These elements are usually well dispersed throughout the matrix. Alkali activation can also change a form of heavy metals from soluble one to the less soluble one. This conversion decrease leaching of heavy metals from geopolymer matrix.

One of only methods available for determining efficiency of hazardous elements immobilization is by leaching tests (Van Jaarsveld et al., 1995). Table 4 shows the results of concentrations for selected hazardous elements after leaching used raw materials and final geopolymer matrix which were washed out from fly ash and CKD.

However the process of geopolymerization (results from matrix) rapidly decreased the concentration of toxic elements. Especially the immobilization of lead, strontium and zinc demonstrate very good fixation capacity.

### 3.3. Application and economic benefit

This building alternative also offers economic benefits over Portland cement concrete. From economical point of view the very expensive sodium hydroxide solution was partly replaced by cement kiln dust. Finally, the geopolymer concrete is about 10 percent cheaper than OPC concrete and moreover processes and stabilizes large amount of dangerous by-product materials. Based on advantageous properties of this geopolymer binder was made the geopolymer concrete in cooperation with ŽPSV a.s. company. The resulting product was transition board (Fig. 6).



**Fig. 6.** Transition board made from geopolymer concrete

## 4. Conclusions

Cement kiln dust (CKD) used in this study is characterized as very usable for alkali activation of

by-product materials such as blast furnace slag (BFS) and low calcium fly ash (LCFA) mixture.

Mineralogical and microstructural analysis identified that the main binder products are Al-containing CSH gel with alkali ions in structure and semi-crystalline alkali silicoaluminate related to zeolites. The results from immobilization tests demonstrated that the manufacturing of geopolymers from waste materials should provide cheap alternative of building material with potential to encapsulate toxic metals in its structure.

Results presented in this work demonstrate that CKD-BFS-LCFA binder has an excellent potential for its application in building industry.

#### References

- Adaska W.S., Taubert D.H., (2008), *Beneficial uses of cement kiln dust*, Proc. 50<sup>th</sup> Cement Industry Technical Conf., Miami, FL.
- Brandštet J., (2007), *Geopolymeric materials ancient and for the 21 Century*, Proc. Conf. 11<sup>th</sup> International Conference Ecology and New Building Materials and Products, Telč, 264-268.
- Davidovits J., (1991), Geopolymers: inorganic polymeric new materials, *Journal of Thermal Analysis*, **37**, 1533-1556.
- Davidovits J., (1994), *Chemistry of geopolymeric systems, Terminology*, Proc. Conf. Geopolymère, Saint-Quentin, 9-40.
- Fernández-Jiménez A., Palomo A., Criado M., (2005), Microstructure development of alkali-activated fly ash cement: a descriptive model, *Cement and Concrete Research*, **35**, 1204-1209.
- Fernández-Jiménez A., Palomo A., Revuelta D., (2009), *Alkali activation of industrial by-products to develop new earth-friendly cements*, Proc. 11<sup>th</sup> International Conference Non-Conventional Materials and Technologies, Bath, UK.
- Fu F., Ni W., Wu H., Tian M., (2011), Strength and microstructural characteristics of slag-fly ash based cementitious materials, *Environmental Engineering and Management Journal*, **10**, 951-954.
- Harja M., Bărbuță M., Gavrilă M., (2009), Utilization of coal fly ash from power plants II. Geopolymer obtaining, *Environmental Engineering and Management Journal*, **10**, 951-954.
- Palomo A., Palacios M., (2003), Alkali-activated matrices for the immobilization of hazardous wastes Part II. Stabilization of chromium and lead, *Cement and Concrete Research*, **33**, 289-295.
- Peethamparan S., Olek J., Lovell J., (2008), Influence of chemical and physical characteristics of cement kiln dusts (CKDs) on their hydration behavior and potential suitability for soil stabilization, *Cement and Concrete Research*, **38**, 803-815.
- Richardson I.G., (2004), Tobermorite/jennite- and tobermorite/calcium hydroxide-based models for the structure of C-S-H: application to hardened pastes of tricalcium silicate,  $\beta$ -dicalcium silicate, Portland cement, and blends of Portland cement with blast-furnace slag, metakaolin, or silica fume, *Cement and Concrete Research*, **34**, 1733-1777.
- Sumajouw D.M.J., Hardjito D., Wallah S.E., Rangan B.V., (2006), Fly ash-based geopolymer concrete: study of slender reinforced columns, *Journal of Materials Science*, **42**, 3124-3130.
- Van Jaarsveld J.G.S., Van Deventer J.S.J., Lorenzen L., (1997), The potential use of geopolymeric materials to immobilise toxic metals: Part I. Theory and applications, *Minerals Engineering*, **10**, 659-669.
- Xu J.Z., Zhou Y.L., Chang Q., Qu H.Q., (2005), Study on the factors of affecting the immobilization of heavy metals in fly ash-based geopolymers, *Material Letters*, **60**, 820-822.